AKADEMIE DER WISSENSCHAFTEN DER DDR

ZENTRALINSTITUT FÜR KERNFORSCHUNG
ROSSENDORF BEI DRESDEN

ZfK – 621

ANNUAL REPORT 1986

ON NUCLEAR PHYSICS ACTIVITIES AND APPLICATIONS

Zentralinstitut für Kernforschung, Rossendorf
Technische Universität, Dresden
Karl-Marx-Universität, Leipzig
Humboldt-Universität, Berlin
Friedrich-Schiller-Universität, Jena
Bergakademie Freiberg
Zentralinstitut für Isotopenforschung, Leipzig

Edited by K. Hennig

Edditorial staff: F. Dönau, F. Flagmeyer, M. Friedrich, W. D. Fromm
K. Möller, J. Mösner, F. Naehring, D. Schmidt,
S. Unterricker, W. Wesch, G. Winter, R. Wünsch

April 1987

ISSN 0138-2950

AKADEMIE DER WISSENSCHAFTEN DER DDR

Z E N T R A L I N S T I T U T F Ü R K E R N F O R S C H U N G

R O S S E N D O R F B E I D R E S D E N

ZfK - 621

ANNUAL REPORT 1986

ON NUCLEAR PHYSICS ACTIVITIES AND APPLICATIONS

Zentralinstitut für Kernforschung, Rossendorf

Technische Universität, Dresden

Karl-Marx-Universität, Leipzig

Humboldt-Universität, Berlin

Friedrich-Schiller-Universität, Jena

Bergakademie Freiberg

Zentralinstitut für Isotopenforschung, Leipzig

Edited by K. Hennig

Edditorial staff: F. Dönau, F. Flagmeyer, M. Friedrich, W.D. Fromm,
K. Möller, J. Mösner, F. Naehring, D. Schmidt,
S. Unterricker, W. Wesch, G. Winter, R. Wünsch

April 1987

CONTENTS

	page
Nuclear Reactions	1
Nuclear Spectroscopy	28
Theory	42
Applied Methods	70
Accelerators	117
Nuclear Electronics and Methods	119
Computational Methods and Codes	147
List of Publications, Academic Promotions, Lectures and Conference Contributions, Scientific Meetings, Patents and Awards of Honour	150

INHALTSVERZEICHNIS

	Seite
Arbeiten auf dem Gebiet der Kernreaktionen	1
Arbeiten auf dem Gebiet der Kernspektroskopie	28
Arbeiten auf den Gebieten der Kern- und Festkörpertheorie	42
Anwendung kernphysikalischer Methoden	70
Berichte zu den Beschleunigern	117
Apparative und methodische Arbeiten	119
Zentrale Rechentechnik und Rechenprogramme	147
Liste der Veröffentlichungen, Diplomarbeiten, Promotionen, Vorträge, Veranstaltungen, wissenschaftlichen Preise, Patente und Auszeichnungen	150

СОДЕРЖАНИЕ

	стр.
Ядерные реакции	1
Ядерная спектроскопия	28
Теория	42
Прикладные методы ядерной физики	70
Ускорители	117
Ядерная электроника и методы измерения	119
Вычислительный центр и программное обеспечение	147
Список публикаций и докладов	150

CONTRIBUTIONS

NUCLEAR REACTIONS

page

Total kinetic energy release in heavy-ion reactions leading to composite systems with $Z \geq 108$
P. Gippner, K.D. Schilling, W. Seidel, F. Stary, E. Will, H. Sodan, S.M. Lukyanov, G.G. Chubarian, Yu.E. Penionzhkevich , V.S. Salamatin 1

Total kinetic energy release in heavy-ion reactions with dominating fusion-fission mechanism
P. Gippner, K.D. Schilling, W. Seidel, F. Stary, E. Will, H. Sodan, S.M. Lukyanov, G.G. Chubarian, Yu.E. Penionzhkevich, V.S. Salamatin 2

Description of the mass distribution in heavy-ion collisions
G.D. Adeev, V.V. Pashkevich, G. Saupe 3

Measurement of the angular distribution of γ-rays in the binary fission of ^{252}Cf
W. Neubert, W. Pilz, H. Märten 4

Energy and angular distribution of $^{252}Cf(Sf)$ neutrons at low energy
H. Märten, D. Richter, D. Seeliger, W. Neubert, A. Lajtai 5

Energy balance in fission
H. Märten, D. Polster, A. Ruben 6

$^{252}Cf(Sf)$ neutron emission at medium and high energy
H. Märten, D. Richter, D. Seeliger, W. Neubert 7

Extended statistical-model approach to fission neutron emission
P. Krimmling, H. Märten 8

Precise estimation of the angular depending neutron source strength for a 14 MeV neutron generator
Bach Ly Bah, B. Hildebrandt, K. Seidel, S. Unholzer 9

Recommended data of the neutron emission from Pb at 14 MeV incidence energy
T. Elfruth, D. Seeliger, K. Seidel, S. Unholzer 10

The neutron multiplication of lead at 14 MeV neutron incidence energy
T. Elfruth, D. Seeliger, K. Seidel, G. Streubel, S. Unholzer, D. Albert, W. Hansen, K. Noack, C. Reiche, W. Vogel, D.V. Markovskij, G.E. Shatalov 11

Correction of the influence of finite sample size on measured neutron emission cross sections
T. Elfruth, E. Rodriguez, K. Seidel, S. Unholzer, K. Noack 12

Neutron emission spectra from the interaction of 14 MeV neutrons with lead
T. Elfruth, D. Hermsdorf, H. Kalka, J. Pöthig, D. Seeliger, K. Seidel, S. Unholzer 13

Search for metastable highly charged recoil ions
H. Schmidt-Böcking, V. Dangendorf, J. Euler, J. Ullrich, S. Schmidt, S. Zschornack, S. Hagmann 14

Influence of Breit and QED corrections to atomic properties in highly ionized krypton
I. Reiche, G. Zschornack 15

page

Absolute measurements of the U-238 fission cross-section at 4.8 MeV and 8.4 MeV neutron energies using the TCAPM

C.-M. Herbach, K. Merla, G. Musiol, H.-G. Ortlepp, G. Pausch, U. Todt, I.D. Alchasov, L.W. Drapchinsky, E.A. Ganza, O.I. Kostochkin, V.I. Shpakov, P.S. Soloshenkov, S.M. Soloviev 17

Associated particle background normalization in TCAPM fission cross-section measurements using the D(D,^{3}He)-neutron production reaction

C.-M. Herbach, K. Merla, G. Musiol, H.-G. Ortlepp, G. Pausch, U. Todt 18

Experimental determination of fission fragment absorption within fission layers of Pu-239

C.-M. Herbach, G. Musiol 19

Final results of the absolute cross section measurements on Pu-239

C.-M. Herbach, K. Merla, G. Musiol, G. Pausch, W. Wagner 20

A simple method of experimental investigation about fission fragment absorption within thin fission layers by using the fragments energy spectrum

C.-M. Herbach, G. Pausch 21

On the correlation between fission fragment detection efficiency and the plateau height in fission chamber spectra for thin fissile layers on scratched backings

G. Pausch, C.-M. Herbach, K. Merla, G. Musiol, W. Wagner 22

ROBER - A Monte-Carlo code simulating the influence of scratched backings on the absorption probability and the energy spectrum of particles emitted from a thin target layer

G. Pausch, K. Merla, G. Musiol, R. Perez, L.V. Drapchinsky, W. Wagner 23

Influence of atomic, molecular, and solid state effects on neutron resonance cross section

K. Seidel, D. Seeliger, A. Meister, S. Mittag, W. Pilz 24

A statistical model for multiparticle production in hadron-hadron interaction

H.W. Barz, H. Müller, H. Schulz 25

Coulomb final-state interaction in identical boson interferometry

H.-U. Gersch 26

NUCLEAR SPECTROSCOPY

Test of large-area silicon detectors in heavy-ion reactions

L. Funke, J.v. Borany, J. Döring, M. Freitag, K.H. Kaun, H. Prade, B. Schmidt, R. Schwengner, A. Johnson, J.D. Garrett, K. Schiffer 28

In-beam experiments with ^{7}Li - the magnetic moment of a new $15/2^+$ isomer in $^{85}_{37}Rb_{48}$

L. Käubler, J. Döring, L. Funke, H. Prade, H. Rotter, R. Schwengner, E. Will, G. Winter 29

Band structures in ^{79}Br

R. Schwengner, J. Döring, L. Funke, H. Rotter, G. Winter, A. Johnson, A. Nielsson 30

High-spin states in ^{79}Kr

L. Funke, G. Winter, R. Schwengner, J. Döring, H. Prade, H. Rotter, A. Johnson, A. Nilsson 31

page

Transition probabilities in the band crossing region of ^{79}Kr
G. Winter, J. Döring, L. Funke, H. Prade, H. Rotter, R. Schwengner, A. Johnson, A. Nilsson 32

Near-yrast spectroscopy of the N=48 nuclide ^{84}Kr
H. Rotter, J. Döring, L. Funke, L. Käubler, P. Kleinwächter, H. Prade, R. Schwengner, G. Winter, A.E. Sobov, A.P. Grinberg, I.Kh. Lemberg, A.S. Mishin, L.A. Rassadin, I.N. Chugunov, A.D. Efimov 33

Magnetic moment of the 12^+ isomer in ^{84}Kr
H. Prade, L. Funke, L. Käubler, H. Rotter, L.O. Norlin, U. Rosengard 34

Investigation of ^{79}Se in the (α,n) and (α,α n) reactions
L. Funke, J. Döring, R. Schwengner, G. Winter 35

In-beam investigation of the N=82 nucleus ^{142}Nd
L. Käubler, W. Enghardt, H. Prade 35

Particle-core coupling description of negative parity states in the Z=50 nuclei ^{109,113}Sn
L. Käubler, W. Enghardt, P. Kleinwächter, H. Prade 36

Neutron $2f_{7/2}$ excitations in ^{139}Ba
H. Prade, W. Enghardt, L. Käubler, G. Winter 37

E1 transitions in N = 82 isotones caused by outer subshell configurations
W. Enghardt, L. Käubler, H. Prade 38

^{106}Ag:p-n multiplets and band-like structures
W. Andrejtscheff, L.K. Kostov L.G. Kostova, P. Petkov, A. Dewald, J. Eberth, K.O. Zell, P. von Brentano, L. Funke, E. Will 39

Enhanced E1 decay of the $K^{\pi} = 6^-$ state in ^{174}Hf
W. Andrejtscheff, L.K. Kostov, L.G. Kostova, P. Petkov, J. Döring, L. Käubler, H. Rotter, E. Will 40

Limits on heavy axion production from p(n,a)d
W. Enghardt, K.H. Kaun, H. Prade, J. Blümlein, K. Lanius 41

THEORY

Exact scaling behaviour of the effective chiral action and stability of the chiral soliton
H. Reinhardt 42

Vacuum instabilities in the effective chiral action
H. Reinhardt, A. Wirzba 43

Nonlocal expansion of the effective chiral lagrangian
F.-M. Dittes, L. Münchow 44

From quark flavour dynamics to a chiral soliton model with dynamical restoration of chiral symmetry
H. Reinhardt, B. Kämpfer 45

Analysis of the isotropic lambda-particle emission in C+C collisions at 3.66 A*GeV
H. Iwe 46

page

Investigation of Σhypernuclei in the framework of the continuum shell-model
R. Wünsch, J. Žofka 47

Two-fluid model applied to ultra-relativistic heavy ion reactions
H.W. Barz, B. Kämpfer, L.P. Csernai, B. Lukács 49

Isotope distribution in nuclear multifragmentation
H.W. Barz, H. Schulz, J.P. Bondorf, K. Sneppen, R. Donangelo 50

Site-percolation approach for mass and isotopic distributions in fragmentation reactions
O. Knospe, R. Schmidt, H. Schulz 51

Subthreshold pion production and statistical multifragmentation in nucleus-nucleus collisions
H.W. Barz, H. Schulz, J.P. Bondorf, J. Lopez, C. Guet 52

Proton emission in and out-of plane within the TSM
M. Biedermann, P. Mädler 53

Some model calculations of linear momentum transfer in intermediate-energy HIC
M. Biedermann, P. Mädler 54

Randomization by collective fluctuations in the early stage of a heavy-ion collision
P. Mädler, L. Münchow, A. Pfitzner 55

Fluctuation-induced relaxation in one-body dynamics
A. Pfitzner, L. Münchow, P. Mädler 56

Validity of the Landau-Zener formula for quasielastic heavy-ion reactions
B. Milek, R. Reif 57

Photo- and electroexcitation of ^{14}C and ^{14}N
A.N. Golzov, N.G. Goncharova, H.R. Kissener 58

On three-body forces
I. Rotter 59

Symmetry violation in the open quantum mechanical nuclear system
I. Rotter 60

Cooperative effects in nuclei and selforganization
I. Rotter 61

The effect of asymmetric ion range distributions on the modeling of oxygen depth profiles in implanted SOI structures
H.U. Jäger 62

On the linear cascade theory for inhomogeneous targets
M. Posselt 63

Scaling phenomena of primary crystallization studied by computer experiments
H.-J. Müller, K.-H. Heinig 64

page

Computer studied of the statistical distribution functions of particles moving in collision cascades I: incident particles
M. Posselt, G. Otto 65

Computer studies of the statistical distribution functions of particles moving in collision cascades II: recoiling target atoms
M. Posselt, G. Otto 66

On the calculation of the multiplicities of quasicrystal diffraction spots
V. Heera, B. Rauschenbach 67

Some remarks on the indexing of the diffraction pattern of icosahedral quasicrystals
V. Heera, B. Rauschenbach 68

Application of the point kernel integration method to three-dimensional neutron flux calculation outside the hexagonally shaped LWR-cores
F. Seidel 69

APPLIED METHODS

PIXE investigation of $A_3^{II}B_2^{V}$-semiconductors
H.U. Frey, A. Hupfer 70

Profiling of (Al,Ga)As/GaAs heterostructures by experimental and computer-simulated backscattering spectra
R. Flagmeyer, H.-E. Zschau, A. Koch 71

Measurements of hydrogen incorporation and of damage density on proton bombarded InP
C. Ascheron, V. Riede, H. Sobotta, R. Flagmeyer, C. Neelmeijer 72

Measurements with the Rossendorf high energy ion microprobe
D. Grambole, F. Herrmann, W. Rudolph 73

Hydrogen depth profiling in H implanted semiconductors using elastic recoil detection
D. Lehmann, C. Ascheron, C. Neelmeijer 74

Depth profile of microhardness on hydrogen implanted GaP and InP single crystals
C. Ascheron, R. Schäfer, A. Schindler 75

A study of vacancy type defects on proton bombarded GaP single crystals
C. Ascheron, G. Dlubek, R. Krause, H. Erhard, D. Klimm 76

Investigations of the annealing behaviour of hydrogen implanted GaP single crystals by means of particle induced gamma-spectroscopy, infrared spectroscopy and Rutherford backscattering channeling techniques
C. Ascheron, H. Sobotta, V. Riede, C. Bauer, R. Grötschel, A. Schindler 77

Swelling of He^+ implanted GaP single crystals
C. Ascheron, A. Schindler, R. Flagmeyer, G. Otto 78

Fission-track ages of natural glasses
A. Docekal, W. Stolz, O. Leeder 79

The possibilities of CPAA in geological samples by the Rossendorf cyclotron Y-120
D. Degering, S. Unterricker, W. Stolz 80

page

Fluorine depth profiling for Caries prevention
H. Zschau, J. Vogt, G. Otto, M. Schneider, A. Treide 81

PIXE analysis of elemental distributions along single hair strands
H.U. Frey, G. Otto 82

γ-spectrometric investigations to the intrinsic radioactivities of shielding materials
Kim Jung Ho, S. Unterricker, W. Stolz 83

Moessbauer spectroscopy of the tempering behaviour of the spring steel 62SiCr5
C. Pietzsch, U. Thieme 84

Wear studies of components using deuteron activation
Ch. Eifrig, K. Eichhorn, P. Hammer 85

Energy and dose dependence of damage produced by low energy Ar ion beam etching of GaAs measured ^{65}Cu adsorption and autoradiography and RBS-channeling
R. Fechner, A. Schindler, R. Flagmeyer, F. Bigl 86

Study of near surface damage depth profiles of Ar ion beam etched GaAs by means of ^{64}Cu adsorption and autoradiographic detection
R. Fechner, A. Schindler, F. Bigl, J. Flachowsky 87

A pattern edge profile simulation for ion beam etching processes
G. Ringel, A. Nickel, F. Bigl 89

Scanning microbeam with a liquid metal ion source
J. Mittenbacher 91

Determination of threshold voltages of liquid metal ion sources
I. Stiebritz, R. Mühle, F. Machalett 92

Mass spectra of Au-Si alloy liquid metal ion sources
R. Mühle, F. Machalett, I. Stiebritz 93

Measurements with an ExB type mass separator
R. Mühle, A. Matthies, I. Stiebritz, F. Machalett 94

Amorphization and electrical properties of silicon after high energy phosphorus implantation
W. Skorupa, R. Grötzschel, E. Wieser 95

Strong dopant dependence of implantation defect accumulation and amorphisation in heavily doped silicon
R. Grötzschel, J. Schöneich, A.V. Dvurechenskii, V.P. Popov, H. Bartsch 96

Modeling of enhanced diffusion and electrical activation of As implanted into Si by rapid thermal annealing
R. Kögler 97

Threshold of the electrical activation of Si implanted GaAs by short time annealing in the solid phase regime
D. Panknin, E. Wieser, Ya.V. Fattachov, J.B. Khaibullin 98

Redistribution of implanted As in a $MoSi_2$/polysilicon structure by short time annealing
E. Wieser, Ch. Weise, E. Vetter, Th. Geßner 99

page

Formation of buried Si_3N_4/SiO_xN_y layers in silicon by high dose implantation at 60 keV
W. Skorupa, K. Wollschläger, R. Grötzschel, H. Bartsch 100

Chemical depth profiling of buried silicon nitride layers in silicon by Auger electron spectroscopy
W. Skorupa, J. Albrecht, J. Götz

Ion beam induced epitaxial crystallization of doped amorphous silicon layers
M. Voelskow, W. Skorupa, J. Matthäi 102

Electrical properties of MOS structures fabricated in lamp recrystallized films on SiO_2
N. Sieber, H. Oertel, M. Voelskow 103

Etch rate modification of thermally grown SiO_2 layers by ion bombardment
H. Münzer, C. Neelmeijer, M. Posselt, B. Schmidt 104

A noval processing technique for the fabrication of thin anisotropically etched single crystalline silicon layers
B. Schmidt, U. Kreißig, H. Münzer, E. Rost 105

Results of high resistivity NTD-silicon slice production
L. Bischoff 106

Effects of 20 keV electron beam radiation on MOS structures using thin anodically grown oxide films
G. Mende, M. Deutscher, H.-J. Döring, H. Flietner 107

Out-diffusion of oxygen during ion bombardment of polymer foils
W. Rudolph, R. Grötzschel 108

A diffraction - related classification of polycrystalline materials
P. Klimanek 109

Sample-induced errors in quantitative diffraction analysis of textures
P. Klimanek, A. Mücklich 110

Determination of the implantation-induced textures by electron diffraction
K. Helming, B. Rauschenbach 111

Analysis of the inner compatibility of experimental pole figures by single pole figure fits
S. Matthies, G.W. Vinel 112

Texture investigations on a fluorite vein structure by neutron diffraction
M. Betzl, K. Helming, W. Voitus, H.J. Franzke 113

Small-angle neutron scattering on silicon nitride powders
F. Eichhorn, J. Bläsing 114

Sans studies on the hydration process of portland cement paste
F. Häußler, U. Miehe, F. Eichhorn 115

The structure of metaphosphate glasses by neutron diffraction
W. Matz, D. Stachel, E.A. Goremychkin 116

page

ACCELERATORS

Operation of the cyclotron U-120
B. Anders, H. Guratzsch 117

Operation of the electrostatic accelerators in 1986
W. Bürger, S. Turuc 118

NUCLEAR ELECTRONICS AND METHODS

Electronic equipment for the 4π-spectrometer PHOBOS
W.D. Fromm, H.-G. Ortlepp, H. Sodan, O.V. Strekulovski 119

The vacuum and gas handling system for the 4π spectrometer "PHOBOS"
W. Seidel, D. Walzog, H. Sodan 120

Further test results with the double grid avalanche counter
W. Seidel, H.-G. Ortlepp 121

A Bragg ionization chamber with large solid angle
W. Seidel, H.-G. Ortlepp, D. Walzog, F. Stary, M. Andrassy, H. Sodan 122

Introduction of digital filtering methods into the Bragg-curve spectroscopy
A. Romaguera, H.-G. Ortlepp 123

A test of the Bragg ionization chamber by using the reaction $^{10}B+^{35}Cl$(32 MeV)
A.A. Kotov, W. Neubert, W. Pilz 124

Properties of a coaxial ionization chamber tested with low-energy heavy ions
A.A. Kotov, W. Neubert, W. Pilz 125

A detector telescope for measuring angular distributions of neutron induced charged reaction products
P. Michel, J. Hutsch, J. Mösner, K. Möller, G. Schmidt 126

Position sensitive multistep avalanche chambers for detection of light charged particles
P. Michel, J. Hutsch, J. Mösner, K. Möller, G. Schmidt 127

Parameter optimization of high-density avalanche chambers
P. Manfraß, W. Enghardt, W.D. Fromm, D. Wohlfarth 128

Extension of the Dubna time-of-flight spectrometer DEMAS for measuring light charged particles in coincidence with fission fragments
H.-G. Ortlepp, K. Heidel, H. Sodan 130

A ΔE-E annular semiconductor detector telescope for light charged particles from heavy ion reactions
M. Deutscher, E. Hentschel, J. Keller, R. Kotte, H.-G. Ortlepp, W. Seidel, F. Stary 131

Investigations on the determination of the Pu isotopic composition by gamma-ray spectroscopy
H. Prade, L. Funke, R. Arlt, W. Lewis 132

page

γ-response matrix of voluminous NaJ(Tl)-scintillators
D. Lucas, H. Märten, W. Neubert, W. Pilz 134

Cosmic radiation induced background of selected detector types at high energies
S. Unterricker, D. Degering 135

Experimental arrangement for investigation of the angular distribution of γ-rays in the ternary fission of ^{252}Cf
N.F. Bondar, W. Neubert and W. Pilz 136

The registration of 3 and 4 parameters from fission experiments
W.D. Fromm 137

The color display unit FD4971 as autonomous 2D-analyzer
W.D. Fromm 138

Electronic developments of the KFM group
W.D. Fromm, F. Schwarzenberg, H.-G. Ortlepp 139

Pseudographics on the personal computer PC 1715
H.-J. Müller, K.-H. Heinig, W.D. Fromm, F. Schwarzenberg 140

An intelligent CAMAC-control unit for the CCD sensor L 110 C
G. Karrasch, D. Kreiseler, K. Kreiseler, G. Musiol, G. Zschornack 141

Detritiation system for a high-flux neutron generator
U. Gohs, D. Schmidt 142

Oxidation of hydrogen in air and in inert gas atmosphere using copper oxide catalyser
M. Bittner, U. Gohs 143

A diffusing system for proton beams
H.U. Frey, U. Lehmann, J. Vogt 144

An inexpensive fast-closing safety valve against vacuum breakdown
B. Krause, D. Lehmann 145

A method for computer controlled regulation or stabilization of detector voltages
N.F. Bondar, J. Mösner, J. Hutsch 146

COMPUTATIONAL METHODS AND CODES

EVMESS - A program for experiment data collection on SM3 computers
E. Will 147

A new program package for the calculation of relativistic X-ray emission rates
I. Reiche, G. Zschornack 148

Properties of a bayes-based spectrum unfolding algorithm
E. Jara, A. Reichmann, G. Zschornack 149

NUCLEAR REACTIONS

TOTAL KINETIC ENERGY RELEASE IN HEAVY-ION REACTIONS LEADING TO COMPOSITE SYSTEMS WITH Z ≥ 108

P. Gippner, K.D. Schilling, W. Seidel, F. Stary and E. Will
Central Institute for Nuclear Research, Rossendorf
H. Sodan, S.M. Lukyanov, G.G. Chubarian, Yu.E. Penionzhkevich and V.S. Salamatin
Joint Institute for Nuclear Research, Dubna

Using the double-arm time-of-flight spectrometer DEMAS /1/ systematic investigations were performed concerning the energy and mass distributions of fragments originating from heavy-ion reactions at various mass asymmetries in the entrance channel. The results have already been published /2-4/. Fig. 1 shows the TKE vs. mass distributions obtained by investigating reactions leading to composite systems with $Z \geq 108$. The parabolic dashed lines indicate the expected TKE release in fission in accordance with the fission systematics /5/, which is scaled /6/ proportional to $M_3M_4/(M_3^{1/3}+ M_4^{1/3})$:

$$\langle TKE(AS)\rangle = \langle TKE(S)\rangle \cdot k \cdot M_3M_4/(M_3^{1/3}+ M_4^{1/3}) \qquad (1)$$

Thereby, the expressions $\langle TKE(AS)\rangle$ and $\langle TKE(S)\rangle$ denote the mean TKE release of asymmetric and symmetric /5/ fission products, respectively. The factor k is chosen in such a way, that both mean values coincide for $M_3=M_4=A/2$, where $A=M_1+M_2=M_3+M_4$. The basic idea of the scaling formula (1) is that $TKE \sim Z_3Z_4/(r_3+r_4)$, with $Z \sim M$ and $r \sim M^{1/3}$, respectively. Fig. 1 shows that formula (1) describes only the general behaviour of the intensity ridges in the measured TKE vs. mass distributions. Calculating the mean values $\langle TKE\rangle$ per mass interval one obtaines results denoted in fig. 1 by the circles, which deviate from the predictions of the systematics. Up to now, the reason for these TKE-deviations is not yet understood. They were found to occure in reactions, which undergo various reaction mechanisms /2,4/. One question is, how far the fission systematics (1) is able to describe exactly the TKE release in quasi-fission processes observed in $^{40}Ar + ^{232}Th$ and $^{40}Ar + ^{238}U$ at E_{lab} = 220 MeV /2,4/. For these reactions the contributions to the fragments TKE caused by the angular momenta of the rotating, rigid composite systems were estimated in the sticking limit. They cannot explain the experimental results. On the other hand, for the reaction $^{22}Ne + ^{249}Cf$, which is believed to undergo fusion-fission /2/ small deviations were also observed.

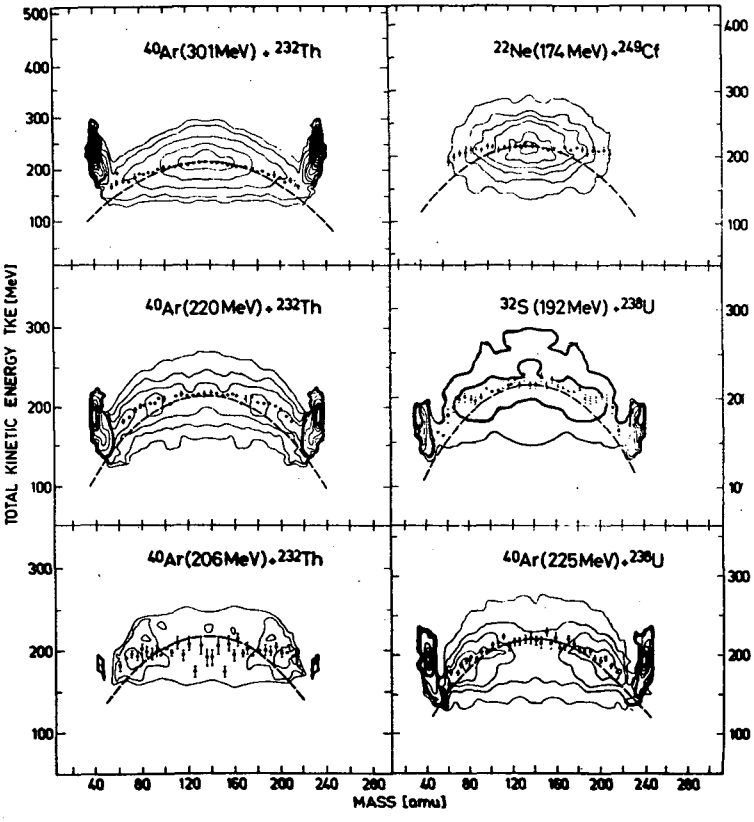

Fig. 1

References

/1/ Schilling, K.D. et al., ZfK-586 (1986), to be published in NIM
/2/ Gippner, P. et al., Z. Phys. A325 (1986) 335
/3/ Sodan, H. et al., JINR Rapid Communications N4-84, Dubna, 1984, p. 13
/4/ Gippner, P. et al., ZfK-592 (1986) 122
/5/ Viola, V.E., Nucl. Data A1 (1966) 391
/6/ Töke, J. et al., Nucl. Phys. A440 (1985) 327

TOTAL KINETIC ENERGY RELEASE IN HEAVY-ION REACTIONS WITH DOMINATING FUSION-FISSION MECHANISM

P. Gippner, K.D. Schilling, W. Seidel, F. Stary and E. Will
Central Institute for Nuclear Research, Rossendorf
H. Sodan, S.M. Lukyanov, G.G. Chubarian, Yu.E. Penionzhkevich and V.S. Salamatin
Joint Institute for Nuclear Research, Dubna

In order to get more experimental material concerning the TKE release in heavy-ion reactions at low incidence energies, the reactions $^{22}Ne + ^{232}Th$ and $^{22}Ne + ^{238}U$ were investigated, both at E_{lab} = 179 MeV. The measurements were performed by means of the time-of-flight spectrometer DEMAS /1/. Because of the mass asymmetries in the entrance channel (η_o = 0.827 and 0.831, resp.) the reactions considered are believed to undergo fusion-fission /2-3/. The excitation energies of the hypothetical compound nuclei are in the region of E^*_{CN} = 105 MeV for both systems /3/. The fig. 1 shows the mass distributions of the measured fragments, fig. 2 the TKE vs. mass distributions. The parabolic dashed lines in fig. 2 indicate the expected TKE release in fission /2,4/. Considering the results of refs. /4,5/ and of the present contribution we found deviations between the obtained mean values of total kinetic energy per mass interval ⟨TKE⟩ and the systematics. These deviations may be characterized by the following features: (i) The ⟨TKE⟩ tend to higher values than predicted for collision systems, which are believed to undergo quasi-fission /2,5/. Collision systems with dominating contributions of fusion-fission show minor deviations. (ii) Reaction products with ⟨TKE⟩ values higher than predicted are observed at energies E_{cm} not far from the Coulomb barrier V_{CB}. These deviations seem to decrease with increasing bombarding energies.
(iii) Within a measured TKE vs. mass distribution the ⟨TKE⟩ excess increases with increasing mass asymmetry of the fragments.

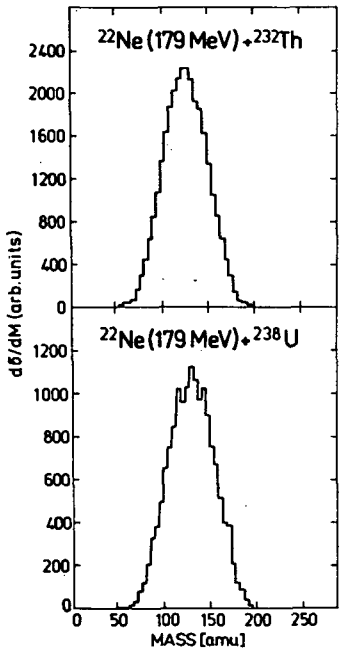

Fig. 1

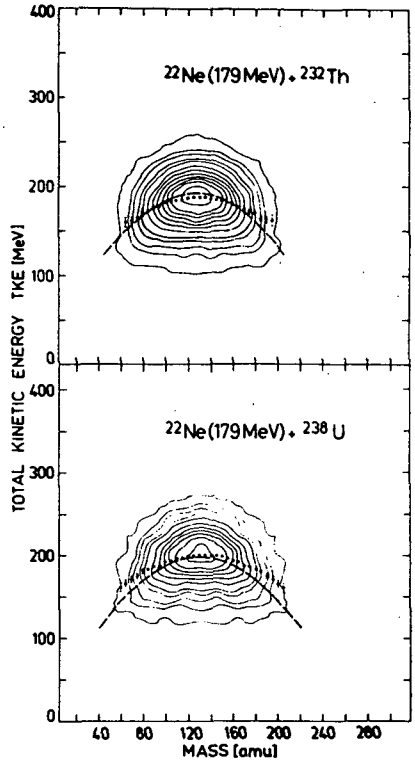

Fig. 2

Deviations of the ⟨TKE⟩ values from the systematics were also observed in the spontaneous fission of ^{258}Fm and of transfermium isotopes /6/. They have been interpreted by a more compact scission configuration of magic fission products resulting in a higher Coulomb-repulsion energy. This argument may be valid for fusion-fission reactions as ^{22}Ne + Th, U, Cf, where a compound nucleus is formed. It is difficult to use it for explaining the behaviour of the ⟨TKE⟩ values in quasi-fission systems as $^{40}Ar(\approx 220$ MeV) + Th, U, where a compactly fused configuration is not attained. The reason for the observed ⟨TKE⟩ deviations remains, therefore, an open question.

References

/1/ Schilling, K.D. et al., ZfK-586 (1986)
/2/ Gippner, P. et al., Z. Phys. A325 (1986) 33
/3/ Gippner, P. et al., ZfK-610 (1987) 42, in print
/4/ Gippner, P. et al., this report, p. 1
/5/ Lukyanov, S.M. et al., Proc. Int. School-Seminar on Heavy-Ion Physics, Dubna, 1986
/6/ Hulet, E.K. et al., Phys. Rev. Lett. 56 (1986) 313

DESCRIPTION OF THE MASS DISTRIBUTION IN HEAVY-ION COLLISIONS

G.D. Adeev
Omsk State University, Omsk, USSR

V.V. Pashkevich
Joint Institute for Nuclear Research, Dubna, USSR

G. Saupe
Zentralinstitut für Kernforschung, Rossendorf, Bereich KF

The aim of the present calculations consists in the interpretation of fragment mass distributions observed in the reactions $^{22}Ne + ^{249}Cf$ and $^{40}Ar + ^{232}Th$ which have been investigated at the heavy-ion cyclotron U 300 of the Laboratory of Nuclear Reactions in Dubna /1/. The symmetric fragmentations obtained in these reactions at the highest incident energies support the idea that compound nuclei have been formed before fission. In these cases the bombarding energy of the projectile is large enough to overcome the conditional and unconditional saddles in the potential landscape of the entrance channel so that fusion can occur. For the corresponding high excitation energies of the compound nuclei /1/ shell effects can be assumed to have been washed out. This leads to an important simplification of the theoretical treatment because only the liquid-drop term of the total potential has to be taken into account when calculating the potential energy surface of the nuclear systems. In the diffusion model presented here a Fokker-Planck equation for the distribution function of the collective variables characterizing the composite system is used as a dynamical equation for the description of the fission path from the saddle to the scission point /2/. The actual relevant variables are the distance R between the centres of mass of the two parts of the fissioning nucleus, the mass asymmetry x, and the neck radius. They are unambiguously connected with the dimensionless variables $\{C, \alpha, h\}$ which have been proposed in ref. /3/ for the parametrization of the nuclear surface. In the numerical calculations two sets of the liquid-drop potential parameters have been used, but the resulting variances of the mass distributions show only a weak dependence on them. The diagonal elements of the friction tensor in the solved diffusion equation have been chosen proportional to the two-body nuclear viscosity parameter which is the only free parameter in this model. In the diffusion tensor also only the diagonal elements have been considered to be non-zero, where the components have been derived from the friction tensor via the Einstein relation. In addition, the influence of the angular momentum of the compound nucleus on the dispersion of the fragment mass distribution has been studied /4/. The inclusion of the angular momentum leads to an additional term in the total potential energy which is given by the rotational energy, where the moments of inertia parallel and perpendicular to the axis of symmetry are functions of $\{C, \alpha, h\}$. Consequently, the stiffness coefficients entering into the Fokker-Planck equation become angular-momentum dependent too, but they change only by a few percent. The main effect consists in a significant shift of the saddle point to that potential region which is characterized by smaller C-values and larger values of the neck radius. This corresponds to a shift in the direction of smaller stiffness coefficients what influences the dynamics of the fission process in such a way that the computed widths of the mass distributions increase importantly. The results for the two nuclear systems shown in fig. 1 are in reasonable agreement with the experimental data /5/.

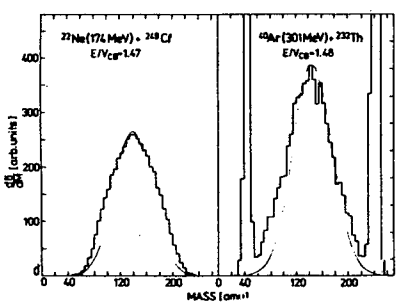

Fig. 1: Calculated (thin lines) and experimentally observed (thick lines) fragment mass distributions for the reactions $^{22}Ne + ^{249}Cf$ and $^{40}Ar + ^{232}Th$.

References:

[1] Gippner, P. et al. Z. Phys. A325 (1986) 335
[2] Adeev, G.D., Gonchar, I.I. Z. Phys. A320 (1985) 451
[3] Ledergerber, T., Pauli, H.-C. Nucl. Phys. A207 (1973) 1
[4] Adeev, G.D. et al. JINR-Report P4-86-247, Dubna, 1986
[5] Saupe, G., Adeev, G.D., Pashkevich, V.V. to be published

MEASUREMENT OF THE ANGULAR DISTRIBUTION OF γ-RAYS IN THE BINARY FISSION OF ^{252}Cf

W.Neubert, W.Pilz
Zentralinstitut für Kernforschung, Rossendorf, Bereich KF
H. Märten
Technische Universität Dresden, Sektion Physik, WB Kernphysik

The average angular momentum of the fission fragments can be derived from the angular distributions of the accompanied γ-rays /1/. The fragments were detected position-dependently in coincidence with the γ-rays registred by a fixed detector (fig.1). The heavy and the light fragment groups were separated by using the time-of-flight method (time resolution $\Delta t \approx 300$ps, L=60mm). Thus, it was possible to cover the angular range from 0 deg to 180 deg for the γ-rays with respect to the emission direction of the light fragments.
The fission fragments were detected by a $20 \times 40 mm^2$ transmission parallel-plate avalanche counter (mounted at a distance of 5mm from the ^{252}Cf source) and a $35 \times 180 mm^2$ position-sensitive avalanche counter. Both of the detectors were operated in a n-heptane athmosphere of 10 torr. The γ-ray detector was a 2x2inches NaJ(TL) crystal coupled to a FEU-110 photomultiplier, resulting in an average energy and time resolutions of 15% and 10ns, respectively. The γ-quanta were distinguished from the promptly emitted neutrons by a flight-path of L=50cm in a second TOF branch. The activity of the ^{252}Cf source amounted to be about 10^4 fission fragments per second resulting in a coincidence counting rate of 6 events per second. The γ-ray spectra were divided into 17 bins from 100keV up to 3MeV in order to obtain energy-dependent angular distributions. The statistical error was less than 4%. The spectra were corrected for scattering radiation which affected the measured distributions up to 30%. For this purpose, a shadow cone was inserted between the source and the γ-ray detector. The responce functions of the NaJ(TL) crystal were measured with calibrated radioactive sources of γ-rays placed at the position of the ^{252}Cf source. The solid angle and efficiency of the position sensitive detector was calibrated by using the 2D plots of the fission fragment TOF and fragment coordinate measured without any γ-ray coincidence condition. The angular distributions were derived with respect to this calibration. Fig.2 shows the results for two bins of the γ-ray energy. These results are in agreement with a recent publication /2/.

References

/1/ Ericson, T., Strutinskii, V., Nucl. Phys. 8 (1958) 284
/2/ Skarsvag, K., Phys. Rev. C22 (1980) 638

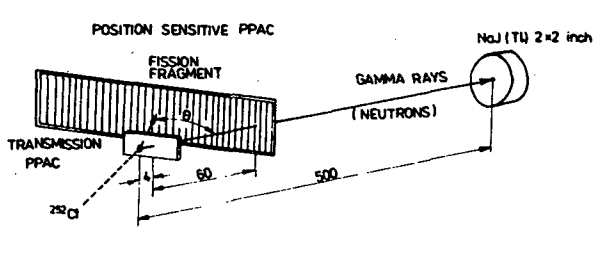

Fig.1

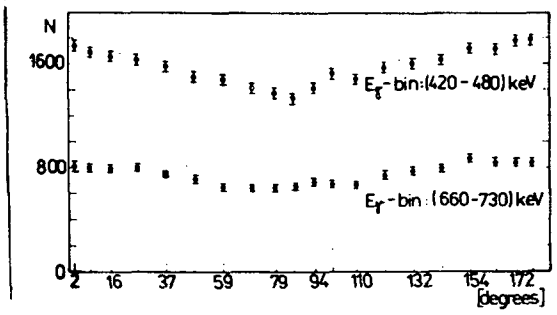

Fig.2

ENERGY AND ANGULAR DISTRIBUTION OF ^{252}CF(SF) NEUTRONS AT LOW ENERGY

H. Märten, D. Richter and D. Seeliger
Technische Universität Dresden, Sektion Physik, WB Kernphysik

W. Neubert
Zentralinstitut für Kernforschung Rossendorf

A. Lajtai
Central Research Institute for Physics, Budapest, Hungary

A new method, i.e. the direction-sensitive spectroscopy of fission fragments based on a special set-up of parallel-plate avalanche counters in connection with neutron time-of-flight spectroscopy, has been applied to measure the energy (E) and the angle (θ) dependent emission probability N(E,θ) of prompt neutrons from spontaneous fission of ^{252}Cf at low energy. The experimental scheme, the multi-parameter data handling, and the analysis procedures were described in ref. 1. Two ^{6}Li-glass scintillators NE 912 have been used at 35 cm flight paths.
In this case, the main background components to be considered are the random background, the background due to scattered neutrons (to be deduced from a shadow cone measurement), and the delayed-γ-ray spectrum (to be measured by means of ^{7}Li-glass detectors NE 913). The method used provided the N(E,θ) distribution for the 0.1 - 2 MeV range and the whole angular range (0-180 deg) with a rather high angle point density (up to 120). The results represented in the figures indicate:

(i) approximately isotropic angular distributions at very low energy ($\lesssim$120 keV),
(ii) a pronounced dip in polar direction (0 deg) at E close to 0.95 MeV (kinematic effect), and
(iii) a raising anisotropy with increasing E.

The measured data can be well reproduced by the use of statistical-model approaches [2,3] assuming that all prompt fission neutrons are evaporated from fully accelerated fragments. As an example, the angular distribution at 1 MeV is shown in comparison with the result of a calculation performed in the framework of an extended version of the generalized Madland-Nix model (GMNM)[3] . T_0 is the lower limit of temperature integration which was introduced to account for the neutron-γ-competition of fragment de-excitation. The N(E,θ) calculation is very sensitive to the choice of T_0 at low energy, whereas the energy spectrum N(E) is little changed. The investigations didn't result in any significant indications of secondary emission mechanisms.

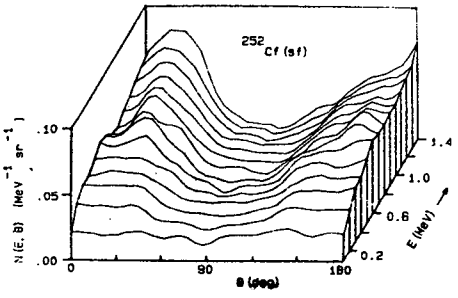

Fig. 1 Experimental N(E,θ) data

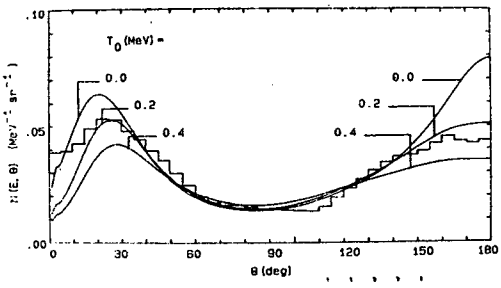

Fig. 2 The angular distribution at 1 MeV (histogram, concentrated data) in comparison with a GMNM calculation for different T_0 parameters.

References

/1/ Fromm, W.D. et al.; Proc. Int. Symp. on Nucl. Phys., Gaußig, 1985 ZfK-592 (1986) 39, H. Märten et al., to be published
/2/ Märten, H., Seeliger, D.; J. Phys. G 10 (1984) 349
/3/ Märten, H., Seeliger, D.; Nucl. Sci. Eng. 93 (1986) 370

ENERGY BALANCE IN FISSION

H. Märten, D. Polster and A. Ruben
Technische Universität Dresden, Sektion Physik, WB Kernphysik

Fission energetics depending on mass asymmetry are studied in the framework of a simple two-spheroid model (TSM) including empirical shell corrections /1/. The potential energy V at scission is considered as the sum of the Coulomb interaction energy V_c and the excess deformation energies E_d of the complementary fragments /2/. Assuming that E_d is quadratic in radius change and V_c is the Coulomb potential of two charges effectively located at the centres of the fragments, V is minimized to describe average fragment energies. The deformability parameters are strongly influenced by shell effects. Their deviation from the liquid-drop model values are related to the shell correction energy δW as in ref. 2.

On the basis of well-known fragment data for $^{252}Cf(sf)$ and $^{235}U(n_{th},f)$, empirical shell correction energies have been deduced in the framework of TSM (fig.1). They are in quite good agreement with calculated shell corrections depending on deformation /3/. Note the influence of closed-shell regions as indicated in fig. 1.

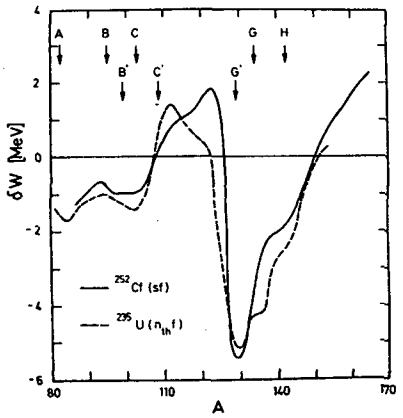

Fig. 1
Shell correction energies deduced from experimental fission data as a function of fragment mass number A. The arrows indicate the position of particular closed-shell regions as calculated in ref. 3. A and G correspond to closed neutron shells at N = 50 and N = 82, respectively. G' indicates the closed-shell region for the proton number 50.

Considering the diminution of shell effects /4/ with increasing temperature and taking into account the excitation energy of the fissioning compound nucleus, the TSM is applicable to any induced fission reaction. The actual δW set is deduced from the accepted empirical data by interpolation.
The calculations reproduce experimental data on the partition of energy in fission as function of incident energy satisfactorily /1/. Presently, the TSM can be applied for the Th-Cf region.

References

/1/ Märten, H. et al.; Proc. Int. Conf. Nucl. Phys., Gaußig (GDR), Nov. 1986

/2/ Kildir, M. and Aras, N.K.; Phys. Rev. C 25 (1982) 365

/3/ Wilkins, B.D. et al.; Phys. Rev. C 14 (1976) 1832

/4/ Bohr, A. and Mottelson, B.R.; Nuclear Structure (Benjamin, New York, 1975), Vol. II, 607

^{252}CF(SF) NEUTRON EMISSION AT MEDIUM AND HIGH ENERGY

H. Märten, D. Richter and D. Seeliger
Technische Universität Dresden, Sektion Physik, WB Kernphysik

W. Neubert
Zentralinstitut für Kernforschung Rossendorf

Based on a new experimental method for the determination of fragment-neutron correlations /1/ the double-differential emission probability N(E,θ), i.e. depending on energy E and angle θ, of ^{252}Cf(sf) neutrons has been measured in order to study the emission mechanism in detail as well as to specify the nuclear standard "Cf neutron spectrum" more precisely. The investigations include complex calculations in the framework of statistical-model approaches. /2,3/

Neutron time-of-flight spectroscopy with two NE 213 scintillators at ~1.6 m flight paths in connection with a direction-sensitive method of fragment spectroscopy (π/4-geometry /1/) has been applied. Experimental data, which cover the whole angular region, are shown in fig. 1 (data normalized to 1.). As in an earlier investigation of emission anisotropy /4/, the equatorial spectrum measured in this work doesn't indicate a pronounced hard emission component, which was concluded /5/ from previous experimental data./6/

The measured distributions can be well reproduced by calculations performed in the framework of the complex cascade evaporation model (CEM) /2/ as well as the generalized Madland-Nix model (GMNM) /3/ as shown in fig. 2 (example). Rather small deviations appearing in the equatorial region at high energy (≳ 6 MeV) specifically are within experimental and theoretical uncertainties. Thus, no significant indications of secondary emission mechanisms have been found. The measured polar spectra extending to 18 and 15 MeV at 0 and 180 deg, respectively, agree with the statistical-model calculations, too.

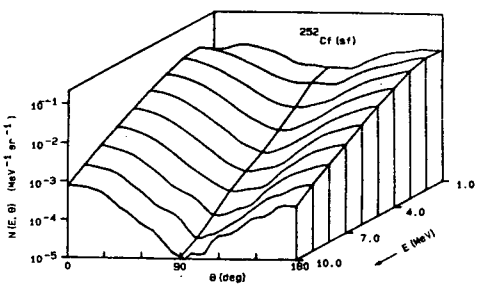

Fig. 1 Experimental N(E,θ) data

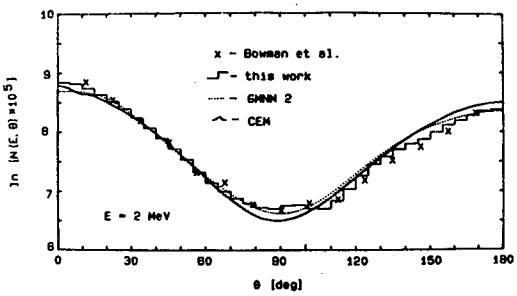

Fig. 2 The measured angular distribution of Cf neutrons at 2 MeV (histogram, concentrated data) in comparison with previous data of ref./6/ as well as theoretical results (CEM, GMNM).

References

/1/ Fromm, W.D. et al.; Proc. Int. Symp. on Nucl. Phys., Gaußig, 1985, ZfK-592 (1986) 39
Märten, H. et al.; to be published

/2/ Märten, H., Seeliger, D.; J. Phys. G 10 (1984) 349

/3/ Märten, H., Seeliger, D.; Nucl. Sci. Eng. 93 (1986) 370

/4/ Seeliger, D. et al.; Yad. Fiz. (1987)

/5/ Märten, H. et al.; INDC (NDS)-146 L (1983)

/6/ Bowman, H.R. et al.; Phys. Rev. 126 (1962) 2120

EXTENDED STATISTICAL-MODEL APPROACH TO FISSION NEUTRON EMISSION

P. Krimmling and H. Märten
Technische Universität Dresden, Sektion Physik, WB Kernphysik

As emphasized in recent review papers /1,2/, accurate predictions of fission neutron emission probabilities have to be based on complex statistical-model approaches to account for the diversity of fragment configurations as well as several emission characteristics like cascade emission, neutron-γ-competition of fragment de-excitation, and influence of fragment angular momentum. The complex cascade evaporation model (CEM) /3/ has been extended to meet these requirements. The new computer code ANNE (EC 1055) takes into account:

(i) the full dependence of fission neutron emission on mass number A and total kinetic energy TKE of the fragments (cf. ref.3),
(ii) excitation energy distribution depending on A and TKE /3/,
(iii) cascade emission /3/,
(iv) neutron-γ-competition (statistical model, empirical γ widths),
(v) neutron width diminution due to angular momentum effects,
(vi) optical-model calculation of transmission coefficients (inverse cross section) depending on A,
(vii) semi-empirical level-density description including shell and pairing effects,
(viii) angular distribution in the center-of-mass system CMS (semi-classical approach).

The code is suitable to calculate multiple-differential emission probabilities depending on emission energy, emission angle, A and TKE. To guarantee a sufficient numerical accuracy as required for detailed studies of the mechanism of fission neutron emission /1/ (in particular for ^{252}Cf(sf)), the total emission probability is obtained as a superposition of about 30.000 single energy distributions. Due to the recent improvements of the CEM, experimental neutron data on the well-investigated ^{252}Cf fission can be reproduced satisfactorily.
Specifically the effects (iii)-(vi) have to be considered to describe the CMS spectra at low energy accurately. Deduced shape parameter agree with data obtained from experiment /4/.

References

/1/ Märten, H. et al., Proc. Int. Symp. on Nucl. Phys., Gaußig, 1985, ZfK-592 (1986) 1
/2/ Märten, H.; Proc. IAEA Advisory Group Meeting on Neutron Source Properties, Leningrad, 1986, to be published
/3/ Märten, H., Seeliger, D.; J. Phys. G 10 (1984) 349
/4/ Seregina, E.A. et al.; Yad. Fiz. 43 (1986) 1092

PRECISE ESTIMATION OF THE ANGULAR DEPENDING NEUTRON SOURCE STRENGTH FOR A 14 MEV NEUTRON GENERATOR

Bach Ly Bah, B. Hildebrandt, K. Seidel and S. Unholzer
Technische Universität Dresden, Sektion Physik, WB Kernphysik

A precise and absolute determination of the neutron flux is made by counting the associated α-particles of the $T(d,n)^4He$ reaction by a Si-SB detector. This method is completed by use of relative monitor counters consisting of a BF_3-long counter and an organic scintillation detector to check permanently the correct function of the α-monitor system. To estimate the energy and angular dependence of the neutron flux the differential neutron source strength - $\frac{dN_n(\theta)}{d\Omega}$ and the neutron energy distribution - $\frac{d^2N_n(E_n,\theta)}{dE_n d\Omega}$ were calculated for a real ^3H-target composition with the code QELL /1/.
The energy distribution of the neutron emission is given in fig. 1 dependent on the emission angle - θ relative to the deuterium beam axis.

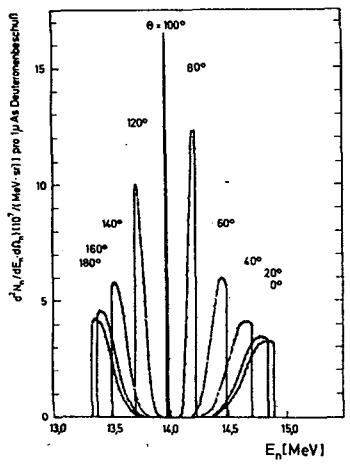

Fig. 1
The angle dependent energy distribution of neutron emission for a 3Ci - 3H-target at Ed=120 keV (Ed-energy of deuteron, Nn - number of neutrons, En - neutron energy θ - angle of emission)

The calculated differential neutron source strength is compared with experimental results in fig. 2.
The dash-dotted line is the weighted mean value of 4 independent activation measurements with Al-samples.
Open circles result from proton recoil measurements with an organic scintillator. The most part of error bars for the absolute scintillation counter measurements results from uncertainties in the neutron detection efficiency and is the same for all points. In contrast to the calculation (full line) the experimental results are influenced by neutron absorption and scattering effects in the target support and the beam tube. Such effects are considerably at θ = 90° and 180° and must be considered.

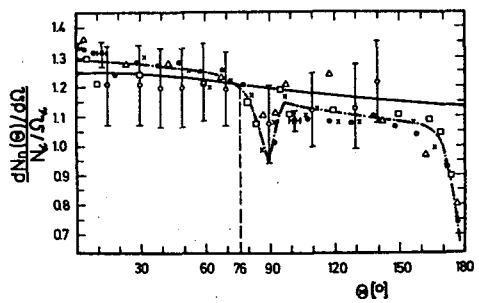

Fig. 2
The differential neutron source strength for a 3Ci - 3H-target. Calculation (full line) and experimental measuring points for a real target construction(□, Δ, o, x /2/ activation of Al-samples (-.-. mean value)
o /3/ organic scintillation measurements)

References

/1/ Seidel, K., S. Unholzer; Internat. TU Dresden 05-09-82 (1982)
/2/ Hildebrandt, B.; Forschungsbeleg, TU Dresden, 1985
/3/ Bach Ly Bah; Abschlußbericht, TU Dresden, 1985

RECOMMENDED DATA OF THE NEUTRON EMISSION FROM PB AT 14 MEV INCIDENCE ENERGY

T. Elfruth, D. Seeliger, K. Seidel and S. Unholzer
Technische Universität Dresden, Sektion Physik, WB Kernphysik

The International Atomic Energy Agency started in 1982 the Coordinated Research Programme on Measurement and Analysis of 14 MeV Neutron Nuclear Data needed for Fission and Fusion Reactor Technology (CRP) to meet the increasing data requests arising mainly from the field of fusion reactor neutronics. One result of the Working Group "Double-Differential Neutron Emission Cross Sections" was a recommended set of neutron emission data from Pb derived from the compilation of experimental data obtained in the CRP or previously published. Pb was used because it is a neutron multiplier candidate for fusion reactor blankets and the material is easily available for groups starting measurements of DDX to compare their results.
The data compiled came from groups of IRK Vienna /1/, Osaka University /2,3/, PINSTEGH Nilore /4/, University of California /5/, and TU Dresden /6,7/. Fig. 1 and Fig. 2 show some of these data.
The recommended distributions are the average of the experimental data points weighted with the inverse of their errors.
It is of interest that the experimental data set obtained deviates from the evaluated data of the ENDF/B-IV library /8/.

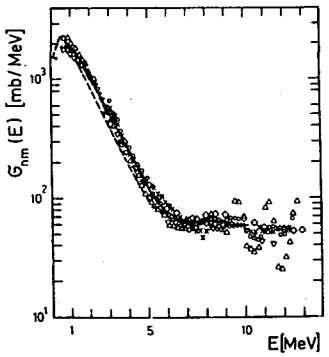

Fig. 1
Angle integrated neutron emission spectrum from Pb measured by several groups (+/1/, ◇▲ /2,3), x /4/, o◇ /6,7), recommended from these data (——) and evaluated in ENDF/B-IV (---).

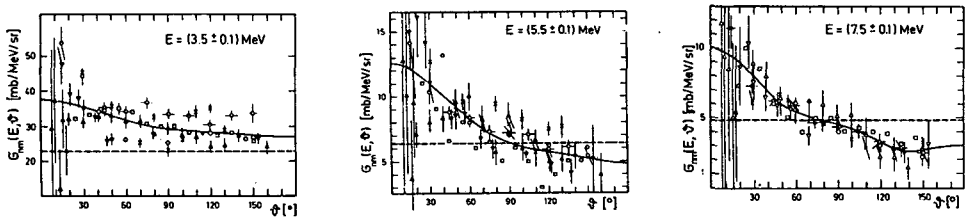

Fig. 2 Angular distributions of neutrons emitted from Pb with the energies inserted. The experimental data are from Refs. /4/ - x, /2,3/ -▲▼/5/ -□ , and /6,7 - o◇ . The recommended average is plotted as full line, the evaluation from ENDF/B-IV as dashed line.

References

/1/ Vonach, H. et al.; Proc. Symp. on Neutron Cross-Sections, Brookhaven (USA) 1980, INDC (USA) - 84/L (1980)
/2/ Takahashi, A. et al; Proc. Int. Conf. on Fast Neutron Physics, Dubrovnik (Yugoslavia) 1986, p. 219
/3/ Takahashi, A. et al.; OKTAVIAN Report A-83-01 (1983)
/4/ Gul, K. et al.; INDC(PAK)-006/GI, Vienna 1986
/5/ Kammerdiener, J.L.; Thesis University of California, Livermoore, UCRL-51232 (1978)
/6/ Elfruth, T. et al.; INDC(GDR)-43/GI, submitted to IAEA for publication
/7/ Hermsdorf, D. et al.; ZfK-277(U), Rossendorf 1975
/8/ Elfruth, T., Seeliger, D. Seidel, K. and Unholzer S.; this report p. 11

THE NEUTRON MULTIPLICATION OF LEAD AT 14 MEV NEUTRON INCIDENCE ENERGY

T. Elfruth, D. Seeliger, K. Seidel, G. Streubel and S. Unholzer
Technische Universität Dresden, Sektion Physik, WB Kernphysik und WB Strahlenschutzphysik

D. Albert, W. Hansen, K. Noack, C. Reiche and W. Vogel
Zentralinstitut für Kernforschung Rossendorf, Bereich Reaktorphysik

D.V. Markovskij and G.E. Shatalov
Institut Atomnoi Energii "I.V. Kurchatova"

In blanket conceptions for D-T-fusion reactors neutron multipliers are used for improving neutronic properties first of all the tritium-breeding coefficients. Multiplier materials must have large (n,xn)-cross sections, small neutron absorption cross sections and appropriate technological properties. Lead is one of the candidates. It is located directly behind the wall of the plasma torus. Therefore secondary neutron spectra from Pb bombarded with 14 MeV neutrons are of immediate interest. Structure and reaction parameters of the closed-shell nucleus Pb remarkably deviate from the mean systematic behaviour of the nuclei. Therefore, files of evaluated neutron data of lead should be more carefully checked against measurements of neutron current, neutron flux and reaction rates at Pb-arrangements than for most of other nuclei.
In the present benchmark neutron leakage spectra were measured with time-of-flight (TOF) and with proton recoil spectrometry (PRS) and activation and fission rates were determined for a lead sphere of 22.5 cm shell thickness fed in its centre with 14 MeV neutrons. The results were compared with neutron transport calculations using the ANISN-, BLANK- and MORSE-code, respectively, based on the ENDF/B and ENDL data files.
Using several independent experimental methods, the uncertainties of consistent results were expected to be smaller than the uncertainties of data obtained with only one of these techniques, for which a critical analysis of possible errors showed that uncertainties of $\lesssim 10$ % as requested are hardly attainable. Also calculated quantities scatter in this range even if the same data set is used.
Neutron spectra measured with TOF and PRS and activation rates indicate a neutron excess of ≈ 10 % total in comparison with calculations based on ENDF/B-IV and ENDL-82 data, which is mostly concentrated in the energy range $E_n \approx 1$-2 MeV. Its description with an increased (n,2n) cross section should be probably combined with a variation of spectral shape parameters (level density, nuclear temperature, ...). At present the shape of the leakage spectrum seems to be some what better reproduced with ENDF/B-IV data.
A detailed representation of the present lead sphere benchmark is given in /1/. The results obtained are discussed in connection with previous lead benchmarks.

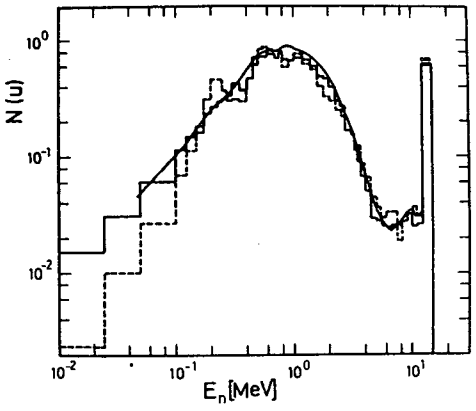

Fig. 1
Neutron leakage spectra per leakage and source neutron
~ ooo experimental results
ENDF/B-IV-calculation
ENDL-82 -calculation

References

/1/ Elfruth, T. et al.; Atomkernenergie-Kerntechnik 48 (1987)

CORRECTION OF THE INFLUENCE OF FINITE SAMPLE SIZE ON MEASURED NEUTRON EMISSION CROSS SECTIONS

T. Elfruth, E. Rodriguez, K. Seidel and S. Unholzer
Technische Universität Dresden, Sektion Physik, WB Kernphysik

K. Noack
Zentralinstitut für Kernforschung Rossendorf, Bereich Reaktorphysik

The neutron time-of-flight spectrometer at TUD was constructed with the view to measure accurate angular distributions of the neutron emission at 14 MeV incidence energy. The experimental arrangement /1/ allows measurements at emission angles from 15° up to 165° under nearly equal experimental conditions. The ring samples used have an outer radius of 6 cm an inner radius of 4 cm and a thickness of about 1/4 mean-free-path of the neutron. Therefore, attention is necessary to correct the influence of finite sample size.
The corrected double-differential cross sections are calculated from the experimentally obtained data, σ_{nM}^{exp}, by

$$\sigma_{nM}(E_o;E,\vartheta) = \sigma_{nM}^{exp}(E_o;E,\vartheta)\cdot f_1(\Phi_o,\vartheta)\cdot f_2(E,\vartheta)\cdot f_3(E,\vartheta). \qquad (1)$$

The factor f_1 is the correction of the anisotropy of the neutron source strength /2/ normalized to the associated α-particles detected at Φ_o and averaged over those neutrons striking the ring sample at a scattering angle ϑ. The factor f_2 is the correction for multiple scattering expressed as ratio of detected neutrons having only one interaction in the scatterer to the total number of neutrons detected. It is calculated by simulating the experimental conditions with the 3-dimensional Monte-Carlo-Code MORSE /3/. The factor f_3 includes both flux attenuation inside the sample and geometry correction of the incoming and outgoing neutrons. It is calculated by integration over the sample volume without any geometrical approximations influencing the result. Fig. 1 shows as an example the correction factors f_2 and f_3 for a lead ring sample of 1.0 cm thickness.

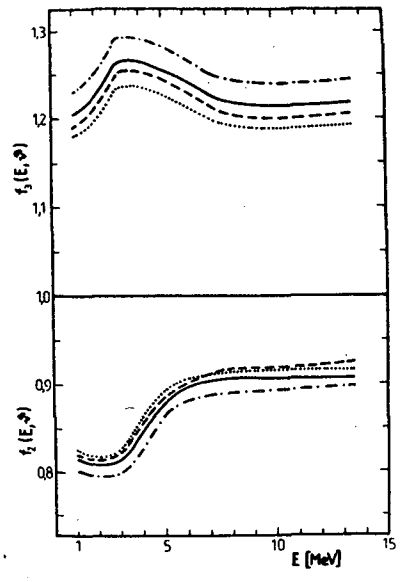

Fig. 1
Correction factors of multiple scattering, flux attenuation and geometry for a lead ring sample of 1.0 cm thickness
(⌒ - ϑ = 30°;
⌒ - 90°;
⌒ - 150°;
~ - angle-averaged value)

References

/1/ Elfruth, T. et al.; INDC(GDR)-34/GI, IAEA Vienna 1985, p. 11
/2/ Bach Ly Bah, Hildebrandt, B., Seidel, K. and Unholzer, S.; this report p. 9
/3/ MORSE-SGC, A Users Guide, Oak Ridge, Nat. Lab., 1976

NEUTRON EMISSION SPECTRA FROM THE INTERACTION OF 14 MEV NEUTRONS WITH LEAD

T. Elfruth, D. Hermsdorf, H. Kalka, J. Pöthig, D. Seeliger, K. Seidel and S. Unholzer

Technische Universität Dresden, Sektion Physik, WB Kernphysik

Because of the importance of lead for the conceptional design of fusion reactors it gives requirements to estimate more precise the neutron emission spectra.
Measurements of n-TOF spectra were carried out on the 14 MeV pulsed beam neutron generator /1/ for scattering angles between $\sqrt{} = 15^{\circ}$ and 165° in steps of 15°.
All spectra of the angular distributions for the lead sample, background and a carbon-standard sample were simultaneously measured.
The mean incident neutron energy was nearly independent from the scattering angle with a value between 14.07 and 14.14 MeV.
In fig. 1 the angle integrated emission spectrum is compared with model calculations, consisting in a superposition of 3 reaction parts:

- a DWBA reaction part /2/ describing collective excitations of the nucleus
- a preequilibrium and compound reaction part, calculated on the base of the Generalized Exiton Model with the code AMAPRE /3/
- a (n,2n) - reaction part, calculated with the code STRAPRE /4/

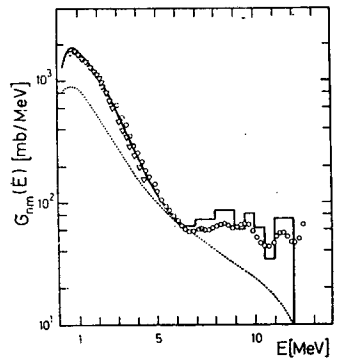

Fig. 1
The angle integrated neutron emission spectrum of Pb (o present data; ▽ 5)) for 14 MeV neutron incident energy compared with the ENDF/B IV evaluation (---) and a theoretical model calculation (...)

In fig. 2 angular distributions for 2 different neutron emission energies E are compared with AMAPRE calculations. With increasing emission energy E the angular distributions are more and more anisotropic and forward peaked caused by the increasing preequilibrium and direct reaction contributions.
For E=5.5 MeV the calculation is in accordance with the experimental data for all scattering angles, at 3.5 MeV appear discrepancies between calculation and experimental data for $\sqrt{} = 15^{\circ}$ and $\sqrt{} = 30^{\circ}$. For E=7.5 MeV the shape of angular distribution is well described but the experimental data are overestimated by the calculation, as it can be seen also for the angle integrated spectrum of fig. 1

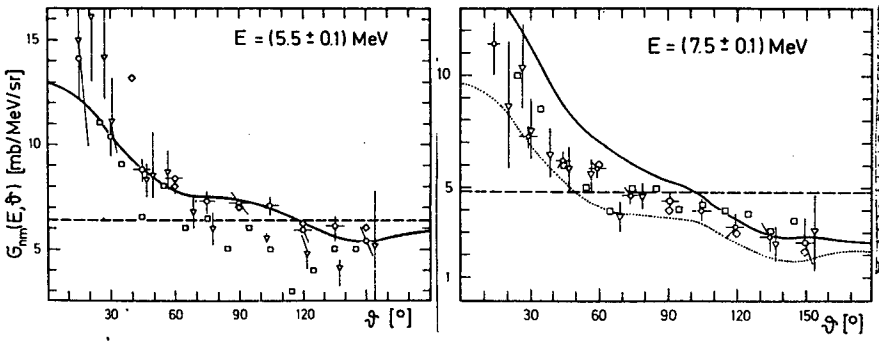

Fig. 2
Angular distributions of neutrons emitted from Pb for 14 MeV neutron incident energy and different emission energies - E. Experimental data (o - present work, ▽ 5), x 6), ◇ 7)) are compared with the ENDF/B IV (---) evaluation and with theoretical model calculations (——)

References

/1/ Helfer, H., et al.; INDC(GDR)-34 IAEA Vienna, 1985, 13
/2/ Ignatyuk, D. and Lunac, V.P.; priv. comm. 1983
/3/ Kalka, H.; Diplom work, TU Dresden, 1983
/4/ Uhl, M., Strohmaier, B.; IRK-76, 1976
/5/ Takahashi, A. et al.; Oktavian-Report A-83-01, 1983
/6/ Kammerdiener, J.L.; Thesis Ph. D. UCRL-51232, 1972
/7/ Hermsdorf, D. et al.; ZfK-277 (Ü), 1975, INDC(GDR)-2/L

SEARCH FOR METASTABLE HIGHLY CHARGED RECOIL IONS

H. Schmidt-Böcking, V. Dangendorf, J. Euler, J. Ullrich, S. Schmidt
Institut für Kernphysik, University of Frankfurt/Main, D-6000 Frankfurt/Main
G. Zschornack
Technical University Dresden, Department of Physics, Division of Applied Nuclear Physics, Mommsenstr. 13, Dresden, 8027, GDR
S. Hagmann
Kansas State University, Manhattan, Kansas 66506, USA

It is well established that fast heavy ion beams are very efficient tools to produce slow highly charged heavy ions. Because of the high outer shell ionization, the fraction of inner shell excited metastable ions should be strongly enhanced compared to light ion bombardment. This might be of particular interest for the production of "beams" of metastable highly charged ions.

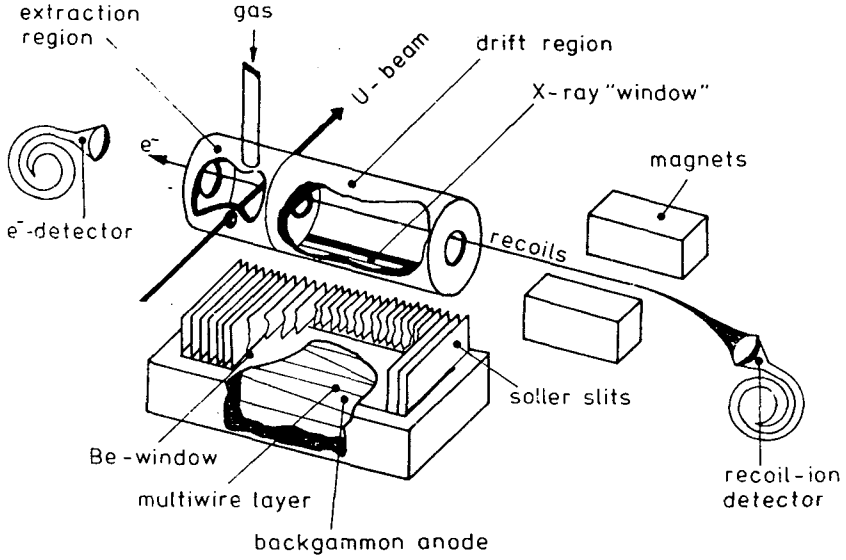

Fig. 1:
Schematic view of the experimental set-up

It is the goal of the present experimental investigation to obtain by x-ray-recoil ion coincidence technique information about the correlation of final recoil charge states and inner-shell x-ray emission in very heavy ion-atom collisions. The apparatus is built in such a way that also delayed x-ray transitions with a lifetime $\tau > 10$ nsec can be detected for x-ray energies above about 500 eV. A schematic view of the whole apparatus is shown in Fig. 1. The collimated 1.44 MeV/u U beam of the UNILAC accelerator of GSI at Darmstadt hits the Ar gas target (differentially pumped cell). The gas pressure was kept below 10^{-4} Torr. The recoil ions are accelerated in the electrostatic extraction field ($V_{ex} \approx 50$ to 2000 Volt) and are then drifting with constant velocity towards the recoil ion detector (channeltron). The emitted x-rays are detected by a position sensitive x-ray detector which is viewing the target cell and the flight path (3.5 cm) of the recoil ions. A Soller Slit is mounted in front of the x-ray detector enabling one to detect the position of x-ray emission with a resolution of better than 0.5 mm in direction of the ion flight path. The position resolution of the detector (backgammon type anode) itself is close to 0.1 mm if the gas pressure in the detector is properly adjusted to the x-ray energy E_x. The time resolution of the x-ray detector is better than 10 nsec for E_x = 2.6 keV. Knowing the position of x-ray emission and measuring the time difference between x-ray and recoil-ion detection, the recoil-ion charge-state can be determined by time-of-flight technique and thus the correlation between x-ray emission and recoil ion charge state can be measured. The "prompt" ($\tau < 10$ nsec) and the delayed x-ray emission can be separated from the position of x-ray detection in the gas detector. Additionally, opposite to the direction of recoil ion extraction the electrons are detected in a second channeltron allowing a high efficient electron-

recoil-x-ray triple coincidence. This triple coincidence is set up to reduce background random events in the x-ray-recoil-ion coincidence. Because the expected real x-ray rate is very low (rate $\ll$ 1/sec) and the detector dark rate due to x-rays from other sources in the experimental area is much higher ($\approx$ 5/sec). This triple coincidence sets a very close time window (< 10 nsec) for possible random coincidences. The measured electron-recoil ion time resolution was better than 10 nsec. Furthermore, to reduce the random coincidence background rate, the recoil ions are deflected in a weak magnetic field thus only the interesting high charge states are detected in the recoil ion detector. First experiments testing the experimental set-up have shown that for 1.44 MeV/u U on Ar, the detected x-ray rate is much lower than the one estimated from the total Ar K-shell excitation cross section. This forced us to increase the efficiency of the detection system and to reduce the background as much as possible. Eliminating the magnetic field components in the target area, the random background in the electron-recoil-ion coincidence could be suppressed below 10^{-4} with respect to the Ar^{1+} intensity.

INFLUENCE OF BREIT AND QED CORRECTIONS TO ATOMIC PROPERTIES IN HIGHLY IONIZED KRYPTON

I. Reiche, G. Zschornack
Technical University Dresden, Department of Physics, Division of Applied Nuclear Physics, Mommsenstr. 13, Dresden, 8027

Using computer programs studying atomic structure or atomic transitions in highly ionized atoms for diagnostics of heavy ion sources or the diagnostics and modelling of plasma devices with relevance to fusion research it is important to know the influence of corrections to the energies, calculated from the multiconfiguration Dirac-Fock formalism. For this purpose we have used a multiconfigurational Dirac-Fock (MCDF) program /1/. This program solved the MCDF equations for an atomic system and dumped the solutions to tape. The adapted program BENA /2/ is able to read this dump and calculates corrections to the MCDF energy levels that result from including the transverse Breit operator /3/ in first order pertubation (E_{Breit}), the second order vacuum polarization /4/ (E_{VP}) and an approximative estimate of the self-energy operator (E_{SE}). Our actual interest was focussed to Krypton ion ground states, because we analyze this species in current experiments on the electron beam ion source "KRYON-2" /5/ of the JINR Dubna. The object of our interest is here the variation of X-ray energies in different Krypton ion ground states.

Table
Contribution of QED and Breit corrections to X-ray energy shifts of $K_{\alpha 1}$- and $L_{\alpha 1}$-transitions in Krypton of ionization stage I. E^{B+QED}-contribution to the X-ray energy due to QED and Breit corrections; ΔE - absolute X-Ray energy shift; ΔE^{B+QED}-X-Ray energy shift contribution of QED and Breit corrections. All shifts are declared relative to the energy of the neutral atom. All shifts are measured in eV.

I	$E^{B+QED}_{K_{\alpha 1}}$	$\Delta E_{K_{\alpha 1}}$	$\Delta E^{B+QED}_{K_{\alpha 1}}$	$E^{B+QED}_{L_{\alpha 1}}$	$\Delta E_{L_{\alpha 1}}$	$\Delta E^{B+QED}_{L_{\alpha 1}}$
2	21,451	0,330	- 0,031	- 1,882	- 1,279	- 0,042
4	21,504	0,926	0,022	- 1,836	0,885	0,004
6	21,471	1,862	- 0,010	- 1,832	2,076	0,007
8	21,451	3,036	- 0,031	- 1,831	3,673	0,008
10	21,442	3,084	- 0,040	- 1,876	19,085	- 0,036
12	21,464	2,307	- 0,017	- 1,894	31,093	- 0,054
16	21,479	1,873	- 0,002	-	-	-
24	21,360	51,965	- 0,121	-	-	-

In Figs. 1-3 contributions from E_{Breit}, E_{VP} and E_{SE} to the electron binding energy to the K-level are shown. In this figures completely ionized subshells are indicated. We notice an shell dependent variation of different contributions. Significant alterations in values of the analyzed contributions appear for ionization of 2p-electrons, whereby changes of QED corrections lies below the eV-level.

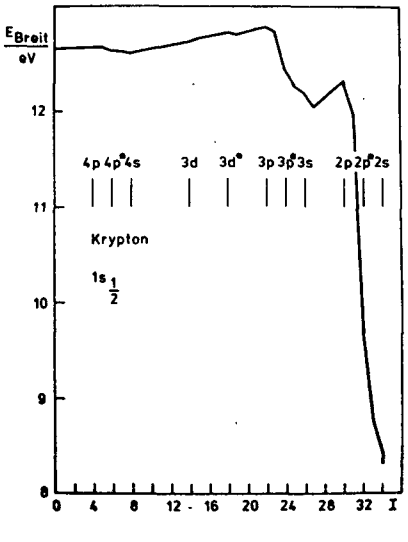

Fig. 1:
Breit contribution to the K-shell electron binding energies for different ionization stages I

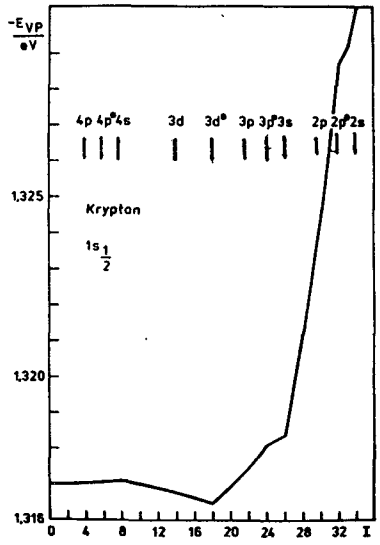

Fig. 2:
Vacuum polarization contribution to the K-shell electron binding energies for different ionization stages I

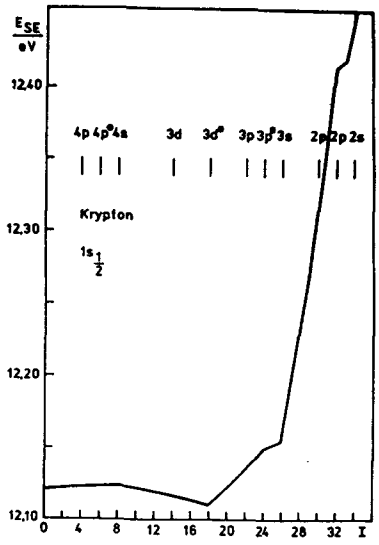

Fig. 3:
Self-energy contributions to the K-shell electron binding energies for different ionization stages I

Consequences of in the graphics for the K-shell demonstrated situation are reflected in the Tabl. for X-ray energy shifts of K_{α_1}- and L_{α_1}-transitions of highly ionized Krypton. We see, that for calculation of X-ray energy shifts the consideration of QED and Breit corrections is in many cases neglegible, because these contributions lie as a rule at about - 1 % of the absolute X-ray shift. Only for calculations of absolute quantities it is inevitable to consider QED and Breit corrections to the MCDF energy levels. This circumstance may be used to economize computer time in a wide class of different studies of atomic inner-shell properties.

Literature:

/1/ Grant I.P. et al., Comp. Phys. Commun., 21, 1980, p. 207
/2/ Mc Kenzie B.J. et al., Comp. Phys. Commun., 21, 1980, p. 233
/3/ Grant I.P. and Mc Kenzie B.J., J. Phys., B 13, 1980, p. 2671
/4/ Grant I.P., Comp. Phys. Commun., 5, 1973, p. 262
/5/ Donets E.D., ECAJA, 13, 1982, p. 941

ABSOLUTE MEASUREMENTS OF THE U-238 FISSION CROSS-SECTION AT 4.8 MEV AND 8.4 MEV NEUTRON ENERGIES USING THE TCAPM

C.-M. Herbach, K. Merla, G. Musiol, H.-G. Ortlepp[+], G. Pausch, U. Todt
Technische Universität Dresden, Sektion Physik, WB Angewandte Kernphysik
[+] since 1984 CINR Rossendorf

I.D. Alchasov, L.W. Drapchinsky, E.A. Ganza, O.I. Kostochkin, V.I. Shpakov, P.S. Soloshenkov, S.M. Solovjev
Khlopin Radium Institute Leningrad

The absolute measurements of the U-238 fission cross-section were continued by a measurement at 8.4 MeV and a short test run with poor statistics at 4.8 MeV neutron energies /1/. The main experimental parameters (neutron production and associated particle (AP) detection) of both measurements correspond to those of the Pu-239 measurements /2/. Considering the parameters of the available ΔE-detectors the AP detection angle in the 8.4 MeV measurement was changed to 41.5 deg.. Due to this, optimum conditions in the AP channel were reached, but the neutron energy was shifted.

Mean neutron energy (MeV)	4.8 ± 0.2		8.4 ± 0.2	
	Corr. (%)	Error contr. (%)	Corr. (%)	Error contr. (%)
Counting of coincidences				
- Statistics of effect	-	2.22	-	0.87
- Random coincidences	0.48	0.17	1.19	0.11
Fission chamber efficiency				
- Pulses below correlated background threshold	1.02	0.07	0.56	0.04
- Extrapolation to zero	0.87	0.27	1.24	0.14
- Fragment absorption	3.07	0.90	2.74	0.81
AP counting				
- Background	3.30	0.60	0.94	0.29
Neutron cone				
- Neutron scattering and effective foil thickness due to the cone aperture	1.07	0.40	1.16	0.40
- Cone neutrons outside the angular extend of the fission foils	-	0.02	-	0.01
Fissile layers				
- Areal density	-	1.15	-	1.15
- Inhomogeneity	-	0.54	-	0.54
Result (10^{-24} cm^2)	0.551		1.022	
Standard deviation (%)	2.82		1.82	

The amount of fissile material in the fission chamber was increased to 177 % compared to /3/ by use of 9 fission-foils. The error contributions of the target parameters were reduced by the application of new fission-foils of better inhomogeneity.
The areal densities of all used fission-foils were determined at the KRI Leningrad by 2π-α-counting (using $T_{1/2}$ = 4.468·10^{9}y ± 0.11 % /4/), and the inhomogeneity by Rutherford-Backscattering-measurements at the CINR Rossendorf /5/. Based on these results, the true chamber design was optimized as explained in /1,2/.
To calculate the fission counting losses by absorption of fission fragments in the target layer a value of $(5.5^{+2.0}_{-1.0})$ mg/cm^2 related to the Uranium content was assumed, based on a value of 7.5 mg/cm^2 for the averaged fragment range in U_3O_8 /6/ and data from the foil manufacturer about microscopic inhomogeneity and admixtures of other elements.
The 4.8 MeV result agrees within the error limits with the ENDF/B-V evaluation (0.540·10^{-24} cm^2), the result at 8.4 MeV lies 2.82 % above this evaluation.

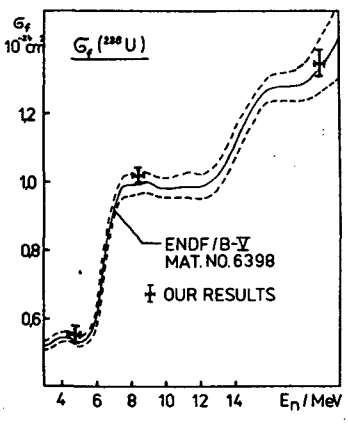

R E F E R E N C E S

/1/ C.-M. Herbach et al., Absolute Measurements of the U-238 Fission Cross-Section at 4.8 MeV, 8.4 MeV and 18.8 MeV Neutron Energies, to be publ. as a TUD-report
/2/ C.-M. Herbach et al., INDC(GDR)-036/G(1985)
/3/ C.-M. Herbach et al., ZfK-584(1986), p. 5
/4/ A. Lorenz (Ed.), INDC(NDS)-149/NE(1985)
/5/ K. Merla, R. Grötzschel, ZfK-584(1986), p. 116
/6/ P.H. White, Nucl. Instr. and Meth. 79(1970)1

ASSOCIATED PARTICLE BACKGROUND NORMALIZATION IN TCAPM FISSION CROSS-SECTION MEASUREMENTS USING THE D(D,^{3}He)-NEUTRON PRODUCTION REACTION

C.-M. Herbach, K. Merla, G. Musiol, H.-G. Ortlepp,+) G. Pausch, U. Todt
Technische Universität Dresden, Sektion Physik, WB Angewandte Kernphysik
+) since 1984 CINR Rossendorf

The associated particles (AP - ^{3}He) in our TCAPM fission cross-section measurements at neutron energies around 8.4 MeV and 4.8 MeV are detected by a telescope of two completely depleted Si-SB-detectors in connection with a fast particle identification circuit /1/. This technique allows:

- to suppress rates of scattered deuterons up to $2.5 \cdot 10^5$ s^{-1}
- to reduce the ^{4}He-background (originating especially in the ^{12}C(d,α)-reaction) essentially by generating a particle significant spectrum (fig. 1) containing all events inside the former selected window around the ^{3}He-peak in the total energy spectrum (fig. 2)/2/.

The portion of the remaining not separated ^{4}He-background is caused by the tail of the ^{4}He-peak and amounts to 0.5...6 %. To determine this background underlying the ^{3}He-peak the particle significant spectrum is collected during the whole measurement. In intervals background spectra are collected using CH_2-foils of comparable thickness and besides particle spectra gated by correlated (incone) neutron signals. The background normalization procedure by spectra fitting is illustrated by fig. 1. This procedure is based only on experimental spectra, not on mathematical descriptions of peak shapes.

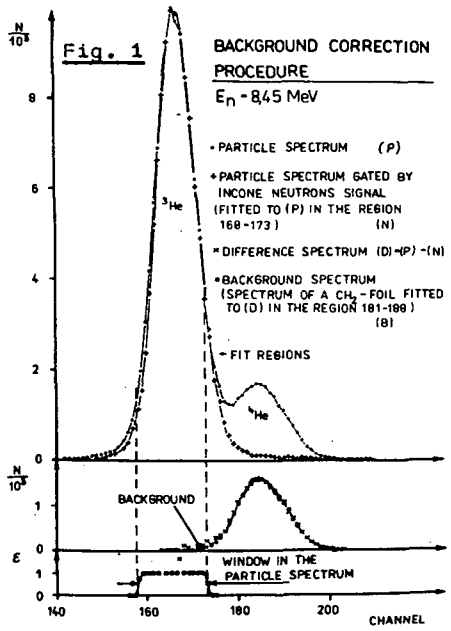

Unfortunately, this method requires a sufficient large ^{4}He peak for the background spectra fitting. Therefore, the energy window in the total energy spectrum of the detector telescope must be choosen wide enough to admit a sufficient part of ^{4}He events in the particle spectrum (Fig. 1, 2). This, of course, enlarges the ^{4}He amount within the AP window, too. In order to reduce the ^{4}He background as much as possible, a new and independent method of background determination was tested in the 4.8 MeV measurement. In the total energy spectrum the events of a separated ^{4}He peak were counted as a monitor rate during both the measurement and the background control runs, using CD_2- and CH_2-foils, respectively. The background particle spectra are normalized to the effect particle spectra by means of the ratio of these monitor rates, and in the normalized background spectra the interesting background amount inside the particle window is determined. The results by using this independent method confirm to these by spectra fitting within the error limits of 0.2 %. But for a general application of this method some experimental modifications are necessary to improve the separation of the used ^{4}He peak, so that small electronic drifts do not influence the result.

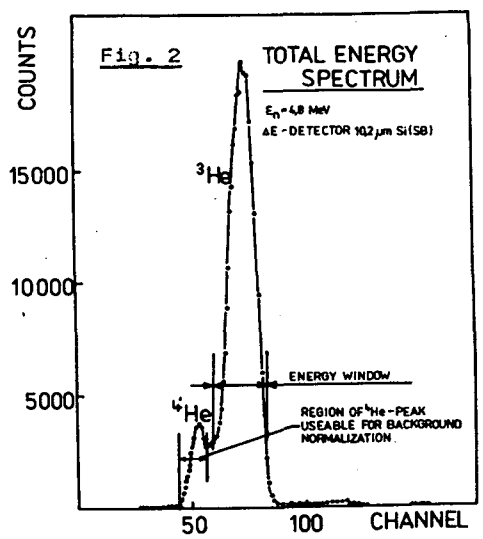

R E F E R E N C E S

/1/ H.-G. Ortlepp et al., Proc. Int. Symp. on Nucl. Phys., Gaussig 1985, ZfK-592(1986), p. 156

/2/ C.-M. Herbach et al., ZfK-584(1986), p. 109

EXPERIMENTAL DETERMINATION OF FISSION FRAGMENT ABSORPTION WITHIN FISSION LAYERS OF Pu-239

C.M. Herbach and G. Musiol
Technische Universität Dresden, Sektion Physik, WB Angewandte Kernphysik

In order to check the absorption correction, experimental investigations as proposed in [1] were carried out at all of the Pu-239 fission layers [2] which were used in our absolute fission cross section measurements [3-5]. A further target (P) with the small thickness of $\gtrsim 40\,\mu g/cm^2$ was inquired additionally to improve the possible accuracy of the measurement. All the fission foils were prepared by thermo-sputtering of PuF_4 with an isotopic purity of 99.97% at the Khlopin Radium Institute Leningrad in the 1977-84 years.

The fissions were induced by neutrons of an Am-Be-source after their thermalization within a block of paraffin. The fission chamber channel was the same as in our cross section measurements [4,6]. For each of the fission events the energy loss of the fragments within the chamber gas was registered. By analysing the amplitude of the current pulse the induction effect was excluded and a sufficient good suppression of α-pile-up-pulses was reached. The normalization to an identical neutron flux was performed by utilizing a "standard" fission foil of U-235 in back-to-back geometry.

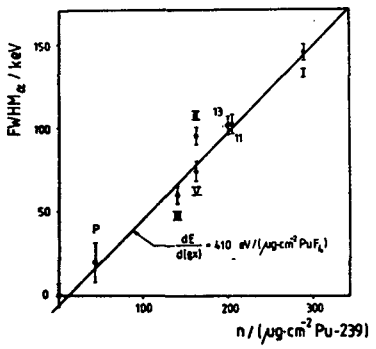

Fig.1: Alpha peak widths caused by stopping power within the fission layers

Based on the registered fission chamber spectra an identical threshold was introduced for the evaluation of the measurements to guarantee uniform conditions of the fission counting independent on small drifts of the electronic. The check up of the stability of the electronic conditions also made it possible to select a fixed plateau range for the determination of the plateau height P_H within the several spectra.

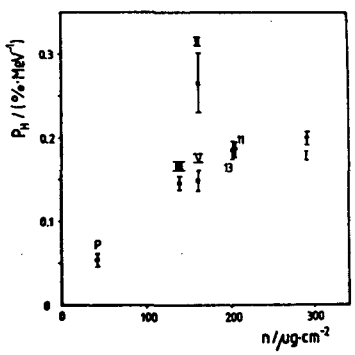

Fig.2: Plateau height of the fission chamber spectrum as a function of foil thickness

By means of α-counting in low geometry a measure of fissionable material within the foils was obtained. The spectra of α- and γ-emission confirmed the identical isotopic composition, the Pu-239 peak widths for perpendicular α-emission indicate an equal chemical structure of the foils. Derived from this measurements, a stopping power of about 20% higher than the Ziegler data [7] of UF_4 was established.

The presented results demand a revision of the absorption correction, which leads to essentially higher cross section data [8]. The analysis of the value $N_{2\pi}/N_{\Delta\Omega}$ as a function of P_H results in effective range parameters of about 2-3 mg/cm^2. Moreover, additional counting losses were found at some of the foils, which can not be explained within the bounds of the model "microscopic inhomogeneous layer". This effect, which is caused possibly by macroscopic surface structures, reduces the accuracy of the used method essentially.

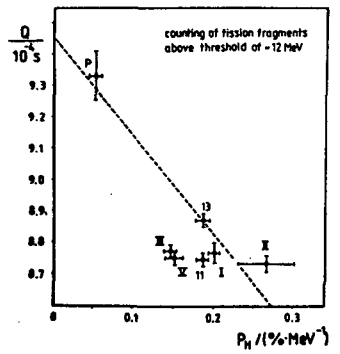

Fig.3: Fission events relative to the layer α-activity as a function of plateau height P_H ($Q=\dot{N}_{2\pi}/(\dot{N}_n \cdot \dot{N}_{\Delta\Omega})$; $\dot{N}_n$=neutr. rate)

References

[1] C.M. Herbach, G. Pausch; this report p. 21
[2] K. Merla et al.; ZfK-584(1986), p.115
[3] W. Wagner; Diss., TU Dresden, 1982
[4] C.M. Herbach et al.; INDC(GDR)-036/G
[5] C.M. Herbach et al.; ZfK-584(1986), p.4
[6] C.M. Herbach et al.; ZfK-559(1985), p.22
[7] J.F. Ziegler; Handbook of Stopping Powers and Ranges in All Elemental Matter, Vol.4, Pergamon Press, New York (1977)
[8] C.M. Herbach et al.; this report p. 20

FINAL RESULTS OF THE ABSOLUTE CROSS SECTION MEASUREMENTS ON Pu-239

C.M. Herbach, K. Merla, G. Musiol, G. Pausch, W. Wagner+)
Technische Universität Dresden, Sektion Physik, WB Angewandte Kernphysik
+) at present Joint Institute of Nuclear Research, Dubna (USSR)

Within the bounds of the joint measuring programme of the Technical University of Dresden and the Klopin Radium Institute Leningrad [1] until 1985 absolute measurements of the fission cross section on Pu-239 have been performed using the time-correlated associated particle method for monoenergetic neutrons at spot points within the 2-20 MeV range.

foil	$\mu g/cm^2$	absorption correction (%)
I	287.9	4.99 ± 1.24
II	163.9	4.58 ± 1.30
III	138.3	5.56 ± 1.21
V	160.6	5.73 ± 1.24
11	199.8	5.40 ± 1.22
13	198.1	4.03 ± 1.24

Tab.1: Exp. determined absorption correction for thermal fissions

Particularly in the result of experimental investigations about the fission detection efficiency [2] a revision of the preliminary published data (see f.i. ref. [3-5]) becomes necessarry. The losses by counting the fission fragments of isotropic fission were determined for the same fission foils, which were used in our cross section measurements. The experiments resulted in values of 2.7%...4.7% higher than calculated using the fragment range of R=7.5 mg/cm^2 as assumed up to now (see tab.1). Additional effects of absorption, which can*not be* explained by "microscopic nonuniformities" [6] led to the large uncertainty of the correction and contribute the dominant error of the cross section data. To consider the fast neutron fission anisotropy the calculations discribed in [7] were performed based on the individual effective range parameters [6] of the foils. Because of the use of the fission foils in forward and backward direction relative to the neutron flux in the cross section measurements, the unknown energy dependence of the additional absorption effect has only a small influence on the resulting error.

The uncertainty of the layers areal density were reduced by low geometry α-counting at the TUD [8] to the value of 0.6%. An estimation of the maximum error of the neutron flux determination due to cone neutrons outside the angle extent of the fission foils were carried out based on [9] and results in an essential contribution only for the 18.8 MeV measurement (0.71%). The neutron energy distributions were corrected in analysis of experimental informations.

The given result of the 14.7 MeV measurement represents a summary of three single runs using the same target (I) [3]. The revised result is in good agreement now with the measurements of Adamov, Li Jingwen and Mahdavi (reviewed in [10]), which confirme within ± 1.8%. Only the data of Cance [11] give 7-8% lower values.

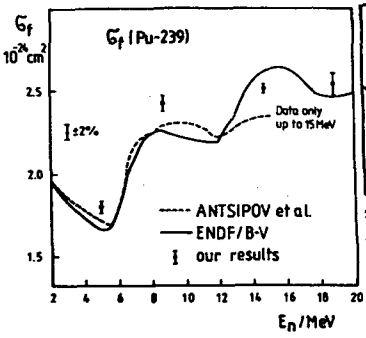

mean neutron energy (MeV)	σ_f (Pu-239) ($10^{-24}cm^2$)	$\frac{\Delta\sigma_f}{\sigma_f}$
4.9 ± 0.08	1.800±0.039	2.18%
8.65± 0.12	2.433±0.050	2.03%
14.7 ± 0.15	2.488±0.038	1.52%
18.8 ± 0.20	2.512±0.068	2.69%

Tab.2: Final absolute cross section data of our TCAPM measurements

Fig.1: Comparision of the presented results with actual fission cross section data files

All the final results are summarized in tab.2, a comparision with current data files is shown in the fig.1. In contrary to the evaluation of Howerton (in [10]) a renormalization of the data files to higher cross sections must be required. It seems to be probable, that the discrepancies of the Pu-239 data are caused by underestimation of the absorption losses due to surface effects by using extremly thin fission foils.

References

[1] R. Arlt et al.; Kernenergie 24(1981), p.48
[2] C.M. Herbach, G. Musiol; this report p. 19
[3] W. Wagner; Diss., TU Dresden, 1982
[4] C.M. Herbach et al.; INDC(GDR)-036/G
[5] C.M. Herbach et al.; ZfK-584(1986), p.4
[6] C.M. Herbach, G. Pausch; this report p. 21
[7] R. Arlt et al.; report TU Dresden, 05-05-79, 1979
[8] K. Merla et al.; ZfK-584(1986), p.115
[9] C.M. Herbach et al.; ZfK-584(1986), p.112
[10] E.D. Arthur; report Los Alamos (USA), LA-UR 85-1674 subm. to the Int. Conf. on Nucl. Data for Basic and Appl. Sci., Santa Fe (USA), 1985
[11] M. Cance, G. Grenier; NSE 68(1978), p.197

A SIMPLE METHOD OF EXPERIMENTAL INVESTIGATION ABOUT FISSION FRAGMENT ABSORPTION WITHIN THIN FISSION LAYERS BY USING THE FRAGMENTS ENERGY SPECTRUM

C.M. Herbach and G. Pausch
Technische Universität Dresden, Sektion Physik, WB Angewandte Kernphysik

Particularly by using the time-correlated associated particle method in the energy range of 2-20 MeV an essential progress was reached for the precision of neutron flux determination in absolute fission cross section measurements [1]. Therefore, it is of great importance now to proof the absolute fission detection efficiency as demanded in [2], to improve the accuracy of the absolute fission cross section data.
The real properties of fission foils are strongly influenced by several parameters of the target production, which can not be checked completely [3,4]. So it must be required, that the experimental investigations about absorption losses are performed by using the same targets as employed in the cross section measurements.

An excellent method to measure the fragment absorption within U-235-targets was developed in [3] by utilizing a gridded ionization chamber and based on an intricate two-parameter analysis. An easier experiment, also useful at targets with higher α-activity (Pu-239), was carried out by P.H. White [4]:
Fission foils with different thicknesses of the active layer n(i) are put into the same thermal neutron field. The number of detected fissions are counted in 2π-geometry ($N_{2\pi}$). The normalization to the number of fissile atoms is performed based on a measurement of alphas or fissions in low geometry ($N_{\Delta\Omega}$). Microscopic nonuniformities within the layer reduce the effective fragment range and are taken into account by the parameter σ/n :

$$N_{2\pi}(i)/N_{\Delta\Omega}(i) = C_o \cdot (1 - n(i) \cdot (1+(\sigma/n)^2)/(2R)) \qquad (1)$$

But by using eq. (1) the fragment absorption can only be determined, if all of the fission foils have the same chemical structure (R=const.) and surface properties (σ/n=const.).

In the result of calculations of the fission fragment energy spectrum after their emission at a plane layer [5,6], the method of White could be modified to enlarge the range of its application. The value of the number of counting losses A below the threshold in relation to the number of fragment pulses P_H within a fixed plateau range of the fission chamber spectrum (fig.) was found to be independent of the parameter n/R. Further calculations simulating selected surface structures [7] indicate the constance of this value also in the case of microscopic nonuniformities. Significant differences are estimated only for surface structures with macroscopic dimensions. If the latter effect is excluded, it becomes possible to determine an individual effective range parameter of each fission foil by using the eq. (2,3) to calculate the absolute absorption without any restriction reflected by chemical structure and microscopic nonuniformities:

$$N_{2\pi}(i)/N_{\Delta\Omega}(i) = C_1 \cdot (1-C_2 \cdot P_H(i)) \qquad (2)$$

$$A(i) = 1-(N_{2\pi}(i)/N_{\Delta\Omega}(i))/C_1 =: 1/2 \cdot n(i)/R_{eff.}(i) \qquad (3)$$

Only relative measurements are necessary, which can be carried out with high accuracy using a comparable simple experimental set-up.

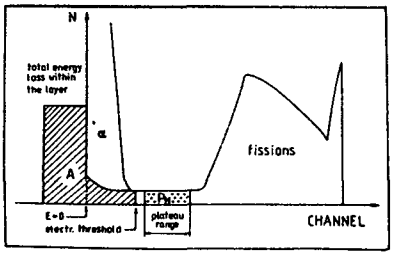

Definition of A and P_H within a simplified fission chamber spectrum

R e f e r e n c e s

[1] C.M. Herbach et al.; INDC(GDR)-036/G
[2] IAEA Consultant's Meeting on the U-235 Fast-Neutron Fission Cross-Section, Smolenice (Czech.), 1983, Conclusions and Recommend., INDC(NDS)-146, p.13
[3] C. Budtz-Jørgensen, H.-H. Knitter; NSE 86(1984), p.10
[4] P.H. White; NIM 79(1970), p.1
[5] B. Sprenger; Dipl. work, TU Dresden, 1984
[6] C.M. Herbach, G. Pausch; ZfK-584(1986), p.114
[7] G. Pausch et al.; this report p. 22

ON THE CORRELATION BETWEEN FISSION FRAGMENT DETECTION EFFICIENCY AND THE PLATEAU HEIGHT IN FISSION CHAMBER SPECTRA FOR THIN FISSILE LAYERS ON SCRATCHED BACKINGS

G. Pausch, C.-M. Herbach, K. Merla, G. Musiol
Technische Universität Dresden, Sektion Physik, WB Angewandte Kernphysik
W. Wagner, Joint Institute for Nuclear Research, Dubna, USSR

Using the Monte-Carlo codes ROBERØ1...Ø3 /1/, first investigations were performed concerning the systematics of fission fragment counting losses due to deviations from the idealized plane target layer. The portion of "forward" fragments from thermal fission which do not leave the fissile layer with an energy above a threshold of 6 MeV, as well as the "plateau" height in the fission chamber spectrum were calculated for three different types of periodic surface profiles (1: covered scratch; 2: filled scratch; 3: scratch with covered bottom /1/) with a period of 30 μm, a scratch width (2b) of 1 μm, and a scratch depth (h) of 1 μm. A mean fragment energy of 84 MeV and mean ranges of 5.8 μm, 9.0 μm and 21.6 mm in the backing material (KOVAR), the fissile layer (U_3O_8), and the fission chamber gas (methane at 110 kPa) were assumed, respectively. The simple stopping power model /1/ allows to compare the results with analytic calculations for a plane target layer of an equivalent effective (i.e. averaged over a period) thickness /2/. Of course, no quantitative description of true counting losses should be expected in this case; the aim was to find out systematic trends, especially in the counting loss / plateau height relation, which help to understand the results of experimental investigations /3/.
Varying the target thickness t, a series of calculations was performed, each of them with a total number of 20 000 fission events. Fig.1-2 show the results; the standard deviations stated were deduced from the scatter of the channel contents in the plateau region of the calculated energy loss spectra. As expected, an additional counting loss occurs, depending on the type of the surface profile (Fig.1). On the other hand, no significant violation of the linear counting loss / plateau height relation was observed in spite of strong deviations from the plane layer model (Fig.2)! Therefore, the "scratch" model does not explain the behaviour observed experimentally /3/.
The "broad valley" calculation (surface type 3: period 20 mm, 2b=10 mm, h=0.1 mm, t=0.24 μm; total spectrum - lower absorption; spectrum of fissions originating inside the "valley" - higher absorption) simulates shifted target edges in a first approximation. Even in this case, the enlarged fragment absorption is followed by a corresponding rise of the plateau height. Further investigations are planned.

REFERENCES: /1/ G. Pausch et al., this report p. 23
/2/ G. Pausch, Dissertation, TU Dresden, 1986
/3/ C.M. Herbach et al., this report p. 19

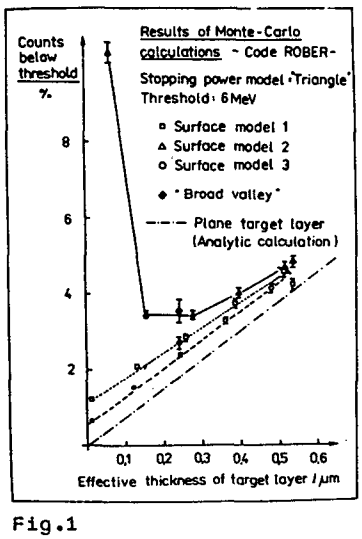

Fig.1

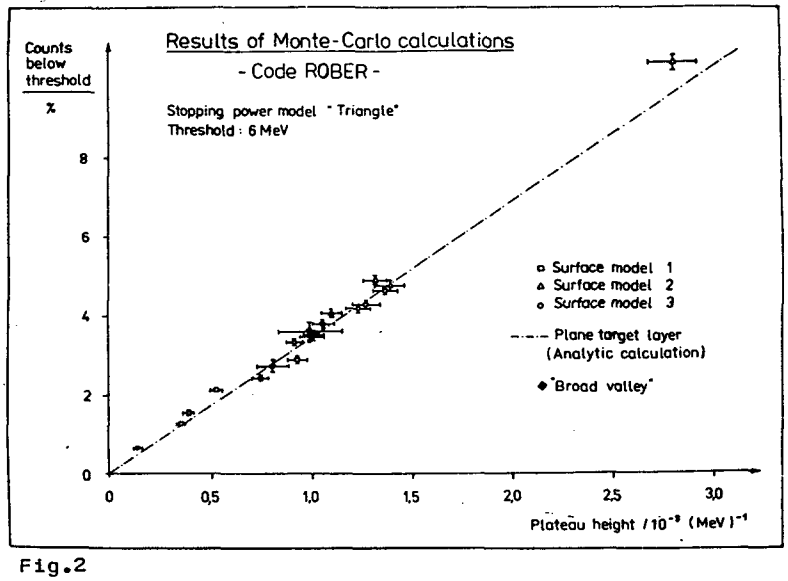

Fig.2

ROBER - A MONTE-CARLO CODE SIMULATING THE INFLUENCE OF SCRATCHED BACKINGS ON THE ABSORPTION PROBABILITY AND THE ENERGY SPECTRUM OF PARTICLES EMITTED FROM A THIN TARGET LAYER

G. Pausch, K. Merla, G. Musiol, R. Perez
Technische Universität Dresden, Sektion Physik, WB Angewandte Kernphysik
L.V. Drapchinsky, Khlopin Radium Institute, Leningrad, USSR
W. Wagner, Joint Institute for Nuclear Research, Dubna, USSR

The experimental examination of Pu-239 targets regarding the fission fragment counting losses /1/ suggested to investigate the influence of a rough backing or target surface on the absorption probability and the energy spectrum of fission fragments or alpha particles originating within a thin target layer. The code ROBER was created to simulate such effects. As a first step, three variants with different kinds of periodic surface profiles (Fig.1) and a simple stopping-power model for fission fragments (Fig.2) were implemented at the CDC-6500 computer of the JINR Dubna. The "scratch" as the dominating type of surface disturbances was suggested by microscopy /2/. The codes ROBERØ1...Ø3 simulate fission chamber spectra, i.e. spectra of energy losses of "mean" fission fragments in a gaseous agent filling the space between the target surface and an electrode. Moreover, separate spectra are built up for fragments which are generated inside the scratch. To reach good statistics for the interesting rare events which cause the "plateau" in the fission chamber spectrum, a non-analogous Monte-Carlo method was applied. Two intuitive parameters allow to favour fission fragment trajectories with small angles relative to the target surface, and with an origin inside the scratch. In a series of test calculations the statistical uncertainty of the plateau height was reduced by a factor of 2...3, choosing optimum parameters.
To verify the correct work of the complete codes, all subroutines and functions were tested separately following a bottom-up strategy; selected sets of input data guaranteed that each order was addressed. As an additional test, the plateau height as well as counting losses were calculated for a plane target layer applying the codes ROBERØ1...Ø3 with a specialized set of geometrical parameters (Fig.3). In this case, it was possible to check the results by analytic calculations /3/.
The chosen structure of the code ROBER allows to modify the geometrical model or to improve the stopping power model by a simple exchange of selected subroutines. In this way, a broad variety of problems can be treated, e.g. simulation of natural alpha and RBS spectra from scratched foils or investigation of targets covered by inactive layers; the only restriction given by the implemented algorithm is that the geometry of the problem must be described by planes.

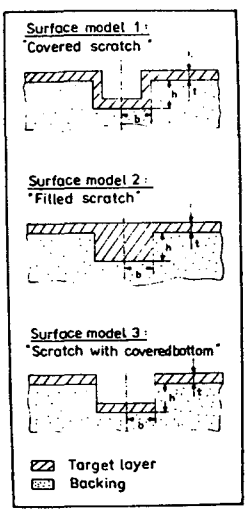

Fig.1: Realized models of scratched backings (cross-sections). Period length (scratch distance) and other parameters must be specified.

REFERENCES

/1/ C.M. Herbach et al., this report p.19
/2/ W. Wagner, Dissertation, TU Dresden, 1982
/3/ G. Pausch, Dissertation, TU Dresden, 1986

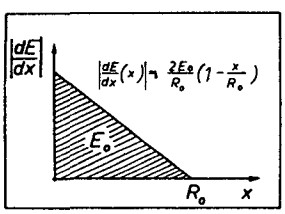

Fig.2: Simple stopping-power model for fission fragments (triangle). The range R_0 of a fission fragment (E^0) in a given material defines the range-energy relation.

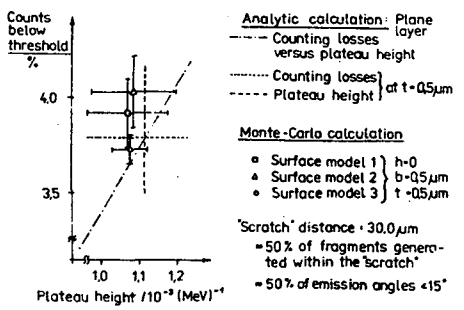

Fig.3: Test calculations for plane backings. Weighted distributions of emission angles and origins; statistics: 20 000 events - CP time ~2 min

INFLUENCE OF ATOMIC, MOLECULAR, AND SOLID STATE EFFECTS ON NEUTRON RESONANCE CROSS SECTION

K. Seidel, D. Seeliger and A. Meister
Technische Universität Dresden, Sektion Physik, WB Kernphysik

S. Mittag
Zentralinstitut für Kernforschung, Rossendorf

W. Pilz
VEB Robotron - Meßelektronik, Dresden

Commonly, nuclear reactions are considered as independent of atomic, molecular, and solid state properties of investigated samples, but the interaction of slow neutrons with atomic nuclei is one of some exceptions. The precise position and shape of neutron resonances depend not only on nuclear properties but also on the nuclear surroundings. The permanent improvement of precision of neutron spectroscopy gave the possibility to investigate a physical field including the properties of nuclei as well as their interaction with the environment in more detail.

A detailed study of low-energy neutron resonances shows clearly an influence of atomic binding on Doppler broadening. The influence of different crystal lattice vibrations and intramoleculare oscillations on Doppler broadening had been observed experimentally /1-3/. In addition, a temperature-dependent shift of neutron resonances was measured /4/. It became evident that the understanding of effects of this type is meaningfull also for applications of neutron resonance data, in particular for nuclear reactor calculations /5,6/.

The observation of hyperfine interactions in neutron resonances gave the possibility to develope a new method for the investigation of nuclei excited in isolated compound-nucleus states at excitation energy close to the neutron binding energy.

In addition to the well-known parameters of these states as energy, spin, parity, and widths, magnetic dipole moments of compound-nucleus states were determined one decade ago /7/. In the last years, we succeeded in determining the mean-square charge radii of different compound-nucleus states /3,8/. In the case of heavy nuclei, these states are often fissionable with quite large fluctuations of fission widths from resonance to resonance.

As a matter of course, it is specifically interesting to search for a correlation between the mean-square charge radii and fission widths of compound-nucleus states /9/.

Such investigations can give new clues for the understanding of the fission process of nuclei caused by resonance neutrons.

A review concerning the influence of atomic, molecular, and solid state effects on neutron cross section at low-energy neutron resonances has been finished recently /10/.

References

/1 / Seidel, K. et al.; JINR-Report P3-11741, Dubna, 1978
/2 / Seidel, K. et al.; Yad. Fiz. 34 (1981) 1173
/3 / Meister, A. et al.; Nucl. Phys. A 362 (1981) 18
/4 / Seidel, K. et al.; Yad. Fiz. 42 (1985) 1041
/5 / Meister, A. et al.; Kernenergie 26 (1983) 313
/6 / Seidel, K. et al.; Proc. Konf. Neutron Physics, Kiev, 1983, Vol. 2, p. 379
/7 / Alfimenkov, V.P. et al.; Nucl. Phys. A 267 (1976) 172
/8 / Mittag, S. et al.; Nucl. Phys. A 435 (1985) 97
/9 / Meister, A. et al.; Proc. 15th Int. Symp. Nuclear Physics, Gaußig, 1985, p. 70
/10/ Seidel, K. et al.; Particles and Nuclei, to be published.

A STATISTICAL MODEL FOR MULTIPARTICLE PRODUCTION IN HADRON-HADRON INTERACTION

H.W. Barz, H. Müller and H. Schulz
Zentralinstitut für Kernforschung Rossendorf, Bereich KF

A statistical model for hadron-hadron interactions is developed by assuming that the reaction proceeds in two steps. First in a violent collision translational energy is transferred into internal excitation energy of two emerging fireballs, which are assumed to decay afterwards indepedently of each other. The decay into the various channels is controlled by the phase space volume of the final hadrons as well as the corresponding flavour content via the underlying quark statistics. By adjusting essentially two parameters, which characterize the size of the fireballs and the energy transfer, a large variety of experimental data for pp and $p\bar{p}$ reactions is succesfully reproduced.

The mean transverse momenta and the mean numbers of various particle types as well as inclusive cross sections for the production of resonances and multiplicity distributions of charged particles are well described up to c.m. energies of about $\sqrt{s} \approx 60$ GeV. As an example we show in fig.1 the mean multiplicity of various particle types as a function of the c.m. energy. Also the invariant cross sections as a function of the Feynman variable x_F and the transverse momentum are in excellent agreement with experimental data below $\sqrt{s} \approx 14$ GeV. Up to this energy the rapidity distributions associated with the fireballs overlap strongly. At higher energies, however, the particle density in the central rapidity region is underestimated. To improve the description of the momentum distributions at higher energies we plan a straightforward extension of the two-fireball picture by including gluon-gluon interactions which give rise to central gluonic fireballs (see refs./2/).

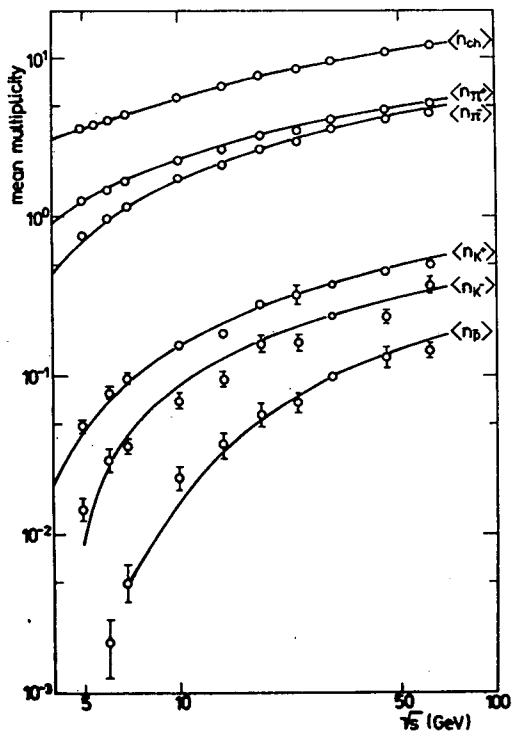

References

/1/ A.M. Rossi et al., Nucl. Phys. B84 (1975) 269

/2/ L. Van Hove and S. Pokorski, Nucl. Phys. B86 (1976) 243
P. Carruther and Minh Doung-Van, Phys. Rev. D28 (1983) 130

Fig.1
Mean numbers of charged particles, π^+, π^-, K^+, K^-, and $\bar{p}$ as a function of $\sqrt{s}$. The curves are fits taken from ref./1/ to experimental data, and the open circles represent the results of our calculations.

COULOMB FINAL-STATE INTERACTION IN IDENTICAL BOSON INTERFEROMETRY

Hans-Ulrich Gersch
Central Institute for Nuclear Research, Rossendorf, GDR

In relativistic nucleus-nucleus collisions second-order interferometry became an important tool for the determination of the size of the region of highly excited nuclear matter. Investigating pion and proton correlations, the radius of the socalled fireball was extracted to be in the range of $R_0 \simeq 2...6$ fm.
The method is based on correlations between identical particles with small relative four-momentum due to quantum statistics. It is assumed that the particles under investigation are emitted during the collision of two heavy ions in a completely stochastic manner (without initial correlations) /1/. Supposing a Gaussian-like distribution ϱ with R_0 (radius) and τ (lifetime) and isotropic emission of the emitted particles, the correlation function takes the form /1/

$$C(q,q_0) = 1 + \exp\left[-\tfrac{1}{2}\left(q^2 R_0^2 + q_0^2 \tau^2\right)\right]. \qquad (1)$$

$\vec{q} = \vec{p}_1 - \vec{p}_2$, $q_0 = /E_1 - E_2/$, p_i and E_i are the momenta and energies of the emitted particles. Usually one neglects the time dependence of (1). Further, a partially coherent generation of the particles is taken into account by a factor $\lambda < 1$ /2,3/. Therefore, the experimental values are often fitted to the function

$$C(q,\lambda) = 1 + \lambda \exp\left(-\tfrac{1}{2} q^2 R_0^2\right). \qquad (2)$$

This pure quantum statistical correlation is modified by the final-state interaction.
Our considerations concern only to charged mesons (e.g. pions) and to the modification of the second-order interference due to the mutual Coulomb repulsion. In the literature this is taken into account by the socalled Gamow factor, G, obtained in a quantum mechanical treatment /2,3,4/:

$$C_\infty(q) = C(q) \cdot G(q). \qquad (3)$$

$$G = \frac{2\pi\eta}{\exp(2\pi\eta) - 1} \qquad \text{with} \qquad \eta = \frac{m\alpha}{q}. \qquad (4)$$

In this way, coincidences of particle pairs with small relative momenta should be suppressed by the mutual Coulomb interaction between them (Fig. 1). The number of particle pairs, once created, is not conserved.
However, under the published experimental results of pion interferometry I did not find any indication for the necessity of the modification via the Gamow factor.
As shown in Figure 1, the data of Zajc et al. /2/ agree well with the results of the pure quantum statistical treatment, given by (2), whereas the other data /4,5,6/ suggest an enhancement instead of the predicted suppression. The enhancement of the experimental pion-data relative to the neutral-particle correlation function can be explaned in a classical picture, in which the charged mesons are repelled by the mutual Coulomb force. Here, compared to the initial (neutral-particle) correlation function, the asymptotic one is simply obtained by shifting the relative momenta toward higher values. Because of particle conservation the correlation function remains normalized.
The effect of mutual Coulomb repulsion for the two outgoing particles can be introduced into an intermediate result of the correlation function (1), in which the inital separation s of the particles is explicitly given:

$$C(q_s) \propto \int_0^\infty s^2 \exp\left(-\frac{s^2}{2R_0^2}\right)\left[1 + \frac{\sin(q_s s)}{q_s s}\right] ds. \qquad (5)$$

The lifetime of the source has been neglected. In a nonrelativistic treatment, a meson pair with an initial relative momentum q_s located at a distance s attains the asymptotic relative momentum

$$q_\infty = \sqrt{q_s^2 + \frac{A}{s}} \qquad \text{with } A = 4\ m\ e2. \qquad (6)$$

(A = 805 and 2880 MeV^2 fm/c^2 for pions and kaons, respectively).
Thus, instead of (5) we obtain an asymptotic correlation function given by

$$C_\infty(q_\infty) \propto \int_{A/q_\infty^2}^{\infty} \frac{s^2}{D} \exp\left(-\frac{s^2}{2R_0^2}\right)\left[1+\frac{\sin(q_\infty s D)}{q_\infty s D}\right] ds \qquad (7)$$

with $$D=\sqrt{1-\frac{A}{s q_\infty^2}} \qquad (8)$$

The lower integration limit, $s = A/q_\infty^2$, is due to the fact that smaller initial separations are not allowed classically. The correlation function gained in this way is shown in Fig. 2. It differs markedly from the correlation function corrected by the usual Gamow factor. Consequently the information gained about the size of the fireball is quite sensitive to the manner of the Coulomb correction.
It should be noted that non-negligible decay times of the fireball will reduce the correlations. Further, until now, relativistic treatment of the Coulomb correction has been missing, in general.
Experiments are now in preparation by Nagamiya /7/ that attempt to measure the correlation of kaons. Considering charged kaon pairs, the predicted correlation is modified even more by the Gamow factor. Further, as Fig. 3 shows, the discrepancy between the quantum mechanical and the classical treatment is more serious for kaons than for pions. Therefore, the size parameter of the fireball generated in relativistic heavy-ion collisions can only be obtained unambigeously if the discrepancies concerning the Coulomb correction are clarified.

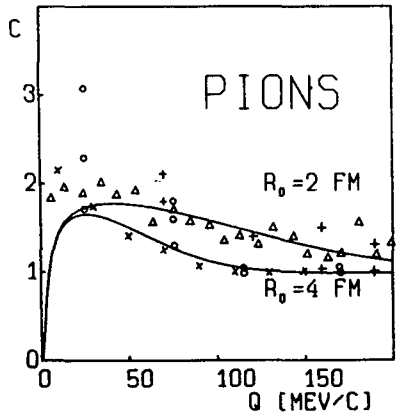

Fig. 1

Experimental correlation coeficients for identical pions from

- o S.Y. Fung et al. /5/
- x D. Beavis et al. /4/
- Δ W.A. Zyjc et al. /2/
- + N. Akhababian et al. /6/

For comparison, the Gamow-corrected correlation functions are shown.

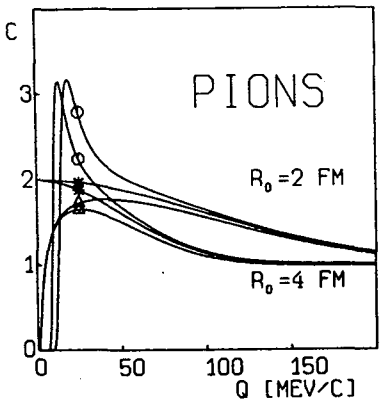

Fig. 2

Identical-pion correlation function for two different sizes, R_0, of the hot source:

- ✱ quantum-statistical effect,
- Δ corrected by the Gamow-factor,
- O Coulomb final-state interaction considered classically.

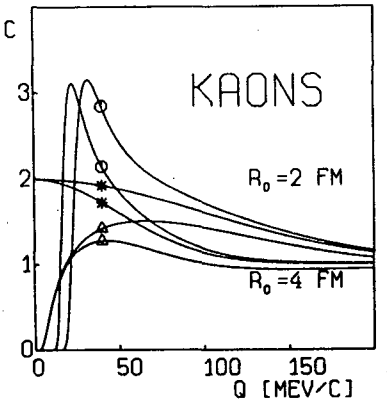

Fig. 3

Identical-kaon correlation function. For details see fig. 2

References

/1/ Yano, F.B., S.E. Koonin, Phys. Lett. 78 B (1978) 556
/2/ Zajc, W.A. et al., Phys. Rev. C 29 (1984) 2173
/3/ Gyulassy, M. et al., Phys. Rev. C 20 (1979) 2267
/4/ Beavis, D. et al., Phys. Rev. C 27 (1983) 910
/5/ Fung, S.Y. et al., Phys. Rev. Lett. 41 (1978) 1592
/6/ Akhababian, N. et al., see J. Bartke, Quark Matter 84, Helsinki and E1-84-587, JINR Dubna Preprint
/7/ Nagamiya, S., Int. School of Nuclear Physics, Erice 1985

NUCLEAR SPECTROSCOPY

TEST OF LARGE-AREA SILICON DETECTORS IN HEAVY ION REACTIONS

L. Funke, J. v.Borany, J. Döring, M. Freitag, K.H. Kaun, H. Prade, B. Schmidt, R. Schwengner
Zentralinstitut für Kernforschung Rossendorf, Bereich KF
A. Johnson
Research Institute of Physics and Royal Institute of Technology, Stockholm, Sweden
J.D. Garrett, K. Schiffer
Tandem-Laboratory Risø, Niels-Bohr-Institute Copenhagen, Denmark

Ion-implanted silicon detectors of about 14 cm^2 sensitive area (42 mm diameter) and a few hundred µm thickness [1] have been tested in connection with ^{16}O induced fusion-evaporation reactions at the tandem accelerator of the Niels-Bohr-Institute Copenhagen in Risø. The goal of these experiments was to find out whether such kind of detectors could be used inside the NORDBALL [2] in order to separate reaction channels with evaporated charged particles involved.

Three different targets (self-supporting Cu and ^{67}Zn foils and ^{67}Zn backed on a Au foil) have been irradiated with the 70 MeV ^{16}O beam of the Risø tandem and the coincident events between charged particles and γ-rays (detected with a germanium detector) were stored in coincidence matrices of 256 x 2048 channels. As shown in fig. 1 the particle spectrum contains three distinct components, similar to spectra measured in α-induced reactions [3,4]. At low energies the protons are dominating since they lose at most 3.5 MeV of their energy in the 100 µm sensitive depth, whereas the energy loss of α-particles ranges up to 14 MeV. In the high-energy part of the spectrum the scattered ^{16}O ions can be seen. With the geometry used in these experiments (up to 4 detectors surrounding the target at a distance of 15-20 mm) a solid angle of about 2π can be covered. Scattered ^{16}O ions reached the detectors only in the experiment with the Au backed ^{67}Zn target. The fairly good distinction between protons, α-particles and heavier ions allows a separation of different reaction channels to be made.

In the case of the Au backed ^{67}Zn target the γ-ray spectra gated with protons, α-particles and scattered ^{16}O ions contain mainly the reaction channels (^{16}O,2pn), (^{16}O,p2n) and (^{16}O,αn), (^{16}O,α2n) as well as (^{16}O,$^{16}O'$), respectively. As expected, channels with only neutrons evaporated are not to be seen in these spectra.

The applicability of such detectors in NORDBALL experiments depends essentially on two questions:

i) How resistent are these detectors against radiation damages caused by scattered or emitted particles and

ii) Can a solid angle of 4π be reached? In the experiments described each of the detectors registered about $5 \cdot 10^8$ charged particles, a dose far below the critical one which is a few times 10^{10} α-particles per cm^2 [5]. The dose of about 10^6 scattered ^{16}O ions that reached the detectors mainly under forward angles also did not deteriorate the resolution. From the present experiments in connection with the investigations of ref. 5 one might estimate that the detectors can be applied for several weeks in such H.I. induced reactions before becoming radiation damaged (provided the number of scattered heavy ions of the beam can be kept relatively small). Furthermore, as shown in ref. [5] there is a great chance for annealing the detectors. Finally, it seems to be possible to manufacture square-shaped detectors of 35 x 35 mm^2. A small box with 6 such detectors surrounding the target (with 2 detectors having an 8 mm hole for the beam) would fit inside the NORDBALL and allow the registration and approximate separation of charged particles in almost 4π geometry.

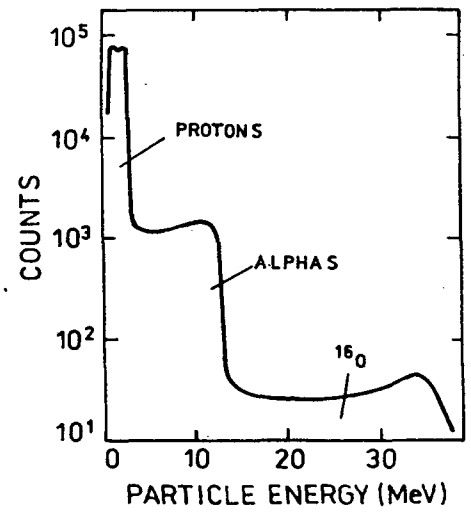

Fig. 1: Particle spectrum measured in the reaction ^{67}Zn (Au backed) + 70 MeV ^{16}O with silicon detectors of 14 cm^2 area, 100 µm sensitive thickness and a resolution of about 100 keV at 8 MeV α-particles.

References:

[1] Borany, J. von, et al.; Annual report ZfK-584(1986)56
[2] Herskind, B.; Nucl. Phys. A447(1985)395
[3] Funke, L., et al.; Z. Physik A324(1986)127
[4] Schwengner, R., et al.; Annual report ZfK-559(1985)34,35,153
[5] Bischoff, L., et al.; ZfK-579(1986)

IN-BEAM EXPERIMENTS WITH ^{7}Li - THE MAGNETIC MOMENT OF A NEW $15/2^{+}$ ISOMER IN $^{85}_{37}Rb_{48}$

L. Käubler, J. Döring, L. Funke, H. Prade, H. Rotter, R. Schwengner, E. Will and G. Winter
Zentralinstitut für Kernforschung, Rossendorf, Bereich KF

By means of a sputter-ionsource used for the ^{7}Li acceleration at the Rossendorf cyclotron, long period in-beam experiments have been performed. In the first experiments enriched (92 %) ^{82}Se targets of different thicknesses have been bombarded with 35 MeV ^{7}Li particles. Spectra of γ-rays delayed to the beam bursts and $\gamma\gamma$-coincidences have been measured so far to investigate different nuclear structure aspects in the final nuclei ^{83}Br, $^{85,86}Kr$ and $^{85,86}Rb$. As a first result a new ns-isomer with $J^{\pi} = 15/2^{+}$ at E_x = 2826.7 keV /1/ has been found (cf. fig. 1) on the basis of the delayed γ-ray spectra.

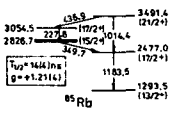

Fig. 1
Schematic partial level scheme /1/ of ^{85}Rb

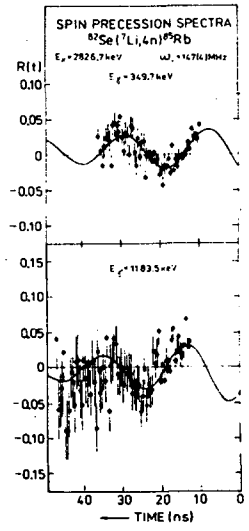

Fig. 2
Spin rotation spectra for two transitions de-exciting the $15/2^{+}$ isomer in ^{85}Rb

In our earlier studies of the nucleus $^{84}_{36}Kr_{48}$, some multiquasiparticle states have been identified /2/ showing the growing importance of spherical shell model aspects close to the magic shell number N=50. In ^{85}Rb the positive-parity yrast states on top of the $9/2^{+}$ isomer are thought to result from the coupling of a proton in the $1g_{9/2}$ shell to the even-even ^{84}Kr core /1/. Thus, these yrast states up to $21/2^{+}$ are suggested to contain 3 qp components resulting from coupling the $1g_{9/2}$ proton to neutron (ν) and proton (π) $1g_{9/2}$ core excitations /1/. No conclusion has been drawn about the configuration of the $15/2^{+}_{1}$ and $17/2^{+}_{2}$ states lying between the $17/2^{+}_{1}$ and $21/2^{+}_{1}$ levels. In this region a backbending like behaviour is supposed /3/.

To clarify this situation, the magnetic moment of the new $15/2^{+}_{1}$ isomer in ^{85}Rb has been determined by the TDPAD-method using a 50 mg/cm^2 ^{82}Se powder target at room temperature. The experimental arrangement is described in ref. /4/. Fitting the usual analytic expression for R(t) to the experimental results (fig. 2), the Larmor frequencies ω_L observed for the 349.7, 1183.5 and 779.4 keV γ-transitions have been determined giving the averaged value ω_L = 147(4) MHz. Taking into consideration the external magnetic field B_{ext} = 2.535(6) T the g-factor amounts to g=+1.21(4) and the magnetic moment of the $15/2^{+}$ isomer in ^{85}Rb to μ=+9.1(3) μ_N. With respect to the large experimental error field corrections have been neglected. The positive sign of the g-factor has been deduced by comparison of the phases of the measured R(t) functions with the phases obtained for known g-factor and A_2 values. From the time distributions a preliminary half-life of $T_{1/2}$ = 14(4) ns has been determined.

The comparison of theoretical estimates for g-factors (table 1) with the experimental value demonstrates that the 3 qp configurations of the type $\nu^{-2}\pi$ are clearly ruled out. The same can be stated for the configuration containing one $p_{1/2}$ proton. The experimental g-factor is within the error limits in agreement with the values calculated for the 3 qp configurations $\pi g_{9/2} f_{5/2} p_{3/2}$, where the configuration $[\pi g_{9/2}(f_{5/2}p_{3/2})_{4^+}]_{15/2^+}$ is the most likely one.

Table 1
Estimated g-factors of 3 qp states

Configuration	g_{calc} [a]
$[\nu(g_{9/2})^{-2}(\pi)^{1}]$ $13/2 \leq J \leq 21/2$ [b]	<0.60
$[\pi g_{9/2} f_{5/2} p_{1/2}]$ $15/2^{+}$	+0.99
$[\pi g_{9/2} f_{5/2} p_{3/2}]$ $15/2^{+} \leq J \leq 17/2^{+}$ [c]	$+1.14 \leq g \leq +1.26$
$[\pi g_{9/2}(f_{5/2}p_{3/2})_{4^+}]$ $15/2^{+}$	+1.21
$[\pi g_{9/2}(f_{5/2}p_{3/2})_{3^+}]$ $15/2^{+}$	+1.19
$[\pi g_{9/2}(f_{5/2}p_{3/2})_{4^+}]$ $17/2^{+}$	+1.21

[a] Calculated by means of the additivity rule of effective g-factors /5/ with: $g(\nu g_{9/2})$=-0.24, $g(\pi p_{1/2})$=-0.14, $g(\pi p_{3/2})$=+1.83, $g(\pi f_{5/2})$=+0.54, $g(\pi g_{9/2})$=+1.37.

[b] (π) stands for all π-configurations mentioned in footnote [a].

[c] For different modes of spin coupling within the configurations.

References

/1/ Zell, K.O. et al., Phys. Rev. C25 (1982) 1379
/2/ Rotter, H. et al., Phys. Lett. 163B (1985) 323
/3/ Lühmann, L. et al., Z. Phys. A313 (1983) 297
/4/ Käubler, L. et al., ZfK-455 (1981) 1
/5/ Lederer, C.M., V.S. Shirley: Table of isotopes. New York: John Wiley 1978

BAND STRUCTURES IN ^{79}Br

R. Schwengner, J. Döring, L. Funke, H. Rotter and G. Winter
Zentralinstitut für Kernforschung Rossendorf, Bereich KF
A. Johnson and A. Nilsson
Research Institute of Physics, Stockholm, Sweden

The in-beam study of ^{79}Br /1/ has been continued. Further experiments were carried out using the ^{78}Se(α,p2n) reaction (E_α=45 MeV) and the ^{77}Se(α,pn) reaction (E_α=27 MeV) at the cyclotrons in Stockholm and Rossendorf, respectively. The level scheme deduced from the present experiments is shown in figure 1. Mean lifetimes of states in ^{79}Br were extracted from Doppler-shift attenuation (DSA) and recoil-distance Doppler-shift (RDDS) experiments. To suppress γ rays from (α,xn) reactions and background radiation a particle-γ coincidence set-up /2/ or a plunger device in connection with a multiplicity filter /3/ were used in DSA or RDDS experiments, respectively, that employed the ^{77}Se(α,pn) reaction. The lifetimes are given in table 1.

Three band-like structures have been identified in ^{79}Br. The level spacings and large E2 transition strengths (B(E2)$\approx$30-40 W.u.) within the yrast band built on the $9/2^+$ isomer are similar to those within the yrast band of the core nucleus ^{78}Se and point to a decoupled motion of the $g_{9/2}$ proton and the core. The transition energies within the $3/2^-$ ground state band decrease above the $13/2^-$ state. This anomaly may indicate a band crossing with the 3qp band observed above the second $13/2^-$ state. The levels of this band are depopulated by rather strong M1 transitions (B(M1)$\approx$0.4 W.u.) and might involve configurations like a $p_{3/2}$ proton coupled to a broken $g_{9/2}$ pair of the core or a $g_{9/2}$ proton coupled to certain negative-parity core states, similar to the 3qp band in ^{81}Br /4/.

References

/1/ Schwengner, R. et al., Annual reports 1984 and 1985, ZfK-559(1985)28, ZfK-584(1986)20
/2/ Schwengner, R. et al., Annual report 1984, ZfK-559(1985)34
/3/ Winter, G. et al., Annual report 1985, ZfK-584(1986)102
/4/ Funke, L. et al., Z. Phys. A324(1986)127

Figure 1. Level scheme of ^{79}Br deduced from the present experiments.

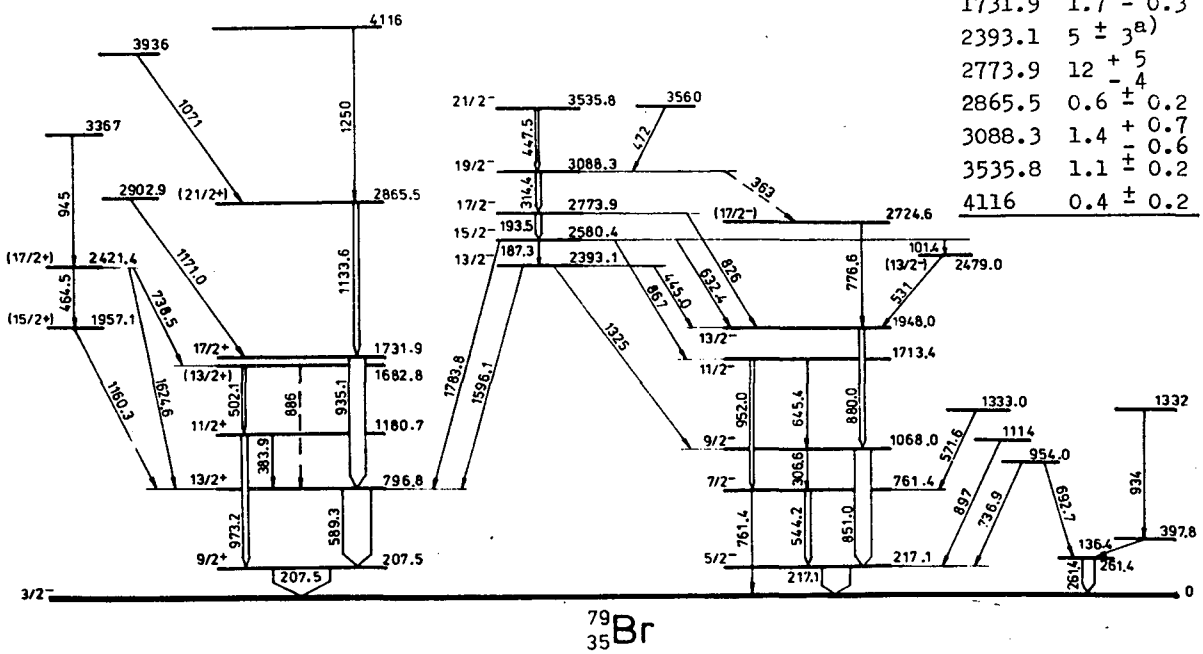

Table 1. Lifetimes of states in ^{79}Br. a) without feeding correction.

E_x/keV	τ/ps
796.8	13 ± 3
1180.7	0.8 ± 0.2
1713.4	0.6 ± 0.5
1731.9	1.7 ± 0.3
2393.1	5 ± 3 a)
2773.9	12 ± 5
2865.5	0.6 ± 0.2
3088.3	1.4 ± 0.7
3535.8	1.1 ± 0.2
4116	0.4 ± 0.2

HIGH-SPIN STATES IN ^{79}Kr

L. Funke, G. Winter, R. Schwengner, J. Döring, H. Prade, H. Rotter
Zentralinstitut für Kernforschung Rossendorf, Bereich KF
A. Johnson, Research Institute of Physics and Royal Institute of Technology, Stockholm, Sweden
A. Nilsson, Research Institute of Physics, Stockholm, Sweden

The investigation of ^{79}Kr has been continued. In order to enhance the excitation of high-spin states in addition to the experiments performed in the reaction ^{77}Se(α,2n) at the Rossendorf cyclotron /1,2/ several experiments in the reaction ^{78}Se(α,3n) have been performed with 45 MeV α-particles at the Stockholm 225 cm cyclotron shortly before its shut-down. In a $\gamma\gamma$-coincidence experiment 3 large-volume HP Ge detectors of more than 20% efficiency have been used. Two of them were positioned at a distance of about 5 cm from the target under 90° relative to the beam direction and one detector about 8 cm apart under an angle of 135° (backward direction). The 3 coincidence matrices of the different detector combinations have been added and the total matrix contains about $2 \cdot 10^8$ coincidence events collected during 25 hours of beam time. Furthermore, the two matrices of the 135°- detector with the two 90°-detectors have been added separately and analysed with respect to Doppler shift effects /3/. The angular distribution and linear polarisation of the γ-rays have also been measured. The present status of the evaluation allows us to establish the level scheme of ^{79}Kr as given in fig. 1, which goes far beyond earlier studies /4/. Besides the yrast sequence of positive parity that is discussed in ref. /3/ the level scheme contains the following level sequences:

i) Both signatures of the 1qp configurations $p_{1/2}$, $f_{5/2}$ and also $p_{3/2}$ with the basis states $1/2^-$ (ground state), $5/2^-$ at 147.1 keV and $3/2^-$ at 384.2 keV. The collectivity, at least in the $p_{1/2}$ and $f_{5/2}$ bands, is relatively large /2/.

ii) Above 2.8 MeV four levels have been found, which show very complicated decay pattern and are likely to form a sequence of levels based on a 3qp configuration of negative parity. Possible low-energy transitions between close-lying states of equal spin and parity ($17/2^-$ to $23/2^-$) are present in the singles γ-ray spectrum but their intensities are too weak to be observed in the coincidence spectra. If they exist a strong mixing of 3 configurations would be suggested.

iii) In addition to the yrast sequence some yrare states of positive parity have been observed, which have counterparts in ^{81}Kr /5/.

To get more insight into the complicated level structure of ^{79}Kr, further evaluation of the extensive experimental material is necessary.

References:

/1/ Schwengner, R. et al., Annual report ZfK-559(1985)29
/2/ Winter, G. et al., Annual report ZfK-584(1986)21
/3/ Winter, G. et al., this report p. 32
/4/ Kajrys, G. et al., Phys. Rev. C27(1983)983
/5/ Funke, L. et al., Nucl. Phys. A455(1986)206

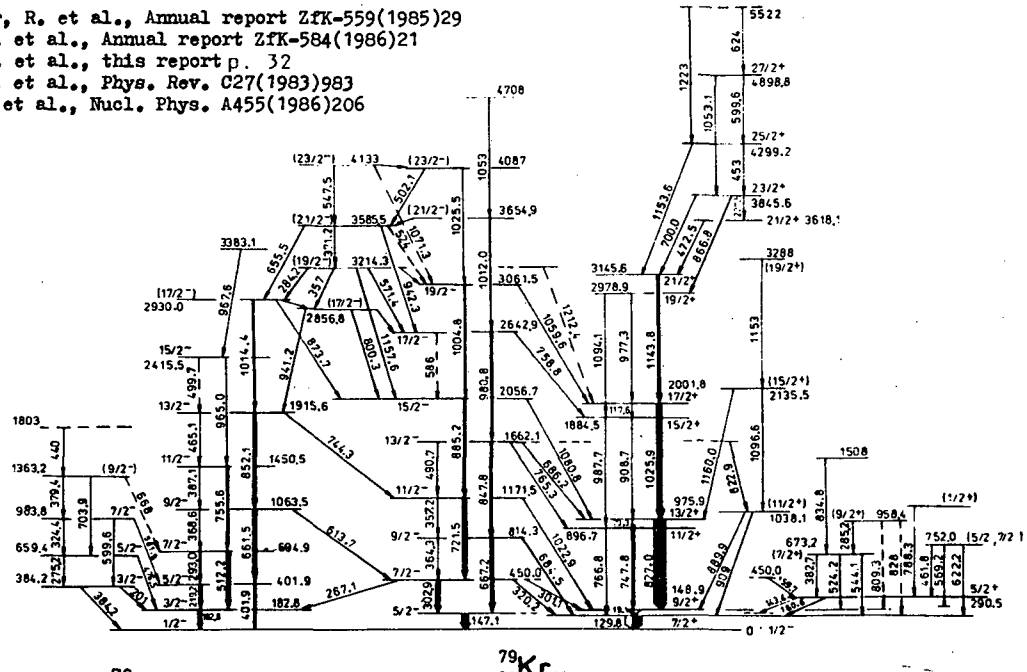

$^{79}_{36}Kr_{43}$

Fig. 1: Level scheme of ^{79}Kr as obtained from in-beam experiments using (α,2n) and (α,3n) reactions.

TRANSITION PROBABILITIES IN THE BAND CROSSING REGION OF ^{79}Kr

G. Winter, J. Döring, L. Funke, H. Prade, H. Rotter and R. Schwengner
Zentralinstitut für Kernforschung, Rossendorf, Bereich KF
A. Johnson
Research Institute of Physics, Stockholm and Royal Institute of Technology, Stockholm, Sweden
A. Nilsson
Research Institute of Physics, Stockholm, Sweden

Excited states in ^{79}Kr have been identified up to $I^{\pi} = (27/2^+)$ and $(23/2^-)$ using in-beam γ-ray spectroscopy in connection with $(\alpha,2n)$ and $(\alpha,3n)$ reactions at the cyclotrons in Rossendorf and Stockholm, respectively. The results are summarised in a level scheme shown in the preceeding contribution to this report /1/. For many levels of the yrast sequence picosecond lifetimes could be deduced from lineshape analysis in Doppler-shift experiments. The results have been obtained either in a common analysis of the two lineshapes found at the observation angles of 25° and 155° or by analysing the lineshape found at an observation angle of 135° in a $\gamma\gamma$-coincidence experiment. Reduced E2 and M1 transition probabilities as derived from these lifetimes are given in table 1.

Table 1. Reduced E2 and M1 transition probabilities given in Weisskopf units.

I_i	I_f	B(E2)	I_i	I_f	B(M1)
$13/2^+$	$9/2^+$	37(5/3)	$11/2^+$	$9/2^+$	0.020(6/4)
$17/2^+$	$13/2^+$	44(4/5)	$15/2^+$	$13/2^+$	0.035(16/13)
$21/2^+_1$	$17/2^+$	54(8/6)	$19/2^+$	$17/2^+$	0.05(2)
$11/2^+$	$7/2^+$	14(4/3)	$21/2^+_2$	$21/2^+_1$	0.4(2/1)
$15/2^+$	$11/2^+$	45(15/11)	$23/2^+$	$21/2^+_1$	0.23(14/8)
$19/2^+$	$15/2^+$	36(14/9)	$23/2^+$	$21/2^+_2$	0.6(6/3)
$23/2^+$	$19/2^+$	46(45/23)	$25/2^+$	$23/2^+$	0.18(6/5)
$25/2^+$	$21/2^+_1$	48(12/7)	$(27/2^+)$	$25/2^+$	0.22(17/9)
$(27/2^+)$	$23/2^+$	57(43/22)			

The errors are given in parentheses in units of the last digit. When asymmetric the notation is (upper/lower) uncertainty.

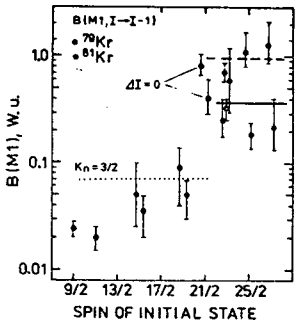

Figure 1. The M1 transition probabilities in the yrast sequence of ^{79}Kr in comparison with the corresponding data in ^{81}Kr /2/. The curves correspond to the prediction of the coupling scheme /2,3/.

The E2 transition probabilities in the yrast sequence of ^{79}Kr have been found to increase slightly with increasing spin (see table 1) but they do not show an irregularity at the band crossing. This behaviour might be interpreted as arising from a considerable mutual mixing of the 1qp and 3qp configurations for several levels in the crossing region. The M1 transition probabilities, on the other hand, are for transitions above spin 21/2 considerably greater than for transitions at lower spin (see figure 1). The increase of the B(M1) values in ^{79}Kr by approximately a factor of four is smaller than in the case of ^{81}Kr where the B(M1) values in the 3qp band are about ten times larger than in the 1qp band.

A plausible explanation for the B(M1) values in the 3qp band being smaller in ^{79}Kr than in ^{81}Kr is found on the basis of the semi-classical coupling scheme of the three particle angular momenta in the 3qp configuration. For the 3qp configuration in ^{81}Kr it was assumed /2/ that the unpaired neutron occupies the $K_n = 7/2$ substate of the $g_{9/2}$ multiplet. Since ^{79}Kr contains two neutrons less than ^{81}Kr it is reasonable to assume that the unpaired neutron in the 3qp states of ^{79}Kr occupies the $K_n = 5/2$ substate. Together with the smaller value of the aligned angular momentum of the two unpaired protons ($i \approx 4\hbar$ in ^{79}Kr compared to $\approx 6\hbar$ in ^{81}Kr), the lower value of K_n in ^{79}Kr gives rise to the reduction of the B(M1) values in the 3qp band of ^{79}Kr as compared to ^{81}Kr (see the broken and full curves in figure 1).

References:

/1/ Funke, L., et al.; this report p. 31
/2/ Funke, L., et al.; Nucl. Phys. A455 (1986) 206
/3/ Dönau, F.; NBI - ZfK Preprint 85 - 36 (1985)

NEAR-YRAST SPECTROSCOPY OF THE N=48 NUCLIDE ^{84}Kr

H. Rotter, J. Döring, L. Funke, L. Käubler, P. Kleinwächter, H. Prade, R. Schwengner and G. Winter
Zentralinstitut für Kernforschung, Rossendorf, Bereich KF
A.E. Sobov, A.P. Grinberg, I.Kh. Lemberg, A.S. Mishin, L.A. Rassadin, I.N. Chugunov and A.D. Efimov
Physico-Technical Institute "A.F. Joffe", Leningrad, USSR

About twenty new levels in ^{84}Kr up to spin 14 ħ and 7.65 MeV excitation energy have been established (see fig.1) as a result of an extensive in-beam spectroscopic study via the $^{82}Se(\alpha,2n)$ reaction at the cyclotrons in Leningrad and Rossendorf. Based on Doppler-shift attenuation or plunger experiments, the mean lifetimes could be determined for thirty of the levels excited. The dominant structure of a new long-lived 12^+ isomer has been identified /1,2/ as the stretched 4qp configuration $\pi(p_{3/2},f_{5/2})\otimes\nu(g_{9/2})^{-2}$ on the basis of the measured g-factor and the sum of the excitation energies of the involved 2qp states 4_2^+ and 8_1^+. Most of the negative-parity states could be grouped into two sequences with $\Delta I = 2$ and $\Delta I = 1$, respectively, built on the two lowest 5^- states. The 2qp configurations $\nu(g_{9/2}^{-1},p_{1/2}^{-1})_{5^-}$ and $\pi(p_{3/2}/f_{5/2}/p_{1/2},g_{9/2})_{5^-}$, respectively, might be ascribed to them, but at least the odd-spin members of the two bands are strongly mixed as indicated by strong interband transitions. The collectivity in the negative-parity bands is rather low ($B(E2)\approx 10 \div 20$ W.u.) as in the ground state band. The (6_2^+) level at 3.95 MeV turns out to have non-collective structure as shown by the low E2 strengths of the transitions deexciting this level. Together with the (8_2^+) and (10_2^+) levels it forms a band-like sequence with enhanced E2 transition strengths (about $30 \div 40$ W.u.) between them. This E2 enhancement might be due to the deformation driving properties of the lowest $g_{9/2}$ orbitals in the proton system indicating the presence of a broken pair of $g_{9/2}$ quasiprotons in this sequence.

References:

/1/ Rotter, H. et al., Annual report 1984, ZfK-559(1985)30; Phys. Lett. 163B(1985)323
/2/ Prade, H. et al., this report p. 34

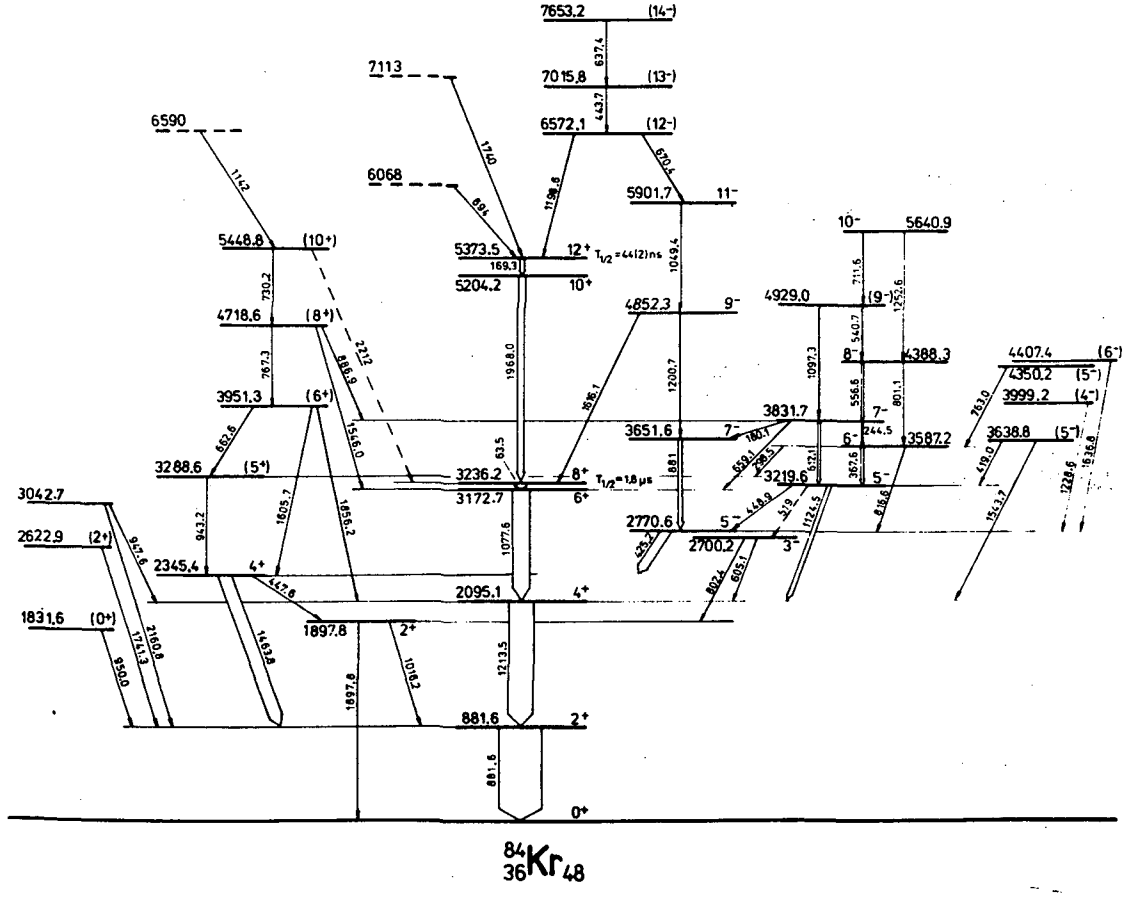

Fig. 1 Level scheme of ^{84}Kr obtained in the $(\alpha,2n)$ reaction at $E_\alpha = 12 \div 27$ MeV

MAGNETIC MOMENT OF THE 12^+ ISOMER IN ^{84}Kr

H. Prade, L. Funke, L. Käubler and H. Rotter
Zentralinstitut für Kernforschung, Rossendorf, Bereich KF
L.O. Norlin and U. Rosengard
Research Institute of Physics, Stockholm, Sweden

Recently we reported on a new four-quasiparticle isomer at E_x = 5373.4 keV with $J^\pi = 12^+$ in ^{84}Kr /1/, which was observed among the about 20 new ^{84}Kr levels established as a result of extensive in-beam spectroscopic measurements. The isomeric state is deexcited by a cascade of two E2 transitions of 169.3 and 1968.0 keV feeding the known 8^+ isomer at E_x = 3236.1 keV. A first measurement of the magnetic moment by means of the TDPAD method at the Rossendorf cyclotron resulted in g = +0.14(3) for the g-factor of the 12^+ isomer /1/. Since this g-factor is rather small, only half an oscillation period could be observed within the given duty cycle of 90 ns causing a relatively large experimental uncertainty.

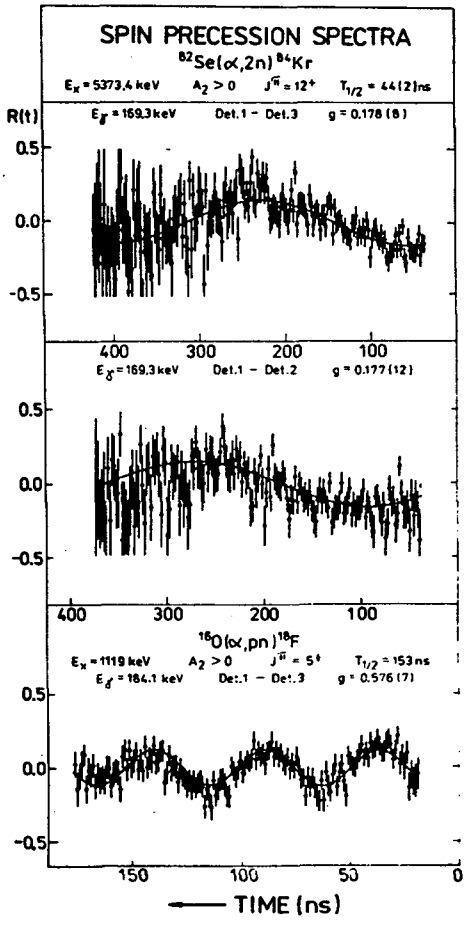

Fig. 1
Time-differential spin precession spectra for the 169.3 keV transition in ^{84}Kr and the 184.1 keV one in ^{18}F. The solid lines represent results of fits.

In order to reduce the experimental error a further g-factor measurement was carried out at the Stockholm 225 cm cyclotron. The isomeric state was populated in the (α,2n) reaction by bombarding a ^{82}Se target (enriched to 92 %) with 30 MeV α-particles. The TDPAD experiment was performed with two big Ge(Li) detectors placed at 135° (Det. 2) and -45° (Det. 3) relative to the incident beam direction as well as with one low-energy photon Ge detector at -135° (Det. 1). The external magnetic field applied perpendicularly to the beam-detector plane amounted to B_{ext} = 2.170(1) T. The beam was pulsed in the 1:9 mode with an electrostatic deflector /2/ giving a repetition time of 1.23 µs. Prompt and delayed signals of all three detectors were stored event by event in a two-parameter mode (E_γ,t) on magnetic tapes. The subsequent analysis was carried out by setting gates on photopeaks and appropriate background intervals in the energy axes of the sorted matrices providing the time distributions for selected γ-rays. From the background-corrected time spectra the normalized ratios R(t) were formed for the 169.3 keV transition in ^{84}Kr and the 184.1 keV one in ^{18}F (fig. 1). Fits of the corresponding analytical expressions /3/ to the experimental R(t) ratios and also to the time curves for the 1968.0 keV γ-ray provided 4 independent g-factor values, the weighted average of which amounts to g = + 0.175(15). The comparison with the R(t) function of the 184.1 keV E2 transition in ^{18}F confirms the positive sign of the g-factor.

Taking into consideration both g-factor measurements we finally got

$$g(12^+,\ 5373.4\ \text{keV}) = +\ 0.168(14) \quad \text{and}$$

$$T_{1/2}(12^+,\ 5373.4\ \text{keV}) = 44(2)\ \text{ns}.$$

As discussed in ref. /1/ on the basis of the additivity rule for effective g-factors this experimental result can only be explained by assuming the 4 qp neutron-proton configuration tion $\nu(g_{9/2})^{-2}_{8^+}\pi(p_{3/2},\ f_{5/2})_{4^+}$ to be dominant in the wave function of the 12^+ isomer.

References

/1/ Rotter, H. et al., Phys. Lett. 163B (1985) 323
/2/ Abrahamsson, K. et al., Nucl. Instr. Meth. 111 (1973) 125
/3/ Käubler, L. et al., ZfK-455 (1981)

INVESTIGATION OF ^{79}Se IN THE (α,n) AND (α,αn) REACTIONS

L. Funke, J. Döring, R. Schwengner, G. Winter
Zentralinstitut für Kernforschung Rossendorf, Bereich KF

Earlier we have found interesting structural effects in ^{81}Kr [1] and also in ^{79}Kr [2] and ^{83}Kr [3], such as a shape transition and enhanced M1 transitions. In the corresponding Se isotones no information on three-quasiparticle (3qp) excitations is known so far. Thus, we have initiated the study of ^{79}Se that cannot easily be reached by in-beam γ-ray spectroscopy. Up to now only one experiment [4] has been performed using the reaction ^{76}Ge(α,n) at α-particle energies of 13 - 16 MeV. As a result of this study low-spin states up to 11/2 have been established in ^{79}Se. In order to get data on higher-spin states we measured $\gamma\gamma$-coincidences in Rossendorf in the (α,n) reaction at 18.5 MeV α-particle energy and the γ-ray singles spectra at 13, 16 and 21 MeV. Because of the low threshold of the (α,2n) reaction the ^{78}Se transitions [5] become dominant already at low beam energies which makes the investigation of 3qp excitations above spin 21/2 practically impossible.
In the preliminary level scheme given in fig. 1 all levels above 2 MeV are newly established but they likely belong to 1qp excitations. Most of the transitions shown in fig. 1 have also been observed by us in the reaction ^{80}Se(α,αn) at E_α = 27 MeV. In this case the weak (α,αn) channel has been selected by using an ion-implanted silicon detector to register the evaporated α-particles and to measure the coincident γ-ray spectrum (see fig. 2 of ref. [6]).
In order to excite 3qp excitations we intend to study ^{79}Se via the ^{76}Ge(^{7}Li,p3n) reaction with the 35 MeV ^{7}Li beam of the Rossendorf cyclotron. The cross section of this reaction is in the order of 10% of the total cross section and the use of Si detectors for the registration of the evaporated protons may clean up the spectra sufficiently well. Furthermore, Doppler-shift lifetime measurements are planned in collaboration with a group of the FTI "Joffe" Leningrad.

References:
[1] Funke, L. et al., Nucl. Phys. A455(1986)206
[2] Winter, G. et al., this report
[3] Kemnitz, P. et al., Nucl. Phys. A456(1986)89
[4] Zell, K.O. et al., Z. Physik A292(1979)135
[5] Schwengner, R. et al., Z. Physik (in press)
[6] Funke, L. et al., Z. Physik A324(1986)127

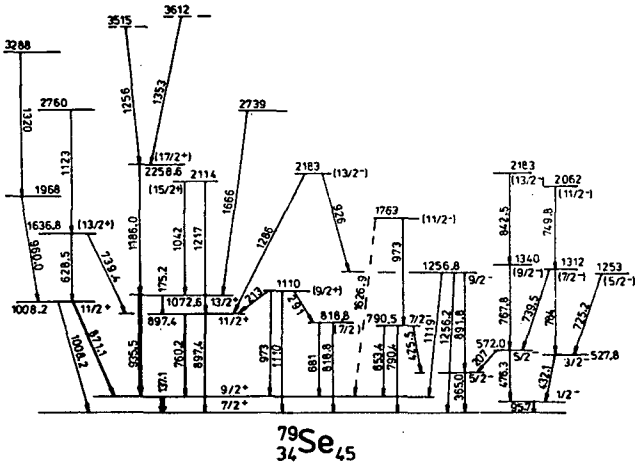

Fig. 1: Preliminary level scheme of ^{79}Se as obtained from investigations in the (α,n) and (α,αn) reactions.

IN-BEAM INVESTIGATION OF THE N=82 NUCLEUS ^{142}Nd

L.Käubler, W. Enghardt and H. Prade
Zentralinstitut für Kernforschung Rossendorf, Bereich KF

In the course of our structure investigations of N=82 isotones also the even-even nuclei ^{138}Ba /1/ and ^{140}Ce /2/ have been studied. To follow especially the behaviour of negative parity states identified in these nuclei, in-beam measurements for the N=82 nucleus ^{142}Nd have been performed at the Rossendorf cyclotron using the reaction ^{140}Ce(α,2n)^{142}Nd with $20 \leq E_\alpha \leq 27$ MeV. In the measurements 10 mg/cm^2 thick $^{140}CeO_2$ targets enriched to 99.5% deposited on lavsan foils have been bombarded. The following experiments have been performed: Measurements of singles γ-ray spectra, relative excitation functions, the γ-linear polarization, prompt $\gamma\gamma$-coincidences and γ-RF time distributions. The evaluation of the data is in progress.
Extended shell model calculations with configuration mixing for the positive parity states /1/ and particle-core coupling calculations for the negative parity states /3/ have been performed.

R e f e r e n c e s
/1/ Enghardt, W. et al., Ann. Phys.(Leipzig) 43 (1986) 424
/2/ Enghardt, W. et al., Nucl. Phys. A449 (1986) 417
/3/ Enghardt, W. and Jäger, H. U., Nucl. Phys. A438 (1985) 141

PARTICLE-CORE COUPLING DESCRIPTION OF NEGATIVE PARITY STATES IN THE Z=50 NUCLEI $^{109,113}Sn$

L. Käubler, W.Enghardt, P. Kleinwächter and H. Prade
Zentralinstitut für Kernforschung, Rossendorf, Bereich KF

Experimentally observed positive and negative parity states and the corresponding electromagnetic properties in the semimagic Z=50 nucleus ^{111}Sn can be successfully described in the framework of the shell model with configuration mixing (SCM) and the particle-core coupling model (PCC), respectively /1/. Further, for positive parity states and half-lives in ^{109}Sn also agreement of the experimental results with SCM-calculations could be found /2/. In the present work this structure investigations are extended to negetive parity states in $^{109,113}Sn$ using known experimental data /3/.

PCC-calculations for semimagic N=82 nuclei are described in ref. /4/. According to this concept the negative parity states of $^{109,113}Sn$ (figs. 1, 2) arise from coupling one neutron in the $1h_{11/2}$ shell to the positive parity states of the corresponding cores $^{108,112}Sn$, respectively. The core states have been computed within the SCM where the N-50 valence neutrons were distributed over the $1g_{7/2}$, $2d_{5/2}$, $2d_{3/2}$ and $3s_{1/2}$ orbits. The model parameters are the same as used in the earlier calculations on excited levels of ^{111}Sn /1/.

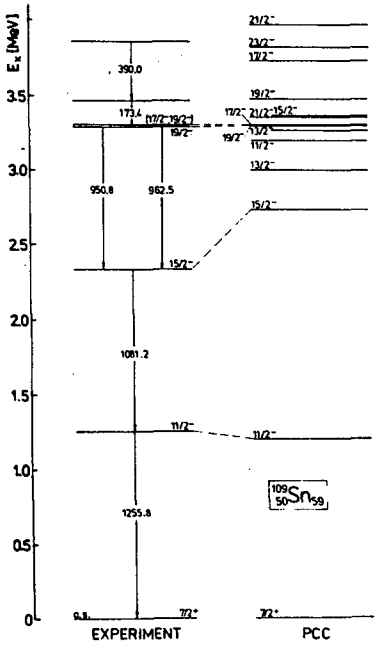

Fig. 1. Comparison of experimental /3/ and theoretical (PCC) energy spectra for negative parity states in ^{109}Sn. In the calculated spectrum for each spin the two lowest states are displayed up to $E_x<4$ MeV.

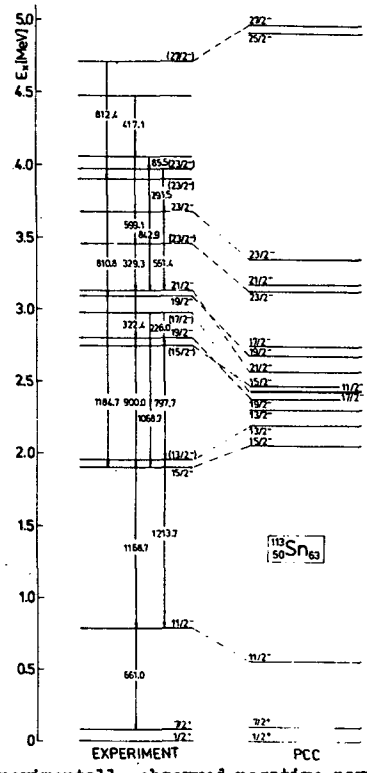

Fig. 2. Experimentally observed negative parity states /3/ in ^{113}Sn compared to PCC calculations. In the theoretical spectrum up to $E_x<5$ MeV the two lowest states for each spin value J are given.

The comparison of the experimental spectra with the theoretical predictions shows the following feature: In the experiments the energy differences between the $11/2^-_1$, $15/2^-_1$ and $19/2^-_1$ states exhibit a vibrator like behaviour. Contrary, the corresponding calculated level spacings are more typical for multiparticle multiplets. For the neighbouring even-even nuclei $^{110,112}Sn$ the comparison of experimental observed low lying 2^+, 4^+ and 6^+ states /5/ with SCM calculations /1/ gives qualitatively the same distinction. Compared with the N=82 nuclei, in the Z=50 nuclei a more complicated situation is found. In the tin nuclei $^{112,114}Sn$ collective positive parity bands have been observed which are interpreted as two-proton two-hole excitations. In the even-even N=82 nuclei no collectivity has been found with the exception of the 3^- states and the shell model approach assuming an inert Z=50, N=82 core has been proved to be an adequate description/6/. The results on tin nuclei show that the $^{100}_{50}Sn_{50}$ core exhibits not so good inert properties for SCM calculations. Systematic experimental and theoretical investigations of half-lives in $^{109,111,113}Sn$ nuclei are in progress.

R e f e r e n c e s

/1/ Prade, H. et al., Nucl. Phys. A425 (1984) 317
/2/ Käubler, L. et al., Abstr. Contr. Int. Symp. on in-beam spectroscopy, Debrecen, 1984, p. 27
/3/ Hashimoto, O. et al., Nucl. Phys. A318(1979)145
/4/ Enghardt, W., H.U. Jäger, Nucl. Phys. A438 (1985) 141
/5/ Van Poelgest, A. et al., Nucl. Phys. A346 (1980) 70
/6/ Enghardt, W. et al., Ann. Phys. (Leipzig) 43 (1986) 424

NEUTRON $2f_{7/2}$ EXCITATIONS IN ^{139}Ba

H. Prade, W. Enghardt, L. Käubler and G. Winter
Zentralinstitut für Kernforschung, Rossendorf, Bereich KF

During our in-beam study of ^{138}Ba by means of the ^{136}Xe(α,2n) reaction we also got some information on ^{139}Ba levels populated simultaneously via the (α,n) reaction channel.
So far mainly low-spin states of ^{139}Ba have been studied in the ^{139}Cs β^- decay, via thermal neutron capture and by means of the (d,p) reaction /1/. The present experiments revealed four new levels on top of the known $11/2^-$ state at 1308.2 keV. The partial level scheme of ^{139}Ba as observed in the (α,n) reaction is shown in fig. 1. The levels at excitation energies of 1828.7, 1977.1, 2091.6 and 2743.4 keV have been established on the basis of the $\gamma\gamma$-coincidence spectra with the 1308.1 and 230.8 keV lines gated. Taking into consideration the angular distribution coefficients obtained for the 148.4 and 520.6 keV γ-rays as well as the small half-life of the 1977.1 keV level ($T_{1/2}$ = 0.40(25) ns) the most probable assignments proposed for the levels at 1828.7 and 1977.1 keV are $J^\pi = (15/2^-)$ and J = (17/2), respectively.

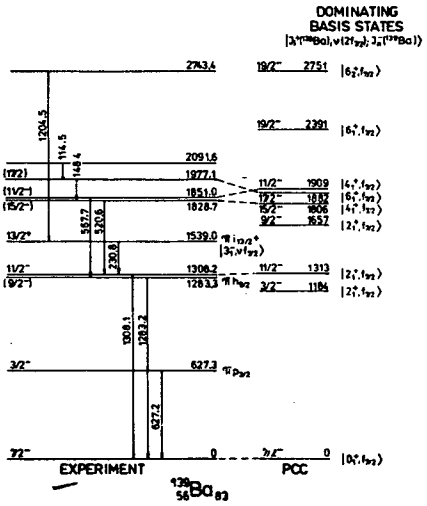

Fig. 1
Partial level scheme of ^{139}Ba as observed in the ^{136}Xe(α,n) reaction

In ^{139}Ba all single-neutron states within the 82 - 126 major shell have been identified /1/, i.e. $2f_{7/2}$ (g.s.), $3p_{3/2}$ (627 keV), $3p_{1/2}$ (1082 keV), $1h_{9/2}$ (1283 keV), $2f_{5/2}$ (1421 keV) and $1i_{13/2}$ (1539 keV). Besides these neutron single-particle excitations various particle-core coupled states are likely to appear in the excitation spectrum of ^{139}Ba. This might be expressed by the high level density between 1.0 and 2.5 MeV experimentally observed /1/. Since the ^{139}Ba g.s. is known to be a rather pure $2f_{7/2}$ neutron state, which reflects the fact that the $2f_{7/2}$ shell is lowest in energy among the single-particle orbitals above the N = 82 gap, the coupling of the $f_{7/2}$ neutron to low-lying ^{138}Ba core states may form some of the yrast states with spin values of $J \geq 11/2$.
Therefore, excitation energies for negative-parity ^{139}Ba states have been calculated within the framework of a particle-core coupling (PCC) model based on coupling one $2f_{7/2}$ neutron to π = +1 proton states of the N = 82 nucleus ^{138}Ba. According to the PCC concept succesfully applied to odd-parity states of N = 82 nuclei /2/ the latter core states are described by means of the shell model with configuration mixing (SCM) adopting a well established SCM approach of Wildenthal /3/. The only new parameter entering the present calculations is the strength of the neutron-proton surface delta interaction between the $f_{7/2}$ neutron and the active protons in the core, which was chosen to be the same as for the proton-proton interaction (A_0 = 0.373 MeV, A_1 = 0.373 MeV).

In fig. 1 (right-hand side) the predicted spectrum of the corresponding odd-parity states for ^{139}Ba is compared with experimental data. For all π = -1 states with $J^\pi \geq 11/2^-$ a good correspondence between experiment and theory is found. Especially, the experimental excitation energies of the $11/2^-$ and $15/2^-$ states at 1308 keV and 1829 keV, respectively, are reproduced very well by the theory. Our simple PCC model predicts the $11/2^-_1$ and $3/2^-_1$ levels to be rather pure states arising from an aligned and antialigned coupling, respectively, of the $2f_{7/2}$ neutron to the 2^+_1 core state, while for all other odd-parity states at least two core states should contribute to their wave functions. Nevertheless, the contributions of the dominating basis states given in fig. 1 are predicted to amount to more than 50 % in the calculated negative-parity wave functions.
In order to compare the whole $2f_{7/2}$ multiplets with experiment more unambiguous spin and parity assignments are needed.

References

/1/ Peker, L.K., Nuclear Data Sheets 32 (1981) 1
/2/ Enghardt, W., H.U. Jäger, Nucl. Phys. A438 (1985) 141
/3/ Larson, D. et al., Phys. Rev. C11 (1975) 1638

E1 TRANSITIONS IN N = 82 ISOTONES CAUSED BY OUTER SUBSHELL CONFIGURATIONS

W. Enghardt, L. Käubler and H. Prade

Zentralinstitut für Kernforschung, Rossendorf, Bereich KF

Investigations on semi-magic N=82 nuclei with $138 \leq A \leq 144$ /1/ have shown that most of their spectroscopic properties at $E_x \lesssim 5$ MeV can be well understood from few proton excitations outside the doubly magic core ^{132}Sn. The valence protons are assumed to occupy $1g_{7/2}$, $2d_{5/2}$, $2d_{3/2}$, $3s_{1/2}$ and $1h_{11/2}$ single particle states. But, it is not possible to account for the rather strong E1 transitions observed for some of these nuclei /1-3/, since they are j-forbidden. The present attempt to explain the E1 transitions is suggested by data of the proton stripping reaction ^{144}Sm(α,t)^{145}Eu /4/, where significant l=3 and l=5 components in the proton strength distributions between $2.7 < E_x < 5.5$ MeV have been observed, which may be attributed to the $2f_{7/2}$ and $1h_{9/2}$ shells above the Z=82 gap. Thus, we conjectured that the wave functions of negative parity may contain admixtures of configurations, where one proton occupies either the $2f_{7/2}$ or the $1h_{9/2}$ shell instead of the $1h_{11/2}$ one. The remaining valence protons are assumed to be on the gds shells /5/. We applied this approach to observed E1 transitions in the N=82 nuclei (cf. fig. 1). The B(E1) values of single-proton transitions between the $2f_{7/2}$ and the $1g_{7/2}$ or $2d_{5/2}$ subshells as well as between the $1h_{9/2}$ and the $1g_{7/2}$ ones were calculated by means of the combination of the particle-core coupling model (PCC) for $\pi = -1$ states and the shell model with configuration mixing (SCM) for $\pi = +1$ states as explained in ref. /5/. The B(σ,L)-values of the competing M1 and E2 transitions have also been computed. Considering the results in table 1 we found that very small admixtures of outer subshell excitations in the $\pi = -1$ wave functions are sufficient to understand the experimental branching ratios or the lifetime in fig. 1. As an example, the E1 decay branch of the 23 ns isomer in ^{140}Ce will be correctly reproduced, if the $J^\pi = 9^-$ state with a predominant structure $(1g_{7/2}^1, 1h_{11/2}^1)$ /1/ contains only 0.007 % of the configuration $(1g_{7/2},2d_{5/2})^3,2f_{7/2}$ or 0.003 % of the configuration $(1g_{7/2},2d_{5/2})^3,1h_{9/2}^1$.

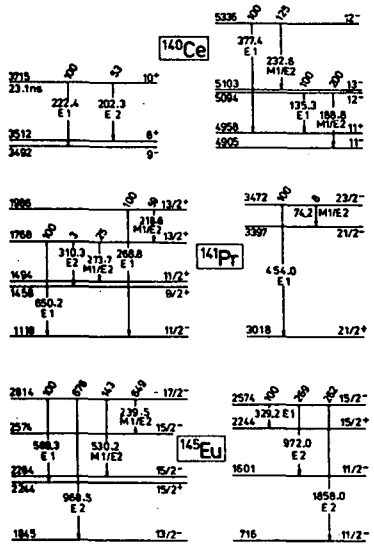

Fig. 1 Levels of N=82 isotones decaying via E1 transitions

Table 1 Predictions obtained from PCC and SCM calculations on the deexcitation of levels which decay via an E1 branch for the nuclei ^{140}Ce, ^{141}Pr and ^{145}Eu

Nucl.	E1 transitions					Competing transitions			
	E_γ(keV)	J_i^π	J_f^π	B(E1,f)[a,c]	B(E1,h)[b,c]	E_γ(keV)	J_f^π	B(M1)[c]	B(E2)[c]
^{140}Ce	222.4	10^+	9^-	0.016	0.032	202.3	8^+		7.4
	135.3	12^-	11^+	0.0044	0.0026	188.8	11^-	0.010	1.6
	377.4	12^-	11^+	0.34	4.7×10^5	232.6	13^-	0.051	93
^{141}Pr	650.2	$13/2^+$	$11/2^-$	2.7×10^{-4}	2.2×10^{-4}	273.7	$11/2^+$	0.0021	8.8
						310.3	$9/2^+$		17
	868.8	$13/2^+$	$11/2^-$	9.4×10^{-4}	0.026	218.6	$13/2^+$	0.028	5.1
	454.0	$23/2^-$	$21/2^+$	2.2	0.30	74.2	$21/2^-$	0.012	130
^{145}Eu	569.3	$17/2^-$	$15/2^+$	0.0064	0.0066	239.5	$15/2^-$	0.0062	95
						530.2	$15/2^-$	0.012	38
						968.5	$13/2^-$		3.8
	329.2	$15/2^-$	$15/2^+$	0.020	0.0014	972.0	$11/2^-$		7.0
						1858.0	$11/2^-$		42

a) Reduced E1 strength of proton transitions between the outer $2f_{7/2}$ shell and the $1g_{7/2}$ or $2d_{5/2}$ shells.

b) Reduced E1 strength of proton transitions between the $1h_{9/2}$ and the $1g_{7/2}$ orbits.

c) The reduced transition probabilities are given in units of e^2fm^{2L} and $\mu_N^2 fm^{2(L-1)}$ for electric and magnetic transitions, respectively.

References

/1/ Enghardt, W. et al., Ann.Phys.(Leipzig) 43(1986) 424
/2/ Haenni, D.R. et al., Nucl. Phys. A331 (1979) 141; Bazzacco, D. et al., Phys. Rev. C21 (1980) 222; Rakel, D.A. et al., Phys. Rev. C21 (1980) 595
/3/ Kostov, L.K. et al., Z.Phys.A325(1986)293
/4/ Gales, S. et al., Phys. Rev. C31 (1985) 94
/5/ Enghardt, W., H.U. Jäger, Nucl.Phys.A438(1985)141

^{106}Ag:p-n MULTIPLETS AND BAND-LIKE STRUCTURES

W. Andrejtscheff, L.K. Kostov, L.G. Kostova and P. Petkov
Institute of Nuclear Research and Nuclear Energy, Sofia, Bulgaria
A. Dewald, J. Eberth, K.O. Zell and P. von Brentano
Institut für Kernphysik der Universität zu Köln, BRD
L. Funke and E. Will
Zentralinstitut für Kernforschung, Rossendorf, Bereich KF

The odd-odd transitional nucleus ^{106}Ag has been thoroughly investigated in (HI,xn) reactions /1/ and in several light-particle induced reactions /2/. An extensive effort has been undertaken /1/ to interpret the spectroscopic data from the (HI,xn) experiments in terms of a model including the couplings of the two odd quasiparticles to a weakly deformed core. Thereby, a long half-life (200 ns) was predicted for the 6^- level at 765.2 keV supposed to have the structure $\pi g_{9/2} \nu h_{11/2}$.

Little is known about the structure of low-spin states in spite of the rich experimental information on energy levels. Earlier, 3^+ isomers were located in the odd-odd neighbours ^{108,110}Ag but so far not in ^{106}Ag. No definite suggestions on the structure of these isomers have been made so far.

In the present work, excited levels of ^{106}Ag were studied using the reaction ^{103}Rh(α,n)^{106}Ag on the Cologne tandem and on the Rossendorf cyclotron. Delayed $\gamma\gamma$-coincidences were performed between germanium detectors (electronic START) and fast scintilators (or signals associated with the beam pulsing) providing the electronic STOP pulses. The data were analyzed according to the generalized centroid shift method /3/.

The time centroid of the 675.5 keV reveals only a small deviation from the zero-time line which indicates an upper limit

$$T_{1/2}(765.2 \text{ keV}) < 0.2 \text{ ns}$$

in contradiction to the above mentioned theoretical prediction. Further,

$$T_{1/2}(364.4 \text{ keV}) = 0.9 \pm 0.1 \text{ ns}$$

could be derived for this 3^- level (364.4 keV). For all levels with $J = 3^+$ a value of

$$T_{1/2}(205.9,\ 389.2,\ 596.1,\ 741.6,\ 835.4 \text{ keV}) < 0.2 \text{ ns}$$

was found.

An estimate of the M1 transition strength of the 87.4 keV transition ($B(M1)_{exp} = 5.3 \cdot 10^{-3}$ W.u.) connecting the 3^- level at 364.4 keV and a lower-lying 2^- level supports the assumption that both states belong to the multiplet $\pi(g_{9/2})_0^{-2} p_{1/2}^{-1} \nu d_{5/2}$. We suggest that the structure of the 3^+ isomers in ^{108,110}Ag arises from the coupling of a $d_{3/2}$ neutron to three $g_{9/2}$ proton holes. Due to the shift of the Fermi level with decreasing neutron number, the $d_{3/2}$ neutron orbital in ^{106}Ag is supposed to lie rather high. This explains the non-existence of a low-lying 3^+ isomer in this nucleus. In this way, the low-lying states in ^{106}Ag can be understood in terms of spherical multiplets. In excitations where the $h_{11/2}$ neutron is involved deformed shapes may occur due to the deformation driving force of the $h_{11/2}$ orbital.

References

/1/ Popli, R. et al., Phys. Rev. C23 (1981) 1085
/2/ Samuelson, L.E. et al., Z. Phys. A294 (1980) 353
/3/ Andrejtscheff, W. et al., Nucl. Instr. Meth. 204 (1982) 123

ENHANCED E1 DECAY OF THE $K^{\pi} = 6^-$ STATE IN ^{174}Hf

W. Andrejtscheff, L.K. Kostov, L.G. Kostova and P. Petkov
Institute of Nuclear Research and Nuclear Energy, Sofia, Bulgaria

J. Döring, L. Käubler, H. Rotter and E. Will
Zentralinstitut für Kernforschung, Rossendorf, Bereich KF

Two-quasiparticle excitations of even-even nuclei in the classical deformed region $150<A<190$ have been the subject of numerous investigations. Of special interest are 2qp band heads with measurable lifetimes as transition probabilities reveal details of their intrinsic structure, which facilitates e.g. a better understanding of the high-spin behaviour.

This work is a continuation of our earlier studies /1/ on this topic. Recently, the nucleus ^{174}Hf has been extensively investigated in (HI,xn) and (α,xn) reactions /2/. Several long-lived ($T_{1/2} > 100$ ns) 2qp states have been found with rotational bands built on top of them. The $K^{\pi} = 6^-$ level at 1713.5 keV appears as the band head of a $\Delta J = 1$ rotational band identified up to $J^{\pi} = 15^-$. The half-life of this level was estimated /2/ as $2 \text{ ns} < T_{1/2} < 10$ ns. We performed delayed γ - r.f. coincidences in the $^{172}Yb(\alpha,2n)$ reaction at the Rossendorf cyclotron. The time distributions were analyzed according to the generalized centroid shift method. The experimental set-up and details of the data analysis are described e.g. in ref. /1/. The level under investigation is de-excited by two E1 transitions of 1105.1 keV (to the 6^+ member of the ground state band) and of 164.3 keV (to a $K^{\pi} = 6^+$ 2qp band head of a $\Delta J = 1$ rotational band) as illustrated in fig. 1. From the time centroids of these two transitions an average value of

$$T_{1/2} \text{ (1713.5 keV)} = 0.45 \pm 0.10 \text{ ns}$$

has been obtained. The configuration of this $J^{\pi} = 6^-$, $K = 6$ level is supposed /2/ to arise from the stretched coupling of two quasineutrons: $\nu(7/2^+/633/, 5/2^-/512/)$. The structure of the $J^{\pi} = 6^+$, $K = 6$ level at 1549.3 keV is suggested /2/ as $92\% \pi(7/2^+/404/, 5/2^+/402/) + 8\% \nu(7/2^-/514/, 5/2^-/512/)$. Thus, the 164.3 keV transition connecting these states should be associated with the 8% admixture: $\nu\, 7/2^+/633/ \rightarrow \nu\, 7/2^-/514/$. However, the Weisskopf hindrance factor $F_W = 3.3 \times 10^4$ of the 164.3 keV transition does not show any appreciable retardation /3/. The E1 transition of 1105.1 keV to the $J^{\pi} = 6^+$, $K = 0$ level is 5-fold K-forbidden. The hindrance factor of this transition, $F_W = 3.8 \times 10^6$, is by two orders of magnitude larger than that of the 164.3 keV transition, but still too low for a 5-fold K-forbidden transition. Moreover, the resulting hindrance per degree of K-forbiddenness $(F_W)^{1/(\Delta K-1)} = 21$ is by far the lowest one among the known values in the region $150<A<190$. This is quite surprising especially for an even spin ($J = 6$) of the initial state where octupole admixtures with $K^{\pi} = 0^-$ are not expected /1/. In ^{172}Yb the $J^{\pi} = 6^-$, $K = 6$ 2qp state decays by a similar E1 transition to the $J^{\pi} = 6^+$, $K = 0$ level with $F_W = 7.3 \times 10^{10}$, i.e. $(F_W)^{1/(\Delta K-1)} = 149$ (cf. /1/). In this way, both E1 transitions depopulating the 2qp state at 1713.5 keV appear strongly enhanced. For a more detailed understanding, configuration mixing of this state associated with a possible rotational alignment of the $i_{13/2}$ neutron $(7/2^+/633/)$ has to be taken into consideration.

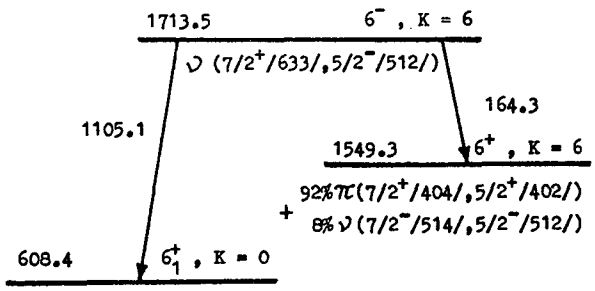

Fig. 1 Partial level scheme of ^{174}Hf

References:
/1/ Kostov, L.K. et al., Nucl. Phys. A376(1982)451, Nucl. Phys. A406(1983)541
/2/ Walker, P.M. et al., Phys. Scr. T5(1983)29, Phys. Lett. 168B(1986)326
/3/ Andrejtscheff, W. et al., ADNDT 16(1975)515

LIMITS ON HEAVY AXION PRODUCTION FROM p(n,a)d

W. Enghardt, K.H. Kaun and H. Prade
Zentralinstitut für Kernforschung, Rossendorf, Bereich KF
J. Blümlein and K. Lanius
Institut für Hochenergiephysik, Zeuthen

The observation of correlated monoenergetic enhancements in the electron and positron spectra measured in heavy ion collision experiments /1/ may be interpreted as signals of a light neutral boson decaying dominantly into e^+e^--pairs. A candidate for such an object is an axion desired for a chiral solution of the strong CP-problem /2/. Up to now the searches for standard axions /3/ have been negative. The data of ref. /1/ suggest an axion mass of $m_a \sim 1.7$ MeV/c^2 and a lifetime of $\tau_a \sim 10^{-13}$ ... 10^{-12} s leading to unnatural parameters /4/ in the standard scenario. These problems and, furthermore, experimental constraints on the standard axion can be circumvented for variant axion models /5,6/ which were proposed recently.

In order to derive limits for the parameters of a class of these axion models we investigated the positron production accompanying the radiative capture of thermal neutrons by protons at an external neutron beam of the 10 MW Rossendorf Research Reactor (Fig. 1), since axions may be produced in competition to the magnetic dipole radiation (E_γ = 2223 keV) from the p(n,γ)d reaction /7/. The decay of these axions would enhance the usual positron production by pair formation (PF) and internal pair creation (IPC) of the γ-radiation. The positrons were detected via their annihilation radiation that was measured by means of a coincidence spectrometer consisting of two NaI(Tl) detectors in colinear arrangement. Simultaneously a γ-ray singles spectrum was taken with a Ge(Li) detector for monitoring the 2223 keV radiation.

The positron yield measured was corrected for IPC and PF and an axion-to-gamma branching ratio of $R^{exp}(x,N) = (0.1 \pm 4.7) \cdot 10^{-4}/\varepsilon(x,N)$ remains, where $\varepsilon(x,N)$ is the acceptance function obtained from a Monte-Carlo-calculation. This has to be compared with the theoretical value /7/ $R(x,N) = 1.1 \cdot 10^{-4}\left[1 - (m_a c^2/E_\gamma)^2\right]^{3/2} \theta(m_a - 2m_e)\left[\varrho^{(1)}/\mu^{(1)}\right]^2$, with $\mu^{(1)} = \mu_p - \mu_n$ the difference of the proton and neutron magnetic moments. The quantity $\varrho^{(1)} = f(x,\xi,N)$ is related to the coupling of axions to nucleons, where x denotes a scale parameter, $\xi \in \{-x^{-1}, x\}$ /6/ and N = 1,2 gives the number of active quark families for variant axions. The mass and the lifetime are obtained from $m_a(x,N) = N \cdot 25$ keV $(x + x^{-1})$ and $\tau_a^{e^+e^-}(x) = 4\pi\eta^2/\left[\sqrt{2}\, G_F\, m_e^3 \sqrt{(m_a/2m_e)^2 - 1}\right]$, $\eta = x^{-1}$ (G_F being the Fermi coupling constant). The standard axion model results from these formulas if N = 3 and $\xi = \eta = x$. The comparison of the experimental and theoretical R allowed us to give limits (90 % confidence level) on the parameters for the standard axion and for the variant axion with N = 1, $\xi = x$ (Table 1). For N = 2, $\xi = x$ and $\xi = -x^{-1}$ as well as for N = 1, $\xi = -x^{-1}$ the 90 % CL for R does not constrain the theoretical predictions.

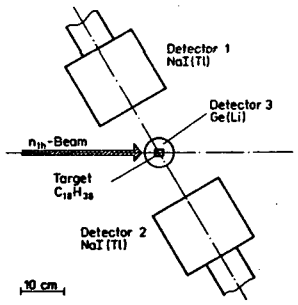

Table 1: Axion parameters excluded by the present experiment at 90 % CL

	N = 1, $\xi = x$	N = 3, $\xi = x$
x	41 < x < 83	0.038 < x < 0.062
m_a (MeV/c^2)	1.05 < m_a < 2	1.2 < m_a < 2
τ_a (ps)	0.33 < τ_a < 9.1	3.3 < τ_a < 23

Fig. 1: Detector arrangement at the external neutron beam for measuring the e^+ creation rate in the p+n reaction

References

/1/ T. Cowan et al., Phys. Rev. Lett. 56 (1986) 444
/2/ G. 't Hooft, Phys. Rev. Lett. 37 (1976) 8; Phys. Rev. D14 (1976) 3432
/3/ S. Weinberg, Phys. Rev. Lett. 40 (1978) 223; F. Wilczek, Phys. Rev. Lett. 40 (1978) 279
/4/ N. Mukhopadhyay and A. Zehnder, Phys. Rev. Lett 56 (1986) 206
/5/ R.D. Peccei et al., Phys. Lett. 172B (1986) 435;
L.M. Krauss and F. Wilczek, Phys. Lett. 173B (1986) 189
/6/ W.A. Bardeen et al., Nucl. Phys. B279 (1987) 401
/7/ T.W. Donnelly et al., Phys. Rev. D18 (1978) 1607

THEORY

EXACT SCALING BEHAVIOUR OF THE EFFECTIVE CHIRAL ACTION AND STABILITY OF THE CHIRAL SOLITON

H. Reinhardt
Zentralinstitut für Kernforschung, Rossendorf, Bereich KF

The effective chiral action of QCD can be assumed to be given by

$$S(U) = - iTr \log i\not{D} \tag{1}$$

where

$$i\not{D} = i\not{\partial} - m(UP_R + U^+P_L),\ P_{R/L} = \frac{1}{2}(1 \pm \gamma_5)\ . \tag{2}$$

Here U is the chiral field living in the coset space $SU(n)_L \times SU(n)_V$ with n being the number of flavours and m is the constituent quark mass, which is assumed to be generated by spontaneous breaking of chiral symmetry. The effective chiral action (1) has been evaluated within a novel improved heat-kernel expansion which includes gradients of the chiral field in a non-perturbative way /1/. The exact scaling behaviour of the effective action of a spatially localized chiral field with respect to a change in the size of the field was found. The energy of the chiral field scales for both $R \to 0$ and $R \to \infty$ like R, showing that the chiral soliton is instable against collapsing. The collapsing of the soliton is, however, accompanied by a vanishing of the baryon charge. The vanishing of the baryon number for $R \to 0$ indicates that the valence quarks have escaped the bosonized theory. In fact, the evaluation of the fermion determinant in Euclidean space fixes the reference state to be that of the physical vacuum; i.e. the state of lowest energy. As an explicit numerical solution of the Dirac equation in the presence of a chiral field with winding number one shows the energy of the valence quarks becomes negative for large spatial extensions of the chiral fields. The physical vacuum is then the state with the valence orbit occupied, and, hence, acquires baryon charge one. As the spatial size of the chiral field is descreased the valence quarks get less and less bounded and eventually their energy becomes positive. The state with the lowest energy (i.e. the physical vacuum) is then that in which the valence orbit is empty. This explains the vanishing of the baryon current as $R \to 0$.

Due to the vanishing of the baryon number for $R \to 0$, the scaling behaviour obtained for the energy ($M \sim R$) does not necessarily imply that the chiral soliton with $N_B = 1$ is instable. Since the baryon number is not independent of the explicit form of the chiral field, to find chiral solitons with given baryon number one should minimize the energy under the constraint of a fixed baryon number. The constrained energy functional may still have a local minimum.

References

/1/ Reinhardt, H., NBI-preprint, NBI-HE-86-46

VACUUM INSTABILITIES IN THE EFFECTIVE CHIRAL ACTION

H. Reinhardt
Zentralinstitut für Kernforschung, Rossendorf, Bereich KF
A. Wirzba
NORDITA, Copenhagen

Many different approaches show that the effective meson action of QCD for a chiral field $U \in SU(n)_L \times SU(n)_R/SU(n)_V$ (n - number of flavors) can be approximated in the absence of external scalar, vector and axial-vector fields by

$$S(U) = -iTr \log i\gamma^\mu D_\mu \qquad (1)$$

where

$$i\gamma^\mu D_\mu = i\gamma^\mu \partial_\mu - m\left(UP_R + U^+ P_L\right), \quad P_{R/L} = \tfrac{1}{2}(1 \pm \gamma_5) .$$

Here m denotes the constituent quark mass. In ref. /1/ the action (1) was calculated in an improved heat kernel expansion which includes gradients of the chiral field in non-perturbative way. This expansion is expected to converge sufficiently fast for both $R \to \infty$ and $R \to 0$. Restricting to next-to-leading order one finds from (1) the following Lagrangian of the chiral field

$$L = -\frac{1}{2} F_\pi^2 \, tr(L_\mu L^\mu) + \frac{1}{32\pi^2} tr\left\{ \frac{m^2}{\mu^2}\left[(L_\mu L^\mu) - (\partial_\mu L^\mu)^2\right] + m^2\left(\Box \frac{1}{\mu^2}\right) L_\mu L^\mu \right.$$
$$\left. - m^2\left[2\left(\partial^\nu \frac{1}{\mu^2}\right) L_\nu (\partial_\mu L^\mu) + \left(\partial_\mu \partial_\nu \frac{1}{\mu^2}\right) L^\mu L^\nu \right] \right\} , \qquad (2)$$

where F_π is the pion decay constant, $L_\mu = U^+ \partial_\mu U$ denotes the left current, and $\mu^2 = m^2 + tr(L_\mu L^\mu)$ a position dependent mass. The energy of a chiral field of the hedgehog form $U = \exp[\vec{\tau}\hat{r}\Theta(r)]$ with a profile function $\Theta(r) = N\pi \exp(-r/R)$ was calculated from eq. (2) as function of the spatial extension of the field, R, for winding numbers N = 1,2,3,4. As one can see in the enclosed fig. 1, for small sizes R the field energy becomes negative and eventually approaches zero linearly. The latter behavior is expected from the general scaling behavior of the chiral action (1) (see ref. /1/). With increasing winding number N the minimum of the energy curve eventually increases. Qualitatively, this behaviour can be found for other profile functions. In physical terms, the negative energy at small R means that the system would gain energy by forming "chiral bubbles" of small size $R \sim 0.04 - 0.08$ fm with non-zero winding numbers. The vacuum would hence not be translationally invariant on a microscopic level, but would consist of a gas of topologically non-trivial "chiral bubbles". Similar results have been found by a numerical evaluation of the fermion determinant in a restricted space /2/.

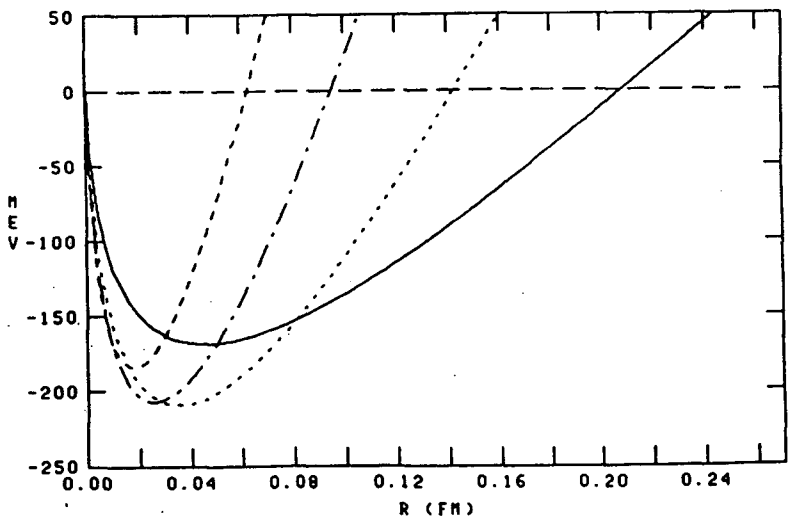

Energy of the chiral field U in MeV as defined in eq. (2) plotted as function of the spatial extension R of the profile function $\Theta(r) = N \exp(-r/R)$ for several winding numbers N. Winding number N = 1 corresponds to the solid line, N = 2 to the dotted line, N = 3 to the dashed-dotted line, and N = 4 to the short-dashed line.

/1/ Reinhardt, H., Niels-Bohr-Institute preprint, NBI-HE-86-46, /2/ Kahana, S., G. Ripka, private communications

"NONLOCAL EXPANSION OF THE EFFECTIVE CHIRAL LAGRANGIAN"

F.-M. Dittes and L. Münchow

Zentralinstitut für Kernforschung, Rossendorf, Bereich KF

We present an explicit expression for the second order term in the nonlocal expansion of the effective chiral action and estimate the corresponding contribution to the field energy.

At present it is widely accepted that low energy hadron physics can be described by the effective chiral lagrangian (see, e.g., /1/, /2/)

$$\mathcal{L} = \bar{\psi} : \not{\partial} \psi \quad , \quad : \not{\partial} = : \not{\partial} - m \mathcal{U} :$$

where the matrix U is usually chosen in the "hedgehog" form

$$\mathcal{U} = \exp(i \vec{\pi} \vec{\tau} \gamma_5) \quad , \quad \vec{\pi} = \vec{r}/r \cdot \theta(r) \, .$$

The real part of the corresponding action can be represented as

$$Re\, S_{eff}[\pi] = -i \frac{N_c}{2} \, Tr \log \frac{\not{\partial}^+ \not{\partial}}{\not{\partial}_0^+ \not{\partial}_0} = i \frac{N_c}{2} \sum_{K=1}^{\infty} \frac{1}{K} \, Tr \left(D^c V \right)^K \, ,$$

where $V = -im \not{\pi} U$ (m being the constituent quark mass, $m \approx 345$ MeV), and $D^c(x_1, x_2)$ is the causal Green function of a scalar field with mass m.
The leading term of this expansion is

$$S_2 = i \frac{N_c}{4} \int d^4 x_1 \int d^4 x_2 \, \left[D^c(x_1 - x_2) \right]^2 \, Tr_{\gamma, \tau} \, V(x_1) \, V(x_2) \, .$$

The corresponding contribution to the field energy ($S = -\int E \, dt$) after some algebra can be brought into the form (for $N_c = 3$)

$$E_2 = E_{kin} + E_{nonloc} \, ,$$

where $E_{kin} = 2\pi f_\pi^2 R \int_0^\infty dr \left(r^2 \theta'^2 + 2 \sin^2 \theta \right)$

is the usual kinetic term with the pion coupling constant f_π renormalized to its physical value $f_\pi \approx 93$ MeV, and

$$E_{nonloc} = \frac{3 m^3 R^2}{\pi} \lim_{\lambda \to 0} \left\{ \int_\lambda^\infty \frac{d\Delta}{\Delta} \, K_1(2mR\Delta) \, d(\Delta) - \frac{K_0(2mR\lambda)}{Rm} \int_0^\infty dr \left(r^2 \theta'^2 + 2 \sin^2 \theta \right) \right\} ,$$

where

$$d(\Delta) = \int_0^\infty dr_1 \left\{ \left[C_1' C_2 \left(r_1^2 - \Delta^2/2 \right) + \left(\frac{S_1}{r_1} \right)' \frac{S_2}{r_2} \left(r_1^4/2 - r_1^2 \Delta^2 + \Delta^4/4 \right) + \frac{1}{2} (S_1 r_1)' S_2 r_2 \right] \Big|_{r_2 = |r_1 - \Delta|}^{r_2 = r_1 + \Delta} \right.$$
$$\left. + S_1 \int_{|r_1 - \Delta|}^{r_1 + \Delta} S_2 \, dr_2 \right\} \, , \quad C_i \equiv \cos \theta(r_i) \, , \quad S_i \equiv \sin \theta(r_i) \, , \quad f_i' \equiv \frac{df_i}{dr_i}$$

stems from the trace $Tr\, V(x_1) V(x_2)$ and all distances are measured in units of the hedgehog "radius" R (K_0 and K_1 are the Bessel functions of imaginary argument).

One sees that E_{nonloc} goes to zero for both $R \to 0$ and $R \to \infty$. A numerical estimate shows, however, that there is a minimum of E_2 for $R \approx 0.3$ fm (cf. the fig. for the parametrization $\theta(r) = 2 \arctan (R/r)^2$). This can be interpreted as an indication for the formation of a bound state of pions with baryon number one.
Of course, all numerical values should be taken with care due to the possible influence of higher order effects and to the importance of heavy mesons at small distances.

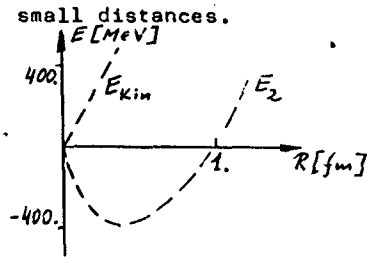

References:

/1/ Ebert D. and H. Reinhardt: Nucl. Phys. A271 (1986) 188

/2/ Dyakonov D.I. and V.Yu. Petrov: preprint INPI 1162 (1986)

FROM QUARK FLAVOUR DYNAMICS TO A CHIRAL SOLITON MODEL WITH DYNAMICAL RESTORATION OF CHIRAL SYMMETRY

H. Reinhardt and B. Kämpfer

Zentralinstitut für Kernforschung, Rossendorf, Bereich KF

Effective meson Lagrangians derived from Nambu Jona-Lasinio type of quark flavour dynamics have proved successful in describing low-energy meson physics /1/. These effective Lagrangians are usually calculated in a gradient expansion around the meson field configuration of the vacuum corresponding to the phase with spontaneously broken chiral symmetry. Here we report an effective meson theory derived from the Nambu Jona-Lasinio model in a generalized heat kernel expansion /2/ around a space time dependent chiral radius field configuration $\phi(x)=\langle\bar{q}q\rangle$ (for details cf. /3/). The resulting chiral meson Lagrangian reads

$$\mathcal{L} = \frac{1}{2}C(\phi)\partial_\mu\phi\,\partial^\mu\phi - V(\phi) - \frac{1}{4}F_\pi^2(\phi)\,\mathrm{tr}\,L_\mu L^\mu + \frac{1}{32e^2}\,\mathrm{tr}\,[L_\mu,L_\nu][L^\mu,L^\nu] \qquad (1)$$

with $e=2\pi$ and $L_\mu = U^+\partial_\mu U$ being the left current of the chiral field $U(x)\in SU(2)_l \times SU(2)_r / SU(2)_l$. Here

$$V(\phi) = \frac{\phi}{2g} + \frac{N\Lambda^4}{8\pi^2}\,\hat{F}\left(\frac{\phi^2}{\Lambda^2}\right), \quad \hat{F}(z) = e^{-z} - z\left(e^{-z} - z\,\Gamma(0,z)\right), \qquad (2)$$

is the effective potential of the chiral radius field ϕ and $C(\phi)=N(\Gamma(0,\frac{\phi^2}{\Lambda^2}) + \frac{2}{3}\exp(-\frac{\phi^2}{\Lambda^2}))$ is a kinetic coefficient. Furthermore

$$F_\pi^2(\phi) = \frac{N}{4\pi^2}\,\phi^2\,\Gamma(0,\phi^2/\Lambda^2) \qquad (3)$$

(N: number of colors, Γ: incomplete gamma function) is a dynamical pion decay constant and Λ is a Euclidian cutoff. The effective potential (2) has the typical "mexican hat" shape and decribes the spontaneous breaking of chiral symmetry in the vacuum where $V'=0$. By putting the vacuum value of the pion decay constant $F_\pi(\phi_0)$ to its physical value of 93 MeV, the cutoff Λ can be fixed in dependence on the vacuum value of ϕ_0, which represents the constituent quark mass.

We have calculated the soliton model solution by exploiting the hedgehog ansatz for the chiral field with winding number one. In Fig. 1 we show the order parameter ϕ and the chiral angle Θ for the soliton as function of the radius. The partial chiral symmetry restoration in the soliton center is a consequence of the symmetry breaking potential V. In case of $\phi=\phi_0$ our model degenerates to the standard Skyrmion model with an energy of 1080 MeV for fixed coupling constants. Our model explains why in almost all chiral soliton models the pion decay constant has to be reduced by about 30% to bring the soliton energy down to the nucleon mass.

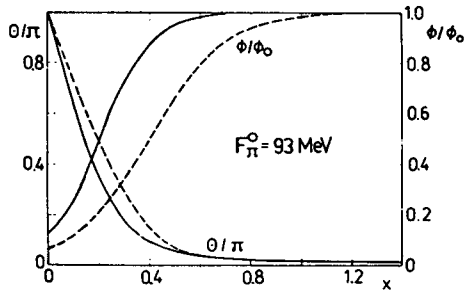

Fig. 1: The chiral angle Θ and the scalar field ϕ as function of the radius $x=rF_\pi(\phi_0)$ (full lines: ϕ_0=320 MeV, Λ=667 MeV, g=0.971, dashed lines: ϕ_0=150 MeV, Λ=2510 MeV, g=0.535).

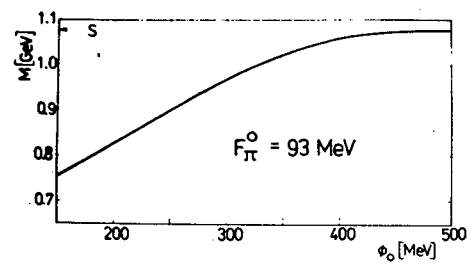

Fig. 2: The soliton mass as function of the constituent quark mass ϕ_0. S denotes the Skyrmion mass.

REFERENCES

/1/ Reinhardt, H., and Ebert D.; Nucl. Phys. B271 (1986) 188 and references therein

/2/ Reinhardt H.; Ann. Phys. in print

/3/ Reinhardt H., and Kämpfer B.; to be published

ANALYSIS OF THE ISOTROPIC LAMBDA-PARTICLE EMISSION IN C+C COLLISIONS AT 3.66 A*GEV

H. Iwe

Zentralinstitut fuer Kernforschung Rossendorf, Bereich KF

At the Dubna synchrophasotron the production of lambda particles was investigated in the reaction C+C at a bombarding energy of E/A=3.66 GeV [1]. The angular distribution dN/dcosθ' (in the NN-system) of the lambda particles stemming only from central collisions shows a remarkable unexpected degree of isotropy (fig. 1d). The lambda particles produced in the elementary reaction p+p ---> lambda + X in the energy region of interest are anisotropicly distributed (fig. 1a) and have a marked forward-backward symmetry. In the reactions {He+Li, C+C} ---> lambda + X without any trigger conditions the Dubna experimentalists have found angular distributions with the same behaviour reflecting the fact that these reactions can be understood to a good approximation as a sum of independent nucleon-nucleon collisions. Central collisions between carbon nuclei including all nucleons of the system into the interaction show the isotropic lambda emission as mentioned above.

This experiment was analysed using our intranuclear cascade code CASIMIR [2]. This code models the interaction process of heavy ions as a sequence of binary collisions of freely moving hadrons. The production of lambda particles proceeds via either direct nucleon-nucleon encounters or else via secondary pion-nucleon encounters. Mean field effects are neglected. Casimir includes completely the rescattering effects of the lambdas with the surrounding matter. The Lamda particles produced via pp ---> NKlambda have been distributed according to $w(\cos\theta')=(1+3\cos^2\theta')/4$ representing a good fit to experiment (fig. 1a). The calculated lambda distribution (fig. 1b) of the reaction C+C differs only somewhat from the input distribution w. On the other side, outgoing from an isotropic input w=1/2 the calculation leads to obviously anisotropic distributed lambdas (fig.1c). In order to compare with experiment the distribution in figs. b) and c) are averaged according to the experimental intervals (fig. 1d). Finally an anisotropic distribution is contained the side points of which lie clearly outside the experimental unaccuracy. The CASIMIR calculations show a lambda emission favoured in forward-backward direction. The considerable pion induced lambda production (about 35%) increases the anisotropy further. In conclusion one can state: on the basis of binary collisions it is impossible to understand the isotropic lambda production in central C+C collisions. Maybe, here, a hint has been found that a new mechanism is at work.

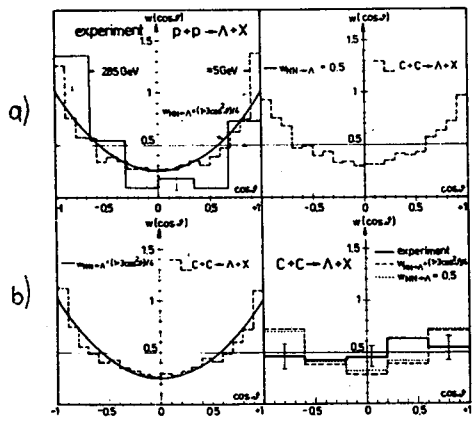

Fig.1
Angular distributions dN/dcosθ' of lambda particles in the NN-system. Fig. a) shows two experiments p+p--->lambda + X together with the fit (full curve) used in CASIMIR. The experiment C+C--->lambda + X (full line in fig. 1d) is compared with CASIMIR calculations.

References:

[1] M. Anikina et al., Z. Phys. C25(1984)1
M. Gazdzicki et al., Dubna report E1-85-949

[2] H.W. Barz and H. Iwe, Nucl. Phys. A453(1986)728

INVESTIGATION OF Σ HYPERNUCLEI IN THE FRAMEWORK OF THE CONTINUUM SHELL-MODEL

R. Wünsch
Zentralinstitut für Kernforschung Rossendorf, Bereich KF

J. Žofka
Nuclear Physics Institute, Czech. Acad. Sci., Řež/Prague, Czechoslovakia

Σ single-particle properties

Numerical calculations showed that the use of the harmonic oscillator potential for the description of Σ hyperons bound in nuclei may be misleading. Binding energy and radial wave function calculated in the more realistic Woods-Saxon potential deviate essentially from the oscillator values, in particular for states close to the threshold and, for angular momenta $l < 2$, above the threshold. These differences are much more important than in the case of nucleons or Λ hyperons, since the average Σ-nucleus potential is still shallower than the Λ potential /1/. The calculations performed have shown that, for light Σ hypernuclei ($A \lesssim 16$), quasi-bound states with $l=1$ do not exist for central potentials with a depth $15\ \text{MeV} \lesssim V_{re} \lesssim 25\ \text{MeV}$ and an arbitrary value of the spin-orbit potential. This is in contradiction to the interpretation of the measured A = 12,16 Σ hypernuclear systems/2/. On the other hand, our calculation stresses the role of atom-like states with a Σ^- hyperon bound mainly by the attractive Coulomb force with a mean square radius of the orbit several times larger than the nuclear radius.

Resonant and quasi-free mechanisms of strangeness transfer

Due to the shallow Σ- nucleus potential, the quasi-free process turns out to give a considerable contribution to the (K^-, π) cross section in the region of Σ production even at small or vanishing momentum transfer /3/.

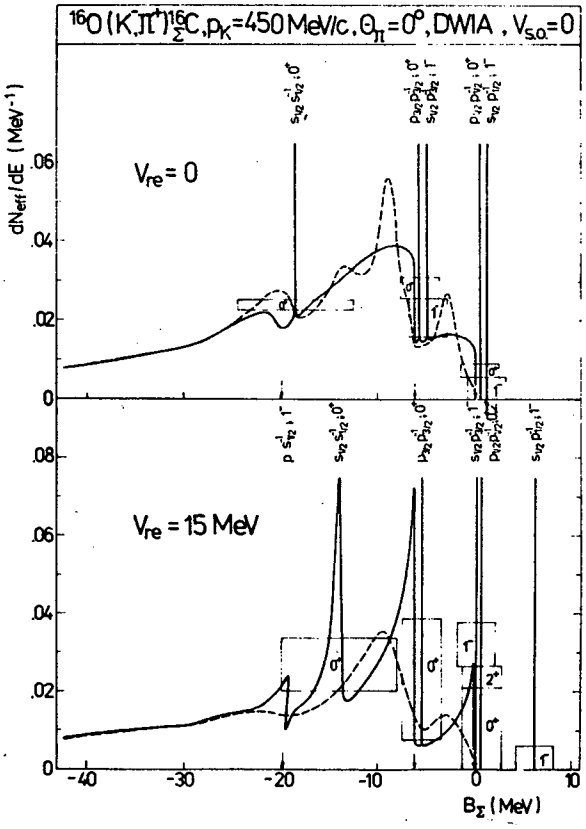

Fig. 1
Calculated $^{16}O(K^-, \pi^+)^{16}C$ spectra vs. Σ binding energy B_Σ for two values V_{re} of the average Σ- nucleus potential, and a vanishing spin-orbit potential $V_{s.o.}$. The arrows indicate the positions of the thresholds of 1h-disintegration channels. The broken lines show the quasi-free contribution, while the boxes indicate the excitation strengths of bound or narrow resonance states. Above the resonance peaks, their dominating 1p-1h structure has been displayed.

Threshold effects which are connected with a pronounced enhancement of the quasi-free process may simulate a resonant behaviour of the Σ hypernuclear system. (See fig. 1) On the other hand, the significant differences between nucleon and Σ hyperon radial wave functions diminish the excitation probability of bound and resonance hypernuclear states (indicated by the boxes in fig. 1). So the quasi-free knock-out of Σ hyperons may account for all the gross structure in the observed spectra. In this case, there is no reason for a strong spin-orbit splitting for Σ hyperons, as has been deduced on the basis of the dominating excitation of substitutional states /2/.

Σ hyperons in a complex nuclear potential

The Σ hyperon undergoes a strong conversion to Λ if it is surrounded by nucleons. In extended nuclear matter, this process is characterized by a width of 20-40 MeV which would cover all the nuclear structure. Nevertheless, structures narrower than 5 MeV have been observed for finite Σ hypernuclear systems. Up to now this discrepancy could not be unraveled and the conversion process is generally neglected in Σ hypernuclear structure calculations. The interpretation of the structures in the experimental spectra as threshold effects may solve this problem. If the observed structures are actually connected with the threshold behaviour of the quasi-free component rather than with the excitation of resonance states, their widths can be smaller. A Σ hyperon in a scattering state has a much smaller probability of meeting a nucleon and converting to a Λ than a Σ hyperon which moves in the nuclear interior.
We investigated the influence of the $\Sigma \rightarrow \Lambda$ conversion on the shape of the $^{16}_{\Sigma}C$ excitation spectrum measured in the (K^-, π^+) reaction on a ^{16}O target. The conversion process was taken into account by an imaginary part of 10 MeV depth in the average hypernuclear potential. Real and imaginary parts were taken to be proportional to the nuclear density. The calculation was performed in continuum shell-model approach /4/. We observed an additional decrease of the strength of the resonance excitations, while the threshold behaviour of the quasi-free process is almost unaffected. Moreover we noticed a remarkable difference between resonance states with a hyperon in deeply bound shells (e. g. in the hypernuclear ground state) and states with a hyperon in a weakly bound Coulomb state. While for the former a width of more than 10 MeV was calculated, for the latter we got less than 1 MeV. Their excitation probability, however, is too small to explain the observed structures.

References

/1/ Proc. Int. HF&K conf. (BNL 1985, ed. R.E. Chrien) Nucl. Phys. A450 (1986)
/2/ Hausmann R.,and Weise W.; Z. Phys. A324 (1986) 355
/3/ Wünsch R.,and Žofka J,; Phys. Lett. (submitted to Phys. Lett. B)
/4/ Barz H.W., Rotter I., and Höhn J.; Nucl. Phys. A275 (1977) 111

TWO-FLUID MODEL APPLIED TO ULTRA-RELATIVISTIC HEAVY ION REACTIONS

H. W. Barz and B. Kämpfer
Zentralinstitut für Kernforschung Rossendorf, Bereich KF
L. P. Csernai
NSCL, Michigan State University, East Lansing, Michigan 48824, USA
B. Lukács
Central Institute of Physics Budapest, H-1125 Budapest, Hungary

Heavy ions colliding with ultra-relativistic energies (E/A >10 GeV) are expected to penetrate one another. To describe this process the target and the projectile are represented by two fluids. If the rapidity difference of the two fluids is large, no particle can be transferred and only energy and momentum can be exchanged. Thus, the model is defined by two sets of equations of motion:

$$(n u^i)_{,i} = 0\,, \quad T^{ik}{}_{,k} = -D n \bar{n} (u^i - \bar{u}^i) \quad \text{and} \quad (\bar{n}\bar{u}^i)_{,i} = 0\,, \quad \bar{T}^{ik}{}_{,k} = -D n \bar{n} (\bar{u}^i - u^i),$$

where n, u^i, and T^{ik} denote the baryon number density, the four-velocity and the energy momentum tensor of the target fluid while the barred quantities refer to the projectile. The coupling term can be related to the longitudinal rapidity loss Δy in a single nucleon-nucleon collision via $D = m\,\sigma_{in}\,\Delta y$, which we estimated to be 1.2 GeV fm^2. The local coupling has the consequence that the energy is conserved within the fluids. Therefore, the model is applicable only for not too high energies, presumably below 100 GeV. For larger energies the leak-out of energy from the fragmentation region into the midrapidity region has to be considered.

The equations are solved using an equation of state that allows for a transition from nuclear matter into the quark-gluon plasma /1/. To reduce the numerical expense only one spatial dimension was considered by investigating the collision of two slabs with thickness d. The energy density attained in the central part is shown in fig. 1 together with the baryon number density. For a thickness od 10 fm most of the matter is in the phase of a hot quark gluon plasma with an energy density of 2 GeV/fm^3.

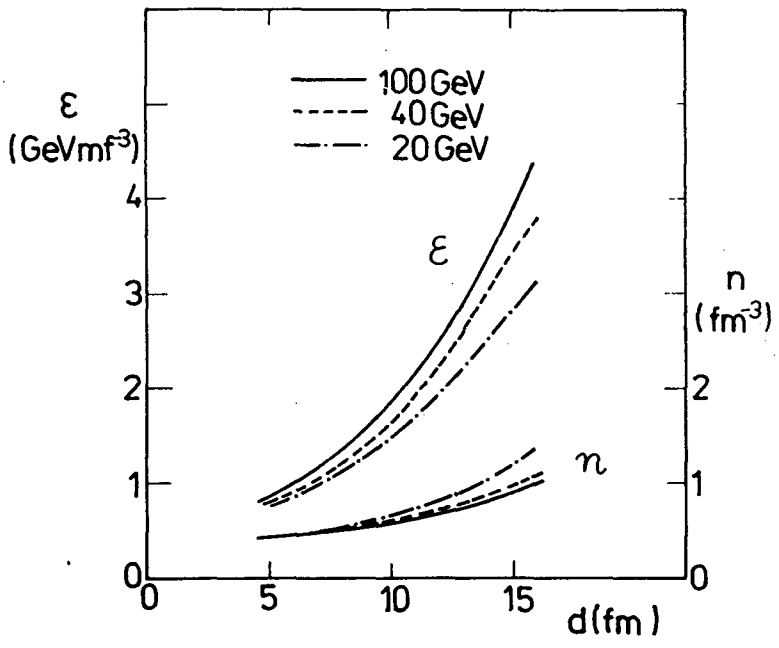

Fig.1. Maximum of energy density and particle number density as a function of slab thickness calculated using a relaxation time of 0.1 fm/c for the phase transition.

Reference
/1/ Barz, H.W. et al., Phys. Lett. 143B(1984)334

ISOTOPE DISTRIBUTION IN NUCLEAR MULTIFRAGMENTATION

H. W. Barz and H. Schulz
Zentralinstitut für Kernforschung, Rossendorf, Bereich KF
J. P. Bondorf and K. Sneppen
The Niels Bohr Institute, 2100 Kobenhavn Ø, Denmark
R. Donangelo
Universidade Federal do Rio de Janeiro, 21944 Rio de Janeiro, Brazil

Several models were developed to describe the process of multifragmentation of nuclei. Most of them were succesfully applied to analyse mass distributions. Now, we use the statistical model of multifragmentation /1/ to calculate the isotope distribution. This model considers the fragmenting nucleus in the moment of the break-up as a thermodynamic ensemble containing different partitions of the nuclear system. To each partition a temperature is attributed which is calculated using particle number, charge and energy conservation. The probability for the occurrence of a partition is taken to be proportional to the entropy factor exp(S). The isotope distribution of the hot fragments is shown in fig. 1 by the thin lines. This distribution is wider than observed in experiment. Taking into account the evaporation of particles from the hot fragments the isotope distribution becomes narrower and the most probable mass number is shifted to the β-stability line. Fig. 2 shows the good agreement to experimental results/2/ obtained in proton induced reactions on Kr.

As a consequence of this cooling process of the fragments the isotope distribution gives only little information about the break- up temperature.

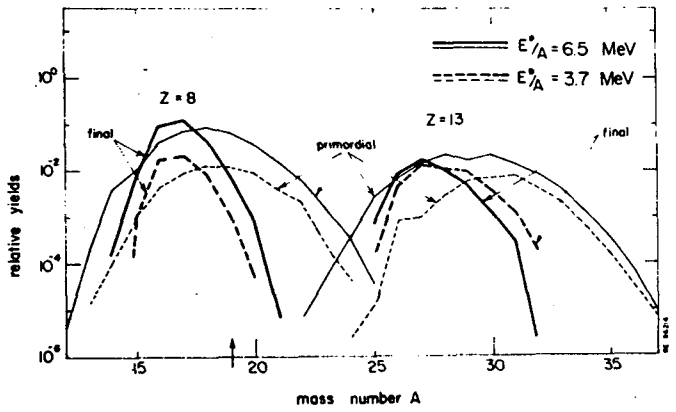

Fig.1. Primordial and final isotope distribution for two different excitation energies per particle of 3.7 MeV (dashed lines) and 6.5 MeV (solid lines) for charge numbers Z=8 and Z=13, respectively.

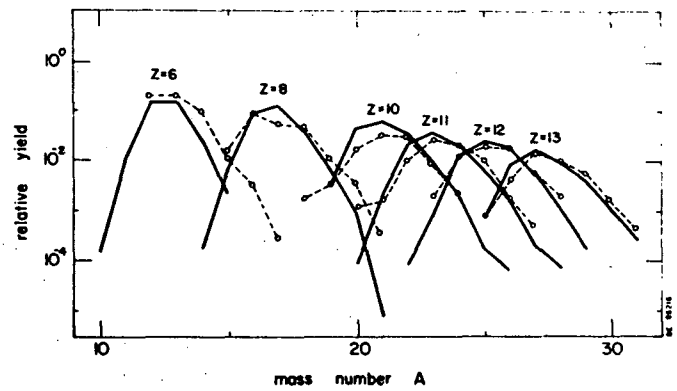

Fig.2. Calculated isotope distributions for different charge numbers Z compared to the data of ref./2/.

References

/1/ Bondorf, J.P. et al., Nucl. Phys. A443(1985)321 and Nucl. Phys. A444(1986)460
/2/ Hirsch, A.S. et al., Phys. Rev. C 29(1984)496

SITE-PERCOLATION APPROACH FOR MASS AND ISOTOPIC DISTRIBUTIONS IN FRAGMENTATION REACTIONS

O. Knospe, R. Schmidt
TU Dresden, Sektion Physik, Wissenschaftsbereich Theoretische Physik
H. Schulz
Zentralinstitut für Kernforschung, Rossendorf, Bereich KF

The production of nuclear fragments has been viewed as a percolation phenomenon. Former percolation models /1/ - /3/ are able to describe the trends of mass distributions only. To describe isotopic distributions the consideration of the isospin degree of freedom is necessary, what was introduced in ref. /4/. This isospindependent percolation model supplemented with isospindependent statistical weights reproduces the experimental features of mass and isotopic distributions in proton induced fragmentation reactions, as it is shown in figs. 1 and 2. The inclusive percolation picture used in ref. /4/ is an approximation of the exclusive percolation /6/ considering mass and charge conservation in every event.

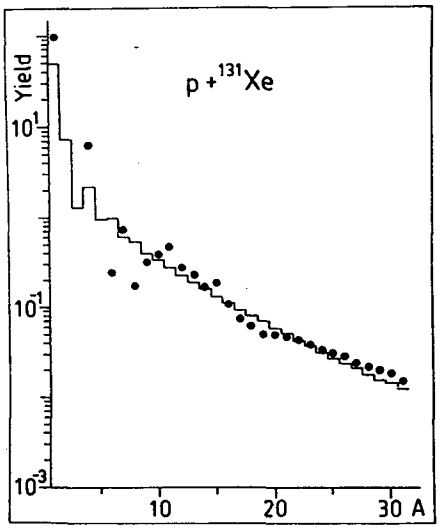

Fig. 1
Mass Distribution

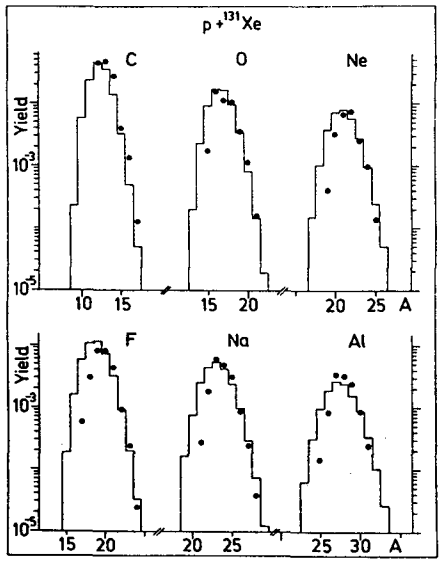

Fig. 2
Isotopic distributions

of the reaction p + Xe for incident protons between 8o and 35o GeV of ref. /5/ (dots) compared to the prediction of the percolation approach (lines)

References

/1/ Campi, X., and Desbois, J.; Proc. 23rd Int. Winter Meeting on Nuclear Physics, Bormio, 1985, p. 497
/2/ Bauer, W. et al.; Nucl. Phys. A452 (1986) 699
/3/ Biro, T.S., Knoll, J., Richert, J.; GSI Preprint 85-67, Nucl. Phys. A in press
/4/ Knospe, O., Schmidt, R., Schulz, H.; Phys. Lett. B182 (1986) 293
/5/ Hirsch, A.S. et al.; Phys. Rev. C29 (1984) 5o8
/6/ Knospe, O., Schmidt, R., Schulz, H.; to be published

SUBTHRESHOLD PION PRODUCTION AND STATISTICAL MULTIFRAGMENTATION IN NUCLEUS-NUCLEUS COLLISIONS

H.W.Barz and H.Schulz
Zentralinstitut für Kernforschung, Rossendorf, Bereich KF
J.P.Bondorf and J.Lopez
The Niels Bohr Institute, 2100 Copenhagen, Denmark
C.Guet
GANIL, 14021 Caen Cedex BP 5027, France

The mechanism for subthreshold production of pions in nucleus-nucleus collisions at a bombarding energy of some tens of MeV per nucleon is - despite many experimental and theoretical efforts - still an open problem. We investigated the probability for producing subthreshold pions at the late stage of heavy ion collisions when multifragmentation occurs. In doing so we assume that pions are in thermodynamical equilibrium with a given nucleonic system at break-up. If they are freely emitted or absorbed in a volume V, their number is given by

$$dN(A_o) = \frac{w(E-m_\pi-\varepsilon_\pi)}{w(E^*)-w(E^*-m_\pi-\varepsilon_\pi)}\, gV \frac{4\pi}{(2\pi\hbar)^3} p_\pi (m_\pi+\varepsilon_\pi)\, d\varepsilon_\pi \,,$$

where ε_π, p_π, m_π, g denote in turn kinetic energy, momentum, mass and degeneracy of the pion. The number of nuclear states for the total excitation energy E^* is denoted by $w(E^*)$ and depends on the mass number A_o. In the limit $\varepsilon_\pi + m_\pi \ll E^*$ the above formula goes over to Planck's formula for black-body radiation. The number of nuclear states at the freeze-out stage is evaluated by means of the statistical multifragmentation model /1/. The differential cross section is calculated according to

$$\frac{d\sigma}{d\varepsilon_\pi} = 2\pi \int b\,db\, \frac{dN(A_o[b])}{d\varepsilon_\pi}$$

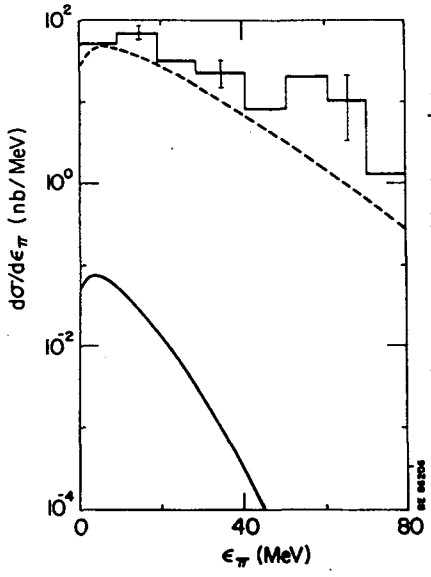

For illustration we consider the reaction $^{40}Ar + ^{40}Ca \rightarrow \pi^0 + X$ at 44 MeV/nucleon /2/. The results are shown in the figure. One sees that the multifragmentation scenario gives a much too small pion cross section, whereas the compound nucleus model (Fermi gas, dashed line) reproduces the data reasonably well enough. Thus we conclude that pions cannot coexist in the interaction volume together with fragments at break-up. If we rely on a statistical process for subthreshold pion production, the emission has to occur early enough before the hot participant zone expands and fragmentation may set in.

/1/ Bondorf, J.P. et al., Nucl.Phys. A443 (1985) 321; Nucl.Phys. A444 (1986) 460
/2/ Heckwolf, E. et al., Z.Phys.A315 (1984) 243

PROTON EMISSION IN AND OUT-OF PLANE WITHIN THE TSM

M. Biedermann and P. Mädler
TU Dresden, Sektion Physik, Wissenschaftsbereich Theoretische Physik

We apply the phenomenological two-stage-model (TSM) for fast particle emission /1/ to calculate the ratio of proton emission cross sections perpendicular ($\phi = 90^{\circ}$) and inside ($\phi = 0^{\circ}$) the reaction plane for different polar angles θ. Corresponding experiments /2/ have been performed for the $^{14}N + ^{197}Au$, E/A = 30 MeV reaction. Possible deviations of the reaction plane from the plane fixed by the fission fragments are taken into account in the same way as in the simple source-model interpretation of /2/ (averaging cross sections over ϕ with a Gaussian-like weight).

The calculated ratio of out-of-plane to in-plane coincidences is shown in Fig. 1 in comparison with the data. The experimentally observed trend of a preferential in-plane emission, especially for fast particles, is generally not reproduced by our calculations.

Owing to the fact that proton-proton correlations calculated within the TSM for similar reactions /3/ qualitatively reproduce experimentally observed /4/ V-shaped azimuthal correlations these discrepancies do not necessarily imply that the physical picture of the TSM fails: For a first look the present calculations have been performed without averaging out substantial unphysical structures in the momentum distribution of emitted particles arising from our pragmatic assumption of particles escaping only perpendicular to the surface of the hot zone.

Our treatment of possible fluctuations of the reaction planes cannot smooth out these structures in polar direction. Furthermore the ratio of cross sections at different angles is much more sensitive to those structures then the cross section itself. Hence, the variety of qualitative trends obtained for different polar angles θ might be a consequence of our "90°-approximation" /1/.

However, to check this statement a corresponding calculation would require two additional angle integrations, which is connected with a very high numerical expense. But only after that conclusions can be drawn from the comparison of TSM predictions with the experimental data.

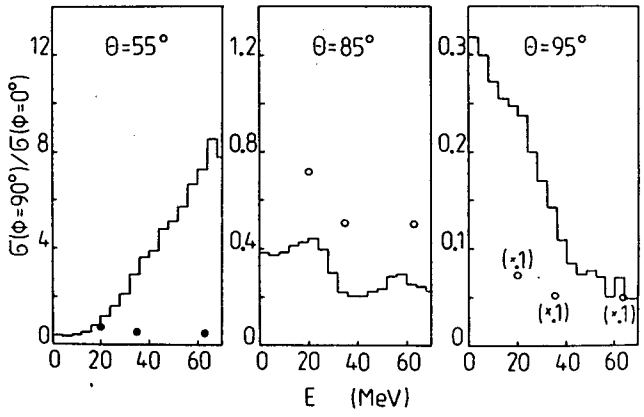

Fig. 1
Calculated ratio of out-of-plane to in-plane coincidences between fission fragments and light particles for 3 different angles θ as a function of proton energy. Experimental points available for $\theta = 55^{\circ}$ only (•) are also shown for a rough qualitative comparison in the other cases (o). Note the different scales.

References

/1/ Biedermann, M., Mädler, P.; Z. Physik A323 (1986) 315
/2/ Tsang, M.B. et al.; Phys. Rev. Lett. 52 (1984) 1967
/3/ Biedermann, M., Mädler, P.; ZfK-584 (1986) 34
/4/ Tsang, M.B. et al.; Phys. Letters 148B (1984) 265

SOME MODEL CALCULATIONS OF LINEAR MOMENTUM TRANSFER IN INTERMEDIATE-ENERGY HIC

M. Biedermann and P. Mädler
TU Dresden, Sektion Physik, Wissenschaftsbereich Theoretische Physik

The most probable amount of linear momentum transfer $\tilde{S} = \langle p_{\parallel} \rangle / p_i$ is an important gross property characterizing intermediate-energy heavy ioncollisions. Of special interest is the question to what extent $\tilde{S}$ is influenced by two-body dissipation (TBD). While in the simple momentum-space model of /1/ a substantial TBD (enhancement of the pure one-body (OB) results) must be incorporated to fit the data, the additional consideration of coordinate space as well of angular momentum has been shown in /2/ to have a similar effect.

We have proved the findings of /2/ by using a 3-dimensional generalization of the quantum-mechanical OB model described for one dimension in /3/. Since that model for any incident energy and mass number combinations only slightly overestimates the missing momentum carried away by fast particles in a corresponding TDHF evolution /3/ we claim that the corresponding 3D results for $\tilde{S}$ shown in Fig. 1 both for direct and inverse kinematics might be close to or somewhat smaller than corresponding (not-existing) realistic TDHF results. This means (cf. Fig. 1) that in the case of direct kinematics realistic TDHF values of $\tilde{S}$ really could be close to the data in contrast to the OB results of /1/ which are also shown in Fig. 1.

For the case of inverse kinematics our 3D-box results are close to unity (like in /2/). Besides the large c.m. momentum of the system this is connected with the fact that in TDHF /4/ as well as in our box model more particles escape in the direction from the smaller nucleus to the heavier one. TBD, however, is expected to at least partially balance this difference (rescattering of nucleons). Hence, a given amount of TBD should lower $\tilde{S}$ for inverse kinematics with respect to the OB result to a larger extent than enhance it in the case of direct kinematics. Consequently, deviations of experimental $\tilde{S}$ values in the inverse kinematics from unity might be more indicative for the role of rescattering than model comparisons in direct kinematics.

For further comparisons in Fig. 1 also results of model calculations within our two-stage model /5/ are included, which - by assumptions - incorporates also two-body effects. Some overestimations of the data probably indicates a slightly too small forward-peaking of preequilibrium particle emission.

Fig. 1 Ratio of transferred linear momentum to incident momentum for varying incident energy for central collisions.

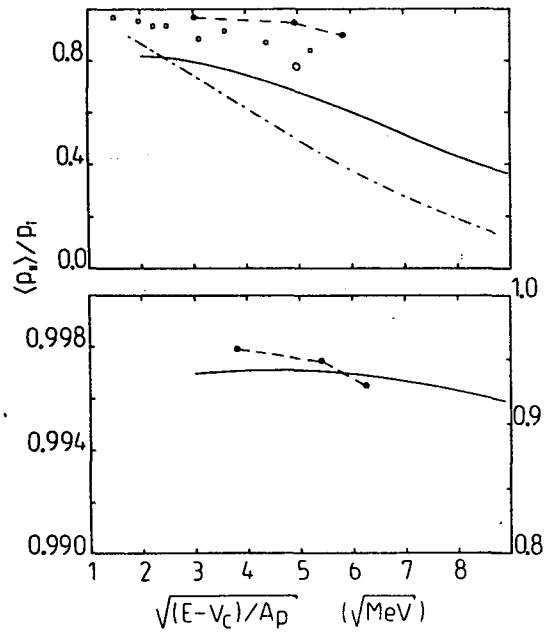

upper case: $^{20}Ne+^{197}Au$ reaction (Ne-projectile)
lower case: $^{197}Au+^{20}Ne$ reaction (inverse kinematics), r.h.s. for TSM results
meaning of the curves: •---• TSM, —— 3D-box model, -•- model calculation of /1/ (one-body part only)
o: exp. point for Ne+Au /6/
▫: some exp. points for different systems taken from /7/

References

/1/ Gregoire, C., Scheuter, F.; Phys. Letters 146B (1984) 21
/2/ Ngô, C., Leray, S.; Z.Phys. A322 (1985) 419
/3/ Biedermann, M., Mädler, P.; ZfK-584 (1986) 33
/4/ Mädler, P.; JINR Communication E7-84-690 (1984)
/5/ Biedermann, M., Mädler, P.; Z. Phys. A323 (1986) 315
/6/ LaRana, G. et al.; Nucl. Phys. A407 (1983) 233
/7/ Viola, V.E. et al.; Phys. Rev. C26 (1982) 178

RANDOMIZATION BY COLLECTIVE FLUCTUATIONS IN THE EARLY STAGE OF A HEAVY-ION COLLISION

P. Mädler
Technische Universität Dresden, Sektion Physik, Wissenschaftsbereich Theoretische Physik
L. Münchow and A. Pfitzner
Zentralinstitut für Kernforschung, Rossendorf, Bereich KF

Since collective fluctuations render effective with respect to a redistribution of occupation numbers ϱ_ν in the contact phase /1/, we apply the same mechanism to the approach phase of a nucleus-nucleus collision. Here, the approximations made in /1/ are not valid. Rather, we have to solve the coupled system for ϱ_ν and the variances /1/ χ, ξ and $\varphi = \langle \delta P^2 \rangle_t$, together with $i|\dot{\nu}\rangle_t \approx h(t)|\nu\rangle_t$, consistently on the computer. The master equation for ϱ_ν reads

$$\dot{\varrho}_\nu = \sum_\beta \int_0^\infty d\tau \left[\left(\chi(t)\cos\Omega\tau - \xi(t)\frac{\sin\Omega\tau}{\mu\Omega} \right) M^{(+)}_{\nu\beta}(t, t-\tau)(\varrho_\beta - \varrho_\nu) - \frac{\sin\Omega\tau}{i\,2\mu\Omega} M^{(-)}_{\nu\beta}(t, t-\tau)(\varrho_\nu \bar{\varrho}_\beta + \varrho_\beta \bar{\varrho}_\nu) \right], \qquad (1)$$

$$\text{with } M^{(\pm)}_{\nu\beta}(t, t-\tau) = F_{\nu\beta}(t) F_{\beta\nu}(t-\tau) \exp\left[i \int_{t-\tau}^{t} dt' (\varepsilon_\nu(t') - \varepsilon_\beta(t')) \right] \pm \text{c.c.}$$

The equations for the variances, together with the (ϱ_ν-dependent) transport coefficients, are quoted in /2/.

The projectile is simulated by a Woods-Saxon potential (V_0 = -50 MeV, α = 0.6 fm, R_0 = 4 fm), which approaches the HF-potential of the target nucleons with $\langle \dot{R} \rangle$ = 0.2 c. The initial conditions are taken at the instant t_0, where the s.p.-potentials begin to overlap: $|\nu\rangle_{t_0}$, $\varrho_\nu(t_0) = \theta(\gamma - \varepsilon_\nu)$, $\chi(t_0) = \xi(t_0) = \varphi(t_0) = 0$.

Preliminary results are shown in figs. 1 and 2 at t = t_0 + 40 fm/c (vanishing s.p.-potential barrier). A comparison with two-body collisions is made using an improved version of the collision term given in /3/. Fluctuations (*** in fig. 1) and two-body collisions (□ □ □) produce each a randomization of the same order of magnitude. Both mechanisms together (• • •) yield a significant amplification, especially for the continuum ($\varepsilon_\nu > 0$). This amplification is due to the reduction of Pauli blocking by the fluctuations. The s.p.-density profiles in fig. 2 exhibit a similar behaviour: the effect of fluctuations (——) is amplified if two-body collisions are added (○ ○ ○ ○). This effect is most important for nucleons outside the s.p.-potential (• • • • •), which is a hint for a new mechanism for pre-equilibrium particle emission.

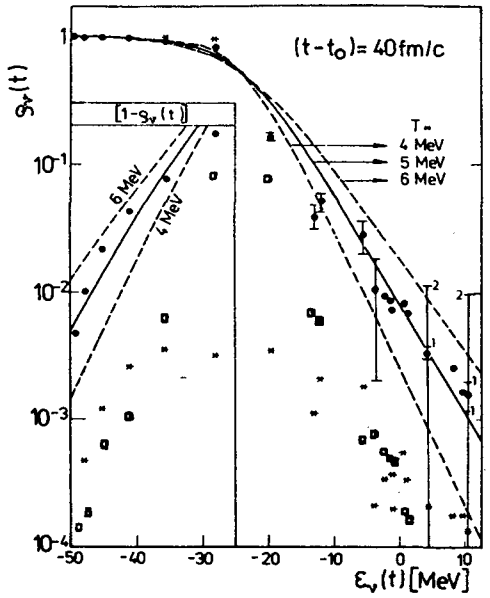

Fig. 1
Randomization of occupation numbers (see text). Fermidistributions for several temperatures are shown for comparison.

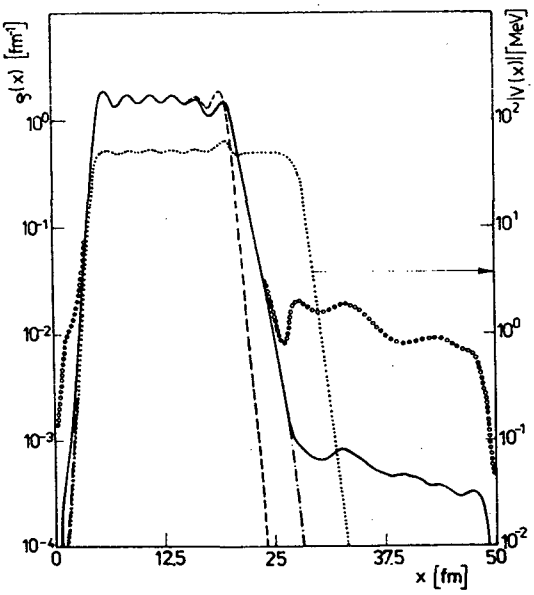

Fig. 2
Change of one-body densities (see text)
---- HF g.s.-state density of the target

References

/1/ Pfitzner, A. et al., this report, p. 56
/2/ Pfitzner, ZfK-596 (1986)
/3/ Wong, C.Y., K.T.R. Davies, Phys. Lett. B96 (1980) 258

FLUCTUATION-INDUCED RELAXATION IN ONE-BODY DYNAMICS

A. Pfitzner and L. Münchow
Zentralinstitut für Kernforschung, Rossendorf, Bereich KF
P. Mädler
Technische Universität Dresden, Wissenschaftsbereich Theoretische Physik

Simulating part of the evolution in a nucleus-nucleus collision by collective dynamics, we have to account for correlations between the collective $\{R,P\}$ and the intrinsic variables $\{x,p_x\}$. They produce not only fluctuation and dissipation in the collective subspace /1/, but also a "collision" term $I(\varrho^{(1)})$ in the equation for the one-body density /2/: $i\dot{\varrho}^{(1)} = [h(t),\varrho^{(1)}] + iI(\varrho^{(1)})$. We refer $\{R,P\}$ to the relative motion and suppose $\delta R = R - \langle R\rangle_t$ to be small. Then, $I(\varrho^{(1)})$ reads ($\bar{\varrho}^{(1)} = 1 - \varrho^{(1)}$)

$$I(\varrho^{(1)}) = \int_0^\infty d\tau \left\{ \left(\chi(t)\cos\Omega\tau - \left[\xi(t) + \frac{1}{i}\right]\sin\Omega\tau/2\mu\Omega \right) \left[F^I(t), \varrho^{(1)}(t-\tau) F(t-\tau) \bar{\varrho}^{(1)}(t-\tau) \right] + h.c. \right\}, \qquad (1)$$

with the collective variances $\chi(t) = \langle \delta R^2 \rangle_t$, $\xi(t) = \frac{1}{2}\langle [\delta P, \delta R]_+ \rangle_t$, the stiffness Ω^2 of the collective potential and the reduced mass μ. Intrinsic transitions are managed by the gradient $F = \partial V/\partial R$ of the coupling $V(x,R)$ ($F^I(t) = g^+(t,t')F(t)g(t,t')$, with $g(t,t')$ the mean-field propagator).

From (1), a master equation for the occupation numbers $\varrho_\alpha = \langle\alpha|\varrho^{(1)}|\alpha\rangle_t$ has been derived /3/. Supposed the evolution proceeds through a contact phase ($\langle\dot{R}\rangle$ small, $\Omega^2 > 0$) a relaxation time can be extracted which reads, for $\varrho^0(\varepsilon_\alpha) = \Theta(\zeta - \varepsilon_\alpha)$, within $\zeta - \Omega < \varepsilon_\alpha < \zeta + \Omega$,

$$\tau_\alpha^{-1} \approx 2g|F|^2 e^{-z\pi}\left[\chi(t) - \chi_0\right], \quad z = \Omega^2\tau^{*2}, \quad \int_0^t dt' \tau_\alpha^{-1}(t') = t/\tau_{eff}(t). \qquad (3)$$

Here, g = A/10 is a level density parameter, $\tau^* = 10^{-22}$ s the memory time, and $\chi_0 = [2\mu\Omega]^{-1}$ the zero-point fluctuation. Stable (damped) and unstable (exponentially increasing) solutions $\chi(t)$ are separated by the line $z = z_{cr}$ in the $\{z, |F|\}$-plane (fig. 1). It is the solution of $z/\tau^{*2} = \mathcal{K}^2(z)$, with $\mathcal{K}^2$ the feed back of the correlations on the collective potential /3/. When approaching this line from above ($z > z_{cr}$), τ_{eff} gets smaller than the collective relaxation time τ_{rel} and attains a few 10^{-22} s at $z \approx z_{cr}$. This is demonstrated in fig. 2, which shows relaxation times along a vertical cut of fig. 1 at $|F| \approx 0.4$ MeV/fm. Since equilibration times from two-body collisions are of the same order of magnitude we conclude that the fluctuation-induced relaxation may compete with two-body collisions if $z \approx z_{cr}$.

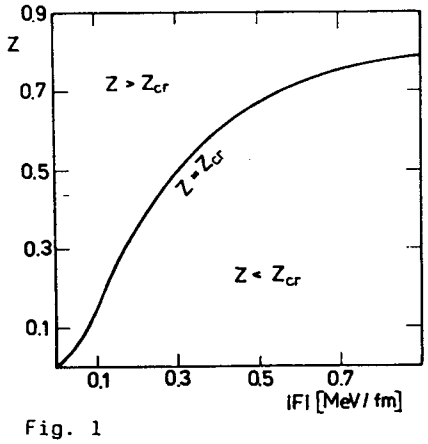

Fig. 1
The line of instability for $\chi(t)$
$A_1 = A_2 = A = 100$

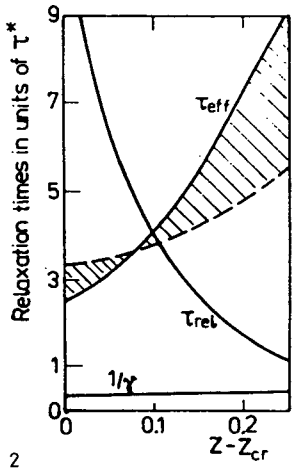

Fig. 2
Relaxation times near $z_{cr} = 0.6$
$\tau_{eff}(t=\tau^*)$: dashed line,
$\tau_{eff}(t=9\tau^*)$: full line
γ is the dissipation coefficient

References

/1/ Gross, D.H. et al., Nucl. Phys. A378 (1982) 375
/2/ Münchow, L., A. Pfitzner, Z. Phys. A314 (1983) 97
/3/ Pfitzner, A., ZfK-596 (1986)

VALIDITY OF THE LANDAU-ZENER FORMULA FOR QUASIELASTIC HEAVY-ION REACTIONS

B. Milek
Joint Institute for Nuclear Research, Dubna
R. Reif
TU Dresden, Sektion Physik, Wissenschaftsbereich Theoretische Physik

In order to test the validity of the Landau-Zener formula for particle promotion between molecular orbits numerical investigations of the same problem have been performed within a semiclassical description of the heavy-ion collision, including a realistic choice of the single-particle scheme of the radial coupling matrix element as well as of the trajectories for the relative motion of the collision partners. As an example we have chosen the inelastic excitation of the first $1/2^+$ state of ^{17}O in a $^{17}O + ^{13}C$ collision /1/, for which a pronounced avoided level crossing between two branches originating from the asymptotic $2s_{1/2}$ and $1d_{5/2}$ levels in ^{17}O occurs. The radial coupling matrix element as a function of the distance between the centers of the ions shows a long-range tail, which is responsible for a strong excitation of the upper level already at rather large distances. This behaviour which does not allow to localize the transition in a narrow region around the crossing point has been discussed in ref. /2/ (see fig. 1). By further calculations it has been confirmed that the jump probability reaches a saturation value even if the system passes the crossing region once with high collective velocity. As a function of the bombarding energy the two-way jump probability exhibits an oscillatory behaviour: it has a first maximum for incident energies near the barrier, which falls down rapidly (half-width of about 1 MeV) and a smaller peak (half-width of about 5 MeV) located at 2o MeV above the barrier, depending on the orbital angular momentum. Such a resonance-like structure cannot be understood within a diabatic picture of two independent jumps but is well known in molecular physics as an interference phenomenon between transitions in the entrance and exit stage of the reaction (Stückelberg phase in the expression for the two-way jump probability).

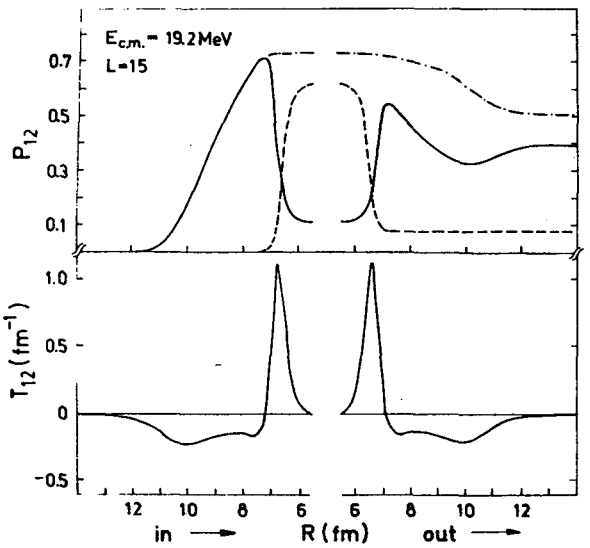

The importance of these features in the jump probability, which are not covered by the Landau-Zener formula, should be further explored.

Fig. 1
Radial coupling matrix element T_{12} and jump probability P_{12} for $^{17}O + ^{13}C$ (from ref./2/).

References

/1/ Cindro, N. et al.; Phys. Rev. C33 (1986) 128o
/2/ Milek, B., and Reif, R.; Phys. Lett. 157B (1985) 134

PHOTO- AND ELECTROEXCITATION OF ^{14}C AND ^{14}N

A. N. Golzov, N. G. Goncharova,
Institute for Nuclear Research, Moscow State University, Moscow, USSR

H. R. Kissener
Zentralinstitut für Kernforschung, Rossendorf, Bereich KF

For the 1p shell nuclei the data on inclusive and partial photodisintegration cross sections through the GDR region are more complete and consistent than those in other mass regions. Thorough checks of microscopic theories against the photonuclear data at photon energies below 50 MeV have been performed for the 1p shell nuclei (for reviews see /1,2/).

The corresponding data for the nucleus ^{14}C have been published only recently for the channels (γ, n_{tot}), $(\gamma,1n)$, $(\gamma,2n)$ and (γ,n_o). These cross sections differ in several respects from the trend observed for the neighbouring nuclei with g.s. isospin $T_o \neq 0$:
(i) there is only little structure in the pygmy resonance region $E_\gamma \lesssim 17$ MeV,
(ii) the $T_>$ GDR peak is found at relatively high energy, and
(iii) the $(\gamma,2n)$ process constitutes a significant part of the inclusive photoneutron cross section.

A shell model study with standard input can explain all important features of the experimental evidence. We have calculated the integral response, the expected prominent partial disintegration channels (γ,N_i) and the particle emission spectra for the decay chain $^{14}C \rightarrow {}^{13}C \rightarrow {}^{12}C$. The dominant disintegration branches of the GDR in ^{14}C feed the 15.1 MeV state in ^{13}C (about 25 %), the g.s. of ^{13}B (about 30 %) and the g.s. of ^{13}C (about 20 % of the dipole sum). In order to discriminate between model versions, more data on the partial disintegration channels are needed. Details are given in /3/.

The same model has been used to calculate excitation strengths, formfactors and disintegration channels of the stretched M4 configurations excited in backward electron scattering on ^{14}C and ^{14}N /4/. Recent high-resolution data for $^{14}C(e,e')_{18C^o}$ at momentum transfer $q \approx 250$ - 400 MeV/c show three narrow 4^- resonances at 11.72, 17.33 (T=1) and 24.3 MeV (T=2); theory reproduces both positions and relative strengths. The T=2 M4 resonance is a good candidate for searching for isospin impurity in the giant resonance region through partial disintegration channels. For the $^{14}N(e,e')$ data theory also provides a good description, but some ambiguity remains in assigning the M4 strength to the observed resonances (5^-, 4^-, 3^-; T=1). Estimates for the disintegration channels of prominent M4 stretched configurations in ^{14}N are given /4/.

References:

/1/ Goncharova, N. G., Kissener, H. R., Eramzhyan, R. A., Sov. J. Particles and Nuclei 16 (1985) 773
/2/ Kissener, H. R., Rotter, I., Goncharova, N. G., Fortschritte der Physik, in print
/3/ Goncharova, N. G., Golzov, A. N., Kissener, H. R., Nucl. Phys. A 462 (1987) 367
/4/ Golzov, A. N., Goncharova, N. G., Kissener, H. R., Nucl. Phys. A 462 (1987) 376

ON THREE-BODY FORCES

I. Rotter
Zentralinstitut für Kernforschung, Rossendorf

The difference between the nucleus and the atom consists in the fact that the central field in the atom, in which the electrons are moving, is created by the nucleus, while the nucleons inside the nucleus move in a central field created by the nucleons themselves. In this central field, essential cooperative aspects of the interplay between the constituent particles are involved. In a shell model description, the single nucleons of the nucleus differ therefore from free nucleons at least by the contribution they give to the central field. Accordingly, the shell model wavefunctions are mixed strongly in the basic wavefunctions in the case of the nucleus, while they are more or less pure in the case of the atom. The nuclear shell model is therefore characteristic of the nuclear many-body problem. A shell model for the description of the motion of one nucleon does not exist in contrast to, e.g., the description of the hydrogen atom where only one electron moves in the central field. But a shell model description has been used already for the four-nucleon system.

Because of the existence of highly excited states above particle decay thresholds, the nuclei should be described by taking into account the coupling to the continuum in a straightforward manner from the very beginning. In the Rossendorf continuum shell model /1/, the starting point is a standard nuclear structure calculation with inclusion of the single particle resonances into the space of bound single particle wavefunctions up to a certain cut-off radius. The coupling to the continuum, including the tails of the single-particle resonances beyond the cut-off radius, is taken into account by the same Hamiltonian $H = H_0 + V$ without additional approximations. The part V contains the residual two-body forces.

The corrections to the results of a standard nuclear structure calculation, which arise from the coupling to the continuum, are connected mainly with the correction term $H_{QP}G_P^{(+)}H_{PQ}$ to the Hamiltonian which takes into account the coupling via the continuum. Here, the Q subspace is the function space of the standard nuclear structure calculation with the Hamiltonian $H_{QQ} \equiv QHQ$, the P subspace is the function space of scattering states with the Hamiltonian $H_{PP} \equiv PHP$ and one particle in the continuum, $H_{QP} \equiv QHP$ etc. and $P + Q = 1$.

A consequence of the replacement of H_{QQ} in the shell model by H_{QQ}^{eff} in the continuum shell model is the appearance of some symmetry violation in the nuclear forces. The matrix elements of $H_{QQ}^{eff} - H_{QQ}$ are

$$\langle \phi_R | H_{QP} G_P^{(+)} H_{PQ} | \phi_{R'} \rangle = \sum_c \int_{\varepsilon_c}^{\infty} dE' \langle \phi_R | H | \xi_{E'}^{c(+)} \rangle (E^+ - E')^{-1} \langle \xi_{E'}^{c(+)} | H | \phi_{R'} \rangle \qquad (1)$$

where ϕ_R is eigenfunction of H_{QQ}, ξ_E^c is solution of the coupled channels equations $(E-H_{PP})\xi_E^{c(+)} = 0$ while c denotes a channel with threshold energy ε_c. The matrix elements (1) do not vanish also at energies where all channels are closed, i.e. for bound states. The eigenvalues of H_{QQ}^{eff} are real in this case, otherwise complex. The real part determines the energy, the imaginary part the width of the state.

The matrix elements (1) induce some charge dependence of the nuclear forces which has nothing to do with the problem of charge symmetry of the nuclear forces in nuclear matter or between free nucleons. This charge dependence is caused by the differences in the scattering wavefunctions ξ_E^c of neutrons and protons owing to the Coulomb interaction as well as by the different threshold energies ε_c for neutron and proton channels. The differences have, according to eq. (1), regularities with general many-body properties of the nuclei as, e.g., binding energy and shell closure /2/, which are in accordance with the trends observed in the Coulomb energy anomaly.

The success of including three-body forces into the calculations for the A = 3 system has been demonstrated by Sasakawa et al. /3/. The three-body forces in the A = 3 case may be of the same origin as the many-body forces (1) in heavier nuclei, since already for A = 4 or 5 the shell model with its cooperative effects can be used.

References

/1/ Rotter, I., Fiz. Elem. Chastits At. Yadra 15 (1984) 762 (translation: Sov. J. Part. Nucl. 15 (1984) 341; ZfK-508 (Rossendorf 1983))

/2/ Rotter, I., J. Phys. G 6 (1980) 185

/3/ Sasakawa, T., S. Ishikawa, Few-Body Systems 1 (1986) 3

SYMMETRY VIOLATION IN THE OPEN QUANTUM MECHANICAL NUCLEAR SYSTEM

I. Rotter
Zentralinstitut für Kernforschung, Rossendorf

The Rossendorf continuum shell model /1/ allows to describe the nucleus as an open quantum mechanical many body problem. The starting-point is a standard nuclear structure calculation with inclusion of the single particle resonances into the space of bound single particle wavefunctions up to a certain cut-off radius. The coupling to the continuum, including the tails of the single particle resonances beyond the cut-off radius, is taken into account by the same Hamiltonian $H = H_0 + V$ without additional approximations.

The corrections to the results of a standard nuclear structure calculation, which arise from the coupling to the continuum, are connected mainly with the correction term $H_{QP}G_P^{(+)}H_{PQ}$ to the Hamiltonian, which takes into account the coupling via the continuum. Here, the Q subspace is the function space of the standard nuclear structure calculation with the Hamiltonian $H_{QQ} \equiv QHQ$, the P subspace is the function space of scattering states with the Hamiltonian $H_{PP} \equiv PHP$ and one particle in the continuum, $G_P^{(+)}$ is the Green function for the motion of the particle in the continuum, $H_{QP} \equiv QHP$ etc. and $P + Q = 1$.

A consequence of the replacement of H_{QQ} by H_{QQ}^{eff} in an open quantum mechanical system is the appearance of some symmetry violation in the nuclear forces for finite nuclei which does not exist in nuclear matter. The nucleus is, indeed, an open quantum mechanical system in relation to the nucleon degrees of freedom. But the threshold for the emission of Δ isobars is so high in energy that the nucleus may be considered as a closed system in relation to these particles. As a consequence, the NN, $\Delta\Delta$ and Δ N correlations in finite nuclei are different /2/ although they may be the same in nuclear matter. The differences correspond to the differences in the effective nuclear forces used, e.g. in the standard shell model and in the continuum shell model calculations.

In the ansatz for the spin-isospin dependent particle-hole interaction, all corrections other than those considered explicitely are summarized in the parameter g' /3/. This parameter is obtained from a fit to the experimental data and involves, therefore, all the effects in finite nuclei which are connected with the coupling to the environment. This parameter should be assumed, for this reason, to be smaller for Δ isobars than for nucleons in finite nuclei although the universality of the spin-isospin correlation, suggested by the naive quark model, holds surely in nuclear matter /4/.

In a similar way, a small charge dependence of the nuclear forces is induced by the environment /5/ which has nothing to do with the problem of charge symmetry of the nuclear forces in nuclear matter.

References

/1/ Rotter, I., Fiz. Elem. Chastits At. Yadra 15 (1984) 762 (translation: Sov. J. Part. Nucl. 15 (1984) 341, ZfK-508 (Rossendorf 1983))

/2/ Rotter, I., Ann. Phys. (Leipzig) 43 (1986) 514

/3/ Migdal, A.B., Rev. Mod. Phys. 50 (1978) 107

/4/ Weise, W., Nucl. Phys. A 374 (1982) 505c

/5/ Rotter, I., Phys. G 6 (1980) 185

COOPERATIVE EFFECTS IN NUCLEI AND SELFORGANIZATION

I. Rotter
Zentralinstitut für Kernforschung, Rossendorf

The Rossendorf continuum shell model (CSM) /1/ describes the nuclear system as an open quantum mechanical many body problem. The starting-point is a standard nuclear structure calculation with inclusion of the single particle resonances into the space of bound single particle wavefunctions up to a certain cut-off radius. The coupling to the continuum, including the tails of the single particle resonances beyond the cut-off radius, is taken into account by the same Hamiltonian $H = H_0 + V$ without additional approximations.

The corrections to the results of a standard nuclear structure calculation, which arise from the coupling to the continuum, are connected mainly with the correction term $H_{QP}\, G_P^{(+)} H_{PQ}$ to the Hamiltonian, which takes into account the coupling via the continuum. Here, the Q subspace is the function space of the standard nuclear structure calculation with the Hamiltonian $H_{QQ} \equiv QHQ$, the P subspace is the function space of scattering states with the Hamiltonian $H_{PP} \equiv PHP$ and one particle in the continuum, $G_P^{(+)}$ is the Green function for the motion of the particle in the continuum, $H_{QP} \equiv QHP$ etc. and $P + Q = 1$.

The CSM /1/ allows to describe longliving states and shortliving ones in a unified manner and can therefore be used in order to investigate the interplay between the shortliving collective states and the longliving states of single-particle nature. The results of numerical calculations obtained show that the collective features of the nuclei may be identified with cooperative effects in self-organizing systems /2/. Structures in space and time are formed since all the resonance states have a finite lifetime due to their coupling to the continuum. The paradigm of synergetics formulated by Haken /3/ seems to be valid also for nuclear structure studies although the mathematical formalism used is completely different. Moreover, the concept of a value parameter defined by Eigen /4/ is included automaticaly into the nuclear structure studies /5/.

A proof of this statement consists in investigating processes which, although very improbable from a pure statistical point of view, may appear due to their large "selective value". A process of such a type is the emission of a high-energy particle in a nuclear reaction by leaving all the remaining nucleons in their energetical lowest states. The concentration of all the energy on one particle is the less probable the higher the available energy is and should be suppressed from a pure statistical point of view at high energies but favoured from the point of view of selforganization.

Another proof bases on the finite lifetime of the compound nucleus resonance states. All the memory to the entrance channel is lost in the limit of a very long lifetime of the resonance states as it has been assumed in the original definition of the compound nucleus. The opposite is true in the limit of a very small lifetime. The reaction proceeds in this case almost without formation of a compound nucleus. The existence of a finite lifetime of the compound nucleus, seen by means of entrance channel effects, points therefore to the fact that in the nuclear reaction considered, structures in space and time appear by self-organization. At high excitation energy, the lifetime of these (dissipative) structures is longer than expected on the basis of naive statistical models.

References

/1/ Rotter, I., Fiz. Elem. Chastits At. Yadra 15 (1984) 762 (translation: Sov. J. Part. Nucl. 15 (1984) 341; ZfK-508 (Rossendorf 1983))

/2/ Rotter, I., J. Phys. G 12 (1986) in press

/3/ Haken, H., Synergetics, Springer-Verlag 1978, and Advanced Synergetics, Springer-Verlag 1983

/4/ Eigen, M., Naturwissenschaften 58 (1971) 465

/5/ Rotter, I., ZfK-598 (Rossendorf 1986)

THE EFFECT OF ASYMMETRIC ION RANGE DISTRIBUTIONS ON THE MODELING OF OXYGEN DEPTH PROFILES IN IMPLANTED SOI STRUCTURES

H. U. Jäger
Zentralinstitut für Kernforschung, Rossendorf, Bereich KF

The phenomenological model [1] developed to describe the evolution of oxygen depth profiles during high dose oxygen implantation into silicon takes into account phenomena such as target swelling, surface sputtering, internal oxidation due to unbonded oxygen, and to a certain extent, also changes in ion range. The model has been generalized [2] to analyse tracer experiments [3, 4]. One finds that the computed oxygen profiles have an incorrect slope in the lower SiO_2/Si interface region (compare fig. 1).

One identifiable parameter in the calculations which can affect this slope is the ion range distribution used. Up to now this was assumed to be a simple gaussian for the pure silicon target (i.e. at low doses). It consisted of parts of three gaussians when a distinct buried layer is formed. If instead of gaussians the skew range distributions of oxygen ions in Si and SiO_2 reported in ref. [5] are adopted and put together by dose matching, we compute the new results shown in figs. 1 - 3.

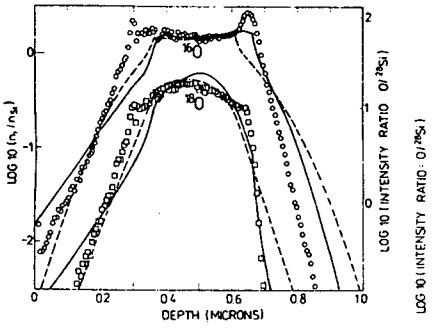

Fig. 1. ^{16}O and ^{18}O depth profiles in a Si sample after two successive implantations: (i) 200keV $^{16}O^+$ ions to a dose of 1.65×10^{18} cm^{-2}, (ii) 210keV $^{18}O^+$ ions to a dose of 3.5×10^{17} cm^{-2}. The theoretical profiles given refer to the left-hand scale and differ from each other by the use of symmetric (dashed lines, ref. [2]) or asymmetric (solid lines) ion range distributions. They are compared with SIMS data of Kilner et al. [3].

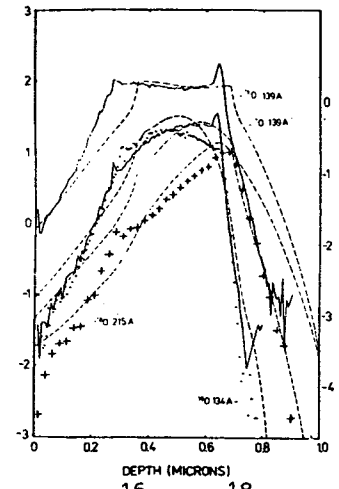

Fig. 2. ^{16}O and ^{18}O depth profiles in as-implanted samples. The SIMS profiles of ref. [4] for the implantation of ^{18}O ions into buried implanted oxide structures are compared with corresponding model results (dashed lines; right-hand scale).

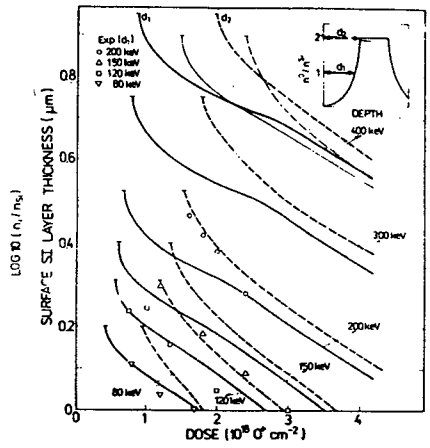

Fig. 3. Surface silicon layer thicknesses versus implanted oxygen doses for various implant energies. For E_{ion}=400keV, the present results are compared to those of ref. [2] (thin lines).

References

[1] Jäger, H. U.: Nucl. Instr. Meth. B 15 (1986) 748
[2] Jäger, H. U. et al.: to be published in Thin Solid Films
[3] Kilner, J. A. et al.: Nucl. Instr. Meth. B 7/8 (1985) 293
[4] Chater, R. J. et al.: IBMM'86 contr. III-31: to be published in Nucl. Instr. Meth. B
[5] Burenkov, A. F. et al.: Tablitsy Parametrov Prostranstvennogo Raspredeleniya Ionno-Implantirovannykh Primesei, Izdatel'stvo BGU im. V. I. Lenina, Minsk, 1980

ON THE LINEAR CASCADE THEORY FOR INHOMOGENEOUS TARGETS

M. Posselt, Zentralinstitut für Kernforschung, Bereich KF

Ion implantation into multilayer targets and into more complicate heterogeneous structures is increasingly used in processing steps of the modern microelectronic technology.
The linear cascade theory describes the phenomena in ion-beam induced collision cascades by linearized Boltzmann equations. For inhomogeneous targets we have to take into account the spatial dependence of the differential cross-sections in the collision terms of the equations. Further, in the case of inhomogeneity the Boltzmann equation cannot be transformed /1/ into the so-called "backward" form which is the fundamental relation of the well-known LSS(WSS) theory. Therefore we have to treat the "forward" equations. In this report we only consider the equation for the incident particles using the following assumptions: (i) The properties of the target only vary with the target depth x. (ii) At x=0 we have a stationary plane source of particles with normal incidence and initial energy E_0. Then our problem depends on: (i) the depth x, (ii) the energy E and (iii) the direction cosine of the particle motion with respect to the x-axis, η . We can derive the following equation for the particle flux $J(x,E,\eta) = F(x,E,\eta)\, v\, \eta$

$$\partial J/\partial x = St_n J + St_e J$$

$F(x,E,\eta)$ is the statistical distribution function. The collision terms $St_n J$ and $St_e J$ describe the interaction of the incident particles with the screened target nuclei and the target electrons, respectively. In the first part of $St_n J = St_{n1} J + St_{n2} J$ the energy transfers from the projectiles to the target atoms are greater than a threshold $T_{min} \ll E$. We obtain

$$St_{n1} J = \frac{C_x(x)}{\gamma(x)} \left[\int_{t_1'(x,E,T_{min})}^{t_2'(x,E,E_0)} dt \, \frac{f(t^{1/2})}{t^{3/2}} \int_{-1}^{1} d\eta' a(x,E,\eta,t,\eta') \frac{J(x,Ee(x,E,t),\eta')}{\eta'} - \int_{t_1''(x,E,T_{min})}^{t_2''(x,E)} dt \, \frac{f(t^{1/2})}{t^{3/2}} \frac{J(x,E,\eta)}{\eta} \right]$$

$$a(x,E,\eta,t,\eta') = \frac{\Theta(\sin\vartheta(x,E,t)(1-\eta'^2)^{1/2}+\eta-\eta'\cos\vartheta)\cdot\Theta(\sin\vartheta(1-\eta'^2)^{1/2}-\eta+\eta'\cos\vartheta)}{\pi\cdot(\sin^2\vartheta\,(1-\eta'^2) - (\eta-\eta'\cos\vartheta)^2)^{1/2}}$$

$$\cos\vartheta(x,E,t)=((m+M(x))/2m)(e(x,E,t))^{-1/2}+((m-M(x))/2m)(e(x,E,t))^{1/2} \qquad e(x,E,t)=(1/2)(1+(1+(4t\gamma(x))/(C_E(x)E)^2)^{1/2})$$

$$t_1'(x,E,T_{min})= (C_E^2(x)/\gamma(x))(E+T_{min})\cdot T_{min} \qquad t_2'(x,E,E_0)=C_E^2(x)\cdot\min((E^2/(1-\gamma(x)),E_0(E_0-E)/\gamma(x))$$

$$t_1''(x,E,T_{min})= C_E(x)^2E\cdot T_{min}/\gamma(x) \qquad t_2''(x,E)= C_E(x)^2\cdot E^2$$

m and M are the masses of the projectiles and the target atoms, respectively. C_E·E and C_x·x are the reduced energy and the reduced length and $\gamma = 4mM/(m+M)$. We assume that collisions with energy transfers below T_{min} do not change the direction of motion of a projectile. Further we take into account that $T_{min} \ll E$. Similar arguments can be applied to all collisions of the incident particles with the target electrons.We get the simple expressions

$$St_{n2} J = (C_x(x)/C_E^2(x)) \frac{\partial}{\partial E} \left[\int_0^{t_1''} dt \, \frac{f(t^{1/2})}{t^{1/2}} \frac{J(x,E,\eta)}{E\,\eta} \right] \qquad St_e J = \frac{\partial}{\partial E} \left[S_e(x,E) \frac{J(x,E,\eta)}{\eta} \right]$$

The electronic stopping power S_e and the function f for the nuclear scattering can be abtained from /2/. The solutions J of our equation have to obey the boundary condition $J(0,E,\eta) = J_0 \delta(E-E_0)\delta(\eta-1) + J_B(E,\eta)\Theta(-\eta)$. J_0 and J_B are the flux of the incident particles and a given flux of backscattered primaries, respectiveley. From J or F we can derive range profiles and other essential informations.Inserting $J=J_+\cdot\Theta(\eta) - J_-\Theta(-\eta)$ into the equation for J we obtain two coupled equations for $J_+$and J_-.For heavy ions and light target atoms we can neglect the contribution of $J_-$to J. The numerical treatment of the remaining equation for $J_+ \approx J$ shows analogies to the iteration schemes of Christel et.al./3/ and Ashworth et.al./4//5/ which have been successfully applied to range profile calculations in homogeneous and multilayer targets.In comparison with the iteration schemes our method has two advantages:(i)It is based on a consequent derivation from the Boltzmann equation.(ii)It is more general.

/1/ Sigmund, P. ;Topics in Applied Physics , vol. 47, ed. R. Behrisch (Springer, Berlin, 1981) p.9
/2/ Ziegler,J.F.,Biersack,J.P. and Littmark,U.;The Stopping and Range of Ions in Solids (Pergamon,New York,1985)
/3/ Christel, L.A., Gibbons, J.F. and Mylroie, S.; J. Appl. Phys. 51(1980) 6176
/4/ Ashworth, D.G., Moulavi-Kakhi, M. and Kranti V. Anand; J. Phys. C 17(1984) 2449
/5/ Moulavi-Kakhi, M. and Ashworth, D.G.; J. Phys. C18(1985) 1135

SCALING PHENOMENA OF PRIMARY CRYSTALLIZATION STUDIED BY COMPUTER EXPERIMENTS

H.-J. Müller and K.-H. Heinig
Zentralinstitut für Kernforschung, Rossendorf, Bereich KF

The term Primary Crystallization (PC) is used for the phase transformation of a metastable solid into a thermodynamically more stable modification, caused by nucleation and growth of nuclei. Besides the problem of the theoretical description of the rates of nucleation and growth, the process is characterized by complicated geometrical constraints inside the grain ensamble induced by grain impingement. This impingement causes a random network of grain boundaries within the final polycrystalline structure.

To study the kinetics of the network formation and its characteristics in the final structure, a computer simulation has been performed. The basic idea of the computer simulation is the combination of macroscopic formulae for the temperature dependence of nucleation and growth rate with an appropriate description of geometrical conditions, deviding space and time into suitable temperature dependent cells /1/. Simulations of isothermal transformations at various temperatures have been accomplished.

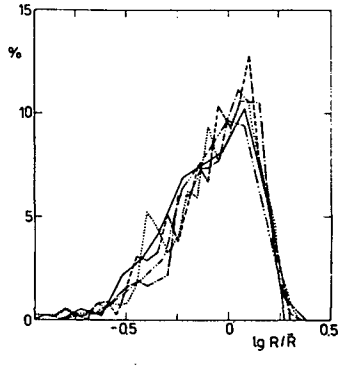

Fig.1: scaled grain-size distribution (—— 700K, -..- 800K, - - 1000K, -.- 1100K, and ... 1200K)

Two main features of the PC have been studied: (i) static analysis of the computer graphics of the final structures with respect to mean grain size, grain edge, and grain size distribution (Fig.1), and (ii) kinetic analysis of transient quantities of the crystallization process like normalized mean grain size (Fig.2), fraction of crystallized material, number of nucleated grains, exhaustion of the crystallizing interface, and exhaustion of the unrecrystallized volume.

Despite of the strong temperature dependence of the mean grain size and the duration of transformation, a fundamental statistical scaling behaviour has been found for the topological static features as well as for all kinetic parameters (see Fig.1 and Fig.2) using appropriate (temperature dependent) scaling factors. Universal laws for these parameters of PC have been found. This is rather surprising, because (i) these laws are independent of the ratio between the rates for nucleation and growth, which varies drastically within the investigated temperature range (800...1300K), and (ii) the computer graphics of the final polycrystalline structures seems to have pronounced differences.

This temperature independence leads to the conclusion that the statistical scaling behaviour must be a result of the topological features within the random network of grain boundaries. It has been pointed out by Rivier /2/ that random cellular networks, which fulfill the conditions of space filling, topological stability (see Ref. /2/), and equal physical constraints of network formation exhibit the same "most probable" cell size distribution of the final network.

The networks of grain boundaries of structures obtained from the computer simulation fulfill these conditions provided that random nucleation (with respect to space and time) and a constant ratio between growth and nucleation rates during transformation are assumed. Therefore, the mean grain size distribution corresponds to the "most probable" cell size distribution. The scaling behaviour of all the other parameters, also of the kinetic parameters, result from the discussed basic features of the random grain boundary network.

The investigation of the scaling phenomena of PC leads to a deeper understanding of analytical transformation formulae, their abilities and their limits of application, and it facilitates the interpretation of experimental data of PC and the transformation conditions.

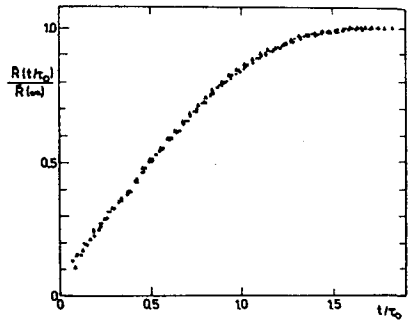

Fig.2: normalized mean grain size vs. scaled time (▲ 900K, ✖ 1000K, ✦ 1100K, and ● 1200K)

/1/ Müller, H.-J., Heinig, K.-H. and Hennig, K.; Computer Simulation of Primary Crystallization amorphous to crystalline, Proceedings of the E-MRS - Strasbourg, June 1986

/2/ Rivier, N.; Philos. Mag. 52 (1985) 795

COMPUTER STUDIES OF THE STATISTICAL DISTRIBUTION FUNCTIONS OF PARTICLES MOVING IN COLLISION CASCADES I: INCIDENT PARTICLES

M.Posselt, G. Otto, Zentralinstitut für Kernforschung, Bereich KF

Extensive informations about the evolution of the ion-beam induced collision cascades can be obtained from the statistical distribution functions of the particle species moving in cascades.
At first let us consider the incident particles. Our calculations are based on the following assumptions: (i) stationary irradiation, (ii) plane source of particles with normal incidence and initial energy E_0 at the target surface and (iii) linear cascades. Then our problem only depends on three variables: (i) the target depth x, (ii) the energy E of the particles and (iii) the direction of motion with respect to the x-axis, $\cos\theta$. Using the last Rossendorf version of the TRIM Monte Carlo simulation program /1//2//3/ we have logged the number of incident particles penetrating marker planes at x during dt with (E,dE) and ($\cos\theta$,d$\cos\theta$)

$$dJ = j(x,E,\cos\theta)\, dE\, d\cos\theta\, dt$$

The statistical distribution function f is obtained from the flux j by a simple transformation

$$f(x,E,\cos\theta) = j(x,E,\cos\theta)/(v\cdot|\cos\theta|) \quad \text{with} \quad v = \sqrt{2E/m}$$

m is the particle mass. The number of particles moving at time t in (x,dx) with (E,dE) and ($\cos\theta$,d$\cos\theta$) is given by $dF = f(x,E,\cos\theta)\, dE\, d\cos\theta\, dx$. Instead of the particle numbers dJ and dF we can define probabilities. For example,

$$d\tilde{J}_N = j(x,E,\cos\theta)\, dE\, d\cos\theta / \left(\int j(x,E,\cos\theta)\, dE\, d\cos\theta \right) = \tilde{j}_N(x,E,\cos\theta)\, dE\, d\cos\theta$$

is the probability that a particle penetrates the marker plane x with (E,dE) and ($\cos\theta$,d$\cos\theta$). The distributions $\left(\partial \tilde{J}_N(x,E)/\partial E\right) = \int j_N(x,E,\cos\theta)\, d\cos\theta$ and $\left(\partial \tilde{J}_N(x,\cos\theta)/\partial \cos\theta\right) = \int j_N(x,E,\cos\theta)\, dE$ are shown below. The two figures illustrate the spatial evolution of the incident particle beam for 50 keV As^+ implantation into Si. It is evident that the peak of the energy distribution must shift from E_0 at x=0 to E_f at sufficiently high values of x. E_f is the final energy in the simulation of the particle motion. We have chosen E_f=15 eV. Fig. 1 shows very broad energy spectra at small and medium depths. Therefore we can conclude that the energy distribution loses the memory of the initial energy E_0 at relatively small depths. On the other hand, the directional distribution in fig. 2 always shows a strong anisotropy which is determined by the direction of incidence at x=0.

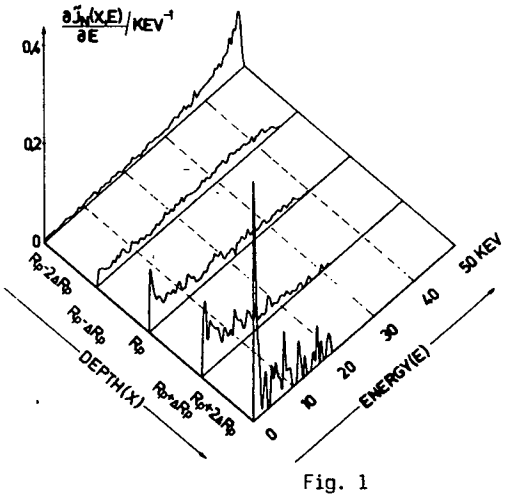

Fig. 1

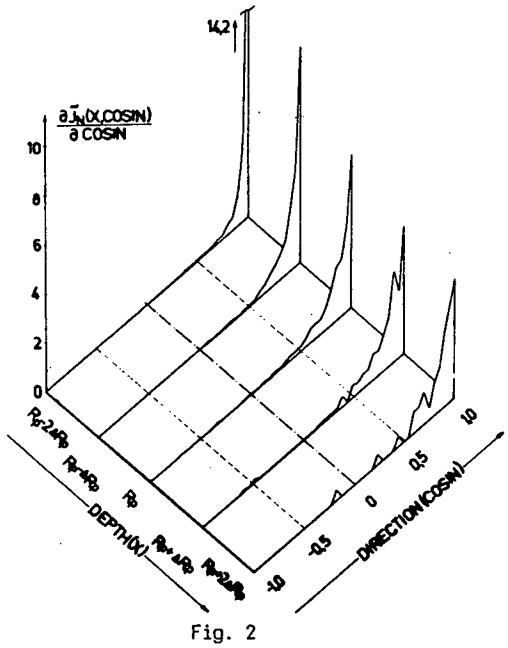

Fig. 2

/1/ Biersack, J. P. and Haggmark, L. G. ; Nucl. Instr. and Meth. 174(1980) 257
/2/ Posselt, M. ,Biersack, J. P. ; Nucl. Instr. and Meth. B15(1986) 20
/3/ Posselt, M. ;Phys. Status Solidi A94(1986) 403

COMPUTER STUDIES OF THE STATISTICAL DISTRIBUTION FUNCTIONS OF PARTICLES MOVING IN COLLISION CASCADES II: RECOILING TARGET ATOMS

M. Posselt, G. Otto, Zentralinstitut für Kernforschung, Bereich KF

The knowledge of the statistical distribution functions of the particles in cascades is not only important for the understanding of the surface effects (backscattering and transmission of the primary particles, sputtering of target atoms) but also for investigations of bulk phenomena (implantation, recoil implantation and mixing). In the present studies we have used the same assumptions as in part I /1/. Similar registration techniques for the recoiling target atoms have been employed. In contrast to part I we have to simulate the motion of all cascade particles which have a chance to penetrate the given marker planes. Target atoms begin to move if the energy transferred from a projectile exceeds the displacement energy E_d.

For 50 keV As^+ implantation into Si we have investigated the energy and directional distributions of the recoiling target atoms penetrating the markers at x. Two cases have been considered: (i) The histories of the particles have been followed until $E_f=E_d=15$ eV. (ii) Only recoils with energies $E \geq E_f = 5$ keV have been simulated. In both cases the energy distribution shows very marked peaks at E_f. The peaks have approximately equal heights at all marker depths. Therefore the great majority of the particles are always the recoils of the lowest energies. The thin high energy tails of the energy distribution are the remaining memory of the energy distribution of the incident particles /1/. The length of the tails decreases with increasing depth x. In the case of $E_f=15$ eV the energy distribution function decreases approximately proportional to $1/E^2$ in agreement with the Sigmund theory /2/. The directional distribution of the particles with energies $E \geq E_f = 5$ keV (fig. 2) shows a stronger anisotropy than the distribution of the recoils with $E \geq E_f = 15$ eV (fig. 1). This is evident since the distribution of the high energy recoils is more influenced by the directional distribution of the incident particles /1/. This influence decreases with decreasing energy and with increasing generation of the cascade recoils. The isotropic limit /2/ is given by the dashed lines. The spatial evolution of the directional distribution is not very pronounced. With increasing marker depth the fraction of the particles moving in a backward direction decreases slightly.

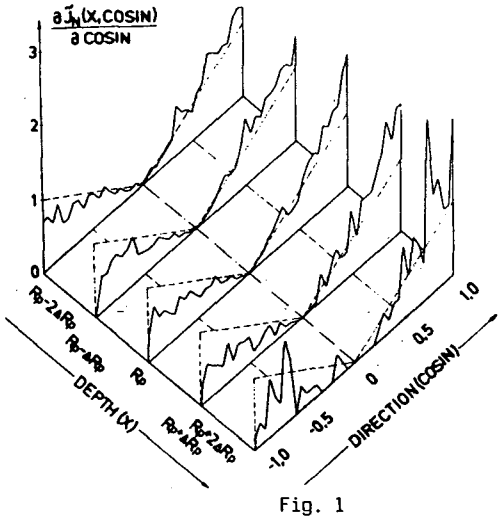

Fig. 1

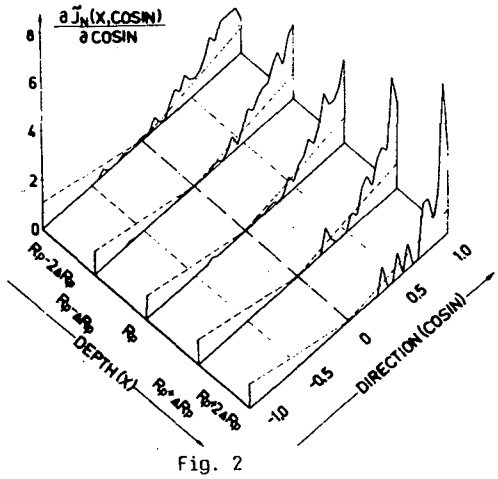

Fig. 2

/1/ Posselt, M. and Otto, G. ; this report p. 65

/2/ Sigmund, P. ; Topics in Applied Physics, vol. 47, ed. R. Behrisch (Springer, Berlin, 1981)

ON THE CALCULATION OF THE MULTIPLICITIES OF QUASICRYSTAL DIFFRACTION SPOTS

V. Heera and B. Rauschenbach
Zentralinstitut fur Kernforschung Rossendorf, Bereich KF

The position $\vec{Q}$ of every icosahedral Quasicrystal (i-QC) diffraction peak in the reciprocal space is given by formulae (1) in /1/. The diffraction spots can be indexed by a set of six integers (n_i), i=1...6. There are various reflexes $\vec{Q}_j$, j=1...M, with the same $Q=|\vec{Q}_j|$. The value M is called the multiplicity of the reflex. The knowledge of the multiplicities is important for e.g. the calculation of the intensities of diffraction rings obtained in powder diffraction experiments.

There exists a simple rule for the calculation of multiplicities in the classical crystallography: The multiplicity is the number of the possible permutations and sign changes of the 3 Miller indices. Because of the linearly dependence of the 6 basic vectors used in the i-QC indexing this rule is not valid. A straightforward computer calculation of the i-QC multiplicities is possible, but very expensive, because 6 integers must be varied independently. In this paper a simple algorithm for the calculation of the i-QC multiplicities should be presented.

Using the notation of Bancel et al. for the 6 Basic vectors given in /1/ and carrying out a simple index transformation $(n_i) \longrightarrow (N_i)$ defined by

$$N_1=n_1+n_2,\quad N_2=n_5-n_6,\quad N_3=n_3+n_4,\quad N_4=n_1-n_2,\quad N_5=n_5+n_6,\quad N_6=n_3-n_4$$

we can obtain Q^2 in the following form: $Q^2 = S + \tau * D$ with $\tau \approx 1.618$ the golden mean and $S=\sum N_i^2$. D can be splittet in 2 terms: $D = S_1 - S_2$ with $S_1=\{(N_1+N_2)^2+(N_3+N_4)^2+(N_5+N_6)^2\}$ and $S_2 = \{N_1^2+N_3^2+N_5^2\}$. Since S and D are integers and τ is a irrational number both are independently constant for all $\vec{Q}_j$ corresponding to a fixed Q. The high symmetry of the term S according permutations and sign changes is reduced by D. The expression D is only invariant under permutations and sign changes of the 3 sums (N_1+N_2), (N_3+N_4) and (N_5+N_6).

Let us now describe the steps of calculating the multiplicities of a reflex with given Q:
- Determine the terms S and D corresponding to the Q under investigation.
- Split up the term S in all possible ordered sets of 6 positive quadratic numbers $[|N_i|]_j$, $|N_1|>|N_2|>\ldots>|N_6|$ with j=1...z and z the number of possible sets.
- Take one of these sets and pick out from these 6 numbers all different ordered triples, which must be assigned to the numbers N_1,N_3,N_5. The residual 3 numbers are the complementary triple.
- Calculate the corresponding S_2 and $S_1=D+S_2$. There is the helpful restriction that S1 cannot be smaller than 0.
- Then split up the sum S_1 in 3 positive quadratic numbers and puzzle out whether there is a possibility to assign this numbers to the terms (N_1+N_2), (N_3+N_4) and (N_5+N_6) so that $|N_2|$, $|N_4|$ and $|N_6|$ are the numbers of the complementary triple. This step determines the sign of the numbers.
- The multiplicity of the found index set $(N_i)_j$ is then $M_{Qj}=2^3*3!/(q*2^m* \Pi m_k!)$ with q=1 for all N_i even or odd and q=2 for N_i of mixed type. m is the number of the zero number pairs $(N_i,N_j)=(0,0)$ and m_k the number of equal number pairs $(|N_i|,|N_j|)$, $(i,j)= (1,2),(3,4),(5,6)$, in the set $(|N_i|)$, i=1...6.
- Repeat this procedure for all sets $[|N_i|]_j$ with S=constant. The total multiplicity is then given by the sum of all M_{Qj}.

In conclusion it should be noted that the diffraction spots related to each other by scaling transformations described in /1/ and discussed also in /2/ have the same multiplicity. Thus it is possible to optimize the procedure described above by using the scaling laws to minimize the value of the sum S.

/1/ Heera, V. and Rauschenbach, B., this report p. 68
/2/ Elser, V. Phys. Rev. B32 (1985) 4892

SOME REMARKS ON THE INDEXING OF THE DIFFRACTION PATTERN OF ICOSAHEDRAL QUASICRYSTALS

V. Heera and B. Rauschenbach
Zentralinstitut für Kernforschung Rossendorf, Bereich KF

Since the discovery of the icosahedral quasicrystals (i-QC) /1/ many papers concerning the interpretation and calculation of the observed diffraction pattern have been published /2/. Because of the noncrystallographic icosahedral point group of the QC pattern, common crystallographic rules for indexing, calculation of multiplicities and intensities of the diffraction spots cannot be used. In addition, different notations in the QC description render the understanding in this matter more difficult and give raise to confusion. The aim of this paper is hence to present the connection between the index notations of Bancel et al. /3/ and Elser /4/. The position of every i-QC Bragg peak in the reciprocal space is given by

$$\vec{Q} = \pi/a^* \sum_{i=1}^{6} n_i * \vec{q}_i/q \qquad (1)$$

with n_i integer, often denoted by the index shorthand $(n_i)=(n_1,\ldots,n_6)$ analogous to the Miller indices in conventional crystallography. The 6 basic vectors $\vec{q}_i$ with length q can be selected from the 12 vectors pointing to the vertices of an icosahedron under the restriction $\vec{q}_i \neq -\vec{q}_j$ for all i,j. There are numerous possibilities to choose the basic vectors in this frame and hence there exist different index notations. The most common notations are given in /3/ and /4/. The connection between this 2 sets of basic vectors is presented in table 1. The co-ordinate reprensentation according Bancel et al. is also shown in this table.

Vectors $\vec{q}_i$ according /3/		$\vec{q}_1$	$\vec{q}_2$	$\vec{q}_3$	$\vec{q}_4$	$\vec{q}_5$	$\vec{q}_6$
	x	1	1	0	0	τ	$-\tau$
co-ordinate representation	y	τ	$-\tau$	1	1	0	0
	z	0	0	τ	$-\tau$	1	1
connection with vectors $\vec{e}''_i$ /4/		$q * \vec{e}_1''$	$-q * \vec{e}_6''$	$q * \vec{e}_2''$	$q * \vec{e}_5''$	$q * \vec{e}_3''$	$-q * \vec{e}_4''$

Table 1: $\tau = (1+\sqrt{5})/2$ is the golden mean; for further explanation see text

It is obvisious from table 1 that the same Bragg reflexes are denoted by different index sets, e.g. the (110000) reflex according Bancel corresponds to the $(10000\bar{1})$ reflex in Elser's notation. There are, however, still further complications in the QC indexing. Because of the self similarity of the QC the indexing is ambiguous in the sense that the diffraction pattern can be scaled (inflation and deflation rules) and then re-indexed. This means that the QC lattice constant a^* in formulae (1) is only defined up to a scaling factor s. Thats why the QC lattice constant follows from the work of Bancel (a^*=1.08 A) strongly differs from the one given by Elser (a=4.60 A). The connection between both is given by the scaling relation $a=s*a^*$ with $s=\tau^3$.

/1/ Shechtman, D., Blech, I., Gratias, D. and Cahn, J. W. Phys. Rev. Lett. 53 (1984) 1951
/2/ see e.g. Levine, D. and Steinhardt, P. J. Phys. Rev. B34 (1986) 596
/3/ Bancel, P. A. and Heiney, P. A. Phys. Rev. Lett. 54 (1985) 2423
/4/ Elser, V. Phys. Rev. B32 (1985) 4892

APPLICATION OF THE POINT KERNEL INTEGRATION METHOD TO THREE-DIMENSIONAL NEUTRON FLUX CALCULATION OUTSIDE THE HEXAGONALLY SHAPED LWR- CORES

F. Seidel[1)]
VEB Kombinat Kraftwerksanlagenbau, Berlin

The strong anisotropic neutron scattering on hydrogen supports the approximated determination of the neutron flux profile in the shield of light water reactors (LWR) using the method of unscattered neutrons. A simple and time saving problem solution can be performed by the well known point kernel integration method (PKM), which offers possibilities to use a flexible geometry mo del. The accuracy of the PKM-results sensitivdy depends on the point kernel parameters fitted to experiment-al results or to reference solutions of high order transport calculations /1/.

The PKM presented here is based on the separation of the whole neutron shielding problem in a one-dimensional multigroup-S_n-calculation to determine the point kernel parameters and a tree-dimensional one-group point kernel integration /2/.

For shield points $\vec{r}$ distributed three-dimensionally the point kernel integration determines the neutron flux spectrum part above the energy limit E_0 (usual 1.0 or 0.5 MeV)

$$\varphi_{E_0}(\vec{r}) = \int_{E_0}^{\infty} \varphi(\vec{r},E)\,dE . \qquad (1)$$

The integration is carried out over all neutron source points $\vec{r}'$ of the source Volume V_c

$$\varphi_{E_0}(\vec{r}) = \int_{V_c} \frac{Q_{E_0}(\vec{r}')}{4\pi\,|\vec{r}-\vec{r}'|^2} \exp\left[-\tau_{E_0}(|\vec{r}-\vec{r}'|)\right] d\vec{r}' \qquad (2)$$

in which the neutron flux contribution resulting from the source

$$Q_{E_0}(\vec{r}') = Q(\vec{r}') \int_{E_0}^{\infty} \chi(E)\,dE \qquad (3)$$

is attenuated on the way $|\vec{r}-\vec{r}'|$ from the source to the shield point in consideration of the optical thickness

$$\tau_{E_0}(|\vec{r}-\vec{r}'|) = \int_0^{|\vec{r}-\vec{r}'|} \Sigma_{E_0}(s)\,ds . \qquad (4)$$

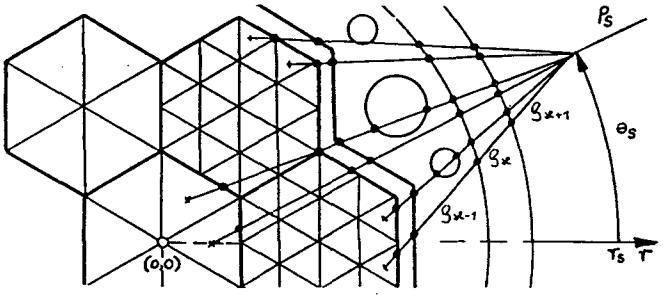

Fig. 1 Schematical representation of the geometry and the ray-tracing of a typical LWR-core-shield arrangement with hexagonally shaped assemblies.

$\chi(E)$ is the fission spectrum and $\Sigma_{E_0}(s)$ is the point kernel parameter depending on the material distribution and averaged over the energy range above E_0. In order to consider the material boundaries $\varkappa$ in eq. (4) the approximation

$$\tau_{E_0}(|\vec{r}-\vec{r}'|) \approx \sum_{\varkappa \in |\vec{r}-\vec{r}'|} \vartheta_\varkappa \Sigma_\varkappa \qquad (5)$$

is performed with respect to hexagonal, coaxial and eccentric-cylindrical boundaries. Such geometry options ensure the practicability of an exact ray-tracing through a core with hexagonally shaped and trigonally discretisated assemblies and through a typical light water reactor shield, s. fig. 1. For each assembly a regular trigonal fine mesh grid of an arbitrary mesh size may be chosen.

Eq.(2) is solved using a semi-analytical integration procedure. The integration along the z-direction is approximated by a sum of line integrals, which correspond to the axial boundaries. To accelerate the z-integration a suitable representation of the SIEVERT-integral table is used.

The efficiency of the method for calculating the neutron fluence of reactor shield materials was demonstrated by some model calculations. The first results offer that an improvement of the point kernel parameter fit will be necessary to obtain accurate fluxes /2/.

Reference

/1/ Wood, J., Computational Methods in Reactor Shielding, Pergamon Press, 1982, c. 6
/2/ Krell, J., Seidel, P., Kernenergie, to be published

1) Aspirant at TU Dresden, Sektion Physik, WB Theoretische Physik

APPLIED METHODS

PIXE INVESTIGATION OF $A_3^{II}B_2^V$-SEMICONDUCTORS

H.U. Frey, A. Hupfer+
Karl-Marx-Universität Leipzig, Sektion Physik, WB Angewandte Kernphysik
Karl-Marx-Universität Leipzig, Sektion Physik, WB Halbleiterphysik+

The XPS and PIXE methods have been used to determine the elemental composition of ultra-high vacuum prepared $A_3^{II}B_2^V$-semiconductors. A quantitative XPS (X-Ray Photoelectron Spectroscopy; information depth of about 5 nm) analysis is complicated by compositional changes due to the preparation (gentle ion bombardment, low temperature annealing) and uncertainties of XPS sensitivity factors. The information depth of PIXE (Particle-Induced X-Ray Emission Spectrometry) is in the range of about 5/um and quantitative application of this method is well established /1/.
Following the UHV-preparation and XPS-analysis the thick semiconductor crystals have been PIXE-analyzed with protons of 1.7 MeV energy and with proton currents between 0.5 nA and 2 nA. It took (40 - 90) minutes to collect charges of (2 - 5)/uC. The quantitative composition was determined using the thick target PIXE formalism /2/.
The quantitative results of both methods (table 1) are in an unexpected good agreement. The stoichiometric composition of the $A_3^{II}B_2^V$ materials with a slight deficiency of the B^V-component was confirmed. In the case of the $(Cd,Zn)_3As_2$ solid solution the PIXE results confirmed the nominal composition of the bulk material showing, that preparative influences disarranged the Cd/Zn ratio on the surface.
While the XPS results were normalized to 100 % absolute concentrations have been determined with PIXE. Only for one sample a total concentration of 100 % was obtained. The lower total concentration of the other samples showed the existence of contamination elements (C,O) that could not been analyzed by PIXE. Impurities of Fe and Cu (in the /ug/g region) could be found and some Cd was analyzed in Zn_3As_2.
Despite of the very different methods important conclusions could be drawn with regard to the analytical description of the UHV-preparation /3/ and the reliability of the used quantitative XPS formalism.

Sample		P	Zn	As	Cd	C	O	Sum
Zn_3P_2	stoich.	240	760	-	-	4.7	15.6	
	XPS	188	792	-	-			
	PIXE	193 ± 15	775 ± 15	-	-			968
Zn_3As_2	stoich.	-	567	433	-	9.2	4.9	
	XPS	-	583	403	-			
	PIXE	-	574 ± 15	411 ± 10	3.5 ± 1			988.5
Cd_3P_2	stoich.	155	-	-	845	9.5	4.2	
	XPS	143	-	-	843			
	PIXE	148 ± 20	-	-	852 ± 15			1000
Cd_3As_2	stoich.	-	-	308	692	34	23	
	XPS	-	-	295	648			
	PIXE	-	-	292 ± 10	688 ± 20			980
$(Cd,Zn)_3As_2$	stoich.	-	214	355	431	7.8	6.3	
	XPS	-	256	363	367			
	PIXE	-	212 ± 10	331 ± 10	424 ± 10			967

Table 1: Elemental composition (concentrations in mg/g) of the semiconductor materials which were supplied by the PAN-IFCS Zabrze (Prof. Dr. W. Zdanowicz)

- The authors thank the staff of the WB Physikalische Chemie (KMU) for the possibility of performing XPS measurements, expecially D. Hirsch for experimental cooperation.

References

/1/ Proc. 3rd PIXE Conference, Heidelberg 1983, Nucl. Instr. and Meth. B 3 (1984)
/2/ H. Frey, J. Vogt, G. Otto, J. Radioanal. Nucl. Chem. 99 (1986) 193
/3/ A. Hupfer, S. Schulze, D. Hirsch, W. Zdanowicz, Cryst. Res. Techn. (in press)

PROFILING OF (Al,Ga)As/GaAs HETEROSTRUCTURES BY EXPERIMENTAL AND COMPUTER-SIMULATED BACKSCATTERING SPECTRA

R. Flagmeyer, H.-E. Zschau, and A. Koch
Karl-Marx-Universität Leipzig, Sektion Physik, WB Angewandte Kernphysik

Quantum well $Al_xGa_{1-x}As$-GaAs structures require uniformity with respect of composition and thickness of individual layers, abruptness of interfaces and high crystalline quality. Recently, the thickness of the individual periodes in (Al,Ga)As-GaAs superlattices were accurately measured by backscattering spectrometry /1/. In order to determine depth profiles of composition of various $Al_xGa_{1-x}As$/GaAs heterostructures we emploied two methods:

(i) Comparison with computer-simulated spectra. The computer code RBSSIM /2/ was used to generate RBS-spectra of multilayered structures and of pure GaAs according to the experimental situation. In all cases thin slabs of 1 nm thickness are chosen. A Gaussian filter with an energy spreading Γ = 15...25 keV was applied for smoothing the generated spectrum to avoid statistical fluctuations.

(ii) Direct evaluation from experimental random backscattering spectrum. A marking routine allows the rapid analysis of multielemental and multilayered structures using an improved mean-energy approximation successively for each layer /3/.

An example of an $Al_xGa_{1-x}As$/GaAs(100) heteroepitaxial structure (T 2) is shown in Fig. 1. The best fit to the experimental spectrum by means of computer simulation (i) was achieved with parameters specified in Tab. 1. Mole fractions x and layer thicknesses are in excellent aggreement with the results using method (ii).

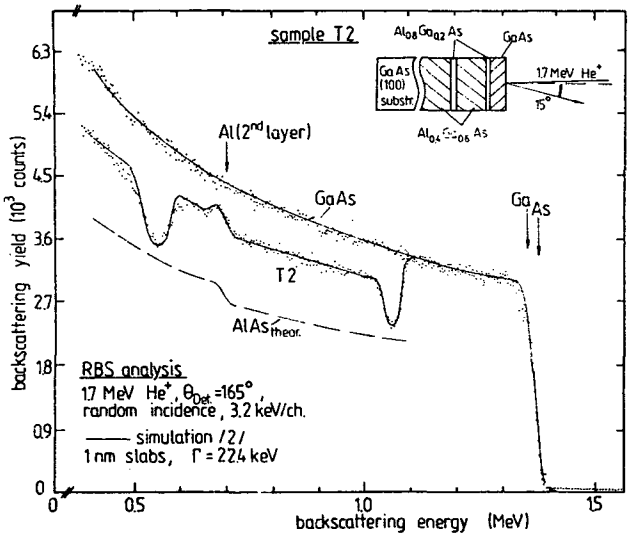

Figure 1:
Observed and simulated backscattering spectra from $Al_xGa_{1-x}As$ / GaAs multilayered structure compared to bulk GaAs

Table 1: Thickness (nm) / Al content x

Layer No.	1	2	3	4	5
Computer simulation	385 / 0	70 / 0.80	725 / 0.40	100 / 0.80	- / 0.40
Direct evaluation	379 / 0	73 / 0.84	733 / 0.39...0.42	103 / 0.82	- / 0.41

The detailed analysis of the first GaAs/$Al_{0.8}Ga_{0.2}As$ interface results in transition width of about 25 nm.

For both methods, the accuracy in measurement of thicknesses d and x values amounts to $\Delta d = \pm(0.05\ d + 5\ nm)$ and $\Delta x = \pm 0.02$, respectively.

R e f e r e n c e s

/1/ Hamdi, A.H., et al., Phys. Rev. B 31, 2343 (1985)
/2/ Zschau, H.-E., Annual Report ZfK-503, 74 (1983)
/3/ Koch, A., diploma work, Karl-Marx-University Leipzig, 1986; Chu, W.K., J.W. Mayer, and M.-A. Nicolet, Backscattering Spectrometry (Academic, New York, 1978)

MEASUREMENTS OF HYDROGEN INCORPORATION AND OF DAMAGE DENSITY ON PROTON BOMBARDED InP

C. Ascheron, V. Riede, H. Sobotta, R. Flagmeyer, C. Neelmeijer+
Karl-Marx-Universität Leipzig, Sektion Physik,
+Zentralinstitut für Kernforschung, Bereich KF

On proton bombarded InP single crystals we have studied the fluence dependences and depth profiles of the incorporated hydrogen, chemically bonded hydrogen and of the implantation induced damage density by use of particle induced γ-spectroscopy, infrared spectroscopy and Rutherford backscattering/channeling technique, resp.. Depth distributions were determined on bevelled samples ($\tan\alpha = 2 \cdot 10^{-4}$).
The investigations show that up to relatively high fluences ($D \approx 3 \cdot 10^{17}$ cm^{-2}) nearly the whole implanted hydrogen is retained within the implanted samples. The hydrogen distribution within InP (fig. 1) nearly coincides with the one measured on as implanted GaP /1/. H is partly contained chemically bonded to P atoms (but probably not to In atoms) as ir absorption measurements show (fig. 2, /2/) and partly contained in relatively stable small bubbles as indicated by scanning electron microscopy.

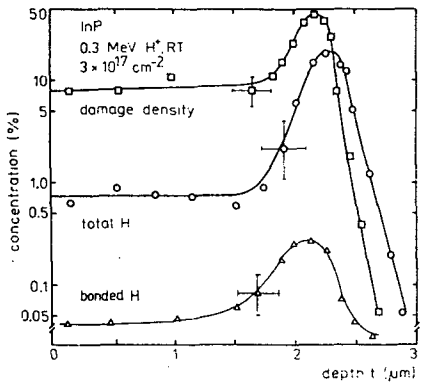

Fig. 1

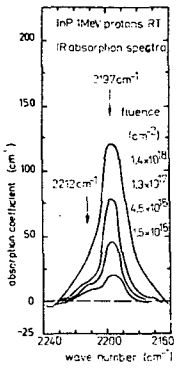

Fig. 2

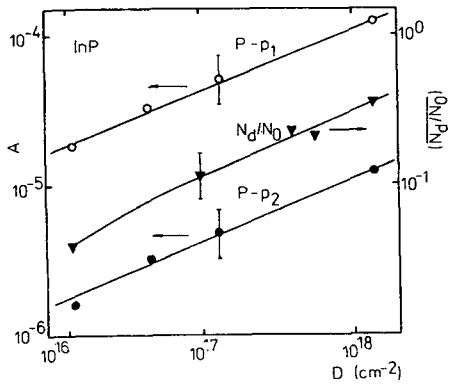

Fig. 3

Fig. 1: Depth profiles of damage density, of total H and of chemically bonded H.
Fig. 2: Variation of the ir absorption of InP due to the P-H valence vibration.
Fig. 3: Fluence dependences of mean damage density N_d/N_0 within the highly damaged region and of integrated absorption A in the ranges of the corresponding local modes shown in fig. 3.

The profile of bonded H is shifted against the one of total H towards the surface and agrees with the profile of radiation damage concerning depth and shape of the maxima. This fact as well as their qualitatively according fluence dependences (fig. 3) let conclude to a chemical bonding of H to P atoms at defect sites. Despite the accordance of the H distributions within as implanted GaP and InP and despite the higher corresponding damage density of InP, in InP about twice less H is bonded then in GaP. This result and the strong difference between the concentrations of bonded and total H (fig. 1) are due to a very low concentration of dangling bonds as indicated by electron spin resonance measurements. The concentration of dangling bonds is two orders of magnitude lower than the damage density. The formation of secondary defects is responsible for the mutual compensation of dangling bonds.

R e f e r e n c e s

/1/ C. Ascheron et al., phys. stat. sol. (a) 89, 740 (1985)
/2/ V. Riede et al., Solid State Comm. 47, 33 (1983)

MEASUREMENTS WITH THE ROSSENDORF HIGH ENERGY ION MICROPROBE

D. Grambole, F. Herrmann, W. Rudolph
Zentralinstitut für Kernforschung Rossendorf, Bereich KF

In the last year the microprobe /1, 2/ was used for first elemental analysis and mapping in the fields of medicine, material science, and corrosion. For this nondestructive ion beam analysis the following analytical methods are available: particle induced X-ray emission (PIXE), Rutherford backscattering (RBS), and nuclear reaction analysis (NRA).

The lateral distribution of Cr deposited in the surface oxid layer of steel samples is a problem of interest. In principle Cr and Fe can be separated by means of PIXE. In our case a very small Cr signal (K_α peak) was observed on the tail of a very strong Fe- K_α peak. Therefore, it was difficult to separate the Cr peak from the background. This leads to a large uncertainty of the Cr intensities.

Nuclear medicine makes increasing use of ^{99m}Tc radiopharmaca. The distribution of these radiopharmaca in the organism of test animals is examined, for instance, by autoradiography of microtome sections. Kidney and brain tissue of rats were measured with the microprobe with the aim of comparing and showing whether the Tc is deposited alone in the tissue or together with the ligands. Tests with the microprobe showed that Tc can be traced by PIXE and RBS measurements at an energy of E_p = 3 MeV up to a concentration of about 0.1µg/mm^2. The results of the microprobe measurements of the tissues showed that the Tc concentration of the specimens was lower than the detection limit. Examinations shall be continued with specimens containing larger Tc concentrations.

Furthermore piezo sinter ceramis consisting of $(Pb_{0.6}Ba_{0.4})Nb_2O_6$ were measured with the microprobe to determine the elemental distribution after the sintering process. Relatively strong structures found in the elemental maps were similar for Pb, Ba, and Nb, respectively. In principle such a behaviour is typically for isolated islands on the surface. But in case of a thick target such islands are not to be expected. Additional SEM (scanning electron microscopy) investigations showed, that the measured lateral elemental distributions are influenced by the surface roughness of the specimens. Fig. 1 shows a SEM picture of a sample surface. Since the X-ray detector was arranged at 120° relatively to the proton beam, some parts of the target were shadowed and some preferred. In case of a strong roughness of the surface it is impossible to get a correct elemental map. Further examinations using smoother specimens are envisaged.

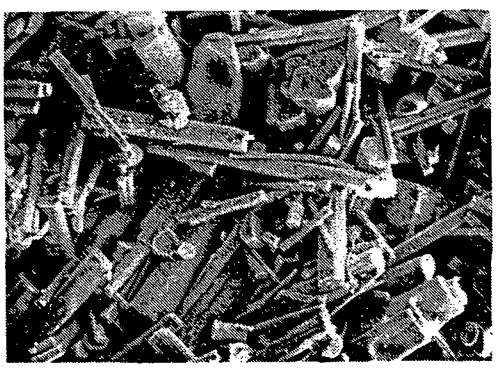

Fig. 1: SEM picture of the surface of a piezo ceramic sample, (140*107)µm^2

References

/1/ Grambole,D. and F. Herrmann; Annual Report 1984, ZfK-559 (1985) 92

/2/ Fromm, W.-D.,D. Grambole, F. Herrmann and F. Schwarzenberg; Proceedings 5th International IMEKO Symposium, June 1986, Jena IMEKO, TC event series No.1,Vol.2, p.271

HYDROGEN DEPTH PROFILING IN H IMPLANTED SEMICONDUCTORS USING ELASTIC RECOIL DETECTION

D. Lehmann, C. Ascheron, and C. Neelmeijer+
Karl-Marx-Universität Leipzig, Sektion Physik, WB Angewandte Kernphysik
+Zentralinstitut für Kernforschung, Rossendorf, Bereich KF

Mechanical, electrical and optical properties of semiconductors and other materials are rather modified by the presence of hydrogen, e.g. /1/. However, most methods of elemental analysis are not successful in the quantitative determination of H without sample destruction. But in the last decade the problem could be solved using ion beam methods (nuclear resonance reaction analysis - NRA and elastic recoil detection - ERD) /2/. Continuing earlier measurements to H profiling on GaP /3/, we investigated the hydrogen distribution of further semiconducting materials (Si and InP). For H detection we used ERD in the earlier described experimental arrangement /3/ with ^{4}He projectiles of 1.5 and 1.7 MeV, respectively. The relatively small analysed depth interval of $t \leq 300$ nm has been extended by one order of magnitude by taking a bevelling technique for preparation of the irradiated areas of the single crystals. After H implantation with 0.3 MeV protons (InP: 3×10^{17} cm^{-2}; Si: 1.7×10^{17} cm^{-2}) the irradiated areas of the samples were sputtered with 1 keV Ar ions. Thus a wedge was prepared with a slope of about 300 nm per mm. The experimental results (fig. 1) for the two materials show, as known from GaP /3/, a strongly marked maximum of H concentration in a depth, which is equivalent to the range of implanted H, and a low H content in regions nearer to the surface. Each measured value was taken in a depth of about 150 nm below the actual surface, to eliminate influences of sample preparation and interferences with the H surface peak. A comparison of the InP results with those of GaP /3/ shows nearly coincidence concerning the maximum H concentration as well as the FWHM of the distribution and the position of the peak, but also the H content near below the surface. In the case of silicon shape and height of the H profile are slightly changed in comparison to InP. A larger content of hydrogen in the region between surface and peak compensates partly the H loss within the peak.

For InP the H profile was also obtained with NRA (^{1}H(^{15}N,$\alpha\gamma$)^{12}C reaction). The two results are in good agreement within the error limits.

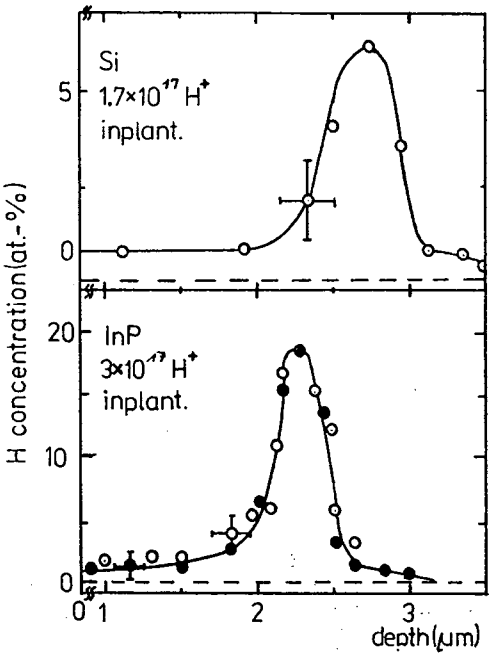

Fig. 1: Hydrogen depth profile in Si and InP.
Implantation: with 0.3 MeV H$^+$.
Analysis: ● - NRA; ○ - ERD

R e f e r e n c e s

/1/ Ascheron, C. et al., Phys. Stat. Sol. A 89 (1985) 549
/2/ Ziegler, J.F. et al., Nucl. Instr. & Meth. 149 (1978) 19
/3/ Lehmann, D. et al., Ann. Rep. 1985 on Nucl. Phys. Activ. and Appl. ZfK-584 (1986) 75

DEPTH PROFILE OF MICROHARDNESS ON HYDROGEN IMPLANTED GaP AND InP SINGLE CRYSTALS

C. Ascheron, R. Schäfer[+], A. Schindler[++]
Karl-Marx-Universität Leipzig, Sektion Physik, WB Angewandte Kernphysik
[+]Martin-Luther-Universität Halle, Sektion Physik
[++]Zentralinstitut für Isotopen- und Strahlenforschung Leipzig, Bereich SF

We have extended our investigations of the effect of proton bombardment on the surface hardness of GaP /1,2/ to depth dependent studies on GaP and InP. The measurements were performed on (111) oriented GaP and InP single crystals implanted with $3 \cdot 10^{17}$ cm^{-2} 0.3 MeV protons and bevelled by 1 keV Ar^+ sputtering. Using a Vickers microhardness tester a load of 20 g was applied for a duration time of 15 s. On unimplanted material values of 8.0 GPa and 4.2 GPa are found for GaP and InP, resp.
In order to interpret the hardness measurements the corresponding distributions of radiation damage and of implanted hydrogen are taken into consideration (figs. 1 a and b/3, 4/). The depth dependent changes of the microhardness of the bevelled samples are shown in figs. 1 c and d. Though the measurements do not exactly represent the hardness at the given depth since there is a gradient in hardness within the region of indentation depth and since effects of deeper layers cannot be neglected, the following qualitative tendency can be recognized:

1. Within the point defect rich region ($t \lesssim 1.5\,\mu m$) hardness increases with damage density.
2. Within the highly damaged region in which extended defects predominate a distinctly smaller increase in microhardness is observed (the effect of gas bubbles can be excluded).
3. Within the H rich region hardness reincreases.

These results make us suppose that point like defects have a stronger hardening effect than more extended defects and that the incorporation of hydrogen hardens material.

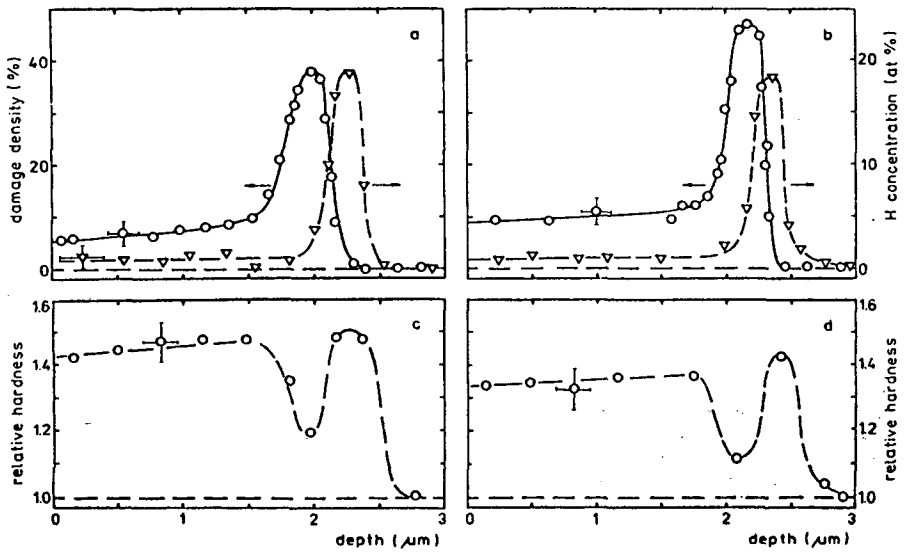

Fig. 1: Depth dependences of the relative changes in microhardness of GaP (c) and InP (d), of the damage density (o) and of the H concentration (▽) of GaP (a) and InP (b) implanted with $3 \cdot 10^{17}$ cm^{-2} 0.3 MeV protons.

References

/1/ C. Ascheron et al., J. Mat. Sci. Lett. 5, 891 (1986)
/2/ C. Ascheron, H. Neumann, Nucl. Instr. Meth. (1987), in the press
/3/ C. Ascheron, et al., Proc. Int. Konf. Nukl. Analysenverf., Dresden, 1983, p. 53
/4/ C. Ascheron, et al., Gemeinsamer Jahresbericht 1986, ZfK (1986)

A STUDY OF VACANCY TYPE DEFECTS ON PROTON BOMBARDED GaP SINGLE CRYSTALS

C. Ascheron, G. Dlubek[+], R. Krause[+], H. Erhard[+], D. Klimm[++]
Karl-Marx-Universität Leipzig, Sektion Physik, WB Angewandte Kernphysik
[+] Martin-Luther-Universität Halle, Sektion Physik
[++] Karl-Marx-Universität Leipzig, Sektion Chemie

Negatively charged and neutral vacancy type defects produced in GaP by proton bombardment (E_p = 1.7 MeV) were studied by use of positron annihilation (Doppler broadening and lifetime measurements). The measurements show with fluence increasing concentration of vacancy defects.

The study of annealing (stepwise conventional annealing for 30 min) shows various stages (fig. 1) which are discussed by taking into consideration the results of internal friction (fig. 2), Rutherford backscattering/channeling and electron microscope measurements:

- Near room temperature and at lower damage densities (below about 0,5 %) isolated vacancies predominate.
- At around 430 K P vacancies become mobile. Here the formation of P-Ga divacancies begins due to the coalescence of isolated vacancies. Measurements of internal friction which respond to unisotropic defects support this assumption (fig. 2).
- The stage near 500 K is supposed to be connected with the annealing of isolated Ga vacancies. This is confirmed by electron spin resonance measurements /1/.
- Near 700 K the formation of mainly vacancy type defect complexes occurs what is also visible in cross-sectional transmission electron microscope patterns /2/.
- The annealing stage near 800 K which is also expressed in Rutherford backscattering/channeling measurements /3/ is believed to be connected with the annealing of smaller defect agglomerates consisting of vacancies, interstitials and antisites.

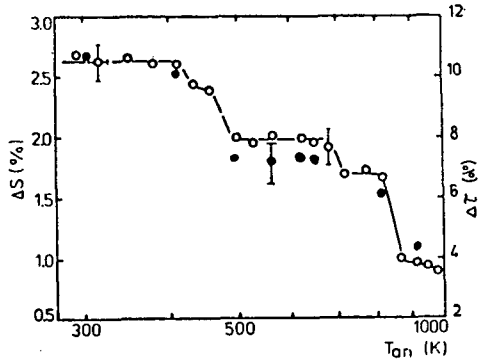

Fig. 1: Temperature dependence of the relative changes ΔS (o) of the S-parameter and Δτ (•) of the mean positron lifetime on proton bombarded GaP

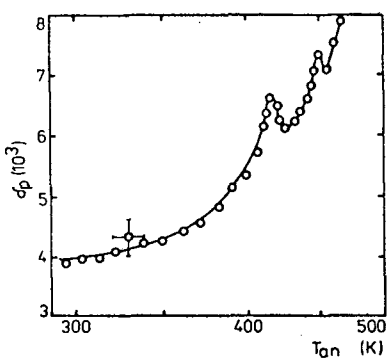

Fig. 2: Internal friction δ_p of proton bombarded GaP as a function of the inverse temperature

References

/1/ E. Yu. Brailowski et al., phys. stat. sol (a), 41 (1980)
/2/ C. Ascheron et al., Nucl. Instr. Meth. (1987), in the press
/3/ C. Ascheron et al., Proc. Int. Konf. Nukl. Analysenverf., Dresden 1987

INVESTIGATIONS OF THE ANNEALING BEHAVIOUR OF HYDROGEN IMPLANTED GaP SINGLE CRYSTALS BY MEANS OF PARTICLE INDUCED GAMMA-SPECTROSCOPY, INFRARED SPECTROSCOPY AND RUTHERFORD BACKSCATTERING CHANNELING TECHNIQUE

C. Ascheron, H. Sobotta, V. Riede, C. Bauer[+], R. Grötschel[+], A. Schindler[++]
Karl-Marx-Universität Leipzig, Sektion Physik, WB AKP
[+] Zentralinstitut für Kernforschung Rossendorf, Bereich KF, der AdW der DDR
[++]Zentralinstitut für Isotopen- und Strahlenforschung Leipzig, Bereich SP, der AdW der DDR

Previous investigations of proton bombarded GaP /1/ were extended to annealing experiments. On GaP single crystals implanted at 300 K, annealed and subsequently bevelled by 1 keV Ar^+ sputtering, the variation of the depth profiles of incorporated H, bonded H and of damage density was studied.

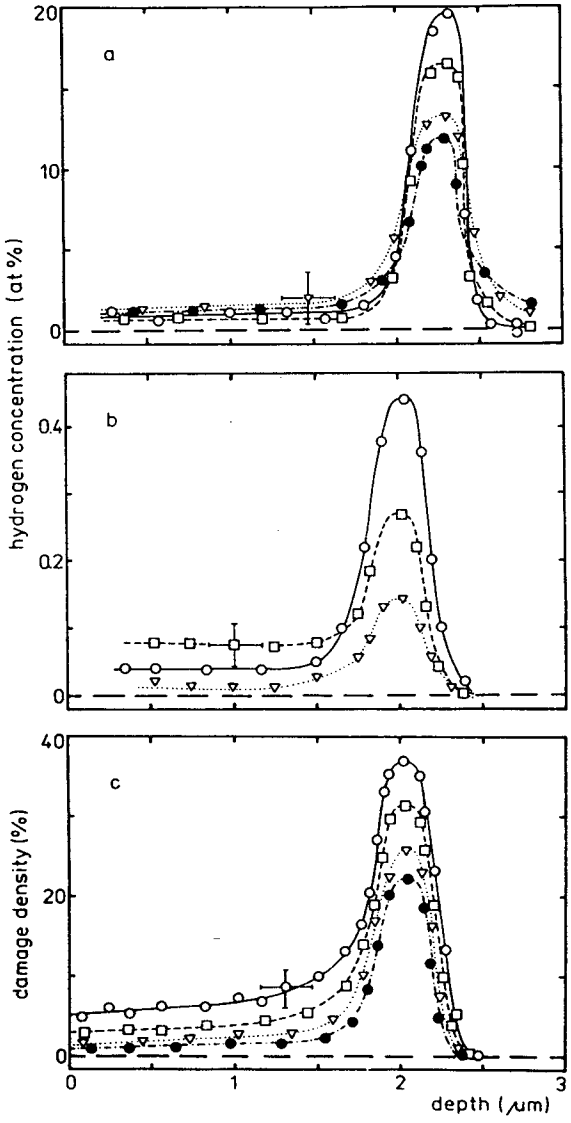

The measurements give the following results:

-With rising temperature, the H profile slightly broadens, increases outside and decreases inside the concentration maximum. Since these variations are not very strong, a very low mobility or a trapping of the implanted H can be assumed.

-The defects in the less damaged region anneal more strongly than in the damage peak region, which points to the predominance of larger defects with higher activation energy within the heavily damaged region.

-The bonded H, which is contained in one order of magnitude lower concentrations than total implanted H and which is bonded at defect sites /1/, exhibits an annealing behaviour similar to the simpler defects. This behaviour suggests that the main H fraction is bonded to smaller defects also present in the damage peak region.

-Immediately below the surface ($t < 0{,}5\ \mu m$) a chemisorption-like gettering effect of the damaged layer to H trapped at the surface is observed after annealing.

References

/1/ C. Ascheron et. al., phys. stat. sol. (a) 89, 740 (1985)

Fig. 1: Depth profiles of (a) total H content (analysis $^1H(^{19}F,\alpha\gamma)\ ^{16}O$ and $^1H(^{15}N,\alpha\gamma)\ ^{12}C$ reactions), (b) concentration of bonded H (IR analysis) and of (c) damage density (RBC analysis with 1,7 MeV He^+ ions) at bevelled GaP single crystals implanted with $3X10^{17}cm^{-2}$, 300 keV protons at 300 K (-o-) and 30 min postannealed at 480 K (-□-), 620 K (-▽-) and 720 K (-●-).

SWELLING OF He^+ IMPLANTED GaP SINGLE CRYSTALS

C. Ascheron, A. Schindler[+], R. Flagmeyer, G. Otto
Karl-Marx-Universität Leipzig, Sektion Physik
[+]Zentralinstitut für Isotopen- und Strahlenforschung Leipzig, Bereich Strahlenforschung, der AdW der DDR

The bombardment of $A_{III}B_V$ materials with He^+ ions offers the possibility to produce isolating regions suitable for gain-guided lasers with high reproducibility /1/.
Changes in volume are due to radiation damage and implanted gas. They are expressed as swelling and strain. These changes were studied together with damage as a function of fluence and post-bombardment annealing temperature. Fig. 1 shows the results of swelling measurements.

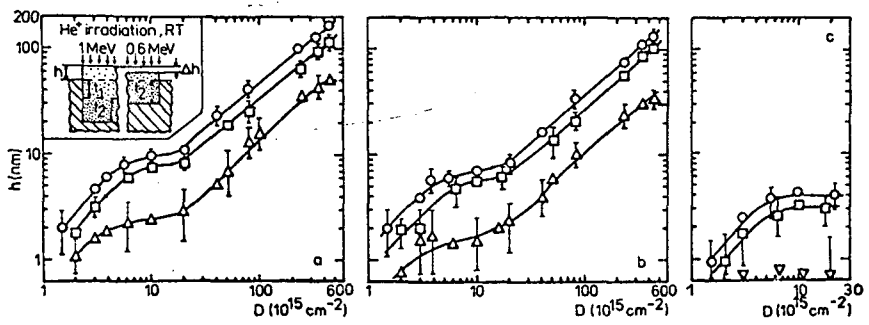

Fig.1 Swelling h of (111) GaP bombarded with 0,6 (□) and 1,0 MeV He^+ ions (○) and difference Δh (△▽) as a function of fluence for implantation at 300K (a) and following annealing at 450K (b) and 720K (c).

The measurement indicate increasing swelling with rising fluence which exhibits saturating behaviour for medium fluences and a stronger reincrease for higher fluences up to volume changes exceeding the amorphization value. At lower fluences ($D < 2X10^{16} cm^{-2}$) the swelling of the near surface layer t_1 and its annealing behaviour are described by the corresponding strain; the fluence dependences of swelling, strain and damage density agree qualitatively which is also observed on H^+ implanted GaP /2/.
At higher fluences, strong swelling occurs since the damage peak broadens towards the surface due to the coalescence of point defects at the front side of the damage peak. Thus, by energy dependent RBC measurements two regions with predominantly different defect types can be distinguished: The near surface region, which contains small defects, and the highly damaged region containing voids and dislocations, which broadens with rising fluence. Annealing at 450 K reduces swelling, strain and damage density for all fluences studied, annealing at 720 K does so for fluences $D < 3X10^{16} cm^{-2}$. At higher fluences flaking occurs during annealing due to the pressure of the implanted gas.

References

1 M.W. Focht, A.T. Macrander, B. Schwartz, L.C. Feldman, J. Appl. Phys. 55, 3859 (1984)
2 C. Ascheron et. al., phys. stat. sol. A 92, 169 (1985)

FISSION-TRACK AGES OF NATURAL GLASSES

A. Docekal and W. Stolz
Bergakademie Freiberg, Sektion Physik
O. Leeder
Bergakademie Freiberg, Sektion Geowissenschaften

By means of the fission-track method age determinations were performed with five native rhyodacitic glasses (volcanic glasses). To this date physical ages of these rocks were not yet determined. Geological-stratigraphic classification is also based on assumptions. Samples were split with one part being retained for later determination of spontaneous track density. The other part was heated in air at 400°C for two houre to erase all spontaneous tracks. These sections were then neutron irradiated with a fluence of about $(1.48 \pm 0.30) \cdot 10^{19}$ m^{-2} in the channel VK III of the nuclear research reactor in Rossendorf. After a series of preliminary examinations the optimum etching conditions were fixed as follows:
Etchant: HF (20 %); temperature: T = 296 K; etching time: t = 10 s.
The geological age /1/ is determined according to

$$t = \frac{1}{\lambda_d} \ln \left(\frac{p_s \lambda_d \Phi \sigma_f I}{p_i \lambda_f} + 1 \right),$$

where: t = age in years; p_s = number of spontaneous fission tracks per area; p_i = number of induced fission tracks per area; λ_d = total changing constant for ^{238}U ($1.6 \cdot 10^{-10}$ a^{-1}); λ_f = changing constant for spontaneous fission of ^{238}U ($8.5 \cdot 10^{-17}$ a^{-1}); Φ = fluence of thermal neutrons; σ_f = cross-section for thermal neutron-induced fission of ^{235}U ($5.82 \cdot 10^{-25} m^2$); I = isotopic ratio of $^{235}U/^{238}U$ ($7.2 \cdot 10^{-3}$).
The etch pits were observed under an optical incident-light microscope at 1000 magnification.
The fission track ages in this study are compared with K-Ar-ages in Table 1.

Table 1: Fission-track ages and K-Ar-ages of the rhyodacitic glasses

sample No./ locality	fission-track age in 10^6 a	error in %	stratigraphic classification	K-Ar-age in 10^6 a	hitherto existing stratigraphic classification
1/Garsebach near Meissen	241 ± 49	20	Triassic	45 ± 4	Upper Carboniferous
2/Garsebach near Meissen	240 ± 53	22	Triassic	98 ± 8	Upper Carboniferous
3/Braunsdorf	185 ± 13	7	Jurassic	136 ± 6	Upper Carboniferous
4/Spechtshausen	no age determination possible	-	-	190 ± 9	Upper Carboniferous
5/Queckhain	131 ± 27	21	Jurassic	82 ± 3	Rotliegendes

Although there are partly relatively great differences between fission-track ages and hitherto existing geological classification, a correspondence relating to the order of magnitude can be found at least for the samples 1, 2 and 3. K-Ar ages which were determined with the same material are in a higher contradiction to the geological assumptions than the fission-track ages.

R e f e r e n c e

/1/ Fleischer, R. L., et al.; Nuclear Tracks in Solids. Principles and Applications. University of California Press, Berkeley (1975).

THE POSSIBILITIES OF CPAA IN GEOLOGICAL SAMPLES BY THE ROSSENDORF CYCLOTRON Y-120

D. Degering, S. Unterricker, and W. Stolz
Bergakademie Freiberg, Sektion Physik

The charged particle activation analysis (CPAA) is well established in analysis of metallic samples /1,2/. We tested the possibilities at the Rossendorf f-f cyclotron for the investigation of geological materials as a complement to the instrumental neutron activation analysis (INAA). The cyclotron accelerates α-particles, deuterons and protons with primary energies of 27 MeV, 13.5 MeV and 6.75 MeV, respectively. An estimation according to /3/ under the assumption that equal amounts of energy are absorbed in the thick targets led to the following results:

- because of the relatively high energy of the α-particles the threshold energies of a number of possible reactions (α,n), $(\alpha,2n)$, (α,p), (α,pn) are exceeded and all deliver thick target yields of about the same order; i.e., helionic activation is non-unique
- for deuterons the (d,n), (d,2n) and (d,p) reactions reach satisfactory thick target yields but somewhat higher than in the case of α-particles; only for light nuclei the (d,α) and (d,2p) reaction must be taken into account
- the activation by protons is based on the (p,n) reaction; only for light nuclei the (p,α) reaction is possible; however, the thick target yields lie about one order below the values for deuteron reactions.

Therefore, activation by deuterons seems to be favourable.

The main problem in the analysis of geological samples is the increased background of the γ-ray spectra as a consequence of major element activation like O, Si, Al, Ca, Mg, Na, K, Fe and H. That's why we investigated geological standard materials with various compositions: ZGI anhydrite AN, ZGI basalt BM, ZGI granite GM, ZGI limestone KH, ZGI slate TB, and fluorite XM. The materials were pressed to rectangular samples (area 5 x 10 mm^2, thickness $\leq$ 1 mm) and four of it were bound on an aluminium target as described previously /4/. With this preparation a beam current of 3 μA for d and α and 6 μA for p in the internal beam of the Rossendorf cyclotron is possible.

The γ-spectra showed strong contributions of the following nuclides, all resulting from the activation of major elements: ^{24}Na (from Na); ^{44}Sc, ^{44m}Sc, ^{46}Sc, ^{47}Sc, ^{48}Sc (from Ca); ^{56}Co, ^{57}Co, ^{58}Co (from Fe). For examination of other elements the method of the internal standard was used /4/. We plotted the concentration ratio of the investigated to the reference element vs. the decay corrected intensity ratio of selected γ-lines from the refering nuclides. The lines used for the standard were the 271 keV line of ^{44m}Sc (Ca-activation) and the 122 keV line of ^{57}Co (Fe-activation). Presuming a unique origin of the considered nuclide, we must obtain a straight line. Naturally, the activation of the major elements hinders the analysis of some elements. The method is suitable for the elements in Tab. 1. Of it are Mg, Ti, Sr, and Y of special interest, because their determination by INAA is difficult or unpossible.

Table 1: List of the elements, whose unique origin could be proved

Element	Reaction	Half life
Mg	^{24}Mg (d,α)^{22}Na	2.6 a
Ti	^{47}Ti (d,n) ^{48}V	16 d
	^{48}Ti (d,2n)^{48}V	
Co	^{59}Co (d,p) ^{60}Co	5.3 a
Zn	^{66}Zn (d,n) ^{67}Ga	3.3 d
	^{67}Zn (d,2n)^{67}Ga	
Sr	^{86}Sr (d,n) ^{87}Y	3.8 d
	^{87}Sr (d,2n)^{87}Y	
	^{87}Sr (d,n) ^{88}Y	107 d
	^{88}Sr (d,2n)^{88}Y	
Y	^{89}Y (d,2n)^{89}Zr	3.3 d

References

/1/ Barrandon, J. N.; Nucl. Instr. Meth. Phys. Res. B14 (1986) 133
/2/ Isshiki, M., et al.; J. Radioanal. Nucl. Chem., Articles 82/1 (1984) 135
/3/ Keller, K. A., J. Lange, H. Münzel; Q-Values and Excitation Functions of Nuclear Reactions, Landolt-Börnstein, New Series Vol. I 5c, Berlin (1973)
/4/ Degering, D. and S. Unterricker; Gemeinsamer Jahresbericht 1984, ZfK-559 (1985) 83

FLUORINE DEPTH PROFILING FOR CARIES PREVENTION

H. Zschau, J. Vogt, and G. Otto
Karl-Marx-Universität Leipzig, Sektion Physik, WB Angewandte Kernphysik

M. Schneider, and A. Treide
Karl-Marx-Universität Leipzig, Sektion Stomatologie, Poliklinik für Orthopädische und Kieferstomatologie

Following preleminary investigations /1,2/ the depth profiling using proton-induced γ-ray emission (PIGE) is an established method ready for routine analysis. Our main object is the fluorine profiling in tooth enamel up to a depth of 500 nm. Applying the resonance at a proton energy of E_p = 340 keV of the reaction $^{19}F(p,\alpha\gamma)^{16}O$ (E_γ = 6.129 MeV, 6.916 MeV, 7.115 MeV and Γ_R = 2.5 keV) fluorine distributions can be measured with a depth resolution of (20...25) nm at the surface. Using proton current of (100... 150) nA, charges of (20...40) uC were collected for each energy at a beam spot of 1 mm diameter. In order to optimize the clinical application of fluorine varnishes the knowledge of the "washing-out" behaviour of the deposited fluorine is an essential question. Hence teeth divided in three parts were prepared as follows. Except the control each sample was touched with the Duraphat laquer and another laboratory drug called D and DAP, respectively. After a 20-hours exposition the laquer was removed and the samples with index "1" were profiled, however those denoted with index "15 T" after a remaining of 15 days in a simulated mouth milieu (Figs. 1 and 2).
From RBS-spectra one obtains a significant lack of phosphorus and oxygen for the sample D 1 which is caused by a 250 nm thick layer rich in CaF_2 at the surface.

R e f e r e n c e s:

/1/ Wolf, U. et al., Annual report 1984, ZfK-559 (1985) 84
/2/ Zschau, H.-E. et al., Annual report (1985), ZfK-584 (1986) 72

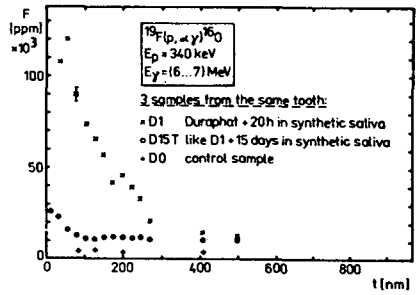

Fig.1

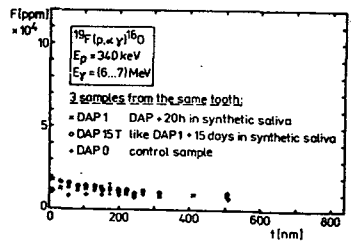

Fig.2

PIXE ANALYSIS OF ELEMENTAL DISTRIBUTIONS ALONG SINGLE HAIR STRANDS

H.U. Frey, and G. Otto
Karl-Marx-Universität Leipzig, Sektion Physik, WB Angewandte Kernphysik

As the trace element levels in the human body can be influenced by the total trace element status and the extent of environmental exposure the medical and environmental research needs concentration values of several elements in various organs of the human body. Slowly growing parts (e. g. hair, nail) may reveal elemental distributions which correspond to the actual elemental supply at the time of their growth. Thus scanning analysis of the concentrational distributions within parts of different age may be helpful in diagnosis of time-depending processes. Human hair seems to be an excellent tissue for non-invasive investigation of the trace element status and is therefore of increasing interest in toxicology, forensic science, nutrition, and environmental technology /1/.
A homogeneous proton beam /2/ with 1.7 MeV energy was used for PIXE analysis of elemental distributions along single hair strands. As high currents resulted in damage of the hair /3/ beam intensities of about 0.5 nA/mm^2 and measuring times of 90 minutes were used. The number of ions falling onto the sample was determined using the diameter of the homogeneous proton beam and the thickness of the hair, which was determined before irradiation by use of a light microscope. Characteristic X-rays were measured by a Si(Li) detector with an energy resolution of 195 eV FWHM at 5.9 keV. Special experimental conditions /3/ and the formalism for thick target PIXE /4/ were used for the quantification of the elemental content.

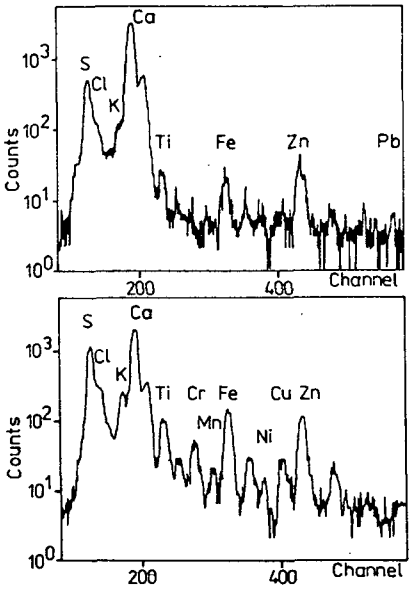

Figure 1:
PIXE spectra of single hair analysis of a female (top, Q = 10 µC) and a male (bottom, Q = 18 µC)

The visible differences in the two PIXE spectra of fig. 1 are the higher natural Ca-content in the hair of the female /1/ and the higher content of metals in the hair of the male. Some results of the analysis of hair of a male are shown in table 1.

Element	x = 15	x = 20	x = 25	x = 30
Ca	729	736	934	1160
Cl	2370	2680	3350	2410
Fe	38	40	74	50
K	411	425	637	392
S	47000	45200	45700	45300
Zn	262	219	204	224

Table 1: Elemental concentrations (µg/g) in the hair of a male analyzed in various distances (x/mm) from the root of the hair

R e f e r e n c e s

/1/ M. Anke, M. Risch, Haaranalyse und Spurenelementstatus (Gustav Fischer Verlag, Jena, 1979)
/2/ H.U. Frey et al., this report, p. 144
/3/ H.U. Frey, Thesis, Leipzig, 1986
/4/ H. Frey, J. Vogt, G. Otto, J. Radioanal. Nucl. Chem. 99 (1986) 193

γ-SPECTROMETRIC INVESTIGATIONS TO THE INTRINSIC RADIOACTIVITIES OF SHIELDING MATERIALS

Kim Jung Ho, S. Unterricker, and W. Stolz
Bergakademie Freiberg, Sektion Physik

For the construction of a low level γ-spectrometer beside the location /1/ also radioactive impurities in the shielding and construction materials are of great importance. Common shielding materials are metals of high atomic number, mostly Pb, Bi, Hg but also Fe, Cu, Sn and Cd. These substances contain natural radioactive impurities. In some cases also man made radioactive nuclides can be detected.

The activities are small in every case, though one must use a very sensitive low background spectrometer to select suitable shielding and construction materials. In our case the γ-spectrometer consists of a 45 cm^3 Ge(Li)-detector shielded by 9 cm of lead at the outside, 2 cm mercury and 0.6 cm electrolytic copper. The cold finger is directly surrounded by a lead plug and the preamplifier is enclosed with low activity copper sheets. The samples were grained and filled into a Marinelli beaker of 3 cm wall thickness.

The contents of radioactivities in the samples are determined by i) the geology and geochemistry of the ores, ii) the metallurgical procedure, and iii) the age of the metals. Beside discrete photopeaks γ-spectra of the samples show remarkable differences in the background continuum below about 0.7 MeV. These preferentially originate from the β^--bremsspectrum of ^{210}Bi which is a daughter of ^{210}Pb (half life 22 a, U chain). For most of the discrete lines there are hardly differences between the blank and the sample. To our experience only the following peaks can be analysed: ^{40}K-1.46 MeV, ^{208}Tl-2.61 MeV, ^{210}Pb-0.24 MeV, ^{214}Bi-0.61 MeV, ^{226}Ra-0.19 MeV. In every case there must be a careful correction for absorption of background radiation by the sample and for the self absorption in the sample. Such corrections can be performed very exactly by a Monte-Carlo procedure /2/. We made approximations with a point detector and a series expansion of the corresponding integral relations. The self absorption correction is problematically for energies below 0.3 MeV and large effective sample thickness. Therefore the bremsspectrum contributions (first column of Tab. 1) are not corrected. Printed are only relative numbers which are comparable because the samples have all an equal effective thickness of about 12 gcm^{-2}. The numbers are differences between a sample and a blank measurement. Owing to the absorption of background by the sample the best shielding material is that with a large negative value. Tab. 1 shows for selected materials beside the bremsradiation contribution the corrected photopeak rates per kg of ^{40}K and ^{208}Tl.

References

/1/ Kim, J. H. et al.; Annual Report 1985, ZfK - 584, April 1986, p. 120
/2/ Nakamura, T. and T. Suzuki; Nucl. Instr. and Meth. in Phys. Res. 205 (1983) 211

Table 1: Counting rates for intrinsic radioactivities of shielding materials

shielding material	counts per 10^4s 0.1 - 1 MeV relative numbers	counts per 10^4s·kg 40 - K 1.46 MeV	208 - Tl 2.61 MeV
yellow lead bricks - radiation protection	12800	0.4(7)	0.3(5)
lead Halsbrücke - electrolytic, 99.99 %	2700	0.2(4)	0.1(3)
lead bars - old lead installation	2600	1.7(7)	0.2(4)
lead slabs - Muldenhütten, 40 a old	800	0.6(6)	0.2(3)
biemuth Halsbrücke - 99.9 %	-260	<0.1	0.6(4)
lead U.S.S.R. - underground laboratory ZfK Rossendorf	-660	0.8(5)	0.1(3)
lead Korea (KDVR) - wire form	-910	0.2(4)	0.6(3)
mercury-China	-1040	0.7(6)	0.1(5)

MOESSBAUER SPECTROSCOPY OF THE TEMPERING BEHAVIOUR OF THE SPRING STEEL 62SiCr5

C. Pietzsch, Bergakademie Freiberg, Sektion Physik
U. Thieme, TU Karl-Marx-Stadt, Sektion Chemie und Werkstofftechnik

The structural changes of martensitic steel owing to the tempering are determined mainly by the decomposition of the state of strain in the supersaturated solid solution and the carbide formation. It influences the properties of the resulting microstructure of the steel in a strong way.
In the literature there exist different opinions on the composition and crystallography of the induvidual carbide phases after tempering which are influenced by the content of alloying, the hardening, and the tempering conditions. The X-ray phase analysis of $\chi(Fe_5C_2)$-carbide and Θ carbide (Fe_3C) mixtures often fails in consequence of the structure similarity of mixture components. If different alloying elements are introduced into the steel matrix the lattice parameters of the single carbide phase change in different extents. We report investigations of the carbide formation in the austenitic steel 62SiCr5 (0.62 C; 1.27 Si; 0.91 Mn; 0.5 Cr; 0.14 Cu; 0.024 P; 0.011 S) after a heat treatment by different tempering temperatures using the Moessbauer effect. The investigations were performed at 293 K and at 80 K.
Table 1 shows the measured results.

Table 1: Moessbauer parameters of carbide phases (δ = isomer shift (rel. α Fe), Δ = quadrupole splitting, H_i = internal magnetic field)

tempering temperature	T = 293 K				T = 80 K			
	δ /mm·s^{-1}	Δ/mm·s^{-1}	H_i/T	carbide	δ /mm·s^{-1}	Δ/mm·s^{-1}	H_i/T	carbide
293 K	0.32	0.83	-	spm ε	0.41 0.16	1.00 0.64	- 2.21	spm ε (χ+Θ)
423 K	0.30	0.79	-	spm ε	0.37 0.11	0.78 0.64	- 2.25	spm ε (χ+Θ)
543 K	0.28 0.28	0.82 0.43	- 1.93	spm ε (χ+Θ)	0.30 0.30 0.26	1.07 0.36 0.21	- 2.33 2.38	spm ε (χ+Θ) Θ
698 K	0.21 0.13 0.17	0.89 -0.07 0.07	- 1.76 1.96	spm ε χ Θ	0.32 0.34 0.34	1.10 0 0	- 2.13 2.35	spm ε χ Θ

The complete set of the spectra shows a central quadrupole doublet. The parameters of this doublet are nearly unchanged in the full region of temperature and can be assigned to a superparamagnetic(spm) ε-carbide (Fe_2C) according to the literature. Up to tempering temperatures of 543 K the magnetically splitted spectra correspond to an intermediate carbide of the χ- and Θ-phases /2/. With rising temperatures the structures of χ- and Θ-carbide appear well separated.
The occurence of spm ε-carbide in the full investigated temperature region is surprising and can be explained only by the high silicon content in the steel matrix /3/. The formation of intermediate carbides is supported by the high content of alloying elements in the steel. With rising tempering temperatures the crystallinity and the portions of the χ- and Θ-carbide phases improve in favour of ε-carbide.

References

/1/ Le Caer, G., et al.; phys. stat. sol. (a) 6 (1971) K97
/2/ Nakagura, S., et al.,; Metall. Trans. 14A (1983) 1025
/3/ Mathalone, Z., et al.; J. Appl. Phys. 42 (1971)687

WEAR STUDIES OF COMPONENTS USING DEUTERON ACTIVATION

Ch. Eifrig
Zentralinstitut für Isotopen- und Strahlenforschung Leipzig, Bereich IA
K. Eichhorn
Zentralinstitut für Kernforschung Rossendorf, Bereich G
P. Hammer VEB dkk Scharfenstein

The deuteron activation of a ball and socket joint at the tandem accelerator makes it possible to determine the wear rate, the transport of abraded material, and the contamination of the sliding parts. A new series of refrigerating compressors with ball and socket joints (fig. 1) is developed in the VEB dkk Scharfenstein.

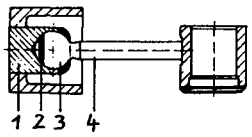

Figure 1: The ball and socket joint (1 Piston with the socket, 2 friction areas at the ball and at the socket, 3 ball, 4 connecting rod)

The compressors must have a service life of 15 years. In the course of years the wear depth may reach only some micrometers. The radionuclide technique was used to study the wear behaviour of the ball and socket joint. The applied thin layer activation is very sensitive in comparison with conventional methods. It allows the on-line control of selcted friction areas during machine operation.

For acitvation the pistons or the balls are adjusted in a vacuum chamber with a position reproducibility better than 0.1 mm. After adjusting the deuteron beam with an energy of 3.5 MeV is passed through a 2 mm diameter collimator and then it is directed to the ring-shaped friction area of the compressor part. 8 activity spots with a diameter of 2 mm are produced in these areas by rotating the part in the beam. The nuclide Co-57 is generated in trace quantities in a 15 µm deep layer. The parts activated in this way require only elementary handling precautions. The activation quality is controlled autoradiographically, and by γ-spectroscopy. Measurements of the micro-hardness of test samples show that this activation leaves the wear properties of the materials unchanged.
After the radioactivation the Co-57 intensity of the parts is measured in relation to a calibration source. The parts are assembled into a complete compressor which is mounted in a test stand with an additional oil circuit and an oil filter collecting the wear particles. The filters are changed after a definite time and their radioactivity is measured with a scintillation detector. After the test run the machine is disassembled, the individual parts are checked for Co-57 contaminations. The Co-57 intensity of the piston or the ball is measured again. With the difference between this value and those value measured before the beginning of the test run, and with the calibrated activation depth profile, the total wear depth can be determined and coordinated to the values of the oil filter measurements (fig. 2).

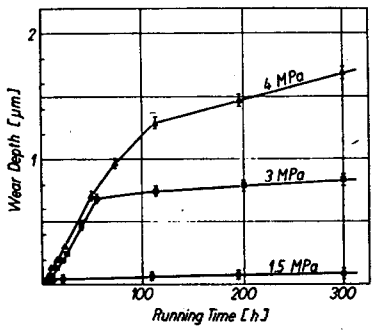

Figure 2: Wear dependence on the running time of selcted compressors at different pressures

This method causes an error of 20%. This is a typical value for wear measurements.
With the described method it is proved that the oil exchange and the lubrication of the joint take place. The measurements show that the wear of the joint has a degressive behaviour. This is important for the durability. Further the fact that only a few wear particles from the activated friction area are found on the opposite surface of the frictional partner shows that the destructive kinds of wear - abrasion and adhesion - are negligible.

ENERGY AND DOSE DEPENDENCE OF DAMAGE PRODUCED BY LOW ENERGY Ar ION BEAM ETCHING OF GaAs MEASURED BY ^{64}Cu ADSORPTION AND AUTORADIOGRAPHY AND RBS-CHANNELLING

R. Fechner, A. Schindler, R. Flagmeyer[+] and F. Bigl
Zentralinstitut für Isotopen- und Strahlenforschung Leipzig, Bereich SF, der AdW der DDR
[+]Karl-Marx-Universität Leipzig, Sektion Physik, WB AKP

Studies of low energy Ar^+-ion bombardment damage of <100> GaAs surfaces by means of ^{64}Cu adsorption, autoradiography and Rutherford backscattering were presented in previous papers /1,2/. In this paper the studies are extended to dependences on Ar ion energy (0.5 to 2.0 keV) and on dose ($1 \cdot 10^{13}$ to $5 \cdot 10^{16}$ cm^{-2}). The experimental conditions are the same as in /1, 2/. ^{64}Cu adsorption was carried out at room temperature in an aqueous solution (1 mg Cu^{II}-ions; 10 ml . 1 nHCl and 15 MBq ^{64}Cu in 100 ml H_2O) for 5 minutes. Autoradiographs were taken with the samples in contact with the film for 1 to 10 hours. Blacking curves were measured by a photometer. A quantitative Cu concentration measurement was made by autoradiographic imaging of calibration standards on the same film.

Fig. 1 shows the adsorbed Cu concentrations as a function of the ion dose for four ion energies. The adsorbed Cu concentrations on the non bombarded areas at the samples are lower than $6 \cdot 10^{13}$ cm^{-2}. The solid curves are only guides for the eye. The adsorbed Cu concentration increases with ion dose and begins to be saturated at a dose of $1...2 \times 10^{15}$ cm^{-2} for 0.5 keV ions. With increasing ion energy the Cu concentration increases for the same dose and the beginning of the saturation shifts to higher doses.

This behaviour is in qualitative agreement with the behaviour of the damage production measured by RBS-channelling, shown in Fig. 2 for GaAs and Si. RBS measurements were carried out with 1.2 MeV He^+ ions using a backscattering angle of 95° (5° grazing exit geometry). With the given detector resolution power of 15 keV the surface depth resolution becomes better than 4 nm. The results of Fig. 2 are in good agreement with previous measurements /2, 3/. Fig. 3 shows ion energy dependences of the adsorbed ^{64}Cu concentration and of the damaged layer thickness at the saturation level of the ion dose ($\geq 10^{16}$ cm^{-2}). Also shown

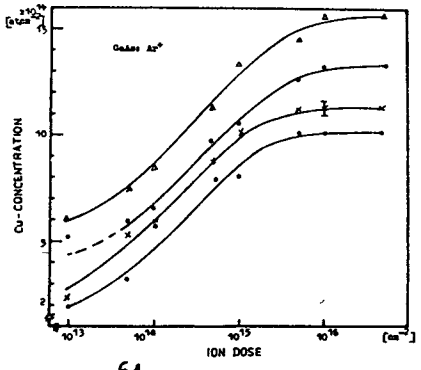

Fig. 1 Adsorbed ^{64}Cu concentration on Ar ion bombarded GaAs surfaces as a function of ion dose for 0.5 keV (—•—), 1.0 keV (—x—), 1.5 keV (—o—) and 2.0 keV (—Δ—) ion energy

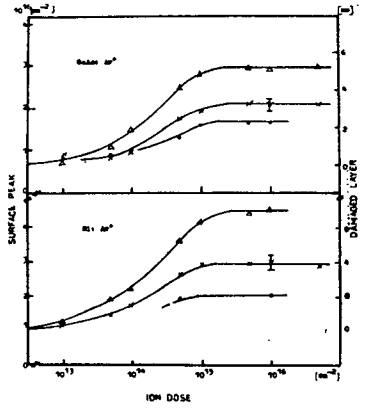

Fig. 2 Total amount of damage measured by RBS surface peak intensities of <100> aligned spectra of Ar-ion bombarded GaAs and Si as a function of ion dose for 0.5 keV (—•—), 1.0 keV (—x—) and 2.0 keV (—Δ—) ion energy. The right-hand scale indicates the thickness of the damaged layer, estimated under the approximation of rectangular damage profiles

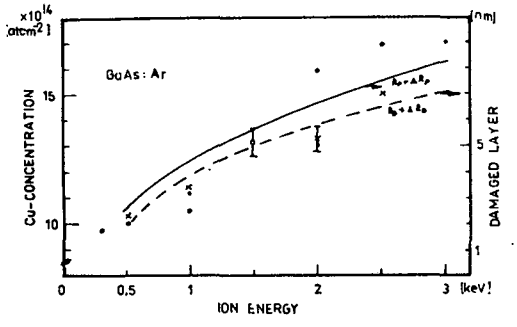

Fig. 3 Comparison of the behaviour of the adsorbed Cu concentration (o), left-hand scale and the damaged layer thickness (x)this work, (•)/3/, right-hand scale of Ar ion bombarded GaAs at saturation dose ($> 10^{16}$ cm^{-2}) as a function of ion energy; also shown: Ar^+ implantation ($R_p + \Delta R_p$), (solid curve) and damage ($R_D + \Delta R_D$) (dashed curve) calculations (right-hand scale) after Pearson /4/ and Sigmund and Sanders /5/ respectively

are the theoretical curves for $R_p + \Delta R_p$ for implanted Ar and for the produced damage $R_D + \Delta R_D$ (projected ranges R_r, R_D plus standard deviations ΔR_p, ΔR_D) after /4/ and /5/ respectively. Fig. 3 demonstrates a rather good qualitative agreement of the behaviour of Cu concentration and damaged layer thickness at the saturation dose level as a function of the ion energy. The experimental results lead us to the conclusion that the adsorbed Cu-atoms penetrate into the damaged layer and are gettered at defect sites. This assumption is confirmed by the high diffusitivity of copper in GaAs. A rough estimate of the copper concentration in the damaged layer for saturation doses gives values of 15 to 20 atom percent. Measurements of the depth profiles verify the distribution of the copper atoms in the damaged layer /6/.

References

/1/ R. Fechner, A. Schindler, J. Flachowsky, Gemeinsamer Jahresbericht ZfK 559, 127 (1985)

/2/ R. Flagmeyer, R. Fechner, Gemeinsamer Jahresbericht ZfK 559, 87 (1985)

/3/ R. S. Williams, Sol. State comm. 41 (1982) 153

/4/ A. F. Burenkov, F. F. Komarov, M. A. Kumachov, M. M. Temkin, Tabellen-Parameter der räumlichen Verteilung implantierter Ionen, Minsk 1980 (in russian)

/5/ P. Sigmund, J. B. Sanders, Proc. Int. Conf. Appl. Ion Beams Semicon. Technol. Grenoble (1967) 215

/6/ R. Fechner, A. Schindler, F. Bigl, this report p. 87

STUDY OF NEAR SURFACE DAMAGE DEPTH PROFILES OF Ar ION BEAM ETCHED GaAs BY MEANS OF ^{64}Cu ADSORPTION AND AUTORADIOGRAPHIC DETECTION

R. Fechner, A. Schindler, F. Bigl, J. Flachowsky
Zentralinstitut für Isotopen- und Strahlenforschung Leipzig, Bereich SF, der AdW der DDR

In previous papers near surface damage of Ar ion beam etched GaAs crystals was investigated by means of ^{64}Cu adsorption and autoradiographic detection /1, 2/. The adsorbed copper concentration dependences on ion etching energy and dose behave qualitatively as the damage layer thickness depends on these etching parameters. On this account it is concluded that the primarily adsorbed copper atoms penetrate into the whole damaged layer where they are gettered. Depth profile measurements of adsorbed Cu atoms on damaged layers made to check this assumption are presented in this paper. The sample preparation for depth profile measurements was done by very low energy ion beam etching (0.2 keV Ar^+ ions) of bevelled sections on the damaged and ^{64}Cu adsorbed GaAs surface. Autoradiographic registration of the Cu distribution at the bevelled section and differentiation of the

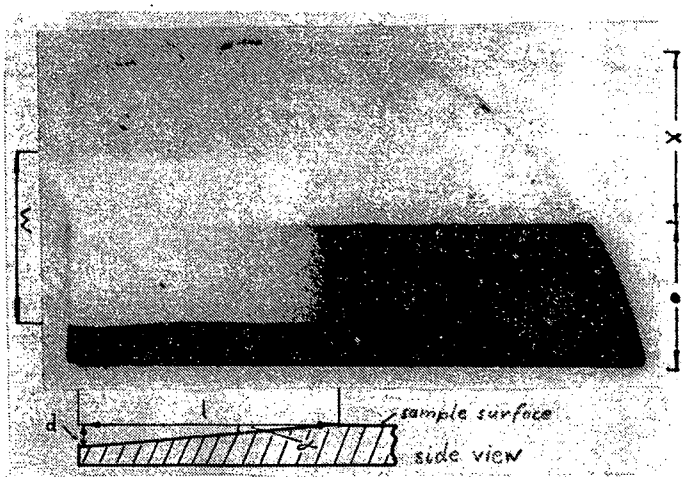

Fig. 1

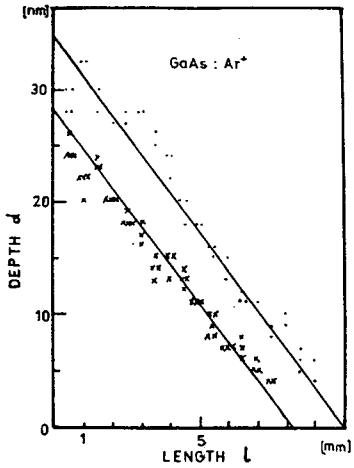

Fig. 2

Fig. 1: Autoradiograph of ^{64}Cu, adsorbed at partly ion beam etched (Ar, 1.6 keV, $1 \cdot 10^{17}$ cm^{-2}), black part of the sample, $< 100 >$ GaAs. A bevelled section for depth profiling made by low energy ion beam etching (Ar, 0.2 keV, 80 μAcm^{-2}) is also shown. The scheme indicates the area (l x w) and the inclination (α) of this section.

Fig. 2: Step height profile of the bevelled section of Fig. 1. All measured points of the Talystep measurements are shown: (— • —) damaged area, (— x —) undamaged area.

blacking curve of the autoradiograph in connection with the mechanical profile measured by the Talystep method give the copper concentration depth profile. Fig. 1 shows the autoradiograph of a sample which was prepared as mentioned above. The bevelled section on the partly damaged sample is indicated. Ion beam etching was done with 1.6 keV Ar ions with a dose of $1 \cdot 10^{17}$ cm^{-2}. In Fig. 2 the mechanical profile of the bevelled section of the sample in Fig. 1 is shown (-x- not ion beam etched, —•—ion beam etched). The differerence in step height between the damaged and the nondamaged part results from the higher sputtering rate of the damaged layer.

There are obvious problems with the used profile measurement technique because damage caused by ion beam etching has to be measured by ion beam etching depth profiling. Absolute concentration profiles cannot be reliably measured in this case but contrasts between different conditions of damage production are easily registered. Fig. 3 shows the copper concentration depth profiles of four different ion energies and of the unetched sample part. The profiles are normalized to unity at the maximum.

The depth profile of the unetched sample part is also shown. The copper concentration is more than one order of magnitude lower than in the damaged layers.

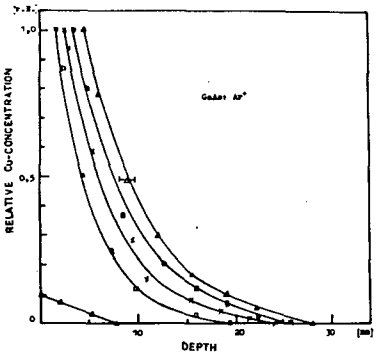

Fig. 3

^{64}Cu depth distribution of adsorbed copper on ion beam etched <100> GaAs. Ar ion beam etching parameters are normal incidence dose 1 . 10^{17} cm^{-2}, ion energy 0.7 keV (●); 1.0 keV (x); 1.6 keV (■), 2.0 keV (△) and unetched (▲). The solid curves are only guides for the eye.

The measurements show clearly that the copper is distributed throughout the damaged layer. It is also shown that there are very deep tails in the profiles, far deeper than the predected and measured /2/ thicknesses of the heavily damaged layers. Similar results were obtained for the depth distribution of implanted Ar-etching gas in Silicon by SIMS /3/. Our experiments suggest that the combination of ^{64}Cu adsorption and bevelled sections is a useful tool for the characterization of near surface damaged layers in GaAs.

References

/1/ R. Fechner, A. Schindler, J. Flachowsky, Gemeinsamer Jahresbericht ZfK, 559, 127 (1984)

/2/ R. Fechner, A. Schindler, R. Flagmeyer, F. Bigl, this report p. 86

/3/ T. Mizutani, C. J. Dale, W. K. Chu, T. M. Mayer, Nucl. Instr. Meth. in Phys. Res. B 7/8 (1985) 825

A PATTERN EDGE PROFILE SIMULATION FOR ION BEAM ETCHING PROCESSES

G. Ringel, A. Nickel, F. Bigl
Zentralinstitut für Isotopen- und Strahlenforschung Leipzig, Bereich SF, der AdW der DDR

The erosion of surfaces by low-energy ion bombardment has important industrial and scientific applications. Ion beam etching is an important process in semiconductor technology for pattern delineation.

A number of mechanisms may be responsible for the formation of ion-induced topography. One of the most important mechanisms under most circumstances relates to the dependence of the etching rate V on the angle of incidence Θ. A typical dependence for ion milling is shown in Fig. 1.

The erosion of a surface profile can be described by the following equation /1/:

$$X(T + t) = X(T) + t\,(V(\Theta)\cdot\sin\Theta + \cos\Theta \cdot dV/d\Theta)$$
$$Y(T + t) = Y(T) + t\,(\sin\Theta\cdot dV/d\Theta + \cos\Theta\cdot V(\Theta))$$

with T, t - erosion time
V(Θ) - etching rate for the edge angle Θ
X, Y - coordinates of the points for the generally discrete points at time T or $(\overline{T} + t)$

It is known that these equations are valid for homogeneous materials. So it is necassary

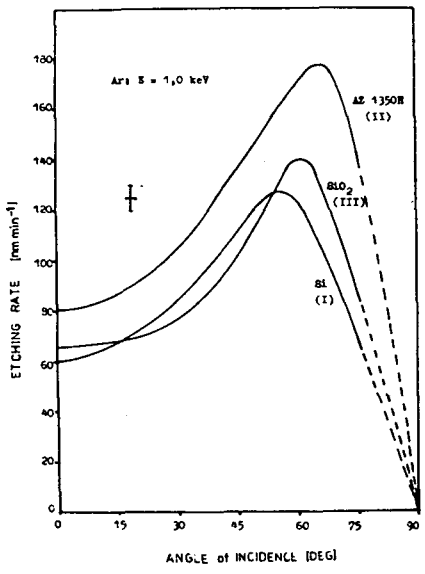

Fig. 1

in addition to solve the following equation for interfaces.

$VM(\Theta)/\sin(\Theta M) = VS(\Theta S)/\sin(\Theta S)$

with $VM(\Theta M)$ - etching rate of the masking material for an edge angle ΘM

$VM(\Theta S)$ - etching rate of the substrate material for the unknown angle ΘS of the substrate profile

Figure 2 shows the time-dependent evolution of the pattern edge profile for the ion beam etching of a 500 nm SiO_2 layer with Ar ions. The SiO_2 layer was over-etched with 100 nm. The edge erosion of the masking material is so high that after a quarter of the total etching time an etching process in the SiO_2 layer has taken place both in the vertical and the horizontal direction. The edge angle in the SiO_2 layer is relatively small.

Though for a lot of materials the differences of the etching rates in ion milling are very small, the next figure shows their considerable influence on profile evolution.

Let us suppose that the smallest etching rate is the etching rate of the masking material and the highest etching rate is the etching rate of the layer which has to be structured, see Fig. 1. The result is shown in Fig. 3. The edge angle of the structured layer would be increased, to about 76°. On the other hand the displacement of the edge would increase to 0.3 µm.

The present program for the modelling of pattern edge profiles during ion milling is also used for reactive ion beam etching.

References

1 M. Cantagrel, IEEE Trans. Elect. Dev. ED 22, 7, 1975

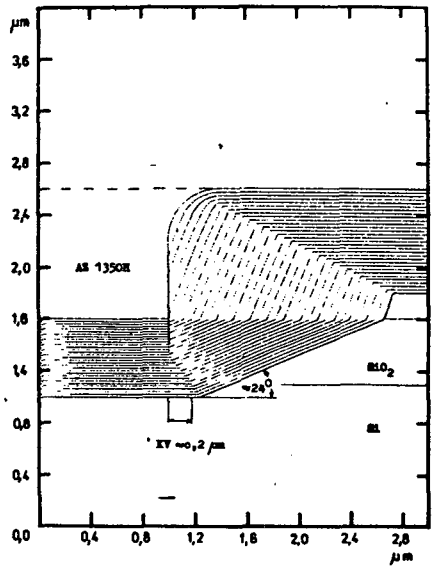

Fig. 2

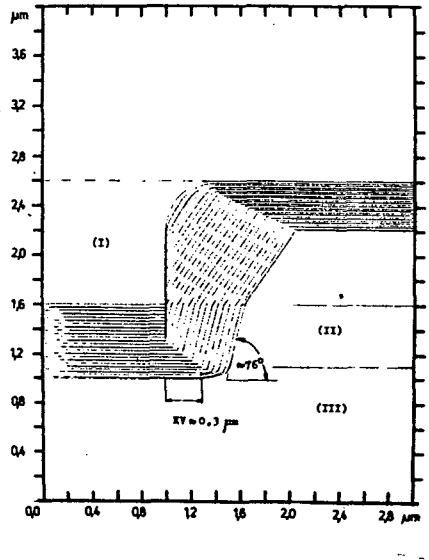

Fig. 3

SCANNING MICROBEAM WITH A LIQUID METAL ION SOURCE

J. Mittenbacher
Friedrich-Schiller-Universtität Jena, Sektion Physik

The focused ion beam (FIB) technology in the future will be applied in many ways in VLSI process. For it, high intensity ion probe systems with liquid metal ion sources (LMIS) have been developed recently. Continuing our work on LMIS /1,2/ an electrostatic optical system has been designed to produce FIB. Using components of an electron microscope ELMI-D an optical column was built up. It consists of the ion gun (emitter, control-electrode, extractor), condensor lens, beam alignment plates, ExB mass filter, octupol stigmator, objective lens and postdeflector. An electron-photon conversion-type secondary electron detector is set close to the work stage. The block diagram of the equipment is illustrated in Fig. 1.

Preliminary operation of this s ystem was done with a Ga^+-LMI-source without the mass filter-stigmator module. The Ga^+ ions are accelerated to 6 - 35 keV and focused on the target. By employing two three-electrode einzel lenses a fixed image and object distance is achieved while variing the beam energy. Lens operation occurs in the acceleration mode. Electrostatic beam deflection control the beam position, while writing various patterns from single point to 64-1024 lines. A CRT driven synchronously is modulated by the z- or y-signal. A typical scanning ion micrograph (SIM) image of an MOS-IC bombarded with 25 keV Ga^+ ions is shown in Fig. 2. The dominant image contrast mechanism is conductivity. SIM resolution of approximately 1 - 2 µm has been achieved till now. In order to obtain spot diameters in the submicron range, improvements to develop a condensor lens with lower aberration and to reduce electrical power supplies ripple are provided for the next time.

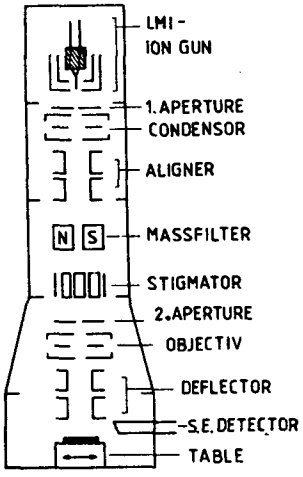

Fig. 1
Schematic diagram of the FIB system

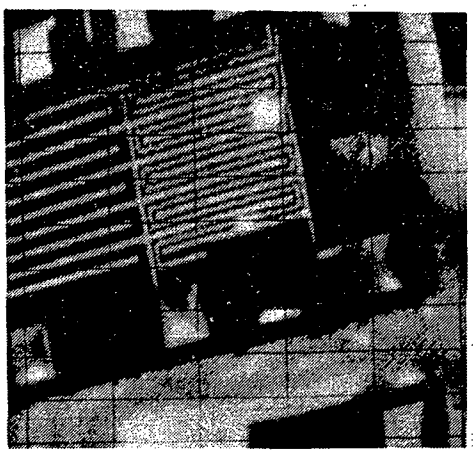

Fig. 2
SIM of an integrated circuit
70 x

References

/1/ Mittenbacher, J., Gemeinsamer Jahresbericht 1984, ZfK-559 (1985) 94

/2/ Mühle, R., J. Mittenbacher, Forschungsergebnisse Friedrich-Schiller-Universität 1986 N/86/31, unveröffentlicht

DETERMINATION OF THRESHOLD VOLTAGES OF LIQUID METAL ION SOURCES

I. Stiebritz, R. Mühle, F. Machalett
Friedrich- Schiller- Universität Jena, Sektion Physik

In the present work the ion source consisted of a needle emitter wetted by liquid gallium and an extraction electrode without aperture.
The dependence of the threshold voltage on geometrical parameters was determined experimentally and computed numerically by a finite difference scheme using a spherical coordinate with increasing mesh size /1/.
The threshold voltage V_t as a function of the tip radius r_t and the distance d is represented in the figures 1 and 2, respectivly (d-distance between extraction electrode and emitter tip).
From the experimental as well the numerical data a simple empirical equation could be derived for calculation of threshold voltages:

$$V_t = 2\sqrt{\gamma/\varepsilon_0}\sqrt[4]{r_t d}$$

(γ- surface tension, ε_0- dielectric constant).
By this expression it is also possible to determine the surface tension of various liquid metals or alloys. For temperatures near the melting point we determined with a precision of 10 percent for:

gallium γ = 0.7 N/m
Au-Si γ = 0.8 N/m
gold γ = 1.1 N/m

in good agreement with tabulated values /2/.

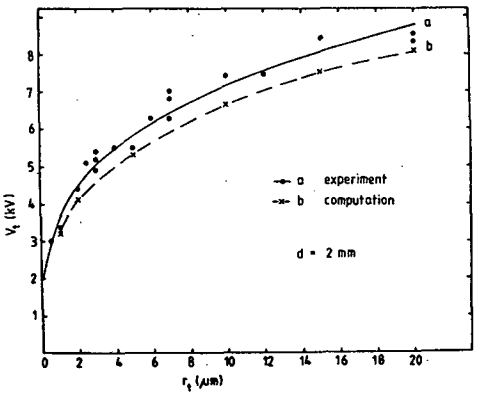

Fig.1 Threshold voltage V_t vs. tip radius r_t for gallium emitters

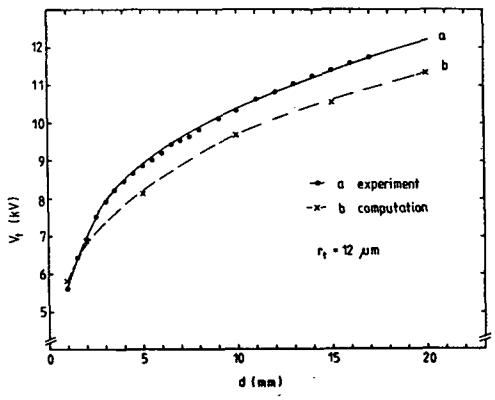

Fig.2 Threshold voltage V_t vs. distance between extractor and emitter tip for one gallium emitter

R e f e r e n c e s ;
/1/ Kang, N.K., Tuggle, D., Swanson, L.W., Optik 1982
/2/ CRC Handbook of Chemistry and Physics, Florida (1980)

MASS SPECTRA OF Au-Si ALLOY LIQUID METAL ION SOURCES

R. Mühle, F. Machalett, I. Stiebritz
Friedrich-Schiller-Universität Jena, Sektion Physik

In order to optimize the working parameters of Au-Si alloy liquid metal ion sources the influence of the alloy composition and the source current on the beam composition was investigated. The measurements were carried out by means of the ion source and the mass spectrometer described in /1/ and /2/, respectively.
The influence of the source feed composition on the intensity of the main ion species in the beam is shown in Fig. 1. It is visible that an increase of the silicon fraction in the source material causes an increase of the proportion of silicon ions and of the Au-Si compounds too. Fig. 2 shows the flux ratios of the various ion species normalized to the total ion flux as a function of the source current. For these measurements the eutectic composition of $Au_{82}Si_{18}$ was employed. It can be seen that for increasing source current the Si^+ and $AuSi^+$ fractions increase while the Au^+ fraction decreases and those of Si^{++}, Si_2^+, Au_2Si^{++}, Au^{++}(beyond 40µA) are nearly constant. The ratios of doubly to singly charged ion fluxes as functions of the source current are shown in Fig. 3. There can be seen that the two ratios decrease with increasing source current.

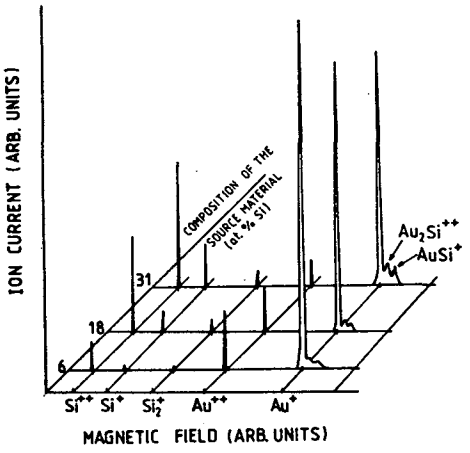

Fig.1 Main ion species of the Au-Si mass spectrum in dependence on the material composition

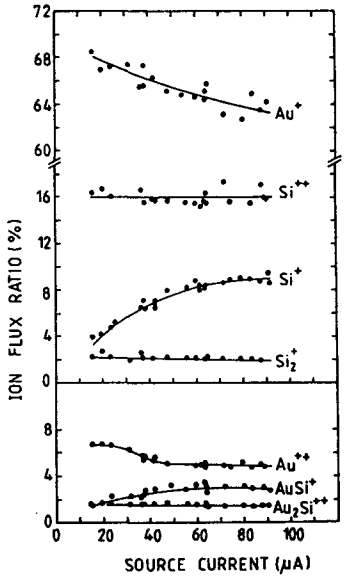

Fig.2 Ion flux ratios of varios ion species normalized to the total ion flux as a function of the source current

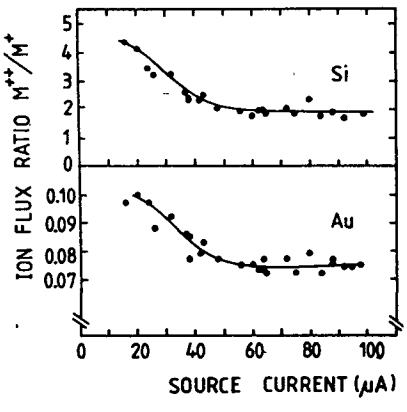

Fig.3 Ratios of doubly to singly charged ion fluxes as a function of the source current

R e f e r e n c e s ;
/1/ Mittenbacher, J., Gemeinsamer Jahresbericht 1984, ZfK-559 (1985) 94
/2/ Mühle, R., Machalett, F., Annual Report 1985 ZfK-584 (1986) 125

MEASUREMENTS WITH AN E*B TYPE MASS SEPARATOR

R. Mühle, A. Matthies, I. Stiebritz, F. Machalett
Friedrich-Schiller-Universität Jena, Sektion Physik

In ion microbeam systems an E*B type mass filter is often employed for the separation of the different ion species, delivered by the liquid metal ion sources. While its mass resolution is considerably lower than that of a sector magnet, use of this filter leads to a simple optical configuration because of its straight beam line /2,3/. The design of the E*B mass separator is described in the article by Seliger /1/.
A schematic diagram of our ion optical column is shown in Fig.1. It consists of the following elements: ion source, condenser lens, E*B mass separator and Faraday cage. The emitted ions are accelerated by the extractor voltage to energies between 5 and 25 keV and are focused by the condenser lens on the separation aperture. The lenght of the field region is L_f=5cm and that of the drift space L_d=7cm. Separation apertures with diameters of 1, 0.5 and 0.1 mm are used. The magnetic field of the strength of 0.1 T is realized by a Maniperm-ceramic magnet. The ions are collected by a Faraday cage.
The atomic composition of the alloys used was $Au_{82}Si_{18}$ and $Au_{80}Be_{20}$. The obtained mass spectra are shown in Fig.2 and 3. The values of source current I_s and of extractor voltage U_{ex} are indicated. Using a 0.5 mm diameter separation aperture, a mass resolution of about 30 was obtained. The silicon isotopes could be separated. The observed Al ions in the Au-Be mass spectrum arise from the corundum ampoule where the alloy was melted. The observed ion species and the related ion flux fractions of the $Au_{82}Si_{18}$ alloy correspond with those measured with a magnetic spectrometer /4/. The values for the $Au_{80}Be_{20}$ alloy are not yet been published and are the following:

ion species	Au_2^+	Au^+	Au^{++}	Al_2^+	Al^+	Al^{++}	Be^+	Be^{++}
ion flux fraction (%)	7.28	65.17	6.84	1.24	0.83	0.36	14.37	3.91

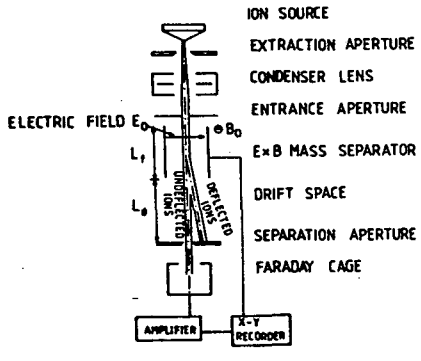

Fig.1 Ion optics column

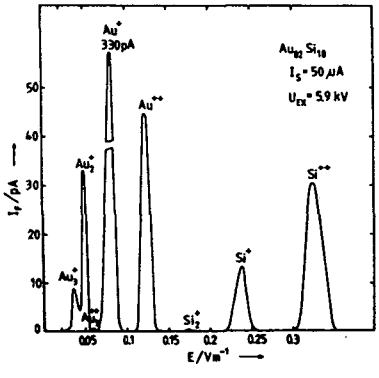

Fig.2 Mass spectrum of the $Au_{82}Si_{18}$ alloy

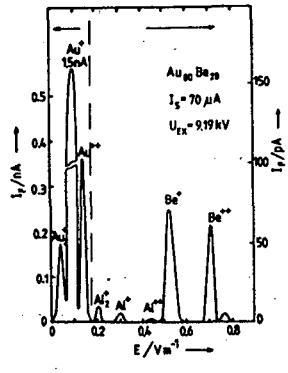

Fig.3 Mass spectrum of the $Au_{80}Be_{20}$ alloy

References;
/1/ Seliger, R.L., J.Appl.Phys. 43 (1972) 2352
/2/ Shiokawa, T. et al., Microcircuit Engineering 1984
/3/ Ishitani, T. et al., Nucl.Instr. and Methods 218 (1983) 369
/4/ Machalett, F., Mühle, R., Stiebritz, I., to be published in J.Phys.D

AMORPHIZATION AND ELECTRICAL PROPERTIES OF SILICON AFTER HIGH ENERGY PHOSPHORUS IMPLANTATION

W. Skorupa, R. Grötzschel and E. Wieser
Zentralinstitut für Kernforschung, Rossendorf, Bereich KF

First results concerning the properties of silicon after 0.99 MeV, $^{31}P^+$-implantation and different annealing schemes have been reported recently /1,2/. Further experiments included the test to amorphize silicon at such high energies and the investigation of the electrical properties after implantation of doses in the range 10^{12} - 10^{16} cm^{-2}.

Previously, it was reported that amorphization is not possible by depositing that energy density into nuclear processes being sufficient at low implantation energies /2/. Implantation with doses higher than $7.5 \cdot 10^{14}$ cm^2 as used in /2/ was performed in the range $0.75 - 6 \cdot 10^{15}$ cm^{-2}. It was shown by RBS (1.7 MeV, $^4He^+$) that a buried amorphous layer was formed after implanting a dose of $4 \cdot 10^{15}$ cm^{-2}. This dose is higher by a factor of about 7 compared with results of Morehead et al. /3/ who reported a threshold dose of $6 \cdot 10^{14}$ cm^{-2} at 200 keV and 300 K. Retarded amorphization at higher energies may be explained by radiation enhanced selfannealing due to charged point defects. They should be formed with a high probability considering the large amount of energy deposited into electronic processes at high energy implantation /2/.

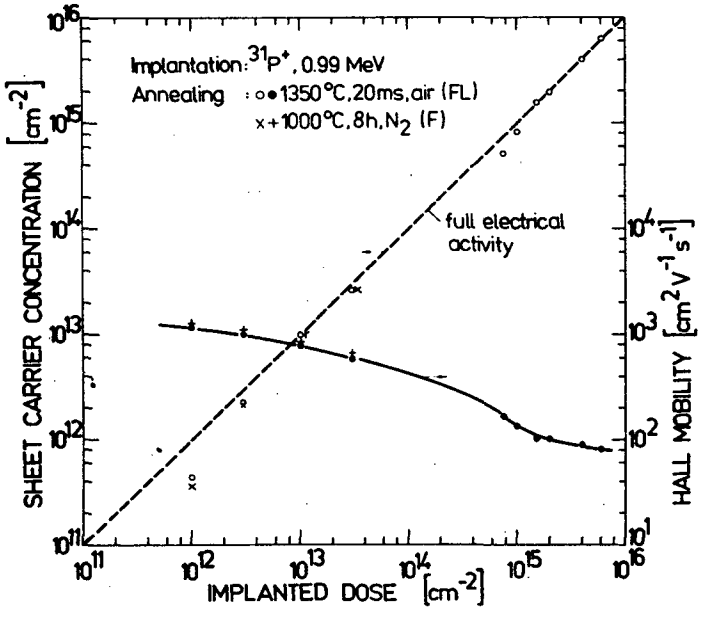

Fig. 1
Sheet carrier concentration and Hall mobility in dependence on implanted dose after 0.99 MeV, P^+-implantation

The results of van der Pauw-measurements are shown in Fig. 1. Post implantation annealing was done by flash lamp irradiation at 1350 °C, 20 ms, air. The dashed line represents an activity of 100 %. Most of the experimental values are in the range 70 - 100 %. The cause for the low activity at 10^{12} cm^{-2} is not clear at present. The Hall mobility behaviour points to impurity scattering indicating well annealed material. For a dose of $7.5 \cdot 10^{14}$ cm^{-2} the mobility was correlated with the volume carrier concentration determined from SIMS profiling. A good agreement with conventional values /4/ for the same volume concentration was reached. For the low dose range also the values reached after furnace annealing at 1000 °C, 8 h, N_2 are included. Only a little difference was found. Such an anneal step was used to simulate the influence of technological processes after CMOS well formation.

References

/1/ Skorupa, W. et al., Gemeinsamer Jahresbericht 1985, ZfK-584 (1986) 45
/2/ Skorupa, W. et al., Proc. 5. Int. Conf. IBMM, Catania 1986
/3/ Morehead, F. et al., J. Appl. Phys. 43 (1972) 1112
/4/ Masetti, G. et al., IEEE-ED 30 (1983) 764

STRONG DOPANT DEPENDENCE OF IMPLANTATION DEFECT ACCUMULATION AND AMORPHISATION IN HEAVILY DOPED SILICON

R. Grötzschel and J. Schöneich
Central Institute for Nuclear Research, Rossendorf, Dept. KF
A.V. Dvurechenskii and V.P. Popov
Institute of Semiconductor Physics, Novosibirsk
H. Bartsch
Institute for Solid State Physics and Electron Microscopy, Halle

The process of defect accumulation and the mechanism of the crystalline-to-amorphous phase transition during ion implantation has been studied widely for elemental and compound crystals /1,2/. The amorphisation is understood as the overlapping of amorphous spikes or, at lower defect creation densities, of collision cascades, where the lattice collapses when a critical relative number of displaced atoms of $\sim$0.1 is reached /3/. In the latter case the defect accumulation - and annihilation processes are mainly influenced by the mobility of the simple defects and their probability for agglomeration, which are dependent on the temperature (e.g. 1/. We have shown that the defect accumulation rate and the amorphisation dose, resp., also depends on the dopant concentration, and in the case of heavily boron doped silicon ($N_B \sim 3$ at.%) the influence is so strong that the amorphisation dose for 80 keV Ne^+ ion implantation has been found to be 10 times higher than for pure silicon /4/.
Heavily doped silicon surface layers were obtained by ion implantation (B^+, As^+, and $B^+ + As^+$) at doses of $5 \cdot 10^{16}$ cm^{-2} and subsequent liquid phase epitaxy by means of PEBA /5/. These samples were implanted simultaneously with 80 keV Ne^+ ions. To avoid thermal effects at elevated temperatures the current density was kept below 0.2 $\mu A\ cm^{-2}$. The implantation was performed in increasing partial doses up to full amorphisation. After the implantation of each partial dose aligned RBS spectra have been taken with the He^+ beam incident along the <100> axis. As a measure for the accumulated damage we used the maximum values χ^D_{max} of the normalized scattering yield from the displaced fraction of the Si atoms.
In Fig. 1 the dependence of χ_{max} on the implanted Ne^+ ion dose D is shown for the different doping atoms.
In the case of silicon crystals and room temperature implantation the crystalline-amorphous transition is complete at the amorphisation dose D_a, when the aligned yield reaches the random yield level. This usually used criterion for amorphisation is in good agreement with the results obtained by electron or X-ray diffraction.

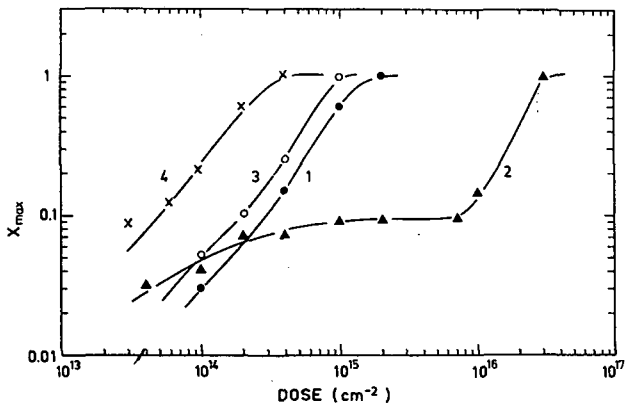

Fig. 1
The χ_{max} values of the normalized backscattering yield of the aligned spectra as a function of the Ne^+ implantation dose D for Si (1), Si <B>, Si <As> , and Si <B+As>

The results, summarized here in Fig. 1, are interpreted qualitatively taking into account the Watkins mechanism /6/.

References

/1/ Thompson, D.A. et al., Radiat. Eff. 25 (1980) 69
/2/ Smirnov, L.S.: Physical Processes in irradiated Semiconductors. Novosibirsk: Nauka 1977, p. 256
/3/ Swanson, M.L. et al., in: Radiation Effects in Semiconductors. Eds. J.W. Corbett and G.D. Watkins. London: Gordon & Breach Ltd. 1971, p. 359
/4/ Dvurechenskii, A.V. et al., Phys. Lett. A116 (19) 8, p. 399
/5/ Dvurechenskii, A.V. et al.: Annealing of Semiconductor Materials. Moscow: Nauka 1982, p. 208
/6/ Watkins, G.D., Journees D'Electronique, Toulouse, 1967, Vol. 1, A1

MODELING OF ENHANCED DIFFUSION AND ELECTRICAL ACTIVATION OF As IMPLANTED INTO Si BY RAPID THERMAL ANNEALING

R. Kögler
Zentralinstitut für Kernforschung, Rossendorf, Bereich KF

A comparison of experimentally determined dopant profiles and sheet carrier concentrations with computer simulations shows a transient enhanced diffusion of As in Si during rapid thermal annealing (RTA, T_{max} = 1000 - 1200 °C, duration 1 to 20 s) with respect to the used computer model by Tsai /1/. The Tsai model describes the diffusion of As in Si according to a vacancy mechanism taking into account neutral and single charged vacancies (V^0, V^-). For maximum As concentrations exceeding the solubility limit the formation of electrically inactive, non mobile As-vacancy clusters is assumed.

The comparison of this model, valid for conventional furnace tempering, with experimental results, obtained by RTA of As implanted Si (energy 100 keV, dose range $5 \cdot 10^{15}$ to $2 \cdot 10^{16}$ cm^{-2}), results in a diffusion coefficient for RTA enhanced by a factor between 2 and 6 depending on As concentration, T_{max} and annealing duration /2/.

This enhanced diffusion coefficient D_{As} can be well described using a model considering beside V^0 and V^- also twofold charged vacancies V^{2-} /3/.

$$D_{As} = D^0 + D^- (n/n_i) + D^{2-} (n/n_i)^2$$

$D^0 = 6 \cdot 10^{-2} \exp(-3.44\ eV/kT)\ cm^2/s$, $D^- = 12 \exp(-4.05\ eV/kT)\ cm^2/s$
$D^{2-} = 125 \exp(-4.6\ eV/kT)\ cm^2/s$

(n = charge carrier concentration in the profile, n_i = intrinsic carrier concentration)

The transient behavior of the diffusion enhancement results from the decreasing carrier concentration due to precipitation or clustering as well as to the diffusional broadening of the profile. The D^{2-} term is only for high carrier concentration important.

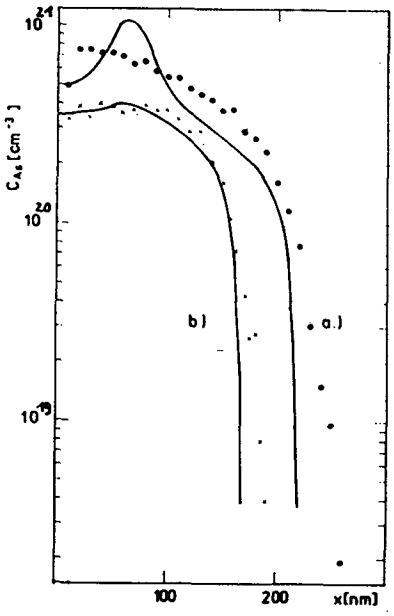

This model describes the diffusion behaviour of As in Si very well as demonstrated by the results in Fig. 1b.
The following conclusions about essential processes during RTA of As in Si are possible:

- For As concentrations $> 10^{21}$ cm^{-3} the assumption is not correct that the clusters of As exceeding the solubility limit are completely non mobile. Such a model gives a profil with a hump in disagreement with the experiment (see Fig. 1a)
- For very short dwell time at T_{max} ($t_d < 5$ s) the computer model results in a too high electrical activation. This points on a higher formation velocity of electrically inactive As in the early stage of annealing than assumed by the Tsai model.

Fig. 1
Depth distribution of arsenic following annealing
computer simulation (line) and RBS depth profile
a) $1 \cdot 10^{16}$ As+/cm^2 (100 keV), T_{max} = 1100 °C, t_d = 10 s
b) $5 \cdot 10^{15}$ As+/cm^2 (100 keV), T_{max} = 1175 °C, t_d = 1 s

References

/1/ Tsai, M.Y., F.F. Morehead, J.E.E. Baglin, A.E. Michel, J. Appl. Phys. 51 (1980) 3230
/2/ Kögler, R., E. Wieser, M. Voelskow, G. Otto, Nucl Instr. and Meth. B in print
/3/ Hoyt, J.L., J.F. Gibbons, Mat. Res. Soc. Conf. Fall Meeting 1985

THRESHOLD OF THE ELECTRICAL ACTIVATION OF Si IMPLANTED GaAs BY SHORT TIME ANNEALING IN THE SOLID PHASE REGIME

D. Panknin and E. Wieser
Zentralinstitut für Kernforschung, Rossendorf, Bereich KF
Ya.V. Fattachov and J.B. Khaibullin
Kazan Physico-Technical Institute, Kazan

The annealing of Si implanted GaAs is characterized by a maximum of the electrical activation for the optimum values with regard to temperature and time. This maximum is caused by the competition of increasing electrical activation due to improved lattice relaxation and of the negativ effect of the surface degradation.

The SI Cr-doped (100) GaAs was implanted in the dose range up to 10^{15} Si/cm^2 at an energy of 200 keV at about 100 °C. Annealing was performed without encapsulant by flash lamp irradiation with pulse durations between 20 and 500 ms or using a set of tungsten halogen lamps with dwell times ≥ 0,5 s.

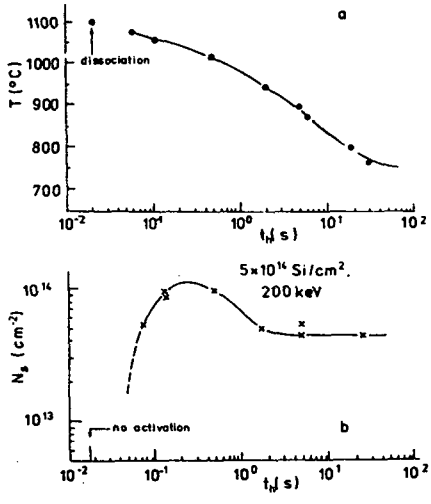

Fig. 1
Dependence of the optimum annealing temperature (a) and of the sheet carrier concentration (b) on the dwell time at T_{max} (capless annealing).

In fig. 1a the dependence of the optimum annealing temperatur on the annealing time is shown for tempering without caplayer. The experiments show a upper temperature limit at about 1100 °C for very short times as well as a smal time dependence at temperatures ≤ 750 °C.
Fig. 1b presents the dependence of the electrical activation on the annealing time for an implantation of $5 \cdot 10^{14}$ Si/cm^2. For each time the optimum temperature according to figure 1a was used. The short time threshold for electrical activation has been found at about 50 ms. For a pulse duration of 20 ms no dopant activation has been measured up to the temperature limit of massive surface degradation (≈ 1100 °C). Annealing with a Si_3N_4 cap up to ≈ 1200 °C gave no better results /1/.

The sheet carrier concentration in fig. 1b is characterized by a maximum of the short annealing time of about 200 ms. This was observed only for Si implanted GaAs with doses ≥ $1 \cdot 10^{14}$ Si/cm^2. An additional annealing at 900 °C, 2 s leads to no remarkable decrease of values observed at annealing < 1 s. This maximum at short annealing times is due to the amphoteric character of Si in GaAs and can be explained by the assumption of a Si concentration on As sites lower than the value for long time annealing /2/

References

/1/ Panknin, D. et al., Nucl. Instr. and Methods (in press)
/2/ Panknin, D. et al., Acta Physica Hungarica (in press)

REDISTRIBUTION OF IMPLANTED As IN A $MoSi_2$/POLYSILICON STRUCTURE BY SHORT TIME ANNEALING

E. Wieser and Ch. Weise
Zentralinstitut für Kernforschung, Rossendorf, Bereich KF
E. Vetter and Th. Geßner
Technische Universität Karl-Marx-Stadt, Sektion Physik/Elektronische Bauelemente, Technikum Mikroelektronik

Refractory silicides combined with a polysilicon layer to a polycide structure are of growing interest for MOS gate metallization schemes. Thereby, short time annealing is now accepted as a very promising process for silicidation tempering and dopant activation within the polysilicon. An important problem is the redistribution of the impurity atoms used for doping the polysilicon within the sheet system. In the present paper the redistribution of As implanted into $MoSi_2$ on undoped polysilicon will be considered. Rapid thermal annealing (RTA) and conventional furnace annealing will be compared and the influence of a SiO_2 cap layer is shown.

<100> p-type Si wafer were covered with 100 nm SiO_2. Following 150 nm undoped polysilicon were deposited. A stoichiometric Mo/2Si sandwich layer was deposited by cosputtering technique. The thickness of the tempered $MoSi_2$ layer amounts to 100 nm (deposition thickness about 130 nm). The sample were implanted with As at an energy of 125 keV up to a dose of $1 \cdot 10^{16}$ cm^{-2}. Annealing was performed in a furnace in H_2-atmosphere for 30 min at 1000 °C or using a set of halogen lamps for 15 s at 1050 °C in air. Before annealing a part of the wafers was covered with a 200 nm cap layer of plasma CVD SiO_2. The depth distribution of As was measured using the SIMS technique.

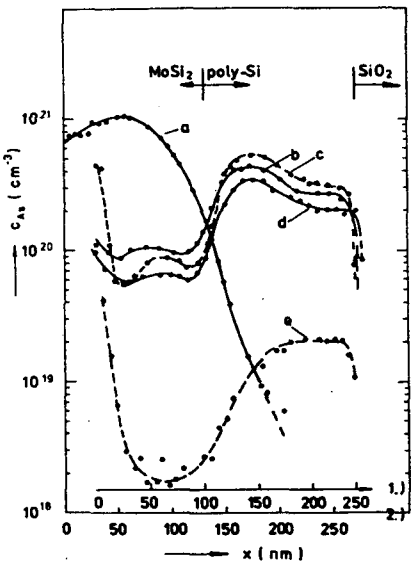

Fig. 1
Depth distribution of As in a $MoSi_2$/polysilicon sheet system: a - as implanted, b - 1050 °C/15 with cap, c - 1050 °C/15 s without cap, d - 1000 °C/30 min with cap, e - 1000 °C/30 min without cap

Figure 1 shows the obtained As profiles. The two different depth scales take into account the shrinking of the $MoSi_2$ by the tempering.

The As depth distributions are very similar for both the short time annealed samples as well for the sample d, tempered at 1000 °C for 30 min with the SiO_2 cap. While the as implanted As profile is mainly concentrated within the $MoSi_2$ layer after silicide formation the largest part of As is found in the polysilicon sheet.
About 40 to 60 percent of the implanted As is lost. After an annealing treatment of 1000 °C/30 min without a cap layer only 1 to 4 percent of the implanted As could be detected.
The present results can be explained in the following way. By the high temperature treatment the hexagonal $MoSi_2$ formed during implantation transforms into the tetragonal phase in a time shorter than 15 s for the considered temperatures. Only a small amount of As is build in the growing tetragonal $MoSi_2$ grains. The main part is concentrated at the grain boundaries and moves very fast in the polysilicon layer and to the $MoSi_2/SiO_2$ interface. Due to saturation of the upper interface and the polysilicon an equilibrium state is approached in about 10 - 15 s for the capped samples. This is proved by the nearly unchanged As distribution after 1000 °C/30 min tempering.

For uncapped samples the evaporation of As leads to a monotonic decreasing As concentration. The As trapped at the $MoSi_2/SiO_2$ interface of the capped samples was removed by the SiO_2 etching.

FORMATION OF BURIED Si_3N_4/SiO_xN_y LAYERS IN SILICON BY HIGH DOSE IMPLANTATION AT 60 keV

W. Skorupa, K. Wollschläger and R. Grötzschel
Zentralinstitut für Kernforschung, Rossendorf, Bereich KF
H. Bartsch
Institut für Festkörperphysik und Elektronenmikroskopie, Halle

Intention

- Formation of buried compound layers at very low implantation energy of 60 keV compared with the usual energy range 150 - 300 keV,
- Synthesis of silicon oxynitride by combined N/O-implantation in alternating sequence,
- Test of the annealing scheme of previous experiments with 330 keV nitrogen beams: T_{target} = 500 °C, post impl. anneal (PIA) = 1200 °C, 5 h, N_2 /1,2/.

Results and conclusions

- Gaussian profile shape in all cases after implanting a total dose of a) 6 N^+ or b) 3 N^+ + 3 O^+ or c) 3 O^+ + 3 N^+ · 10^{17} cm^{-2} as deduced from the silicon part of RBS random spectra; see channels 200 - 250 in Fig. 1 for case c)

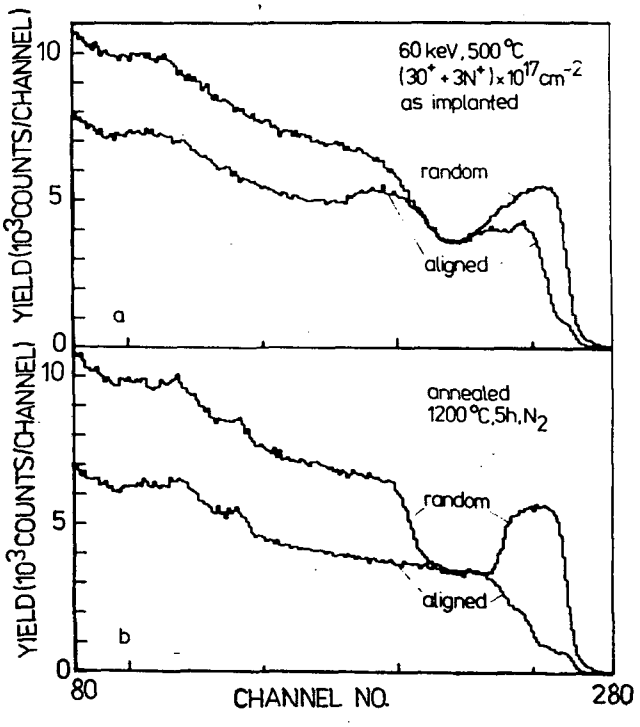

Fig. 1
RBS spectra (1.2 MeV, 4 He^+) after combined N^+, O^+-implantation (a) and annealing at 1200 °C (b)

- By RBS oxygen and nitrogen profiles of the SiO_xN_y layers can not be evaluated separately (channels 100 - 150 in Fig. 1). Other methods are to be used.
- PIA leads to nearly rectangular profiles with steep interregions Si_3N_4/SiO_xN_y-Si due to precipitate dissolution /2/.
- The damage density is lowered drastically after PIA to values of about 5 % for case a), 10 % for b) and 15 % for c). The higher values for the last two cases are caused by the lower dissolution velocity at 1200 °C of precipitates containing oxygen.
- By IR spectroscopy the importance of oxygen for crystallization inhibition in silicon nitride was emphasized /3/. Only SiO_xN_y compounds have random bonding structure before and after PIA at 1200 °C.
- Little crystallites of silicon within the SiO_xN_y layers were found by XTEM. That means the total dose may be somewhat too low for the synthesis of stoichiometric compounds.

References

/1/ Skorupa, W. et al., Gemeinsamer Jahresbericht 1985, ZfK-584 (1986) 46
/2/ Skorupa, W. et al., Proc. 5. Int. Conf. IBMM, Catania 1986
/3/ Skorupa, W. et al., DDR-WP, H 01 L/291 3642

CHEMICAL DEPTH PROFILING OF BURIED SILICON NITRIDE LAYERS IN SILICON BY AUGER ELECTRON SPECTROSCOPY

W. Skorupa
Zentralinstitut für Kernforschung, Rossendorf, Bereich KF
J. Albrecht and J. Götz
VEB ZFTM Dresden

In extending previous studies of ion beam synthesized compounds in silicon with Infrared spectroscopy and X-ray photoelectron spectroscopy /1/ Auger electron spectroscopy with a scanning probe was used to study the chemical structure of buried silicon nitride layer systems. In detail, the depth profiles of bonded silicon and nitrogen and free silicon were recorded. Two modes of profiling were tested: conventional sputter profiling and scanning of a focused electron beam (d ≤ 0.4 µm) on a bevel. The latter method is more advantageous because compound decomposition by sputtering leading to errors in determining the chemical state and the depth scale is avoided. Sputtering was used only for surface cleaning of the bevel before the measurement. Moreover, this method is much more time saving.

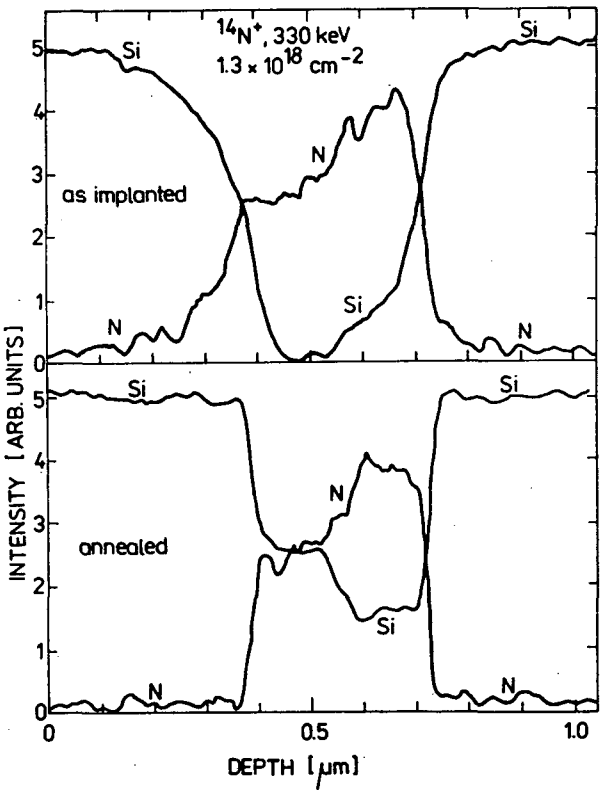

Fig. 1
AES depth profiles of silicon after high dose nitrogen implantation and annealing

First results reached by the scanning method are given in Fig. 1. The buried layer system was produced by implanting a dose of $1.3 \cdot 10^{18}$ N^+cm^{-2} at an energy of 330 keV. Furnace annealing was performed at 1200 °C, 5 h, N_2.
The nitrogen rich region between 0.4 µm and 0.7 µm represents the buried silicon nitride layer. Both, after implantation and annealing a layered structure is visible which is more distinct after the anneal step. An overstoichiometric peak as found by RBS in the centre of such layers after annealing /2/ was not seen. Furthermore, the interfaces between silicon nitride and silicon are steepened after annealing. The steepness is then twice as high as before and comparable to that one of an interface between a Si_3N_4 surface layer deposited by rf-sputtering and the silicon top layer. This Si_3N_4 layer was used at bevel measurements as a surface marker.

References

/1/ Hensel, E., W. Skorupa, Thesis, AdW der DDR, 1985
/2/ Skorupa, W. et al., Proc. 5. Int. Conf. IBMM, Catania 1986

ION BEAM INDUCED EPITAXIAL CRYSTALLIZATION OF DOPED AMORPHOUS SILICON LAYERS

M. Voelskow, W. Skorupa and J. Matthai
Zentralinstitut für Kernforschung, Rossendorf, Bereich KF

Ion beam induced epitaxial crystallization (IBIEC) has become an interesting new method for solid phase epitaxy of amorphous silicon at temperatures below that of conventional furnace variant (> 550 °C). Firstly, this method was reported for silicon by Golecki et al. /1/.

Because the recrystallization rate is proportional to the energy of the annealing ions deposited into nuclear process the use of low implantation energies should be advantageous for a high recrystallization velocity. However, most of the previous work was concerned with high energies > 300 keV. Otherwise, only self ion amorphized layers were studied systematically.

In this letter we report about a peculiarity of IBIEC at relatively low energy of 165 keV applied to arsenic doped (100 keV, $1 \cdot 10^{15}$ cm^{-2}) amorphous silicon layers. Target heating as necessary for IBIEC was firstly done by the ion beam itself. A target temperature of 400 °C was realized using 165 keV N^+ (330 keV, N_2^+) ions with a beam current density of 8 µA cm^{-2}.

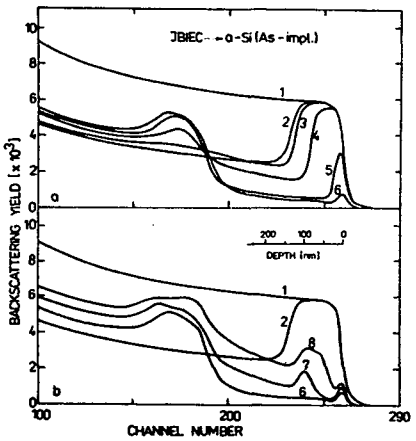

Fig. 1
RBS spectra (1.2 MeV, He^+) of amorphous silicon layers (100 keV, As^+, $1 \cdot 10^{15}$ cm^{-2}, RT) on monocrystalline silicon after different steps of IBIEC (165 keV, N^+, 400 °C); random (1), aligned (2-8)
2 - as amorphized; 3 - $1 \cdot 10^{16}$ cm^{-2}; 4 - $3 \cdot 10^{16}$ cm^{-2}; 5 - $5 \cdot 10^{16}$ cm^{-2}; 6 - $7 \cdot 10^{16}$ cm^{-2}; 7 - $9 \cdot 10^{16}$ cm^{-2}; 8 - $12 \cdot 10^{16}$ cm^{-2}

In Fig. 1 RBS spectra of an amorphous silicon layer with an initial thickness of 140 nm after different regrowth steps by IBIEC are shown. The regrowth process begins at doses $\geq 1 \cdot 10^{15}$ cm^{-2} and after implanting a dose of $7 \cdot 10^{16}$ cm^{-2} full recrystallization is reached. At a depth corresponding to the projected range of the nitrogen annealing ions ($\sim$ 380 nm) a defect peak grows due to the high nitrogen concentration in this region. Surprisingly, further irradiation up to a dose of $1.2 \cdot 10^{17}$ cm^{-2} leads to the evolution of a second defect peak in the region of the regrown amorphous layer (lower part of Fig. 1). The depth of this peak corresponds well to the projected range of 70 nm of the arsenic atoms used for amorphization. To circumvent the influence of arsenic in our experiment self ion amorphized layers were regrown by IBIEC in the same manner as the arsenic amorphized ones. As shown by RBS measurement no defect peak was found in this experiment. That means, the presence of arsenic within the amorphous layer of the first experiment is of crucial importance for the evolution of the second defect peak.

The formation of this defect peak may by explained by point defects which will by created especially at the projected range of the annealing ions. Due to the high target temperature they are expected to migrate during IBIEC. A part of those moving to the surface may be trapped by arsenic atoms forming point defect clusters or secondary defects like loops.

References

/1/ Golecki, I., G.E. Chapman, S.S. Lau, B.-Y. Tsaur, J .W. Mayer, Phys. Lett. A71 (1979) 267

ELECTRICAL PROPERTIES OF MOS STRUCTURES FABRICATED IN LAMP RECRYSTALLIZED FILMS ON SiO_2

N. Sieber, H. Oertel and M. Voelskow
Zentralinstitut für Kernforschung, Rossendorf, Bereich KF

Recent investigations have shown, that lamp recrystallized silicon (r-Si) exhibits n-type conductivity with a free carrier concentration between $3 \cdot 10^{15}$ and $1 \cdot 10^{17}$ cm^{-3} /1/. Values for the generation lifetime range from 0.1 µs to 1 µs /2/. These different values of the generation lifetime are probably caused by different preparation prior or after the recrystallization.

It is the purpose of this paper to investigate the effect of some process steps, such as chemical cleaning, preoxidation and HCl oxidation on the electrical properties of MOS structures prepared in 0.45 µm thick silicon films recrystallized by lateral zone melting. The effect of preoxidation was investigated by growing a thermal oxide approximately 60 nm thick in dry O_2 which was subsequently etched away. Other samples were prepared by standard chemical cleaning of the silicon films only.

Planar MOS capacitors were fabricated growing a 70 nm thick gate oxide in dry O_2 at 1000 °C with or without HCl. The electrical properties of these MOS structures have been investigated using high-frequency and quasistatic capacitance voltage (CV), triangular voltage sweep (TVS) and Halleffect measurements.

As a result the doping concentration in the r-Si films gives a value of $1.4 \cdot 10^{16}$ cm^{-3}. This relatively high unintentional doping concentration could be due to diffusion and/or segregation of impurities such as N, C, O and P /1/ from the cap layers and the underlying oxide during the recrystallization process.

The other electrical properties, such as interfacial effective charge N_f at flat band condition of high frequency CV characteristics, density of interface states N_{st} at midgap point of the quasistatic CV characteristics, sodium concentration N_{Na} determined at 250 °C, Hall mobility μ_H and generation lifetime τ_g are summarized in Table 1.

Table 1

Process	N_f /eV^{-1} cm^{-2}/	N_{st} /eV^{-1} cm^{-2}/	N_{Na} /cm^{-2}/	μ_H /$cm^2V^{-1}z^{-1}$/	τ_g /µs/
		Gate-Oxide without HCl			
Chemical cleaning	$5.6 \cdot 10^{10}$	$4.1 \cdot 10^{10}$	10^{10}-$8 \cdot 10^{10}$	750	$\leqslant 0.1$
Preoxidation	$5.3 \cdot 10^{10}$	$4.0 \cdot 10^{10}$	10^{10}-$8 \cdot 10^{10}$	760	$\leqslant 0.1$
		Gate-Oxide with HCl			
Chemical cleaning	$4.6 \cdot 10^{10}$	$3.8 \cdot 10^{10}$	$<10^{10}$	860 - 900	2.4
Preoxidation	$4.6 \cdot 10^{10}$	$3.0 \cdot 10^{10}$	$<10^{10}$	900	2.4 - 2.6

The data of Table 1 demonstrate that preoxidation of r-Si has no advantageous effect on the electrical properties against chemical cleaning only for both kinds of oxide. A comparison of the data for the samples oxidized with and without HCl shows an appreciable improvement in the electrical parameters and especially in the generation lifetime due to the HCl oxidation.

References

/1/ Tsaur, B.-Y., John C.C. Fan, M.W. Geis, Appl. Phys. Lett. 41 (1982) 83
/2/ Vu, D.P., A. Chantre, H. Mingam, C. Vincent, J. Appl. Phys. 56 (1984) 1682

ETCH RATE MODIFICATION OF THERMALLY GROWN SiO_2 LAYERS BY ION BOMBARDMENT

H. Münzer, C. Neelmeijer, M. Posselt, B. Schmidt
Zentralinstitut für Kernforschung Rossendorf, Bereich KF

Thermally grown silicon oxide layers are widely used as both dielectric layers in MOS-structures and passivation layers against moisture penetration and alcali ion contamination. Defects, impurities as well as clusters of both creating during the semiconductor device production change the structure of the amorphous SiO_2-network in connection with changed bonding states. The chemical reaction velocity between SiO_2 and the etching solution is determined by the bonding state.

We present experimental results for enhanced etching rates owing to ion bombardment induced defect creation in comparison to calculated defect profiles in thermally grown SiO_2. Thermal SiO_2 films were deposited on <100> p-type polished silicon wafers by wet oxydation at T = 1150 °C. Wafers with different SiO_2 layer thickness (715 nm and 414 nm) were implanted with He^+ and Ne^+ ions respectively. The implantation was curried out at E = 60 keV and $D = 1 \cdot 10^{15}$ cm^{-2}. After ion implantation the wafers were etched with 2.7 % HF at T = 25 °C. The thickness of the removed SiO_2 layer was measured both mechanically by means of a Talystep and by the optical interference technique. Combining these methods it was possible to determine the refractive index n in dependence of the layer depth. No change of n was observed. For nonimplanted SiO_2 layers the etch rate of $v_o = 16.5$ nm·min^{-1} was found.

Fig.1 presents the etch rate profiles. The ion induced defect profiles were simulated using Monte-Carlo-calculations [1] . To get information about the relative location and shape of the experimental etch profile with respect to calculated defect distribution the theoretical peak maximum was normalized to the maximum of the etch rate v_{max}.

In the case of Ne^+ the position of experimental and theoretical peak maxima agree well independent of the nuclear potential applied for calculations. This agreement is generally not observed for He^+. The introduction of a Moliere-potential instead of an universal potential improves the theoretical description slightly. However we assume the major part of diviations to be caused by uncertainties of the model (Lindhard, Scharff - Bethe, Bloch, LSBB) for electronic stopping applied. In both cases the shape of the defect profiles is less affected by the nuclear potential. For Ne^+ implantation the remaining diviations at the high energy tail have been not completely understood until now.

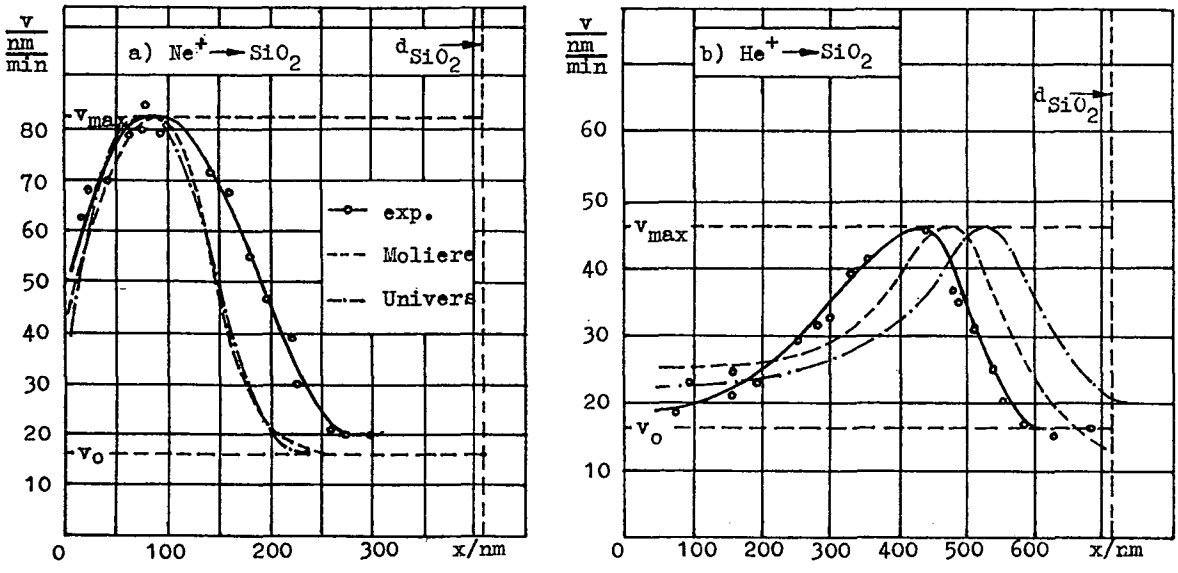

Fig. 1: Etch rate profiles and calculated defect distributions for Ne^+ (a) and He^+ (b) implanted SiO_2

References

[1] Posselt, M. and J.P. Biersack, Nucl. Instr. and Meth. B, 15 (1986) 20.

A NOVAL PROCESSING TECHNIQUE FOR THE FABRICATION OF THIN ANISOTROPICALLY ETCHED SINGLE CRYSTALLINE SILICON LAYERS

B. Schmidt, U. Kreißig, H. Münzer, E. Rost

Zentralinstitut für Kernforschung Rossendorf, Bereich KF

There are several etch stop techniques that exhibit strong dependence of the etch rate on the dopant concentration of single crystalline silicon [1,2] . For the usually used alkaline solutions (ethylenediamine-water and potassium-hydroxide-water mixtures) the etch stop is realized by heavy boron doping ($N_B \sim 1 \cdot 10^{20}$ cm^{-3}). Insulating etch stop layers such as SiO_2 and Si_3N_4 to this time are only used for poly-silicon or nonsemiconducting layers [3,4].
In the present work at the first time ion implanted buried Si_3N_4-layers are used as an etch stop for epitaxial silicon layers. For the investigation the starting material was <100>-oriented polished silicon wafers with ρ_n = 1...10 Ωcm and 40% KOH-water mixture as selective anisotropic etchant was applied. The wafers were implanted with nitrogen at E = 330 keV and D = $1.2 \cdot 10^{18}$ cm^{-2} to form the buried Si_3N_4-layer. The mean layer depth was about 600 nm and the layer thickness about 300 nm. Undoped epitaxial layers with $0.5 \leq d_{epi}/\mu m \leq 5$ were deposited on the single crystalline silicon top layer above the buried Si_3N_4-layer. The anisotropical etching was chosen through a mask from the backside of the wafer (Fig.1).

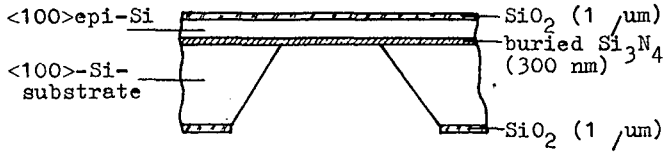

Fig.1:
Cross section of the anisotropically etched wafer with buried Si_3N_4 as an etch stop layer

The etch process stops excellent when the buried Si_3N_4-layer is reached. We have observed a high selectivity with an etch rate ratio of $R_{100\ Si}/R_{Si_3N_4} \geq 10^2$. In comparison, the etch rate in heavely boron doped p^+-layers is lowered by a factor 10...100 [1]. Good flatness for small etched areas until 135x135 µm^2 and 135x2135 µm^2 was observed. Etched areas until 10x10 mm^2 were wavy but mechanical very stable.
Possible applications of this noval etch stop technique for example are the construction of sensor elements, micromechanical devices and the manufacturing of thin masks for X-ray lithography.

References

[1] Petersen, K.E., Proc. of the IEEE 70 (1982) 420
[2] Csepregi, L. et al., Forschungsbericht BMFT-FB-T 84-209 (1984)
[3] Müller, J.E. et al., Proc. 2nd Symp. Measurement in Ind. & Sci., Suhl (1984) 179
[4] Choi, I.H., K.D. Wise, Proc. 3rd Int. Conf. Transducer '85, Philadelphia (1985) 132

RESULTS OF HIGH RESISTIVITY NTD - SILICON SLICE PRODUCTION

L. Bischoff

Zentralinstitut für Kernforschung Rossendorf, Bereich KF

The Neutron Transmutation Doping (NTD) technique to produce high resistivity n-type Si ($\varrho_n \geq$ 10 kΩcm) became a standard process in ZfK last year /1/. This NTD-Si is necessary to manufacture nuclear radiation detectors (NRD) with depletion layers up to 1 mm and detectors for backscattered electrons in the energy range 10...30 keV with very low capacities. The electron-detectors (ED) are installed in the Electron-Beam Inspection System ZRM 20 of Carl Zeiss Jena.

Table 1 gives a survey about the several irradiation cycles. The starting material used in the present work was p-type Si (ϱ_p = 2...5 kΩcm) from the Central Institute of Electron Physics Berlin. The application of a two-step-annealing to reduce the phosphorous concentration and to improve the minority carrier livetime τ /2/ led to an increase of the yield (Yield parameters: $\varrho_n > 8$ kΩcm, $\tau > 200\mu s$).

The doping rates $K\Phi = N_p$ and their deviations are represented in Table 2. On an average an overirradiation according to $1.65 \cdot 10^{11}$ cm^{-3} was found.

The failure was caused by slices with too low resistivity, by broken slices during the NTD-process and by slices for calibration.

cycle	No. of cassettes	No. of slices	No. with two-step-a.	yield slices	%	application
I	2	8	-	-	-	calibration
II	2	23	-	23	100	ED
III	2	35	18	35	100	ED, NRD
IV	2	59	-	58	98	ED
V	2	65	40	26	40	ED
VI	2	59	10	54	92	ED
VII	3	96	-	69	72	ED, NRD
VIII	2	12	-	-	-	calibration
IX	2	27	-	15	56	ED, annealing exp.
Σ	19	384	68	280	73	

Table 1 Results of the several irradiation cycles

cycle	II		III		IV		V		VI		VII			IX	
cassette D 40-	28	52	53	54	56	57	58	59	60	61	85	86	87	90	91
$K\Phi^{aim}$ $10^{12}cm^{-3}$	4.1	5.1	3.0	4.4	3.4	2.0	1.8	2.8	1.6	3.2	2.5	3.8	3.7	3.0	3.4
$K\Phi^{real}$ $10^{12}cm^{-3}$	4.0	5.0	3.7	4.9	3.5	2.1	3.0	3.2	1.7	3.7	2.0	3.5	3.6	2.8	3.3
$\Delta K\Phi$ $10^{11}cm^{-3}$	1.0	1.0	7.0	1.0	1.0	1.0	12	4.0	1.0	5.0	5.0	3.0	1.0	2.0	1.0
± %	-3	-2	+22	+11	+2	+7	+69	+15	+5	+14	-20	-8	-4	-7	-3

Table 2 Doping values of the several irradiation cycles

References

/1/ L. Bischoff Dissertation, Academy of Sciences of the GDR 1986

/2/ L. Bischoff Annual Report 1985, ZfK-584 (1986) 52

EFFECTS OF 20 keV ELECTRON BEAM RADIATION ON MOS STRUCTURES USING THIN ANODICALLY GROWN OXIDE FILMS

G. Mende and M. Deutscher
Zentralinstitut für Kernforschung, Rossendorf, Bereich KF
H.-J. Döring
VEB Carl Zeiss Jena
H. Flietner
Zentralinstitut für Elektronenphysik, Berlin

Annealed anodically grown SiO_2 films are comparable in quality to thermally grown SiO_2 /1/ although there are structural differences between anodically and thermally grown films /2/.

It is known that exposure to ionizing radiation can cause an increase in the fixed oxide charge density and in the surface state density of the interface between thermally grown SiO_2 and Si.

In the present work we investigated the influence of 20 keV electron beam radiation (dose = $3.6 \cdot 10^{-5}$ As) on MOS structures using anodically grown oxide films at first time.

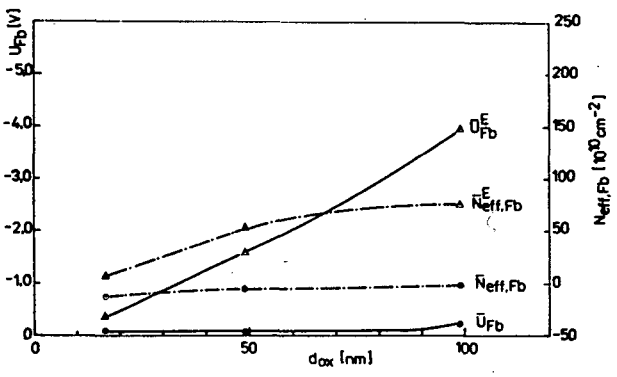

Fig. 1
Flatband voltage shift and fixed oxide charge density of anodically grown silicon oxide films before and after electron beam irradiation

Before and after irradiation the fixed oxide charge density ($N_{eff,Fb}$) and the surface state density in the midgap ($N_{st,Mg}$) depend on anodization technique, oxide film thickness, post-anodization cleaning and annealing conditions.
However, the influence of post-anodization cleaning and of annealing conditions diminishes with decreasing of oxide film thickness.

The influence of oxide film thickness on the flatband voltage shift (U_{Fb}) and the fixed oxide charge density ($N_{eff,Fb}$) of anodically grown silicon oxide films annealed at 400 °C in a nitrogen stream is shown in Fig. 1 before and after electron beam irradiation (U^E_{Fb}, $N^E_{eff,Fb}$).

The radiation hardness of anodically grown oxide films annealed at 800 °C and of thermal SiO_2 films grown in dry oxygen at 1000 °C is practically identical (Table 1). Best results could get with ultrathin anodic oxide films (Table 1).

Table 1
Electrophysical properties of MOS structures using anodically grown or thermally grown oxide films before and after irradiation

oxide type	d_{ox} /nm/	U_{Fb} /V/	U^E_{Fb} /V/	$N_{eff,Fb}$ /10^{10} cm^{-2}/	$N^E_{eff,Fb}$ /10^{10} cm^{-2}/	$N_{st,Mg}$ /10^{10} eV^{-1}cm^{-2}/	$N_{st,Mg}$ /10^{10} eV^{-1}cm^{-2}/
thermal	24	-0.15	-0.24	-15.2	-7.8	2	140
anodic	20	-0.26	-0.28	-5.8	-3.79	2	80
"	15.5	-0.24	-0.26	-10.4	-5.92	-	33

The leakage current of electron detectors passivated with ultrathin anodically grown oxide films (d ≈ 17 nm) is stable under high-vacuum conditions.
The increase of leakage current generated by electron beam irradiation diminishes with oxide film thickness.

Reference

/1/ Mende, G. et al., Thin Solid Films 102 (1983) 65

/2/ Mende, G. et al., 16. Arbeitstagung "Physik der Halbleiteroberfläche", Tagungsbericht, S. 253

OUT-DIFFUSION OF OXYGEN DURING ION BOMBARDMENT OF POLYMER FOILS

W. Rudolph, R. Grötzschel
Zentralinstitut für Kernforschung Rossendorf, Bereich KF

During ^{15}N and ^{19}F ion bombardment of plastic foils a strong hydrogen out-diffusion was observed /1/. In those measurements we found slightly increasing yields of the $^{1}H(^{15}N,\alpha\gamma)^{12}C$ and $^{1}H(^{19}F,\alpha\gamma)^{16}O$ nuclear resonance reactions at low ion fluences for oxygen containing foils. This effect could be explained by an additional out-diffusion of oxygen.

To test this assumption we measured the oxygen to carbon ratios of polyester (Mylar) and polycarbonate (Lexan, Makrofol E) in dependence upon the $^{4}He^{+}$ ion fluence by means of 1.32MeV ^{4}He backscattering analysis. The results are shown in Fig.1. For both materials a strong oxygen out-diffusion is found at the beginning of the irradiation process, whereas for larger ion fluences a constant oxygen content is observed.

For polycarbonate the oxygen out-diffusion is already finished at a He^{+} fluence $\phi \approx 4*10^{14}$ He^{+}/cm^{2}, whereas in the case of polyester the constant oxygen level is only reached for $\phi \gtrsim 25*10^{14}$ He^{+}/cm^{2}. Therefore, the out-diffusion of oxygen depends on the irradiated material. On the other hand our results hint to a constant and material independent oxygen to carbon ratio for large He^{+} fluences (see Fig.1).

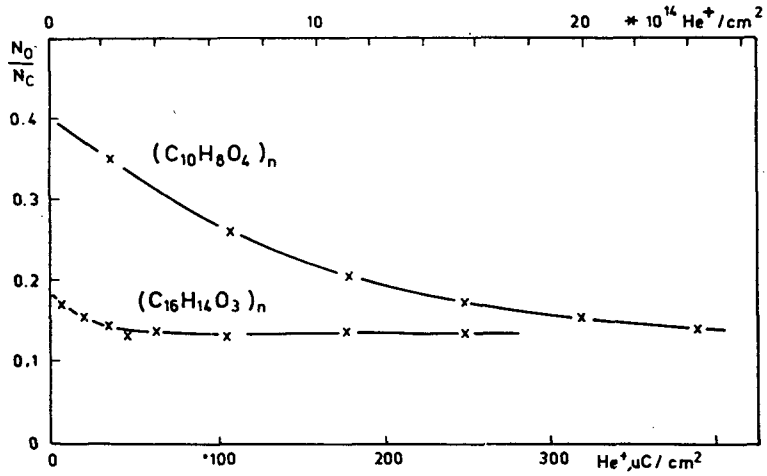

Fig.1: Oxygen to carbon ratios in dependence upon the ^{4}He fluence for polyester $(C_{10}H_8O_4)_n$ and polycarbonate $(C_{16}H_{14}O_3)_n$

Reference

/1/ Rudolph, W. et al.; Nucl. Instr. Meth. B15 (1986) 508

A DIFFRACTION - RELATED CLASSIFICATION OF POLYCRYSTALLINE MATERIALS

P. Klimanek
Bergakademie Freiberg, Sektion Metallurgie und Werkstofftechnik

Theoretical consideration on X-ray or neutron diffraction by polycrystals are often related to a single-phase model structure (ideal polycrystal /1,2/), whose scattering phenomena can be described by averaging the intensity distribution of its single-crystallite scattering over all orientations of the diffraction vector $\vec{g} = (\vec{s} - \vec{s}_0)/\lambda$. The diffraction peaks associated with families of crystallographically equivalent nodes $|\vec{h}|$ = const. of the reciprocal space may be called diffraction singlets in this case. Of course, in order to interprete diffraction by real polycrystals (e.g. by real powders or massive materials interesting in materials science and technology) physically realistic structure models must be used. In the following table a hirarchy of such models is proposed which takes into account the chemical (phase) composition of a microstructure, physical (structural) homogeneity of the crystallites and the spatial arrangement (distribution of positions and orientations) of grains with different structure (arrows indicate interrelations between the structures).

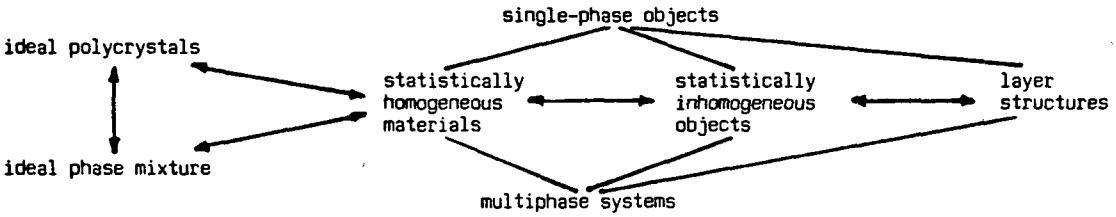

Realization by

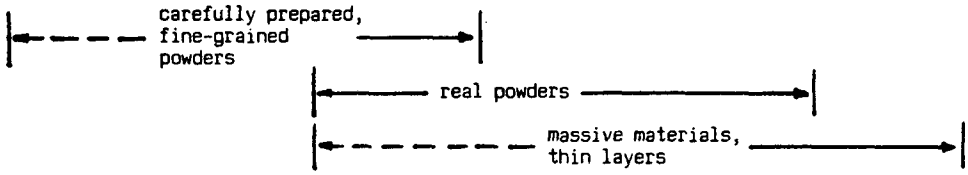

A more detailed discussion of the scheme will be given in /2/. Here only the following explainations may be given:

- Statistically homogeneous polycrystals shall be defined as objects with random (isotropic) spatial arrangement of sufficiently (i.e. with regard to the actual scattering object volume) small grains with similar geometry and only small fluctuations of the lattice disorder. On such conditions all beam pathes are statistically equivalent with respect to absorption in both single-phase and multiphase materials, and the diffraction peaks are practically diffraction singlets yet.
- Statistically inhomogeneous polycrystals are objects, the crystallites of which are nearly randomly (isotropically) distributed but have significantly different size (and shape) and/or non-random orientation distribution (i.e. texture) and/or must be devided into fractions with different lattice disorder. X-ray or neutron reflections of such structures are so-called diffraction multiplets (i.e. weighted sum of partial reflections due to the crystallite fractions with different lattice disorder) /1,2/, which in multiphase systems with various grain diameters D or absorption parameters μD are influenced by the effect of so-called microabsorption (/3/, for instance).
- Layer structures are inhomogeneous polycrystals with anisotropic arrangement of crystallites having different lattice disorder (e.g. in deformation gradients), orientation distribution or grain size (e.g. in thin layers) and/or phase composition (multiphase layers). As in the case of statistically inhomogeneous structures the reflections (hkl) of such structures are diffraction multiplets, but the intensities of the partial reflections are additionally weighted by absorption now, depending on the position of a crystallite fraction within the layer structure. Moreover, the effect of absorption on the partial reflections is different for transmission and backreflection scattering.

Experimental realization of the effects mentioned just will be discussed in /4/.

/1/ Klimanek, P., Cryst. Res. & Technol. 18 (1983) K15
/2/ Klimanek, P., Dissertation B, Bergakademie Freiberg 1987
/3/ Taylor,A., X-Ray Metallography, J.Wiley & Sons, New York, London, 1961
/4/ Klimanek, P., A.Mücklich, p. 110

SAMPLE-INDUCED ERRORS IN QUANTITATIVE DIFFRACTION ANALYSIS OF TEXTURES

P. Klimanek
Bergakademie Freiberg, Sektion Metallurgie und Werkstofftechnik
A. Mücklich
Zentralinstitut für Kernforschung, Rossendorf, Bereich KF

Texture analysis by diffraction methods is based on the fact, that the observed intensity $I_h(y)$ of a reflection $h = \{hkl\}$ associated with a direction y in the sample related axis system of a polycrystal is connected with the orientation distribution of the crystallites by

$$I_h(y) = \sum_j w_j \, P_{h,j}(y) \, \Delta I_{h,j}(y) \qquad (1)$$

where w_j is the volume fraction of a texture component having the pole density $P_{h,j}(y)$ and reflecting the intensity $\Delta I_{h,j}(y)$ into the detector. If $\Delta I_{h,j}(y) = \Delta I_h$ is equal for all texture components, normalization of (1) leads to the quantity

$$P_h(y) = \frac{I_h(y)}{I_h^0} = \sum_j w_j \, P_{h,j}(y); \qquad I_h^0 = \int I_h(y)\,dy \qquad (2)$$

which represents the direct pole figures defined in quantitative texture analysis (/1/, for instance). On practical conditions the equation (1) is valid if

- all crystallites are equivalent with respect to the operating scattering mechanism,
- absorption can be treated as a volume effect and taken into account by a correction factor for all texture components,
- statistical errors due to grain-size induced local fluctuations of $P_{h,j}(y)$ are sufficiently small and
- the detector in all positions of pole figure registration measures the integrated intensity (or the same constant position of it, respectively) of all scattering crystallites.

However, real polycrystalline materials with textures are often structurally inhomogeneous objects and do not fulfil the conditions just mentioned. In this case the equation (2) must be replaced by

$$\frac{I_h(y)}{I_h^0} = P_h'(y) = \sum_j w_j \, P_{h,j}(y) \, \alpha_{h,j}(y) \qquad (3)$$

where the weight factors $\alpha_{h,j}(y) = I_{h,j}(y)/I_h^0 \leq 1$ depend on the special properties of the microstructure of the scattering object. According to /2/, in this connection two types of structural inhomogeneities must be taken into account:

- statistical inhomogeneity due to randomly (isotropically) distributed crystallites of various texture components with significantly different grain size and/or lattice disorder as realized, for example, by mixtures of deformed and recrystallized grains in hot-worked materials and
- inhomogeneity due to anisotropic spatial arrangement of the crystallite fractions associated with different texture components in so-called layer structures as caused, for instance, by strain or temperature gradients in plastically deformed or annealed metallic materials, respectively.

In the first case the parameters $\alpha_{h,j}(y) = \alpha_{h,j}$ are independent of the direction y, but usually different for various reflections h. That means, statistical inhomogeneity of a polycrystal essentially gives rise to systematic errors of the volume fractions of the texture components but does not influence the distribution functions $P_{h,j}(y)$. However, in layer structures absorption is different for various textures components even in single-phase materials and the parameters $\alpha_{h,j}(y)$ depend on both the direction y and the type of the reflection. Moreover the beam geometry of the diffraction experiment (transmission or backreflection technique) have to be taken into account, too. For this reason in diffraction experiments with layer structures both the volume fractions w_j and the distribution functions $P_{h,j}(y)$ of the texture components can significantly be modified. In order to check the considerations sample inhomogeneity was experimentally simulated by neutron diffraction with model objects composed from Cu sheets having different, well-known microstructures and textures. The investigations show that significant changes of pole figures due to sample inhomogeneity are possible.

References

/1/ Bunge, H.-J.: Mathematische Methoden der Texturanalyse. Berlin: Akademie-Verlag 1969
/2/ Klimanek, P., this report p. 109

DETERMINATION OF THE IMPLANTATION-INDUCED TEXTURES BY ELECTRON DIFFRACTION

K. Helming and B. Rauschenbach
Zentralinstitut für Kernforschung, Rossendorf, Bereich KF

The formation of textures induced by implantation is a phenomenon not investigated up to now. Because of the small thickness of the texturized material ($\approx$ 100 nm) the determination of such textures is only possible using electron diffraction. At this the measured values (pole figures, see fig. 1) are usually insufficient for a quantitative texture analysis (reproduction of the orientation distribution function (ODF) of the crystallites). With the help of an extended MPDS-conception /1/ the ranges of measurement of the pole figures absolutely necessary for an ODF-calculation may easely be determined. They have at least to be large enough in order to solve the problem of determination of a single orientation unambiguously.

With the MIMV-method /2/ modified for treatments of incomplete pole figures /1/ the first ODF based on electron diffraction was calculated /3/. Fig. 2 shows the fibre texture of the TiN-crystallites induced by implantation of N in Ti (direction of implantation parallel to the direction of the normal $\vec{N}$ of the sample). It describes the density of probability to find crystal planes with the normal $\vec{h}_i = (\vartheta_i, \varphi_i)$ parallel to $\vec{N}$.

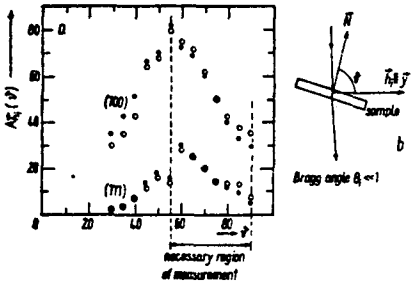

Fig. 1
a) Diffraction intensity of (100) and (111) planes (● experimental, o theoretical)
b) measurement scheme

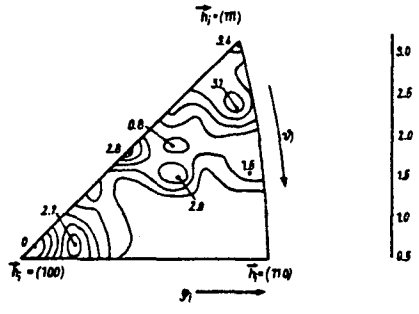

Fig. 2
ODF of the normals of crystal planes $\vec{h}_i = (\vartheta_i, \varphi_i)$ parallel to $\vec{N}$

References

/1/ Helming, K., Dissertation A, ZfK Rossendorf, 1985
/2/ Matthies, S., G.W. Vinel, Phys. Status Solidi B112 (1982) K111, K115
/3/ Helming, K., B. Rauschenbach, Phys. Status Solidi B138 (1986) K1

ANALYSIS OF THE INNER COMPATIBILITY OF EXPERIMENTAL POLE FIGURES BY SINGLE POLE FIGURE FITS

S. Matthies
Zentralinstitut für Kernforschung, Rossendorf, Bereich KF
G.W. Vinel
Zentralinstitut für Kernforschung, Rossendorf, Bereich G

Independently on the variation width of an orientation distribution function (ODF) reproduced from diffraction pole figures in quantitative texture analysis (the variation width is connected with the ambiguity of the results of the central problem /1/ and can in principle be reduced by conditional ghost corrections /2/) erroneous experimental data lower the value and reliability of a reproduced ODF. If the degree of falsification of the experimental data is too great the sense of a reproduction activity itself may be questionable. For this reason criteria are of interest permitting to characterize the quality of the experimental data already before the beginning of the expensive solution of the reproduction problem ($i = 1,2,\ldots,I$; $j = 1,2,\ldots,J$):

$$\tilde{P}_{\vec{h}_i}(\vec{y}_i) = \sum_{n=1}^{\tilde{N}_b} \int_0^{2\pi} f(\{\tilde{g}_{b_n} \cdot \vec{h}_i, \bar{\varphi}\}^{-1} \cdot \{\vec{y}_j, 0\})/(2\pi\tilde{N}_b)\, d\bar{\varphi}. \qquad (1)$$

Erroneous experimental data are not compatible, i.e. several pole figures as well as the values in different pole points ($\vec{y}_j$) of a given pole figure correlated by the crystal symmetry $\tilde{\mathcal{G}}_8$ cannot be interpreted as projections of one and the same ODF f(g). The first circumstance ("outer compatibility") can be investigated with the help of group theoretical invariants /3,4/. For a characterization of the inner compatibility there was not a quantitative approach up to now.

In difference to the harmonic method /5/ considering (1) as a linear problem and using the FOURIER-apparatus the WIMV-method /2/ (solving (1) together with the non-linear condition $f(g) \geq 0$) is able to get an approximative solution even for a single pole figure without any formally mathematical restrictions. The quality of such solutions can be characterized by the RP-values (mean value of the relative deviations of the recalculated from the experimental pole figures).

Due to the underdeterminate character of a single pole figure fit its minimized RP-values provide a lower estimation of the RP-values that can be expected for the whole problem (consideration of some pole figures, additional falsifications for a perturbed outer compatibility). At this the ODF's determined in single pole figure fits are completely out of interest. Test calculations using model distributions as well as experimental data confirm the statements just given. So for the test example MIX-2 (cf. /2/) we got following $RP0_i$-, $RP1_i$-values of the pole figures (111), (001), (110) for the 3-pole figure fit respectively single pole figure fits (in parentheses):

$RP0_i$ /%/: 0.46(0.41), 0.86(0.35), 0.57(0.55)

$RP1_i$ /%/: 0.56(0.52), 1.05(0.71), 0.80(0.73).

References

/1/ Matthies, S., ZfK-480 (1982), ISSN 0138 - 2950

/2/ Matthies, S., G.W. Vinel, Phys. Status Solidi B112 (1982) K111, K115

/3/ Matthies, S., G.W. Vinel, Gemeinsamer Jahresbericht 1984, ZfK-559 (1985) 81; ISSN 0138 - 2950

/4/ Matthies, S., Annalen der Physik 43 (1986) 299

/5/ Preferred Orientation in Deformed Metals and Rocks: An Introduction to Modern Texture Analysis. (Ed. H.R. Wenk) New York: Academic Press 1985

TEXTURE INVESTIGATIONS ON A FLUORITE VEIN STRUCTURE BY NEUTRON DIFFRACTION

M. Betzl, K. Helming and W. Voitus
Zentralinstitut für Kernforschung, Rossendorf, Bereich KF
H.J. Franzke
Zentralinstitut für Physik der Erde, Potsdam

In rocks texture features are of interest in two aspects for geosciences because they provide information about the history of rock formation, deformation and metamorphic processes. On the other hand, the rock texture is responsible for the forming and orientation of megascopically measurable anisotropies of physical parameters. This gives the way to special applications of the neutron diffraction method in the future.
More recent investigations have a more or less methodical and orientation character and concentrate on megascopical and light-to scaning electron microscopical examination of undeformed and deformed Fluorites of hydrothermal vein structures of the Thuringian forest (3 samples) and the Eastern Harz mountains (3 samples).

According to the similarity of results in both occurences, here we report only about the deformation profile of the Harz mountains.
Fig. 1a - 1c show the pole figures of a undeformed fluorite, fig. 2a - 2c the pole figures of a deformed sample. As for the position of peaks one has to take into account that the determination of sample coordinates axis has a deviation of $\pm 10^{0}$ from the exact position, because the sampling in practice is always related to megascopically visible structural features.
The undeformed sample has a clearly distinct texturation ($\tilde{P}^{max}_{(111)} \approx 20$; $\tilde{P}^{max}_{(100)} \approx 25$). Besides a very distinct main component $\{111\}\langle 112\rangle$ a less intensive secondary component $\{100\}\langle 010\rangle$ is formed. This type of fluoride was not influenced by further deformations. Thats why we conclude that this strongly ordered texture pattern is mainly a product of recrystallization under static conditions.
The deformed sample has not reached such a highly oriented texture, but we notice also 4 preffered orientations which, however, are hardly ever determined only by discussion of pole figures.
Nevertheless, it is fundamental to conclude that the primary highly ordered texture pattern with preffered orientations of (100)- and (111)-lattice planes parallel to the vein walls in the deformed Fluorite is regularly partially moved into new positions, so that seems to be axiomatically possible to explain deformation stages of Fluorite veins by texture analysis with help of neutron diffraction.

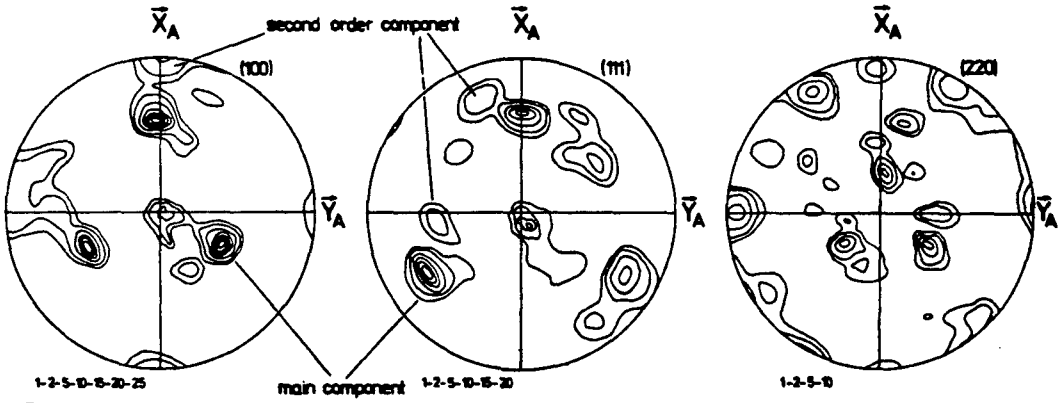

Fig. 1a - 1c: Pole figures of the undeformed sample

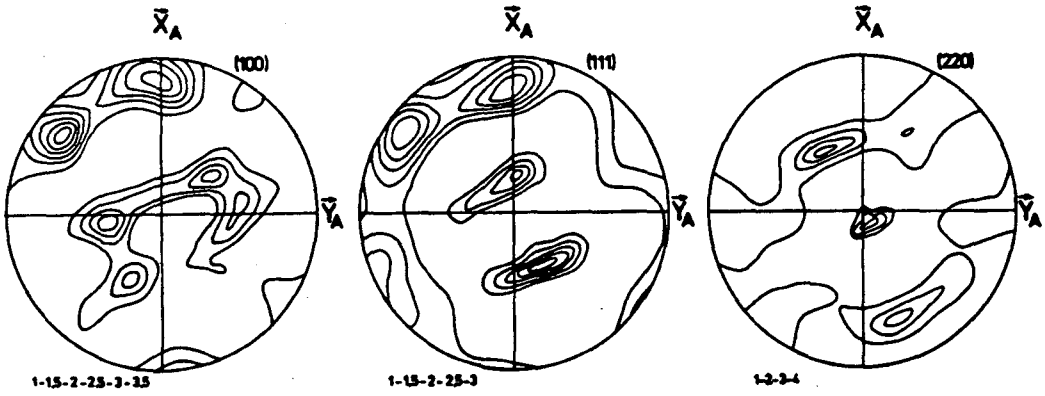

Fig. 2a - 2c: Pole figures of the deformed sample

SMALL-ANGLE NEUTRON SCATTERING ON SILICON NITRIDE POWDERS

F. Eichhorn
Zentralinstitut für Kernforschung, Rossendorf, Bereich KF
J. Bläsing
Technische Hochschule "Otto von Guericke" Magdeburg, Sektion Mathematik und Physik

Silicon nitride is a prefered substance for future materials. Because the construction details must be processed by sintering of powders the shape and the size of grains have to be in a suitable range. We used small-angle neutron scattering in order to determine these properties. By the help of this method the material can be investigated in a nearly original state. As the volume of samples used can reach the order of 1 cm^3 a representative portion of grains takes part in the scattering of neutrons.

In the two-phase approximation (the sample consists of particles within a matrix) the differential cross section of small-angle scattering /1/ is

$$\frac{d\sigma}{d\Omega}(\vec{Q}) = \frac{N_p V_p^2}{N} \underbrace{(\varrho_p - \varrho_M)^2}_{\text{I}} \underbrace{\left| \frac{1}{V_p} \int_{V_p} \exp(i\vec{Q}\vec{r})\, d^3\vec{r} \right|^2}_{\text{II}}$$

with N_p - number of particles with the volume V_p,
ϱ_p, (ϱ_M) - scattering length density of the particle (matrix),
N - number of atoms in the sample,
$|Q| = 4\pi \sin\theta/\lambda$,
λ - wavelength,
2θ - scattering angle.

Term I determines the scattering contrast and term II is the single particle form factor. The scattering of thermal neutrons ($\lambda \approx 0.1$ nm) into the scattering angle range of few seconds of arc contains information on structure elements with a size of several µm. Samples produced by nitriding silicon powder and chemical reaction of ammonia with silicon chloride, respectively, have been tested on a double crystal diffractometer equipped with perfect crystals. After the separation of the apparatus function /2/ the measured scattering cross section was expanded within the frame of the Guinier approximation into components of particles with different shape or size.

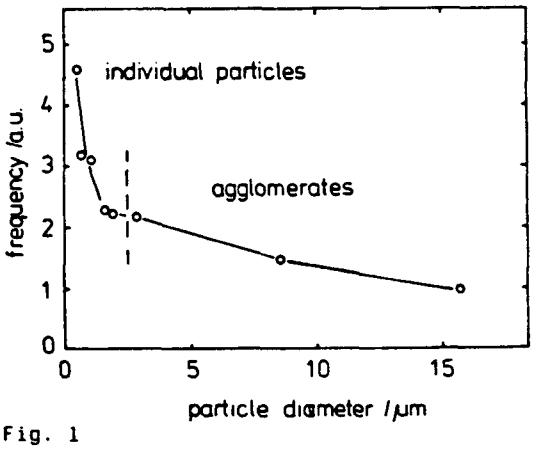

Fig. 1
Particle size distribution of a silicon nitride powder produced by direct nitriding of silicon

Figure 1 shows the obtained particle size distribution function of a nitrided silicon powder. Taking into account not only the results of the particle shape determination but also the data of sedigraphic and electron microscopical analyses particles with a diameter of equivalent spheres less than 2.5 µm are individual ones whereas the greater sizes are caused by agglomerates of 20...150 single particles.

References

/1/ Kostorz, G., Treatise on Materials Science and Technology. Vol. 15, ed. G. Kostorz, Academic Press 1979, p. 227

/2/ Schild, L., Dissertation A, Technische Hochschule Magdeburg 1982

SANS STUDIES ON THE HYDRATION PROCESS OF PORTLAND CEMENT PASTE

F. Häußler and U. Miehe
Technische Hochschule Leipzig, Sektion Naturwissenschaften
F. Eichhorn
Zentralinstitut für Kernforschung, Rossendorf, Bereich KF

Small-angle neutron scattering (SANS) was applicated to problems of material research in civil engineering. Hydrating Portland cement paste was investigated on a double crystal diffractometer equipped with perfect crystals.
Portland cement paste contains many crystallographic phases existing in various ranges of size. Therefore the scattering curve is a superposition of these phases and structures. Following formula can describe this fact /1/:

$$I(\Theta) = K\,\hat{U} \sum_{i=1}^{s} p_i\, u_i \int_{V_{pi}} V_{pi}(a)\, W_i(a)\, |f_i(Q,a)|^2\, da \qquad (1)$$

$$Q = 4\pi \sin(\Theta/2)/\lambda \qquad (2)$$

The measured SANS curve $I(\Theta)$ is a function of the rocking angle Θ of the second diffractometer crystal. $|f(Q,a)|^2$ characterizes the particle form factor. The variable a is the characteristic linear size of the scattering objects, while W(a) represents the distribution function of a. V_p describes the volume of the scattering particles with the volume-concentration p and with a SANS contrast u. The summation is extended over s types of scattering objects with different phases and geometries. The constant K and the smearing operator $\hat{U}$ take into account properties of the diffractometer device.

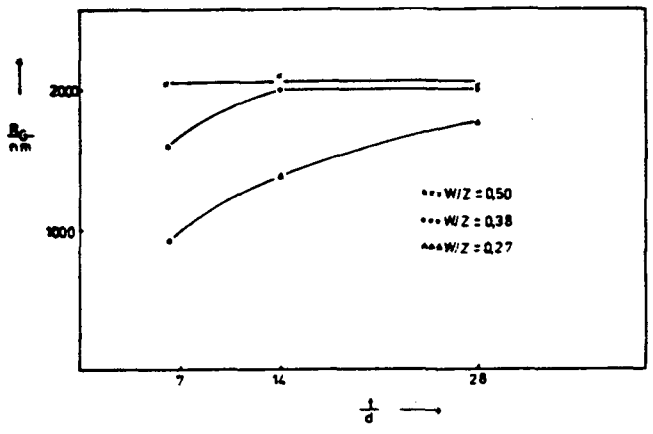

Fig. 1
Gyration radius for cement paste of different water/cement ratio versus hydration time

First experiments /2/ showed the development of the scattering curves during the initial 24 h after the beginning of hydration. The changes of the scattering curves are caused by the microstructural development confirmed by measurements of temperature, electrical resistivity and dielectric constant /3/, too. Now, fig. 1 shows the development of radii of gyration during 28 days after the onset of hydration /4/. The radii of gyration vary with the water/cement ratio in the range from 500 to 3000 nm. 0.38 is the calculated water/cement ratio for complete hydration of the Portland cement used. In contrast to the other samples the sample with a water/cement ratio of 0.27 shows another asymptotic cinetic behaviour. The existing deficiency of water causes both a prolonged hydration process and a decrease of the gaps between the individual cement phase grains.

References

/1/ Häußler, F., Dissertation A, Technische Hochschule Leipzig 1986
/2/ Eichhorn, F. et al., Annual Report 1985, ZfK-584 (1986) 71
/3/ McCarter, W.J., A.B. Afshar, J. Materials Science Letters 4 (1985) 405
/4/ Miehe, U., Diplomarbeit, Technische Hochschule Leipzig 1987

THE STRUCTURE OF METAPHOSPHATE GLASSES BY NEUTRON DIFFRACTION

W. Matz
Zentralinstitut für Kernforschung. Rossendorf, Bereich KF
D. Stachel
Friedrich-Schiller-Universität Jena, Otto-Schott-Institut
E.A. Goremychkin
Joint Institute for Nuclear Research Dubna, Laboratory of Neutron Physics

In connection with the development of athermal optical glasses with anomalous partial dispersion there is a growing interest in phosphate glasses. Up to now the structural reasons for the athermal behavior of the glasses are not known.

We studied the atomic structure of a series of metaphosphate glasses, $Me(PO_3)_2$ with Me = Zn, Mg, Ca, Sr, Ba, by neutron diffraction. In such glasses exist very short interatomic distances. To resolve these distances the structure factor S(Q) have to be measured up to high values of Q (= $4\pi\sin\vartheta/\lambda$). With a conventional neutron diffractometer at the RFR a maximum value Q_{max} = 93 nm^{-1} can be achieved. In order to extend the Q-range of the structure factor time-of-flight neutron diffraction experiments were performed at the pulsed reactor IBR-2 of the JINR Dubna. With Q_{max} = 168 nm^{-1} a good resolution in real space was obtained /1/. For the interpretation of the diffraction data the function T(r) was used.

$$T(r) = 4\pi r \rho_0 + \frac{2}{\pi}\int_0^{Q_{max}} Q\left[S(Q)-1\right]\frac{\sin(\pi Q/Q_{max})}{\pi Q/Q_{max}}\sin(Qr)dQ$$

Here ρ_0 is the mean particle density of the sample. The figure shows the T(r)-curves for the investigated glasses.

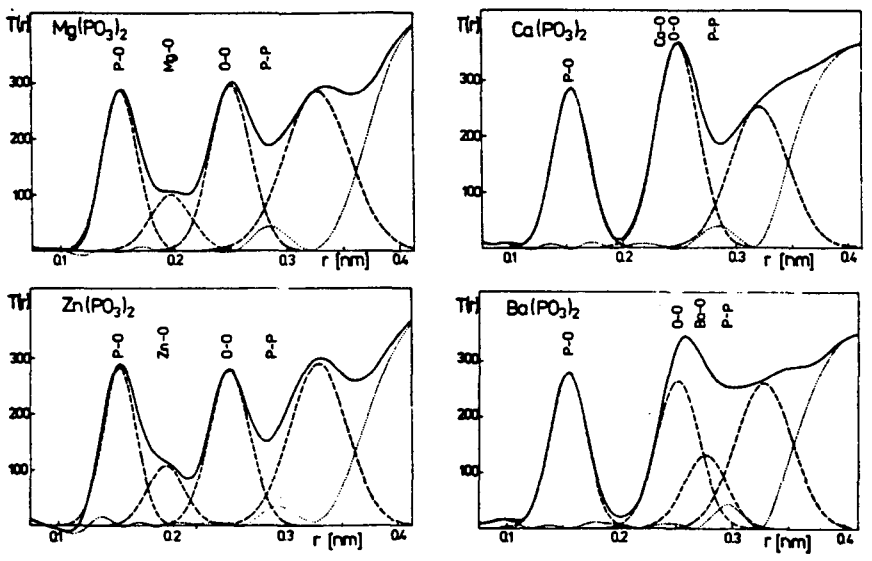

Fig. 1
Reduced radial distribution functions T(r) of metaphosphate glasses as deduced from neutron diffraction experiments (continuous lines). The dashed lines are the fitted Gaussians attributed to different atomic pairs and the dotted lines are the residuals.

The separated peaks in T(r) especially for $Mg(PO_3)_2$ and $Zn(PO_3)_2$ indicate the the possibility to divide T(r) into single peaks. The procedure of dividing T(r) into single Gaussians was performed at a graphical display. To obtain a good quality of the fit the difference between experimental and fitted peaks (dotted line) was minimized. These peaks can be attributed to distinct atomic pairs according to the different ionic radii of the samples constituents. The pairs are indicated in the figure. From the results of the peak separation procedure the following description of the structure of the glasses can be given. The main structural elements are PO_4-tetrahedra with a mean P-O-distance of 0.155 nm. The tetrahedra are only a little distorted, as indicates the O-P-O bond angle distribution deduced from P-O- and O-O-distances. The O-O coordination number of 4.5 allows the conclusion, that tetrahedra are connected up via two bridging oxygen ions in chains. The P-O-P bond angle distributions have a maximum around 140 ° , so that the chains are not linear. The metal ions are located between the chains of PO_4-tetrahedra and are surrounded by oxygen ions. For the glasses with Zn,Mg,Ca the metal has 4 nearest oxygen neighbors and in the Ba glass 8. The structure of strontium metaphosphate glass seems more complicated.

/1/ Matz, W., U. Hoppe, Gemeinsamer Jahresbericht 1984, ZfK-559 (1985) 77

ACCELERATORS

OPERATION OF THE CYCLOTRON U-120

B. Anders and H. Guratzsch
Zentralinstitut für Kernforschung Rossendorf, Bereich G

In the past year the total operation time of the cyclotron has been 5650 hours. The beam has been used mainly for basic nuclear research (1508 hours) and isotope production (1489 hours).
Table 1 shows the complete time distribution.
Table 2 gives the survey of accelerated particles with their percentages of beam time.

For the generation of Li^{3+} ions an internal ion source with an indirect heated cathode was put into operation. This has given the possibility to increase the beam time with Li ions used for nuclear spectroscopy studies.

Table 1

Beam time distribution for 1986

Cyclotron operational	5650 h
Turning on and off; Maintenance	502 h
Scheduled revision	476 h
Total beam time:	4672 h
Nuclear physics	1508 h
Isotope production	1489 h
Neutron therapy	200 h
Thin-layer activation	100 h
Cyclotron improvement	510 h
Others	865 h

Table 2

Accelerated ions and their percentages of beam time

D^+	52 %
H_2^+	3 %
$^4He^{2+}$	34 %
$6;7_{Li}{}^{3+}$	11 %

OPERATION OF THE ELECTROSTATIC ACCELERATORS IN 1986

W. Bürger and S. Turuc
Zentralinstitut für Kernforschung Rossendorf, Bereich G

Tandem-Accelerator

The accelerator has been operated in a 3-shift mode. It has been used for experiments of nuclear physics, solid state physics, thin layer activation, irradiation of polymer foils and for experiments directed to the development of accelerator components.

Characterizing parameters of accelerator employment are given in table 1 and 2.

	hours	species of ions	rel. op. time
Available time	5802	p	22 %
Accelerator under voltage	4421	d	21 %
Experiments with beam	4139	d (pulsed)	14 %
Development	692	C	3 %
		N	24 %
Maintenance and planned stand	971	Si	5 %
		Cl	11 %
		Br, O	< 1 %

The accelerator did not need an opening of the vessel for maintenance during the past year. The life time of the charging belt (Greengate) is now about 12000 hours.

The equipment for foil irradiation in connection with the production of nuclear track microfilters has been improved. Because of the insufficient long term stability of ion current the relation "ion current/foil speed" has to be kept constant. The foil belt tension is controled in order to achieve exact winded finished rolls.

A test stand for experiments with an external ion beam has been built up. First activities using this possibility dealt with investigation of art objects.

With respect to beam diagnostic at present we study a decelerator lens assembly for measuring the energy spread of a low energy ion beam.

In connection with our development of sputter ion sources we delivered and set up into operation an ion source MISS 483 at the tandem accelerator of the University of Helsinki.

Van de Graaff Accelerator

The 2 MV VdG accelerator has been used 3200 hours mainly for nuclear analysis (protons, deuterons, helium ions). During that time the rf-source was running without any maintenance.

We changed the charging belt and we use now a Poly-C-belt. At present the life time of this belt is about 2300 hours. The charging with brushes was not satisfying because of the high dust generation. Now we use a conventional needle arrangement with good success.

The activities for improving the energy stability of the ion beam have been continued.

NUCLEAR ELECTRONICS AND METHODS

ELECTRONIC EQUIPMENT FOR THE 4π- SPECTROMETER PHOBOS

W.D. Fromm and H.-G. Ortlepp
Zentralinstitut für Kernforschung, Rossendorf, Bereich KF
H. Sodan and O.V. Strekalovski
Joint Institute for Nuclear Research, Dubna, Laboratory of Nuclear Reactions

At present the installation of the 4π-spectrometer PHOBOS /1/ for reaction products of medium energy heavy ion collisions is prepared at the JINR Dubna, Laboratory of Nuclear Reactions. Parallel with the development and test work on models of the gas-filled detection modules/2,3/ parts of the electronic equipment have been developed /4/. The conception for the whole electronic system has been worked out. It includes:

i) special timing and spectroscopic equipment which has been optimized with regard to the chosen gas detectors,
ii) the first level trigger logics for events exceeding a certain multiplicity level,
iii) the CAMAC multiparameter data acquisition system based on the system crate principle,
iv) the computer configuration for data collection, control and on-line analysis,
v) the preliminary conception of the electronics for the phoswich scintillation detectors.

The concept is based on maximum simplicity and economy with the technology presently available at the JINR Dubna and the CINR Rossendorf. At the first step the event selection is performed only by a multiplicity criterion (fig.1). Later the majority coincidence may be replaced by a more sophisticated set-up, but the individual detector-specific modules organizing analysis or fast reset must not be changed. A second level trigger is not foreseen, but may be introduced later, too, e.g. by replacing the system crate by a faster multiprocessor bus system.
The computer-controlled detection electronics for the chamber and the scintillator part for each of the 30 modules of PHOBOS is realized as dedicated CAMAC-units. Therefore, a CAMAC-system consisting of several branch highways has to be chosen.
The data-taking computer will be connected to a specialized CAMAC-crate, the system crate, via a crate controller KE001 /5/ with DMA-capability. As branch drivers single width CAMAC units KK008 /6/ placed in the system crate are used. Also the trigger electronics is located in the system crate allowing in this manner fast service of the interrupt by first transferring the response pattern to the computer which then selects the crates with hit modules. Their information is read blockwise with DMA into a buffer which is periodically written to magnetic tape.
A second, more powerful computer is coupled to the bus of the data-taking machine and can use parts of the event-data for on-line analysis. Singles and two-dimensional spectra can be displayed and stored on magnetic disk. Several small computer systems control subsystems of the spectrometer, e.g. the vacuum system, the gas-supply and the high voltage system. The status of these autonomous systems is supervised by the data-analysis computer during the experiment.

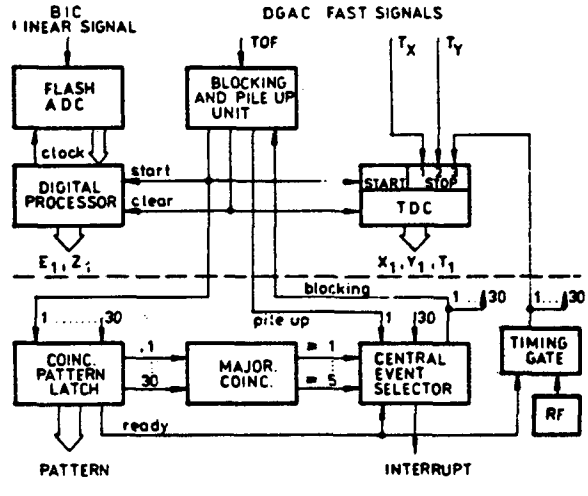

Fig.1:
Read-out electronics for one of the 30 double-grid avalanche counters (DGAC) - Bragg ionization modules (upper part) and the first level trigger (lower part) of the PHOBOS gas detector

REFERENCES

/1/ Sodan, H. et al.; Annual Report 1984 ZfK-559(1985)144
/2/ Seidel,W. et al.; Annual Report 1985 ZfK-584(1986) 94
/3/ Andrassy, M. et al.; this report p. 122
/4/ Ortlepp,H.G. et al.; Annual Report 1985 ZfK-584(1986) 95,98
/5/ Churin, I.N. et al.; Preprint 10-81-755 VIK Dubna 1981
/6/ Churin, I.N. et al.; Preprint 10-83-594 VIK Dubna 1983

THE VACUUM AND GAS HANDLING SYSTEM FOR THE 4π SPECTROMETER "PHOBOS"

W. Seidel and D. Walzog
Zentralinstitut für Kernforschung, Rossendorf, Bereich KF
H. Sodan
Joint Institute for Nuclear Research, Dubna

The vacuum and gas handling system for the 4π spectrometer PHOBOS /1/ was designed. From this conception practical demands were derived for the technical specifications of the main components of the vacuum and gas handling system which are to be regarded in the practical design work. Several considerations have to be addressed regarding the feasibility of such a design:

(1) In the reaction chamber a vacuum of 10^{-4} - 10^{-5} Torr should be attained.

(2) The 30 Bragg ionization chambers (BIC) /2/ and 30 double grid avalanche counters (DGAC) /3/ have to be evacuated initially to 10^{-2} - 10^{-3} Torr.

(3) The 60 counters and the reaction chamber should be simultaneously evacuatable or aeratable.

(4) The counters must operate with a steady gas flow and one has to control the pressure and gas flow.

(5) The control system must prevent wrong manipulations.

Fig. 1 shows the concept of the vacuum and gas handling system (pumps, gate valves, bellows etc.), which is based on NW250, NW100, NW40 and NW25 components. The BIC and DGAC operate in a continuous gas flow mode with different highly purified gases. For easy exchange of the detector modules the whole spectrometer PHOBOS is planned to be turnable by ± 90°. All detectors are, therefore, connected by flexible tubes with a movable system of four ring tubes, which provide the evacuation and a separate gas flow through both counter types. The outlets of the counters are connected to vacuum pumps and the amount of gas flow is regulated by needle valves behind the detectors. The gas pressures can be adjusted with a precision of about 1 % by means of automatic valves VBR 40 /4/ located before the detectors.

The corresponding reference signal is given by a vacuum meter M 501 /4/. It is planned to use one of such systems for each group of 3 BIC working with the same gas pressure. The 30 DGAC are provided with one common control system only. A prototype of the gas flowing control system is under test.

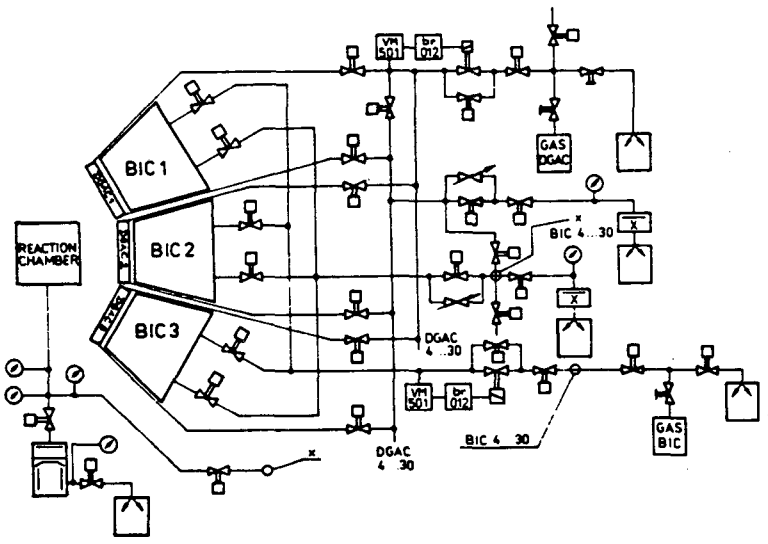

Fig. 1
Vacuum and gas handling system for the 4π spectrometer PHOBOS

References

/1/ Sodan, H. et al., Annual report 1984, ZfK-559 (1985) 144
/2/ Seidel, W. et al., this report p. 122
/3/ Seidel W. et al., Annual report 1985, ZfK-584 (1986) 94; this report p. 121
/4/ VEB Hochvakuum Dresden

FURTHER TEST RESULTS WITH THE DOUBLE GRID AVALANCHE COUNTER

W. Seidel and H.-G. Ortlepp
Zentralinstitut für Kernforschung, Rossendorf, Bereich KF

The overall design of the double grid avalanche counter (DGAC), provided for the 4π spectrometer PHOBOS /1/, and first test results have been described previously /2/. During the last year the time and position resolutions could further been improved. Fig. 1 shows the measured time resolution for the light group of ^{252}Cf fission fragments versus the gas pressure for two different wire distances. Both counters had the same anode-cathode gap of 3 mm and were operated 15 V below the (pressure dependent) voltage, where the spark discharge sets in. For 1 mm wire distance the minimum at about 2.5 Torr is caused by the contrary action of the pulse height and the drift time dispersion which decrease with decreasing gas pressure. For 1.5 mm wire distance this minimum cannot be attained due to the much higher field inhomogeneities between the wires. For different gas pressures the position spectra of fig. 2 were measured with the 1 mm DGAC irradiated with α-particles through the diaphragm depicted (upper part). The signal processing has already been described in /3/. At low pressure ($p < 3$ Torr) the electron diffusion causes a lateral spread of the avalanche surpassing the wire distance. A continuous position information may be obtained from the centre of gravity. For $p > 5$ Torr the wire structure is resolved, corresponding to an avalanche width of about 1 mm, in agreement with /4/. Fig. 3 shows an etched Cu diaphragm (above) and its image (below) produced with α-particles and the 1 mm DGAC.

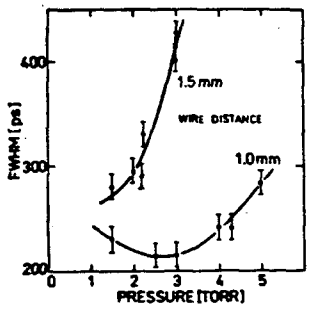

Fig. 1

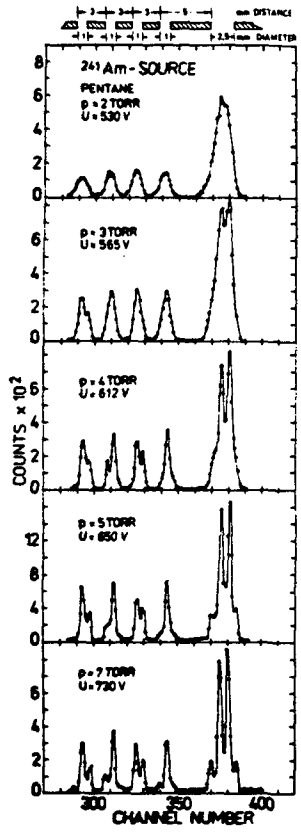

Fig. 2

Fig. 3

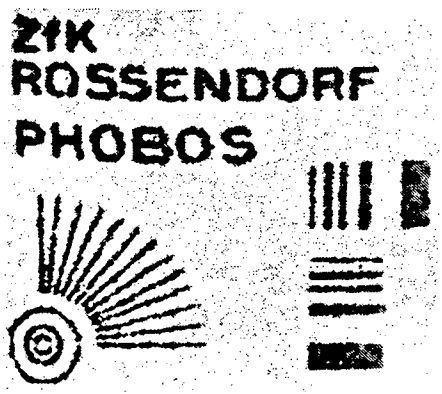

References

/1/ Sodan, H. et al., Annual report 1984, ZfK-559 (1985) 144
/2/ Seidel, W. et al., Annual report 1985, ZfK-584 (1986) 94
/3/ Ortlepp, H.G., W. Seidel, Annual report 1984, ZfK-559 (1985) 149
/4/ Breskin, A. et al., Nucl. Instrum. Methods 217 (1983) 107

A BRAGG IONIZATION CHAMBER WITH LARGE SOLID ANGLE

W. Seidel, H.G. Ortlepp, D. Walzog and F. Stary
Zentralinstitut für Kernforschung, Rossendorf, Bereich KF
M. Andrassy and H. Sodan
Joint Institute for Nuclear Research, Dubna

We present here the prototype of a Bragg ionization chamber (BIC) with a solid angle of 30 msr designed for the second detector layer of the 4π spectrometer PHOBOS /1/. By using the Bragg curve spectroscopy /2/, one measures the energy and the atomic number Z of high energy heavy ions stopped in a gas-filled ionization chamber with the electric field parallel to the incoming particle trajectory. The principle of operation and the analogue signal processing were already described in /3/; first test results obtained with a digital signal processing system are described in /4/. Compared to conventional ionization chambers with the electric field perpendicular to the particle trajectories, the BIC offers the additional advantage of close packing, necessary to follow the demands for high solid angle efficiency of PHOBOS. The schematic view of the detector is shown in fig. 1. The BIC consists of a truncated hexagonal pyramid made from stainless steel. The entrance window has a diameter of 13 cm and was made of 3 μm (340 μg/cm^2) thick aluminized polyethylene, supported by horizontally stretched steel wires (diameter 0.2 mm) with 2 mm spacing. The grounded window withstands a pressure difference of about 400 Torr. The 1 mm wide and 1 mm spaced field shaping electrodes were etched from copper-plated fiberglass epoxy laminates glued together in form of a truncated hexagonal pyramid. The voltage divider of totally 100 MΩ resistance supplies a field strength $E \sim 1/r^2$, necessary for position-independent Z calibration. The distance between the cathode and the Frisch grid amounts to 22 cm, that between grid and anode to 1.5 cm. The Frisch grid consists of copper-beryllium wires of 70 μm diameter, separated by 0.4 mm. The screening inefficiency was calculated to be 0.25 %. The preamplifier signals were fed into two different shaping amplifiers - a standard spectroscopic amplifier with 6 μs shaping time for the energy determination and a second one with 0.5 μs shaping time corresponding to the electron drift time between the Frisch grid and the anode. The chamber was operated in a stationary regime with 90 % Ar + 10 % CH_4 non-purified gas at a pressure of 150 Torr. First tests were performed with α-particles from ^{210}Po and ^{241}Am sources. Fig. 2 shows the measured energy spectrum. Subtracting the contributions of the energy straggling in the entrance window ($\Delta E \sim 40$ keV) and the electronic noice ($\Delta E = 49$ keV) from the observed value of $\Delta E = 71$ keV, the intrinsic energy resolution of the BIC is estimated to be $\Delta E = 32$ keV ($\Delta E/E = 0.6$ %). From the α-particle Bragg peak spectrum shown in fig. 3 a Z resolution of 3.6 % was deduced. Further optimizations of the energy and Z resolutions are under work.

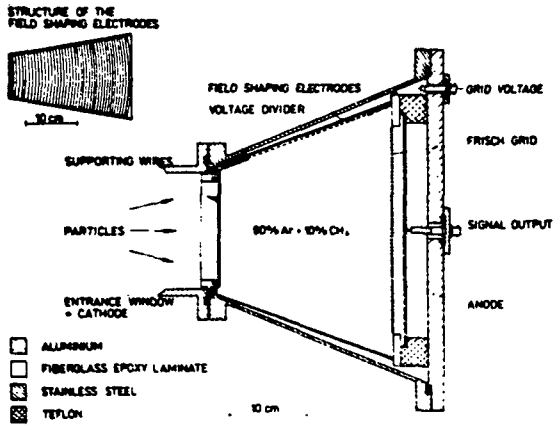

Fig. 1
Schematic view of the BIC

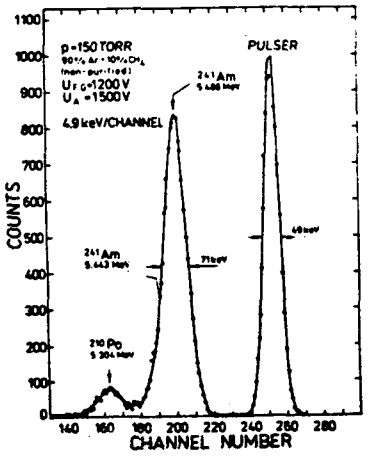

Fig. 2
α-particle energy spectrum

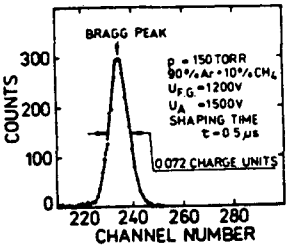

Fig. 3
α-particle Bragg peak spectrum

/1/ Sodan, H. et al., Annual report 1984, ZfK-559 (1985) 144 /3/ Kotte, R. et al., ZfK-591 (1986)
/2/ Gruhn, C.R. et al., Nucl. Instrum. Methods 196 (1982) 33 /4/ Romaguera, A., H.G. Ortlepp, this report p. 123

INTRODUCTION OF DIGITAL FILTERING METHODS INTO THE BRAGG-CURVE SPECTROSCOPY

A. Romaguera and H.-G. Ortlepp
Zentralinstitut für Kernforschung, Rossendorf, Bereich KF

During the development and test of a small Bragg ionization chamber (BIC) at CINR /1/ it became clear that the usually applied signal processing /2,3/ is not optimal, especially with regard to pile-up problems. Therefore, the introduction of digital filtering methods was considered. A complex study has been started including:

i) model calculations of expected errors due to the quantization in dependence of the analogue shaping and the flash ADC resolution and sampling period

ii) storage of real BIC wave forms of alpha praticles and low mass heavy ions from the CINR 5 MV tandem accelerator by use of a transient recorder (fig. 1)

iii) off-line test of several algorithms for obtaining the Z information applied to the stored waveforms (fig. 2) in order to optimize the digital filter operation

iv) real time processing of BIC signals digitized by a 8 bit video ADC with 200 ns sampling period in a model digital filter arithmetics for gaining the energy information (fig. 2).

In these first attempts both the E and Z resolutions did not attain the values of the analogue method. Reasons are the small number of only 14 samples and the unsufficient stability of the used ADC. The stability requirements for pulse spectroscopy are at least one order of magnitude higher than for video applications. A new digital system based on an 8 bit flash ADC chip is under construction.

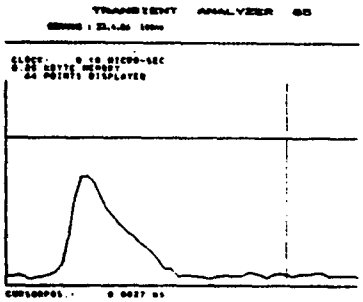

Fig. 1
BIC pulse shape recorded with the CINR transient recorder

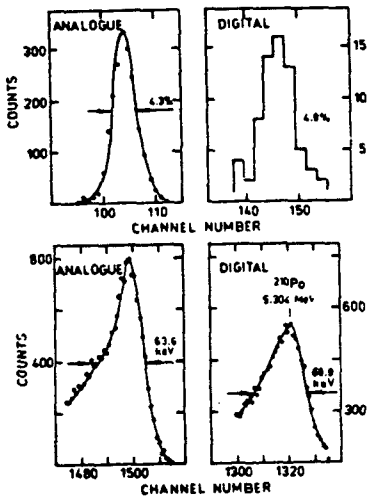

Fig. 2
Alpha-particle Bragg-peak (upper part) and energy (lower part) spectra obtained by analogue and digital signal processing

References

/1/ Kotte, R. et al., ZfK-591 (1986)
/2/ Assalineau, J.M. et al., Nucl. Instrum. Methods 219 (1984) 508
/3/ Shenhav, N.J., H. Stelzer, Nucl. Instrum. Methods 228 (1985) 539
/4/ Koeman, N., Nucl. Instrum. Methods 123 (1975) 161

A TEST OF THE BRAGG IONIZATION CHAMBER BY USING THE REACTION $^{10}B+^{35}Cl(32MeV)$

A.A. Kotov*), W. Neubert and W. Pilz
Zentralinstitut für Kernforschung Rossendorf, Bereich KF

The observation of various charged particles produced in inelastic H.I. reactions at very low energies is restricted to some light target nuclei. A sensitive test of the ionization chamber was performed with a target enriched in ^{10}B(mixed with ^{12}C) which was bombarded by a 32MeV ^{35}Cl-beam. In this case the incidence energy exceeds the Coulomb barrier of about 22 MeV and the production of reaction products is favoured by the positive Q-values. Indeed, we observed pronounced branches of C, N and O out of the products of elastic scattering. The ^{10}B and ^{12}C constitutents of the target scatter the incoming ^{35}Cl ions elastically into narrow cones which are not accepted by the ionization chamber mounted at 27.5 deg with respect to the beam axis. This feature enables us to follow the low intensity branches of nitrogen and oxygen down to about 8 MeV. Nevertheless, the upper branch in fig.1 belongs to the scattered beam particles. Ions of ^{35}Cl with energies up to 23 MeV can be produced by elastic scattering from the Al target holder. The lower branch in fig.1 is formed by the $^{10}_{5}B$ target recoils. The range of these recoils($\approx$2.5mgcm^{-2}) exceeds somewhat the depht of the ionization chamber (corresponding to1.85mgcm^{-2}of butane) and the non fully stopped boron ions lead to the vertical fringe. On the other hand, the track of the ^{12}C recoils of about the same energy fits within the chamber lenght. The branches of nitrogen and oxygen are lower in the intensity. An inspection of the kinematics shows that both nuclei may be produced by ^{35}Cl induced reaction on ^{10}B and ^{12}C. As a consequence of the low energies, all branches in the BP-E plot are inclined and a somewhat modified data processing is required. We subdivided the energy range from 9.6 MeV to 15.2 MeV into 20 bins and determined the centres of gravity. Fig.2 shows the projections onto the BP-axis whereby the distances between the peaks refer to the energy-averaged values. We find a good separation of adjacent nuclear charges in the $5 \leq Z \leq 8$ region regardless of their low energy and moderate energy resolution of the detector. The charge resolution amounts to be about $Z/\Delta Z \approx 16$. The BP-response (for a shaping time of 0.25 µs) fulfills the linear relationship Z=0.125*BP+1.35.

*) On leave from LNPI, Gatchina, U.S.S.R.

Fig.1

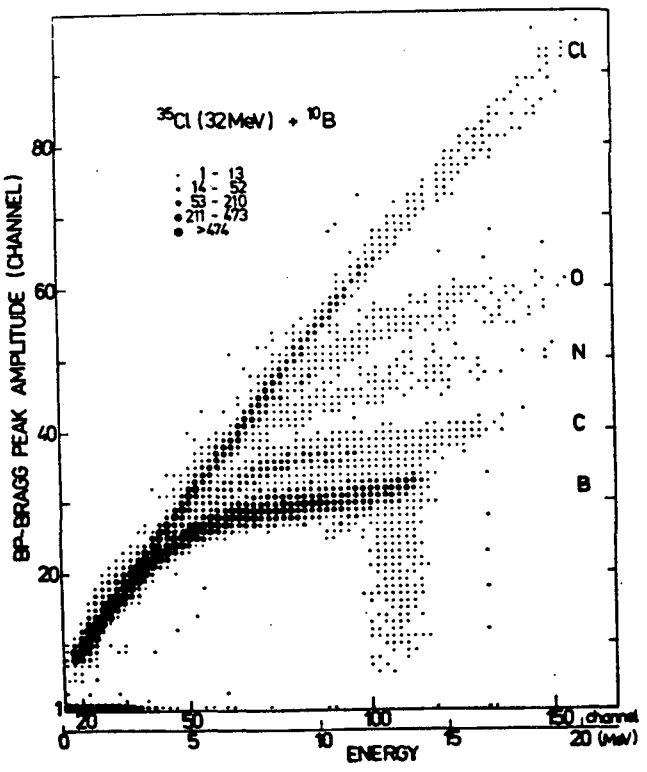

Fig.2

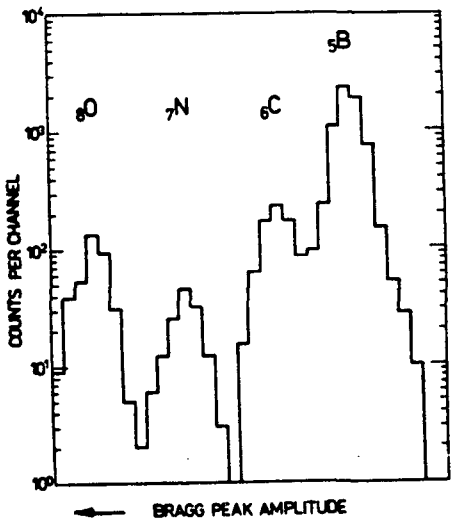

PROPERTIES OF A COAXIAL IONIZATION CHAMBER TESTED WITH LOW-ENERGY HEAVY IONS

A.A. Kotov*), W. Neubert and W. Pilz
Zentralinstitut für Kernforschung Rossendorf, Bereich KF

Experiments with purified n-pentane resulted in good energy and charge resolutions /1/. However the purification is time-consuming and a simple alternative is the use of other alkenes. Commercial butane which contains up to 68% of isobutane was used in the experiments at the Rossendorf Tandem Accelerator. A disadvantage is that the signal amplitude for heavy ions goes down by about 2% per hour in our ionization chamber /2/ newly filled with this gas.
A series of tests was performed with $^{12}C^{4+}$ions of E_0=20 MeV. The ions elastically scattered by a Au target (290µgcm^{-2}) enter the ionization chamber under 27.5 deg. with respect to the beam axis. The entrance window (18mm in diameter, supported by a Ni grid) was made from Formvar with a thickness corresponding to 57µgcm^{-2}. The ionization chamber was operated at 6.,8., 9.and 10.10^{3}Pa. In order to maintain the same E/p-values the voltage was always adjusted. The total charge released by the ionization was measured with a pulse shaping of 2µs by using spectroscopic amplifiers SPV 5024. The measurements cover the range 0.75 V/Torrcm ≤ E/p ≤ 2V/Torrcm in the space between cathode and Frisch grid. The peak position-remains unshifted for E/p ≥1.8 V/Torrcm indicating full charge collection. At fixed E/p, the amplitude of the energy signal (E) rises to a pressure of 9.10^3 Pa where total absorption is reached for 18.7 MeV carbon ions. This result is confirmed by calculations of the Bragg curves using the input data of ref. /3/. The Bragg-Peak signal (BP) was generated by using the spectroscopic amplifier SPV 5023 with a shaping time of 0.25µs which becomes comparable with the collection time of the electrons produced around the Bragg peak. A Gated Biased Amplifier (ORTEC model 444) allowed the necessary µs-delay of these analog signals required for the two-dimensional data processing. Both the E and the BP signals were fed into stretchers followed by 8 bit ADCs. The digitized information was combined in a 16 bit interface (SWB 4901) and processed by a microprocessor-controlled 2 D-analyzer with colour display. A two-dimensional BP-E plot subsequently generated at E/p=2.35 V/Torrcm by ions of $^{12}C^{3+}$(14.7 MeV), $^{28}Si^{7+}$(27.3 MeV) and $^{35}Cl^{7+}$(26.2 MeV) shows fig. 2. The values in the brackets are the energies after the entrance window. This plot shows a good separation for silicon and sulfur above 15 MeV. A linear relation between the BP-amplitude and the nuclear charge Z is fulfilled for the three ions (and ions of B,C,N,O, next contribution) as seen in the insert of fig.2.

R e f e r e n c e s

/1/ Kotte,R., Ortlepp,H.-G., Keller,H.-J., Stary,F., Annual Report 1985, ZfK-584(1986) p.97
/2/ Andronenko, L.N. et al., Annual report 1985, ZfK-584 (1986) p.99
/3/ Northcliffe, L.C. and Schilling, R.F.
Nucl. Data Tables A7 (1979).

*)On leave from LNPI, Gatchina, U.S.S.R.

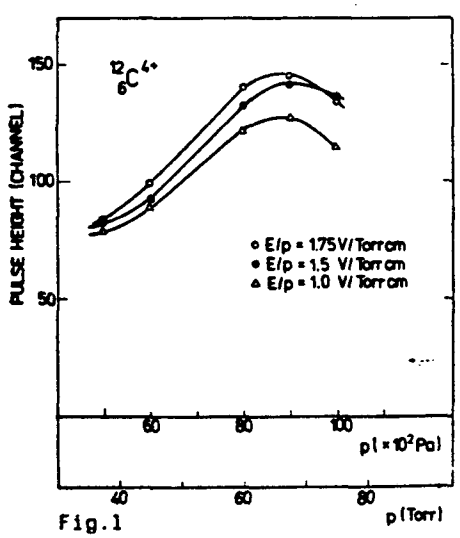

Fig.1

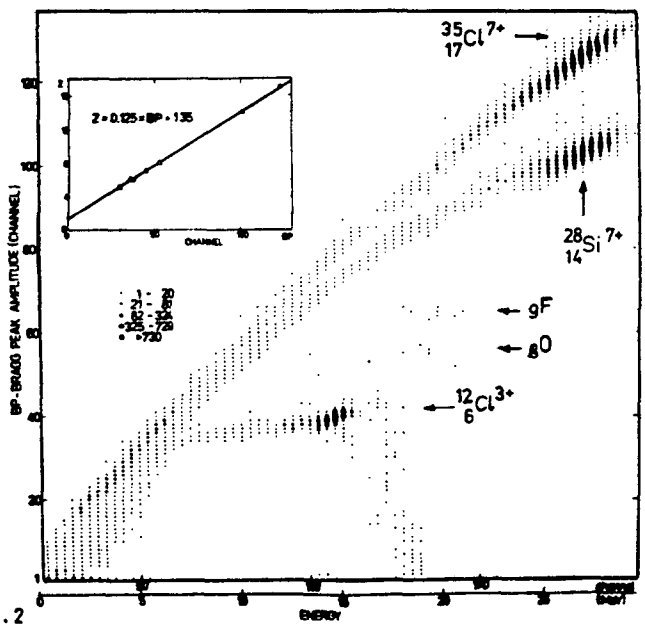

Fig.2

A DETECTOR TELESCOPE FOR MEASURING ANGULAR DISTRIBUTIONS OF NEUTRON INDUCED CHARGED REACTION PRODUCTS

P. Michel, J. Hutsch, J. Mösner, K. Möller and G. Schmidt
Zentralinstitut für Kernforschung Rossendorf, Bereich KF

A charged particle spectrometer, described in /1/, has been changed in several details and completed by two position sensitive multistep avalanche chambers (MSCs) /2/ in order to measure the differential cross section of neutron induced charged particles in forward direction. At present we use this upgraded spectrometer for a measurement of the zero degree differential cross section of the n-p capture reaction at E_n = 25 MeV. In a former experiment we determined the total cross section of this reaction /3/.

The n-p capture reaction and its inverse, the deuteron photodisintegration, has recently recieved much attention from both the experimental and theoretical sides. Especially the 0° cross section excitation function seems to give deeper insight into details of the N-N interaction, see e. g. /4/.

Fig. 1 shows the spectrometer consisting of a gaseous target and a detector system. The gas cell contains two MWPCs which ensure that detected particles are originated within the cell. The two scintillation counters (SC1, SC2) serve for measuring the time of flight and the response of the charged particles and the two MSCs are used for the determination of the track coordinates in order to reconstruct the neutron-deuteron angle. The position resolution of the MSCs allows a determination of this angle with an accuracy of 1.7 mrad (FWHM).

The spectrometer was designed in order to minimize multiple scattering and energy loss. The exit window of the gas call was made of 13.5 mg/cm^2 mylar foil, the thickness of the plastic scintillator of SC1 is 5.2 mg/cm^2 and the MSC1 has an average mass density of 3.8 mg/cm^2 tungsten. In order to avoid windows for the MSCs the whole vessel is filled with isobutan corresponding to a density of 2.4 mg/cm^2 along the path between the gas cell and SC2. The MSCs operate in the gas flow mode ($\approx$ 100 cm^3/min) using a system to maintain a constant pressure of (16 $\pm$ 0.1) mbar. A mean scattering angle of about 28 mrad for 10 MeV deuterons results from these values taking into account additionally the multiple scattering within the gas cell containing hydrogen at a pressure of 0.4 MPa.

The spectrometer has a mean opening angle of $\pm$ 107 mrad resulting from the distance of 700 mm between the centre of the gas cell and the SC2 and the diameter of 150 mm of the SC2.

The other components of the experimental setup are similar to that described in /1/. In order to obtain a larger rate of capture deuterons a Ti-T target of 2.5 · 10^{12} Bq/cm^2 and a neutron collimator with enlarged opening angle are applied. Thereby, the neutron flux crossing the gas cell amounts to about 4 · 10^5 n/s at a pulsed deuteron beam of 1.5 µA. Consequently the total rate of capture deuterons per hour is about 80, that means a factor 20 larger than formerly.

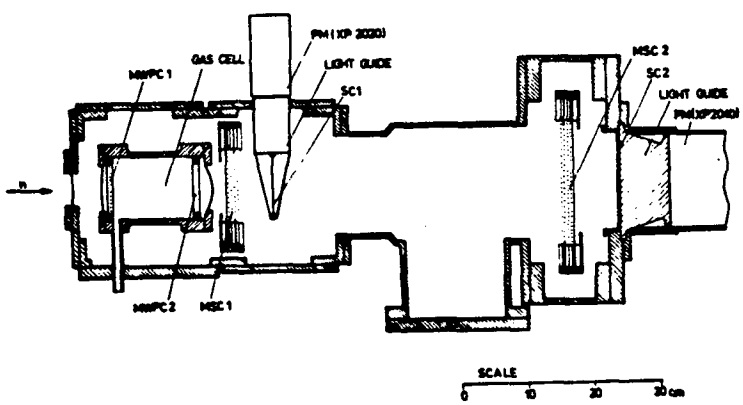

Fig. 1
Schematical view of the telescope

References

/1/ Stiehler, T. et al., Nucl. Instrum. Methods A 236 (1985) 343
/2/ Michel, P. et al., this report p. 127
/3/ Stiehler, T. et al., Phys. Lett. B 151 (1985) 185
/4/ Zieger, A., Grewer, P. and Ziegler, B., Few-Body Systems 1 (1986) 135

POSITION SENSITIVE MULTISTEP AVALANCHE CHAMBERS FOR DETECTION OF LIGHT CHARGED PARTICLES

P. Michel, J. Hutsch, J. Mösner, K. Möller and G. Schmidt
Zentralinstitut für Kernforschung Rossendorf, Bereich KF

Two low pressure position sensitive multistep avalanche chambers (MSCs) have been developed for an experiment measuring the differential cross section of the n-p capture reaction at E_n=25 MeV /1/. This kind of detectors have been chosen due to the spezific conditions of the experiment resulting in the following demands. The mass density of the chambers has to be small in order to minimize multiple scattering and energy loss, the efficiency for detection of deuterons up to 15 MeV should be nearly 100 %, track localization of better than 0.5 mm (FWHM) is required in order to obtain a sufficient angular resolution and a stable operation is necessary with respect to position response and efficiency during several weeks at pulse rates up to 10^5c/s.
We have built two MSCs with effective areas of 100x100 mm^2 and 190x190 mm^2, respectively. Fig. 1 shows the arrangement of the electrodes, where A is a 50 $\mu g/cm^2$ formvar foil with 40 $\mu g/cm^2$ gold evaporated, B is a 1 x 1 mm^2 mesh of 20 µm Au-tungsten wires, C and E are the cathode grids made of 28 µm Au-tungsten wires in 1 mm distance and D is the anode grid consisting of 13 µm Au-tungsten wires 2 mm apart. The PPAC gap (A-B) is 3.7mm, the gap of the drift space and the distances between cathode and anode wire planes are 5.3 mm. The E-grid is orthogonal to that of D and C. The principle operation mechanism of low pressure MSCs has been investigated by several authors /2/. We applied delay-line read out using special low noise preamplifiers /3/.
The two MSCs have been tested with 5.5 MeV α-particles (^{241}Am), 5.9 keV γ's (^{55}Fe), protons (5 to 25 MeV) and deuterons (5 to 22 MeV) at pressures of 8 and 16 mbar isobutan. Position resolution of 320 µm (FWHM) for α-particles and 480 µm for 5.9 keV γ's have been obtained in both coordinates over the whole active areas of the chambers. A differential and integral nonlinearity of track localization of smaller than 0.8 % has been measured with an α-source using a computer controlled mechanical scanner. Fig. 2 shows the result of the determination of the efficiency for protons and deuterons at 16 mbar which have been obtained by operating the chamber in coincidence with a scintillation counter telescope described in /1/.
More details about the properties of the chambers will be published. Finally it should be noted that excellent operation stability of the chambers including electronics and gas flow system has been observed during several days under the real conditions of the experiment.

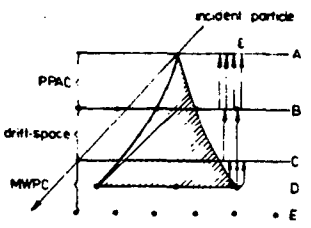

Fig.1: The arrangement of the electrodes of the MSCs.

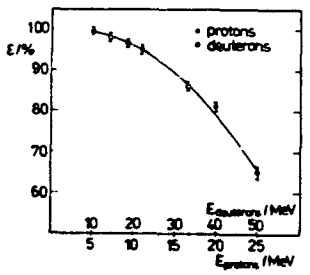

Fig.2: The efficiency of the MSCs for protons and deuterons.

References

/1/ this report p. 126
/2/ Breskin, A. et al., Nucl. Instrum. Methods A 161 (1979) 19 and 221 (1984) 363
Sanewsci, Ju.W. et al., Dubna Preprint P 13-84-563 (1984)
/3/ Ortlepp, H.G. and Seidel, W., Gemeinsamer Jahresbericht 1984 ZfK-559 p. 149

PARAMETER OPTIMIZATION OF HIGH-DENSITY AVALANCHE CHAMBERS

P. Manfraß, W. Enghardt, W.D. Fromm and D. Wohlfarth
Zentralinstitut für Kernforschung, Rossendorf, Bereich KF

High-density avalanche chambers as proposed by Jeavons et al./1/ are intended for use as position sensitive detectors of a positron emission tomograph (PET) which is under construction. The PET is planned to consist of a hexagonal arrangement of such detectors, each having a size of 50*28 cm^2. Before finally designing the positron camera the essential properties of the detectors had to be studied. The results of these investigations are summarized in this report.

The detectors were operated with different filling gas mixtures at normal pressure:
(i) Ne + 4% Hexan + (0.07, 1.3 or 2.6)% i-propanol,
(ii) Ne + (10 or 20)% CO_2 + (0, 1.3, 2.6 or 4.0)% i-propanol.

Layout of the γ-ray converters

The multi-hole converters consisting of 0.2 mm thick PbSn3Sb2.5 foils insulated by layers of glass fabric reinforced epoxy-resin were made in the KSG Gornsdorf by means of machines that are commonly used for producing multi-layer printed circuit boards.

We tested four kinds of converters with holes of 0.8, 1.05 and 1.7 mm diameter. The minimum thickness of the remaining converter material between the holes is 0.2 mm. It could be shown that for both gas mixtures the converters with holes of 1.4 and 1.7 mm diameter allow the detection of all escaping electrons by the MWPC. Therefore, converters with 1.4 mm diameter holes will be used for the positron camera.

Time resolution

The aim of this investigation was to get information on the maximum time resolution ($2\tau_0$) that is achievable for this detector type, where special interest was focused on the change from the drift to the avalanche regime of converter operation. For this purpose the anode voltage of the MWPC was adjusted at 1.4 kV that ensures a convenient registration of the time distributions of the conversion electrons in the drift mode, and the the electric field strength at the converters (E_c) was increased. Fig.1 shows the typical time spectra in the drift and avalanche modes as well as in the transition phase. The latter is limited to a rather narrow field strength interval of about 1 kV/cm. The avalanche regime begins for electrons escaping the converter foils on lowest potential and extends over the whole converter with increasing E_c. For a converter consisting of 20 layers (0.2 mm Pb + 0.1 mm insulator) and Ne + 4% Hexan + 2.6% i-propanol as filling gas the maximum field strength is limited to E_c=7.2 kV/cm by electric discharges in the converters because of the roughness of the inner surfaces of the holes. The corresponding time resolution amounted to $2\tau_0$ = 16 ns at FWHM.

Using converters with thicker insulation layers (10 times 0.2 mm Pb + 0.2 mm insulator), the practical limit of the electron amplification (Raether's condition) is reached at E_c=8.7 kV/cm, i.e. electric discharges occur during the irradiation with the γ-rays of a ^{22}Na source. The time resolution attained at this field strength was $2\tau_0$ = 14 ns FWHM. Basing on these results the converters of the positron camera will consist of 16 layers of 0.2 mm Pb and 0.2 mm insulator each.

Efficiency and yield

Fig.2 shows the detection efficiency for 511 keV γ-radiation of a MWPC with one converter consisting of 20 layers (0.2 mm Pb + 0.1 mm insulator) in dependence on the converter field strength E_c; the MWPC anode voltage was kept constant. The efficiency amounts to ε = 4.8% at E_c=6 kV/cm. Since the absorption of 511 keV radiation in the converter was experimentally found to be 16%, the converter yield is 30%. Thus stacking 8 such converters will give a detector with an efficiency of ε=22.5% for E_γ=511 keV.

Electron amplification and discrimination against low-energy Compton-scattered radiation

The electron amplification in the converter depending on E_c at constant anode voltage was measured for the 6.3 keV photons emitted from a ^{55}Fe source. The experimental setup and the results are displayed in fig. 3.

The source was mounted on top of the converter and their radiation was collimated parallel to the converter surface by means of Pb-foils. Using the filling gas Ne + 10% CO_2 + 2.6% i-propanol a maximum gain of M_c=35 at E_c=6.2 kV/cm was measured. This preamplification in the converter is sufficient to reject the low-energy signals of the MWPC by pulse-height discrimination.

Reference

/1/ A. Jeavons et al.; Nucl.Instr.Meth.176(1980)89

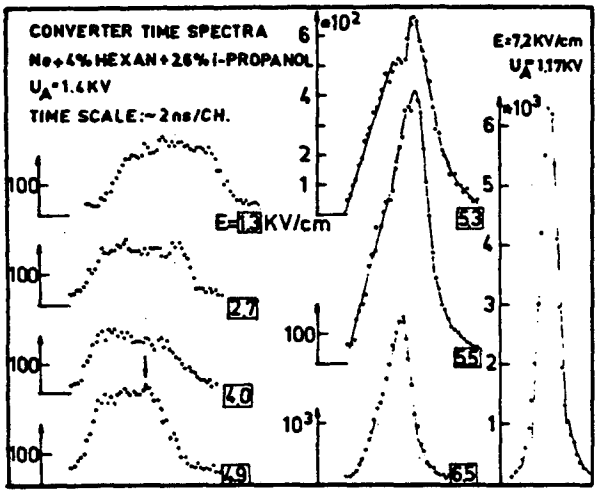

Fig.1:
Electron time spectra in dependence on the electric field strength at the converter.

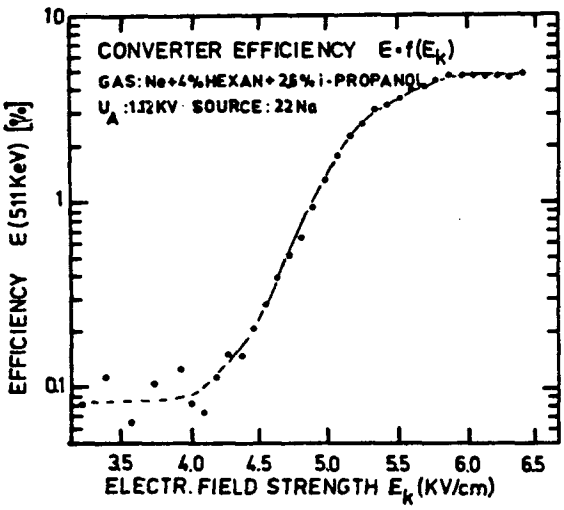

Fig.2:
Detection efficiency of a combination of one converter and a MWPC for 511 keV γ-rays plotted versus the converter electric field strength.

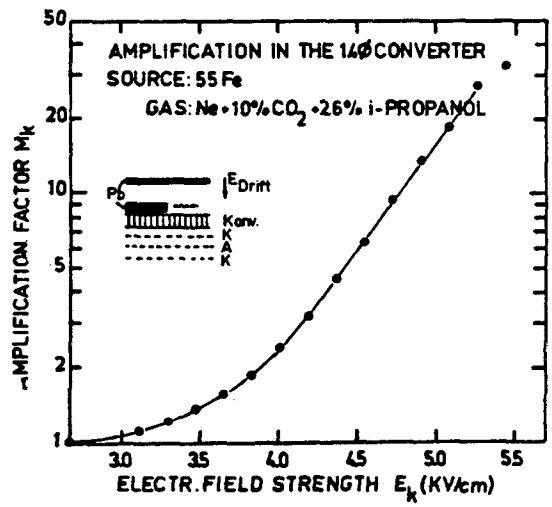

Fig.3:
Electron amplification in the holes of the converter depending on the converter field strength measured for the 6.3 keV γ-radiation of a ^{55}Fe source. The inset shows the experimental arrangement.

EXTENSION OF THE DUBNA TIME-OF-FLIGHT SPECTROMETER DEMAS FOR MEASURING LIGHT CHARGED PARTICLES IN COINCIDENCE WITH FISSION FRAGMENTS

H.-G. Ortlepp
Zentralinstitut für Kernforschung, Rossendorf, Bereich KF
K. Heidel and H. Sodan
Joint Institute for Nuclear Research, Dubna, Laboratory of Nuclear Reactions

New experimental information about the fusion-fission process at about 10 MeV/u is expected from light charged particle (mainly alpha particles) - fission fragment coincidence measurements. The Dubna double-arm time-of-flight spectrometer DEMAS /1/ has been used for the spectrometry of two correlated heavy reaction products only. Recently a 5 cm diameter ΔE-E silicon detector telescope manufactured at the CINR Rossendorf /2/ has been included. The telescope is placed inside the reaction chamber at 20 degrees with respect to the beam direction (fig. 1). In addition to the quantities TOF, E, X, Y measured in both DEMAS arms the values ΔE and E of the telescope and the time ΔT between the light particle and one of the fission fragments had to be recorded. For that aim the event trigger logics (fig. 2) and the data acquisition system were modified. The system is triggered by a majority coincidence unit if at least two of the three signals TOF 1, TOF 2 and ΔT are in coincidence within the 1 µs resolving time. In this case the gates of each of the 11 CAMAC ADC's are opened and, after conversion, 11 codes are transferred to the SM-3 computer. In the analogue ΔE and E channels linear gate and stretcher units (ORTEC 542) serve to suppress pile-up and to match the timing conditions at the ADC input gates. A first measurement was performed with 178 MeV ^{22}Ne ions bombarding a gold target. The data analysis is under way.

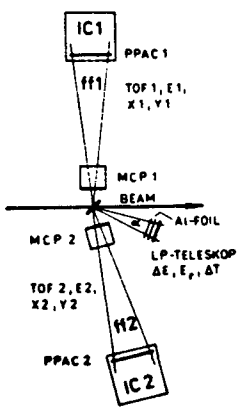

Fig. 1
Detector arrangement of the α-ff-experiment

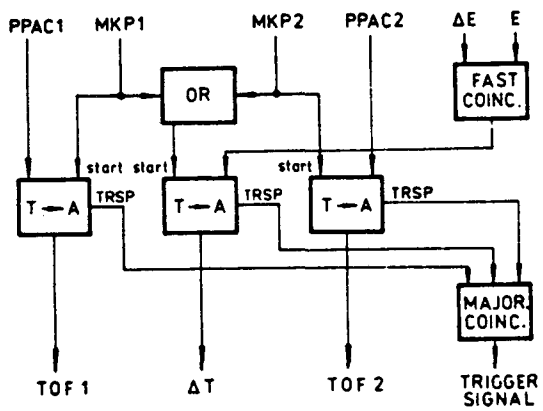

Fig. 2
Block diagram of the event trigger logics (TRSP - true stop)

References

/1/ Schilling, K.D. et al., ZfK-586 (1986)
/2/ Deutscher, M. et al., annual report 1985, ZfK-584 (1986) 54

A ΔE-E ANNULAR SEMICONDUCTOR DETECTOR TELESCOPE FOR LIGHT CHARGED PARTICLES FROM HEAVY ION REACTIONS

M. Deutscher, E. Hentschel, J. Keller, R. Kotte, H.-G. Ortlepp, W. Seidel and F. Stary
Zentralinstitut für Kernforschung, Rossendorf, Bereich KF

For measurements of forward peaked fast light particles in coincidence with other products of heavy ion reactions an annular detector together with its readout electronics /1,2/ was developed. In a first step a ΔE-E telescope in ring like geometry consisting of a silicon surface barrier diode with 6 concentric sensitive areas and a plastic scintillator /2/ was used. Based on the experience with large Si(Li) particle detectors /3/ a modified type with a central hole was developed to replace the scintillator. The preparation and performance of this type is similar to the full plane one /3/. Fig. 1 shows its cross section and the dimensions. The design allows a radiation sensitivity up to the edge of the hole.
During a test experiment at the Rossendorf U-120 cyclotron a 0.2 mg/cm^2 $(CD_2)_n$ target was bombarded with 7 MeV protons, 13 MeV deuterons and 27 MeV alpha particles. The elastically scattered particles were detected by the ring telescope at 72 mm distance downstream. The ΔE, E and ring number codes were collected event by event. Off-line the events were sorted for each ring number into separate ΔE-E plots. Fig. 3 shows the added spectra of the p, d and alpha runs.

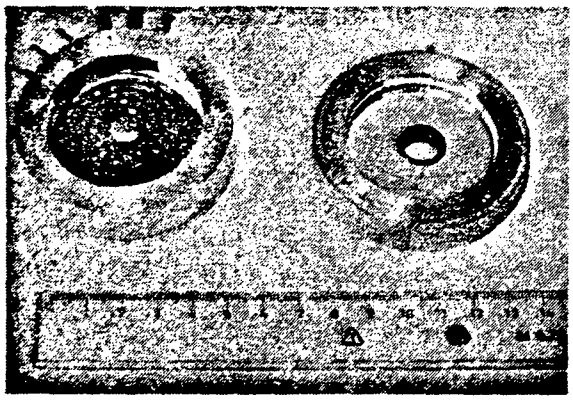

Fig. 1
The ΔE (left) and E (right) ring detectors

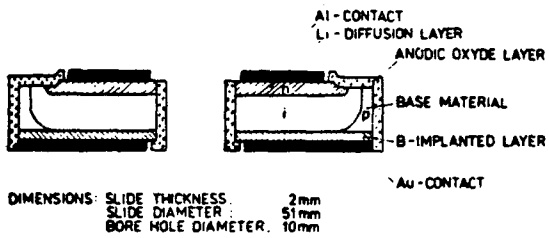

Fig. 2
Cross section of the Si(Li) detector

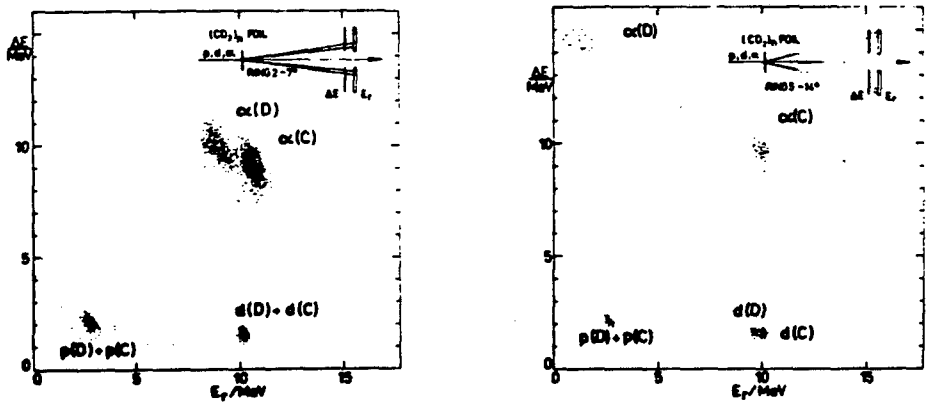

Fig. 3
ΔE-E plots of events related to the second (left) and fifth (right) ring

References

/1/ Schmidt, B. et al., Annual report 1984, ZfK-559 (1985) 152
/2/ Kleinwächter, P. et al., Annual report 1985, ZfK-584 (1986) 92
/3/ Deutscher, M. et al., Annual report 1985, ZfK-584 (1986) 54

INVESTIGATIONS ON THE DETERMINATION OF THE Pu ISOTOPIC COMPOSITION BY GAMMA-RAY SPECTROSCOPY

H. Prade[+] and L. Funke
Zentralinstitut für Kernforschung, Rossendorf, Bereich KF
R. Arlt and W. Lewis
International Atomic Energy Agency, Vienna, Department of Safeguards

In-field measurements of the isotopic composition of plutonium samples for safeguards purposes are usually carried out by using high resolution γ-ray spectroscopy (HRGS). The influence of some of the most important experimental factors (e.g. counting statistics, resolution, absorber thickness), which can be controlled by the inspectors, on the accuracy of the determination of Pu isotopic composition has been studied in order to judge measured values of isotopic ratios and isotopic abundances and to optimize the equipment, measurements and data evaluation. The sensitivity of the uncertainty of the measured values has been determined by varying only one of the parameters keeping all the other measurement conditions constant at the same time. Special attention was paid to process high counting rates, which is required to minimize the measurement time and also is a general problem in nowadays γ-ray spectroscopy.

The γ-ray spectrometer used in the present investigations was the standard HRGS equipment used by IAEA inspectors in the field (13 cm^3 planar HPGe detector and series RG-11 preamplifier made by Princeton Gamma Technical Corporation, 8K CICERO MCA of the Silena Corporation). For some of the measurements the PGT detector (Det. 1) was replaced by a 2.6 cm^3 ORTEC planar HPGe detector (Det. 2) and a Tennelec amplifier TC 244 was used instead of the CICERO amplifier. The data evaluation was performed by means of the standard LLNL plutonium isotopic evaluation software implemented on the DEC-PRO 380 computer. Altogether 164 Pu spectra (4K length) have been measured and processed. The plutonium γ-ray measurements have been performed in the Safeguards Analytical Laboratory in Seibersdorf using Pu samples of 10 g and 30 g. In fig. 1 an example of a Pu spectrum is shown. The Pu isotopic composition is obtained from the γ-ray spectra between 122 keV and 382 keV by analyzing the six peak groupings indicated in fig. 1.

To study the influence of the counting statistics, resolution and Cd absorber thickness in front of the detector on the accuracy of the determination of the isotopic composition of Pu samples the relative errors of three different criteria have been regarded:

$^{240}Pu_{eff}$ = 2.49 wt% ^{238}Pu + wt% ^{240}Pu + 1.57 wt% ^{242}Pu,

the ratio $^{240}Pu/^{239}Pu$ and the peak area of the 160.31 keV peak, which is the principal source of the ^{240}Pu value.

In fig. 2 the dependence of these parameters on the counting statistics are shown as obtained with the PGT detector (Det. 1), 2 µs shaping time and 30 % busy time. The relative errors first decrease rapidly with the integral number of counts (up to $\sim 10^7$), while further increase of the measuring time leads to a moderate improvement only.

Taking into account also the results on the influence of the resolution and the absorber thickness the following conclusions can be drawn:

1. It is very important to collect Pu spectra with good statistics. "Good" means more than 10^7 integral counts (provided the Cd absorber thickness is chosen between 1.4 mm and 2.4 mm).
2. For the data analysis code used in this investigation the influence of the resolution is of less importance as far as it does not exceed the end of the plateau region (850 – 900 eV) at 208 keV (*cf. fig. 3*). Good resolution leads to a remarkable improvement only if it can be made < 700 eV at 208 keV.
3. It seems to be very important to optimize the spectrometer for high throughput, even if some compromise to the resolution has to be made. In this case it might be helpful to use with the present systems a 1 µs shaping time and the peak detection mode of the ADC.

[+] Consultant to the IAEA from 29 May to 2 July 1986

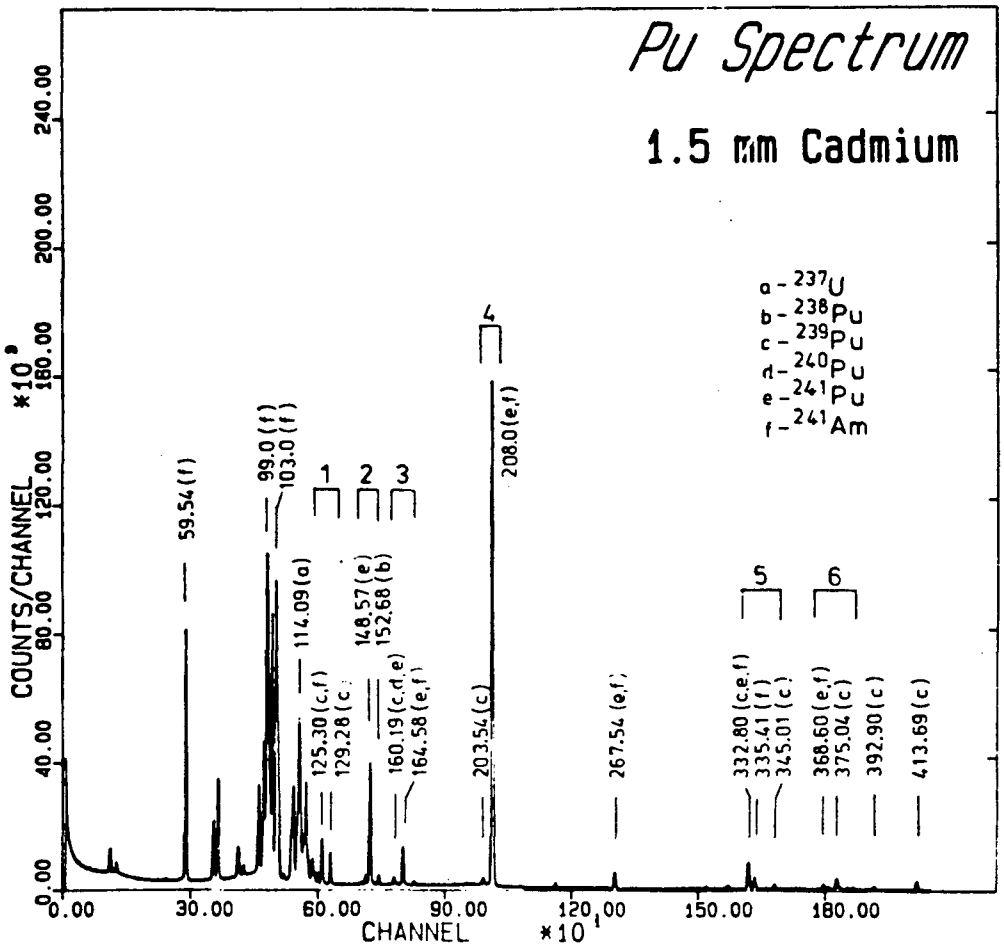

Fig. 1
Example of a plutonium spectrum. The peak groupings indicated are used by the evaluation software to determine the isotopic composition.

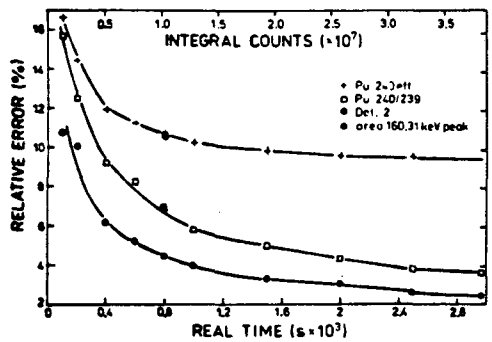

Fig. 2
Relative errors of Pu parameters versus counting statistics. The measurements are mainly performed with Det. 1 at a busy time of 30 % and 2 µs shaping time.

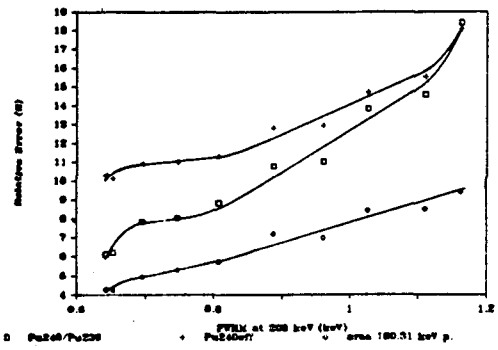

Fig. 3
Relative errors of Pu parameters versus resolution (Det. 2, 15 % busy time, 2 µs shaping time). The resolution was changed by adding a constant noise level to the preamplifier-detector noise at the main amplifier input.

γ-RESPONSE MATRIX OF VOLUMINOUS NaJ(Tl)-SCINTILLATORS

D. Lucas and H. Märten
Technische Universität Dresden, Sektion Physik, WB Kernphysik

W. Neubert and W. Pilz
Zentralinstitut für Kernforschung Rossendorf

For the analysis of continuous γ-spectra measured by the use of thick NaJ(Tl)-scintillators, it is necessary to take into account the inverse response matrix. In order to determine the detector response with high precision an analytical method has been developed. For this purpose, the treatment of Gardner /1,2/ based on rather simple parametrizations of the response spectra has been extended concerning additional terms (peak due to back scattering, maximum at the Compton edge) to improve the agreement with measured detector response distributions. Furthermore, the parameters, which define the ratio of the escape peak areas to the photo peak area, have been modified.
All parameters are considered as continuous functions of γ-ray energy. The detector resolution depending on energy has to be deduced from measurements.
A FORTRAN code has been developed to calculate the response matrix for cylindrical sodium iodide crystals with eligible geometry. The calculations based on an optimized parameter set yield a rather good agreement with measured response functions. Examples are represented in the figures for a (2"x2")-scintillator.
In fig. 1, a result of a Monte Carlo calculation /3/ (MCC) is shown for comparison.

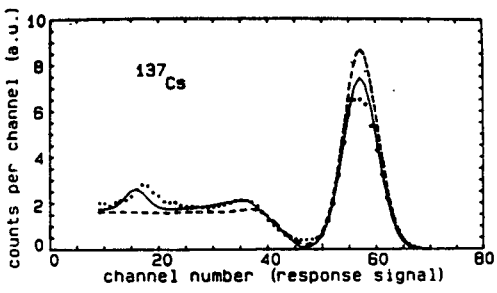

Fig. 1
Response function of a (2"x2")-NaJ(Tl)-scintillator for 0.662 MeV γ-quanta (^{137}Cs) (dotted - experimental data corrected for scattering effects, dashed - MCC, continuous - this work).

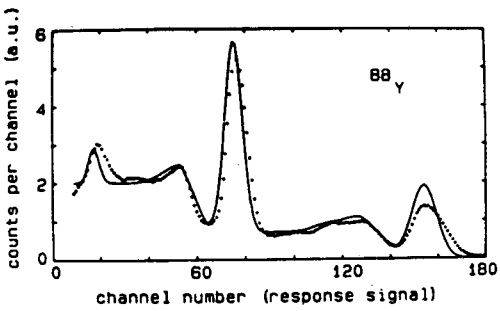

Fig. 2
The same as fig. 1 for γ-quanta from a ^{88}Y source (0.898 and 1.836 MeV).

References

/1/ Gardner, R.P.; Nucl. Instr. Meth. 138 (1976) 287
/2/ Porelli, A., Gardner, R.P.; Nucl. Instr. Meth. 159 (1979) 177
/3/ private communication, Šeda, J., Technical University Prague

COSMIC RADIATION INDUCED BACKGROUND OF SELECTED DETECTOR TYPES AT HIGH ENERGIES

S. Unterricker and D. Degering
Bergakademie Freiberg, Sektion Physik

The main component of cosmic radiation at sea level is the muonic component. Its intensity is of the order of 160 $\mu^{\pm}/m^2 s$ and the muonic energies range to more than 10^{15} eV. For the stopping of muons by matter nuclear processes have no importance, that means ionization processes are dominant. The differential energy loss at energies > 200 MeV is approximately 2 MeV/gcm^{-2}. Therefore, the high energy muons have a great range.
If a muon crosses an energy sensitive detector the pulse height is proportional to the path length in the detector and the muon induced background will show an extended maximum at an energy $\hat{E}$ corresponding to the most probable path length $\hat{l}$. The muonic energy distribution is practically unimportant for this muonic background spectrum as shown in Fig. 1. A geological shielding by 200 m we (water equivalent) shifts the energy distribution of the muons to higher energies. The pattern of background spectrum, especially the 'muonic peak' of the NaI(Tl)-detector, is not influenced by thick geological layers. Only the intensity is diminished by a factor of 100.
The shape of the muonic background spectrum is determined by i) the effective dimensions of the detector, ii) the zenith angle dependence of muonic intensity, iii) the energy dependence of the differential energy loss, and iv) the response of the detector to the products of muon interaction. Maximum path length l_{max} in the detector and maximum differential energy loss define a maximum deposited energy E_{max}.

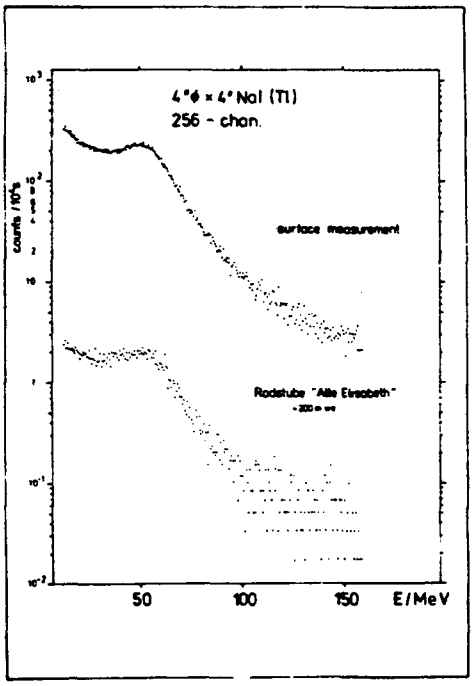

Figure 1: High energy spectrum of a large NaI(Tl)-detector without and with a geological shielding of 200 m we.

In Tab. 1 theoretical values for $\hat{E}$ and E_{max} of different detector types are summarized. In the cases of NaI, Ge and Si good agreement with the experiments (see for instance Fig.1) could be achieved. All of these detectors show also some pulses with $E > E_{max}$. For NaI and coaxial Ge detectors the 'muonic peak' is in an energy region which has hardly importance in the field of spectroscopy, while in the case of Si detectors the muon energy deposition is important for the background of α - and β-spectra. Large proportional counters show the 'muonic peak' at X-ray energies.

Table 1: $\hat{E}$ and E_{max} for selected detector types

detector	NaI(Tl)	Ge(Li)	Si(Li)	proportional counter
geometry	cylindrical 100mmØ x 100mm	'coaxial' 45cm^3	planar 16mmØ x 3mm	cylindrical 50mmØ x 400mm
$\hat{E}$/MeV	59	30	1.2	0.012
E_{max}/MeV	114	50	5	0.050

EXPERIMENTAL ARRANGEMENT FOR INVESTIGATION OF THE ANGULAR DISTRIBUTION OF γ-RAYS IN THE TERNARY FISSION OF ^{252}Cf

N. F. Bondar**), W. Neubert and W. Pilz
Zentralinstitut für Kernforschung, Rossendorf, Bereich KF

The detection of ternary fission events requires an optimization of the registration efficiency and an effective suppression of disturbing events. High detection efficiency of the γ-rays is achieved by two large (5x6inches) NaJ(Tl) crystals (SC1,SC2) coupled to FEU-110 photomultipliers. Both detectors are adjusted at a distance of 54cm on both sides of the ^{252}Cf source (*) in order to check the forward-backward emission symmetry. The fission fragments are detected by a transmission parallel plate avalanche counter (PPAC-START) and a position sensitive PPAC which covers an angular range of 98° degrees. The coordinate of the registered fission fragment is read out by an inductive delay-line. Perpendicularly to the plane defined by the transmission PPAC, PS PPAC (θ=25°) and the centre of the NaJ(Tl) crystals we arranged two silicon detectors D1 and D2 of $\rho \approx 150 \Omega cm$. Each of these silicon detectors covers an angular aperture of 40 degrees and they are shielded by a 36μm Al foil in order to stop the 6.12MeV alpha particles of the g.st.decay of ^{252}Cf. The preamplifier /1/ was modified for large-area silicon detectors with capacities $C > 100pF$. The observed counting rate of about 1 particle per sec. of light charged particles (mainly α's) allows to join the timing signals from both detectors after fast discrimination. The corresponding energy signals were amplified by shaping amplifiers (τ=0.25μs). The agreement of the energy scales of both spectroscopic branches was checked with a ThC' source. The threshold was set at 1MeV in the following CFTs adjusted for this long rise time. Both of the logical output signals are connected and then they are fed into the slow coincidence input 1.

A cut-off of the neutrons in the γ-branches became possible by a careful adjustment of the CFTs delivering a minimum walk of small signal amplitudes. The logical output signals (M) of the corresponding TACs 4 and 5 are fed into the slow coincidence units. The time correlation between α's and γ's is measured within 100ns by TAC 3. The M output signals of this TAC and TAC 2 deliver the remaining slow coincidence input signals. The coincidence outputs of both γ-branches are connected by a TTL OR module with adjustable μs-delay. The output of the OR triggers both ADCs (E1 and E2) and then the two 7 bit words are connected by a mixer. The three words FF TOF, POSITION and E1+E2 enter a multiplex interface based on the SI 1.2 standard which allows a data storage via the DMA channel onto the magnetic disc of the KRS 4201 computer.

**) On leave from LNPI, Gatchina, U.S.S.R.

R e f e r e n c e s

/1/ Ortlepp, H.-G. and Schuster, E., Annual Report ZfK-584 (1985) p.101

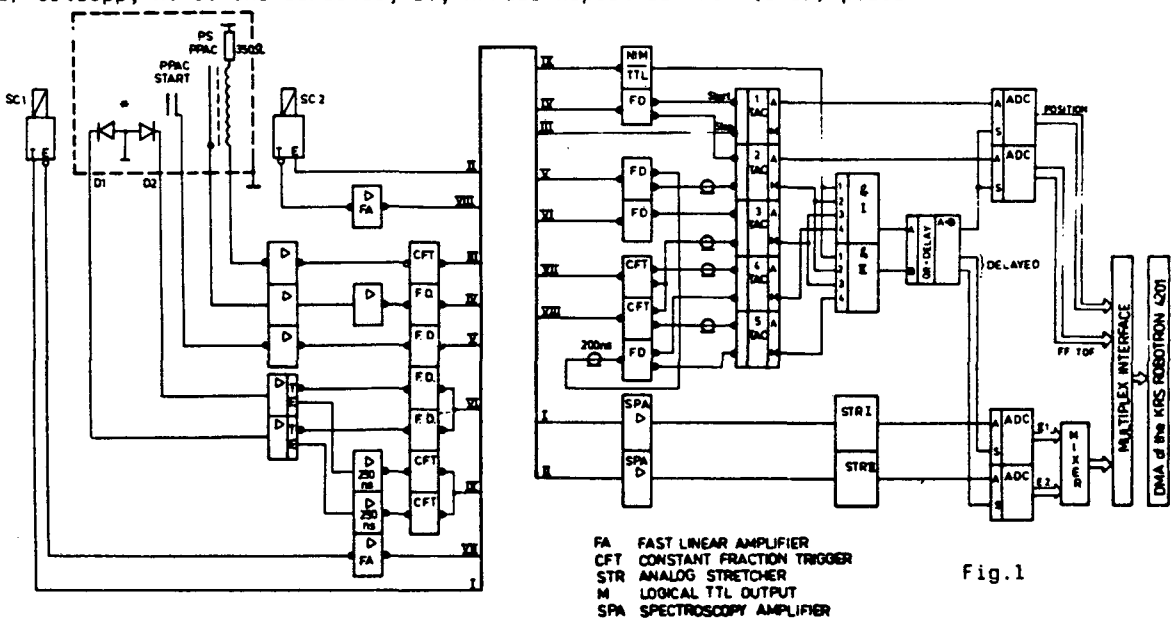

Fig.1

THE REGISTRATION OF 3 AND 4 PARAMETERS FROM FISSION EXPERIMENTS

W.D. Fromm
Zentralinstitut für Kernforschung, Rossendorf, Bereich KF

For a certain class of experiments the recording of events consisting of several quantities on a mass-storage device is necessary. Typically magnetic tape units are employed which provide capacities of tens of megabytes. At the KRS4201 computers installed at the Rossendorf tandem generator only magnetic disk storage is available. Therefore, the event format was optimized to fulfil the following experimental requirements:

- every parameter is represented by 1 byte (256 channels),
- every record contains 63 events of up to 4 parameters,
- 600000 events per disk cartridge can be stored.

The event format is used for 3 as well as 4 parameter measurements (Fig.1). The following set of programs was implemented:

Prog-Nr.	Task	3 Param.	4 Param.
3	Control of 2D-Display	FADI	FADI
4	Measurement	TRIP	VIRP
5	On-line Sorting	TROS	VISO
6	Protocoling	PROT	PROT

For the quality of the measurements the excellent display of linear and two-dimensional spectra is essential. Singles spectra of each parameter are continuously updated and presented on a high resolution vector display (1024*2048). For two selected parameters a two-dimensional representation with full resolution (256*256) is produced on the color display unit during the data-taking /1/.

The on-line sorting is performed according to a two-dimensional information held in a table. This information can be provided either directly from the color display unit after marking a region of interest with the joystick or by the input of a papertape containing 256 values for the lower and upper limits each. This papertape can be produced by a program which uses physical knowledge concerning the information needed for sorting. The table remains in core and can be used several times. An additional condition for another parameter can be implied for 4-parameter data. Again, a two-dimensional distribution for 2 selected parameters and singles spectra are produced for events fulfilling the conditions. The choice of the parameters is unrestricted, therefore, an easy self-checking procedure is available. Because the sorting is performed from the disk it is very fast (few seconds).

The content of the disk can be protocoled, too. The experiments number, the according disk space and the number of blocks occupied are printed for every run.

The following fission experiments were performed so far:

1) multiple differential neutron emission probabilities from spontaneous fission of Cf^{252}
   parameters: TOF fragment, fragment direction, TOF neutron /2/
2) measurement of neutron spectra from n-induced fission of Th^{232}
   parameters: TOF neutron, scintillator light output, pulse shape (off-line n_γ-separation)
3) angular distribution of γ-rays in the binary fission of Cf^{252}
   parameters: TOF fragment, fragment direction, γ-energy
4) angular distribution of γ-rays in the ternary fission of Cf^{252}
   parameters: TOF fragment, fragment direction, γ-energy, ΔT γ-fission (n-separation)

All the experiments are long-time measurements with typical data-taking times of 1000 to 2000 hours. The superior stability of the KRS4201 system has to be emphasized. In periods of unattended running of the experiment the display-monitors are switched off. The detailed physical evaluation was also performed or is in progress at the KRS4201 computer with programs written in FORTRAN language by the experimenting physicists.

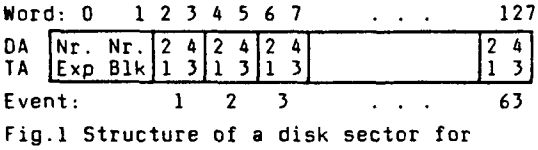

Fig.1 Structure of a disk sector for the storage of fission-events

References

/1/ Fromm, W.D. et al.; Annual Report 1983 ZfK-530(1984)131

/2/ Märten, H. et al.; Annual Report 1985 ZfK-584(1986)123

THE COLOR DISPLAY UNIT FD4971 AS AUTONOMOUS 2D-ANALYZER

W.D.Fromm
Zentralinstitut für Kernforschung, Rossendorf, Bereich KF

The measurement and the presentation of two-dimensional (2D) intensity distributions is an essential method in nuclear reaction studies. The adaption of the color display unit FD4971, originally developed for the investigation of multispectral images of the earth's surface, to nuclear physics applications /1/ has opened new possibilities for complex measurements at the accelerators and in the methodical work in the laboratory. The large display memory of the unit (1,28 KB) allows high resolution of the parameters (256*256 channels) and the registration of up to 65535 counts per channel (16 bit). The device can work in an autonomous manner or coupled to a host minicomputer via a 16 bit parallel interface. The display unit is controlled by the microcomputer system MPS4944 which can be easily expanded. New regimes for data-storage or presentation required for a certain experiment can be programmed.
In the autonomous regime the possibility to store the content of the large display memory has to be provided. The magnetic cassette tape unit K5200 equipped with the controller for the standard interface SIF1000 /2/ was connected to the display unit. On one side of the tape cassette 250 KB can be stored which amounts to slightly less than two pictures. The direct (1:1) output of the pictures is not only tape- but also time-consuming (> 2 min per picture). If one uses the fact that a large part of the memory contains zeros and the maximal intensity is well below 2^{15}, then the number of consecutive zeros can be counted and treated as one negative number. This sparse data scan procedure was implemented in the magnetic tape software with very large savings observed (compaction up to 20-fold).
Several experiments are searching for small effects on a large background. The separation is based often on the position of the intensities in the two-dimensional array spanned by the parameters. Formerly /1/ only linear transformations from intensity to color hue and vice versa were provided. For the above-mentioned measurements a logarithmic transformation was implemented. The 16 bit intensity is transformed into a 4 bit exponent with a 3 bit mantissa pointing to the 7 bit address for the continuous color scale. The reciprocal transform reproduces the data within the 4 most significant bit.
Furthermore the possibility of a hardcopy output of the recorded intensity distributions was a necessity. Every channel of the intensity distribution is printed as graphical element consisting of 3*3 points on a robotron 1154/5200 graphical matrix printer (768 points/line). The number of points printed (0..9) is connected to the intensity again in a logarithmic manner. All points are filled if the intensity is larger than 256 counts. An example of such an output is shown in the figure.

References

/1/ W.D. Fromm and M. Kahlenbach; Annual Report 1983, ZfK-530(1984)131

/2/ F. Schwarzenberg and W.D. Fromm; Annual Report 1983, ZfK-530(1984)129

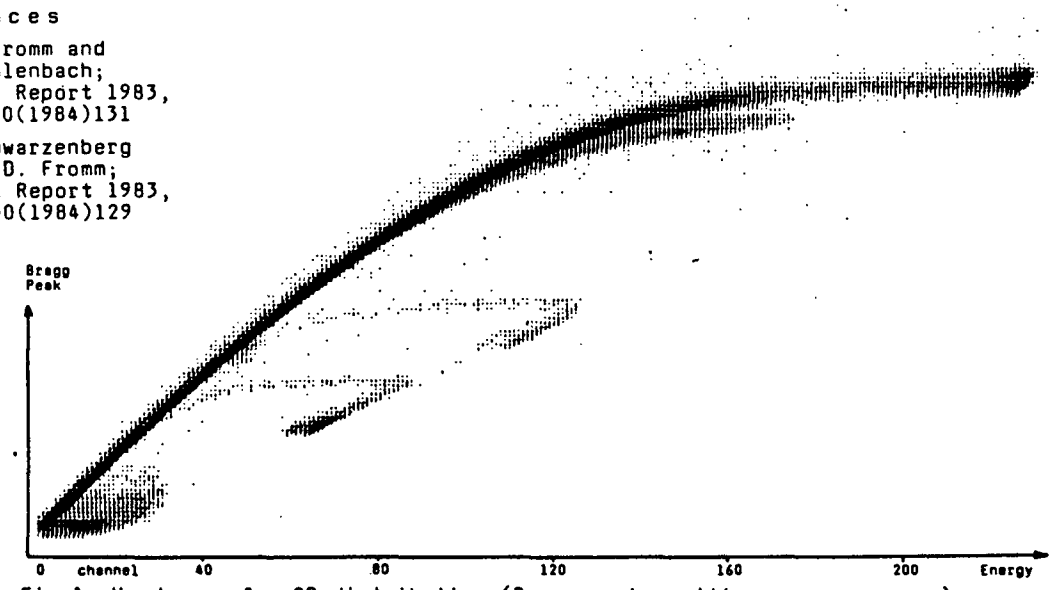

Fig.1: Hardcopy of a 2D-distribution (Bragg peak position versus energy)

ELECTRONIC DEVELOPMENTS OF THE KFM GROUP

W.D. Fromm, F. Schwarzenberg and H.-G. Ortlepp
Zentralinstitut für Kernforschung, Rossendorf, Bereich KF

Analog-Digital-Converter ADC 9908-30

For the microcomputer system MPS 4944 a spectroscopic ADC module was developed. The ADC is of the Wilkinson type and works with a clock frequency of up to 50 MHz. Resolutions of 256, 1024 and 4096 channels are selectable by the microcomputer. The data are output on the front panel connector as parallel information of up to 16 bit taking 2 sign-bit into account which are determined by front-panel BNC connectors. A coincidence regime is provided with a programmed waiting time for the coincidence signal of 2 to 8 µsec.

Interface Module V.24/IFSS/PIO VIF 9909-10

The overwhelming number of new peripheral devices are nowadays equipped with serial interfaces. For their usage in connection with the microcomputer system MPS 4944 an interface module for V.24 and the 20mA current loop IFSS was developed using the peripheral IC U856 (SIO). For V.24 the interface-IC 75150 and 75154 are used. The IFSS was realized with optocouplers and active current sources. In addition the parallel interface IC U855 (PIO) can be used for specific interface requirements (e.g. CENTRONICS).

Adapter for the Electronic Typewriters S6011/S6010 9910-10

These electronic typewriters can store one line of text only. Therefore, the use of lift-off or cover-up tapes in the correction process is obligate. The adapter board /1/ adds 2K of RAM (6116) to the text-memory and upgrades the typewriter to a memory-typewriter. One full page of text (4 KB) can now be held in memory and by means of a self-contained algorithm very easily corrected, updated and checked using the 8-character LED-display and function keys. Furthermore, a normal magnetic tape cassette unit can be connected to the adapter in order to archive the typed information. The pages are stored on tape with a 4-character filename and can be read back whenever necessary.

Video Display Unit Controller VDU 9911-10

A VDU controller board for the UPC880 single-board computer /2/ was developed. It was realized on a small PC-board (95*170 mm^2) for the display of 25 lines with 80 characters each. The character-RAM (6116) is mapped into the memory of the microcomputer. 128 characters are stored in a 8*12 pixel field in the character-ROM (2716). The generation of the video-signals for the TV monitor was facilitated by using an integrated CRT controller chip (6845). The VDU board 9911 is functional equivalent to the robotron K7024-board.

Adapter V.24-IFSS 9912-10

The delivery of a number of personal computers PC1715 has stimulated the use of computers in areas as economy, bureau automation, text processing and others. The need for adequate hardcopy-devices had initially to be fulfilled using existing printers which do not possess the necessary V.24 printer interface for the PC1715. Therefore, a small adapter-board for the current-loop IFSS was developed which is connected to the bidirectional V.24-port of the PC1715. More than 30 adapters were built and distributed so far.

Serial Interface for the Electronic Typewriter S6009 9915-10

Under certain circumstances the connection of an electronic typewriter to a personal computer is the preferable solution because of the high quality of the output. For the S6009 electronic typewriter a small interface board for V.24 or IFSS was developed. The unit is attached to the internal test connector and fits under the plastic cover of the typewriter. The mode for printing is selected by a special key combination on the typewriter. The output speed of 15 char/sec is much higher than reached by emulating the keyboard /3/. Only 8 IC are used for the IF-board (SIO, CTC, EPROM, level converters). A first batch of 10 units was produced.

References

/1/ G. Fell et al.; Neuerervorschlag NV 3/85, VEB Robotron Optima Büromaschinenwerk Erfurt
/2/ F. Schwarzenberg and W.D. Fromm; Annual Report 1983, ZfK-530(1984)129
/3/ G. Strauch et al.; Interface S0012, VEB Robotron Elektronik Dresden

PSEUDOGRAPHICS ON THE PERSONAL COMPUTER PC 1715

H.-J. Müller, K.-H. Heinig, W.D. Fromm and F. Schwarzenberg
Zentralinstitut für Kernforschung, Rossendorf, Bereich KF

On the international market, in personal computers of a performance compareable with the PC 1715 high resolution graphics is usually implemented. Thus, it is an essential drawback that the PC 1715 allows quasigraphics only with the aid of a restricted character set of 12 graphic symbols. In order to overcome this drawback partly, a graphic ability with reduced resolution ("pseudographics") has been developed. The problem has been solved by a minimum demand for hardware and software: a 2 kByte EPROM has to be put into an existing socket and a short machine program has to be loaded (using interpreters) or linked (using compilers). Although the presented solution requires considerable less effort than a "semigraphics" for the PC 1715 proposed recently /1/, a broad spectrum of unpretending CAD problems as well as graphics-oriented computer simulations can be accomplished.

The PC 1715 offers the possibility to expand the character-ROM by a 2 kByte EPROM. Therefore, 128 user-defined quasigraphic characters can be added to the alphanumeric character set. Rather than using special characters, the generation of graphics by free addressable points is a suitable method for general problems. The dot-array of a character consists of 12 rows with 8 dots each. Dividing this array into six fields with 4x4 dots each, we can establish a pseudographics of 80*2*24*3=160*72=11580 "pixels" on the standard monitor. In doing so, 2^6=64 new pseudographic characters have to be defined in order to permit all possible pixel configurations within the dot-array of a character. As the 2 kByte EPROM expansion can store 128 characters, two different kinds of pixels can be defined. We use a "full" pixel (all 4x4 dots of the pixel are bright) and a "small" pixel (only the inmost 2x2 dots are bright). It should be noted that the two kinds of pixels can be used simultaneously within one graphic presentation, but they cannot be intermixed within the dot-array of one character.

The figure shows an example for the application of the pseudographics. Full pixels have been used for the frame, whereas small pixels are taken for the curves. Alphanumeric symbols can be used within the graphics by so-called field-attributes /2/.

The application of the pseudographics is supported by a short machinecode routine. The method to load or to link this routine with user programs is described in the special documentation contained in the PLOT.DOC and PLOTBAS.DOC files obtainable from the authors.

The usual screen memory area ($F800...$FF80) or an additional one ($B800...$BF00) can be taken for storing the pseudographics. Manipulating a pixel on the sreen is accomplished by the call of PLOT(IX,IY,IT), where IX is the x-coordinate (0...159) and IY is the y-coordinate (0...71). IT is a control parameter with the meaning:

IT=	0	1	5	2
	pixel erased	set(full)	set(small)	tested

The screen is cleaned by the call of the subroutine RUB.

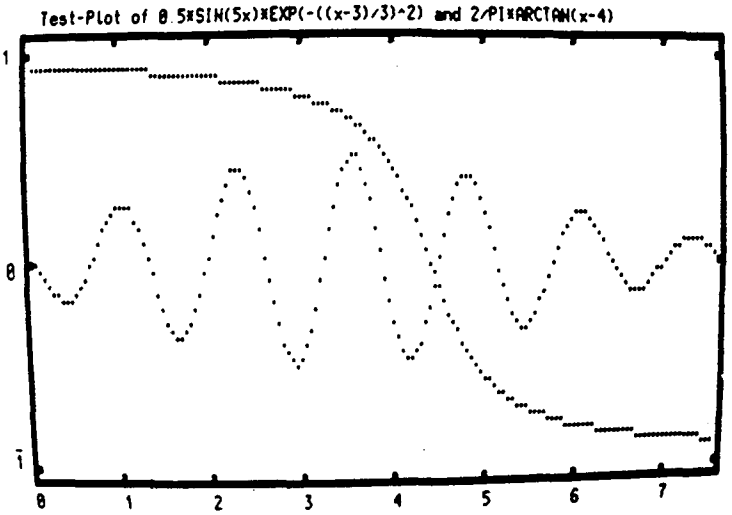

REFERENCES

/1/ Herden, D. et al.; rechentechnik, datenverarbeitung 23(1986)12

/2/ Systemhandbuch SCP; VEB Robotron Büromaschinenwerk Sömmerda, Januar 1985

Fig.1: Example for the pseudographic representation of mathematical functions on the PC1715

AN INTELLIGENT CAMAC-CONTROL UNIT FOR THE CCD SENSOR L 110 C

G. Karrasch, D. Kreiseler, K. Kreiseler
Joint Institut for Nuclear Research Dubna, ONMU, UdSSR

G. Musiol, G. Zschornack
TU Dresden, Department of Physics, Division of Applied Nuclear Physics

At the curved crystal diffraction spectrometer of the Department of New Acceleration Methods at the JINR Dubna a computer controlled adjustment of diaphragms, localized on the spectrometer focussing circle is realized /1/. In order to get comparable measurements it is necessary to make a reproducible adjustment of the diaphragms. For this purpose, an optical measurement system based on a CCD sensor L 110 C in connection with a CCD controller in CAMAC standard with a microprozessor Z 80, has been developed. The operation conditions of the CCD controller are shown on Figure 1.

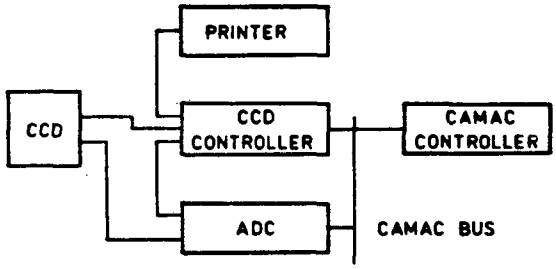

Fig. 1:
Operating conditions of the CCD controller

The CCD control unit realizes the generation of a tact sequence for performing variable exposure time and control of ADC-data reading out.

The data are intermediately stored in the RAM of the control unit. The start of the working cycle can be done either manually from the front panel of the microprocessor system (case A) or via CAMAC bus from an other computer (case B). In the working regime A the data are transferred via a SI 1.2 interface to a printer.

In the regime B either the position of diaphragms or the data of all CCD pixels are given via CAMAC interface to an external computer.

Furthermore, it is planed to test the system for X-ray position sensitive measurements.

/1/ G. Karrasch et al.; Preprint JINR P 13-83-474, Dubna, 1983

DETRITIATION SYSTEM FOR A HIGH-FLUX NEUTRON GENERATOR

U. Gohs and D. Schmidt

Technische Universität Dresden, Sektion Physik, WB Kernphysik

Tritium handling is an important precondition for the operation of high-flux neutron generators with an open target system. Sputtering, diffusion and replacement in the target result in tritium losses and, hence, in the contamination of the vacuum systems as well as the generator exhaust gas. In order to meet the requirements concerning the alowed maximum tritium concentration in air /1/ and the safe handling of contaminated generator components a detritiation system /2/ has been elaborated for the high-flux neutron generator INGE-1 /3/.

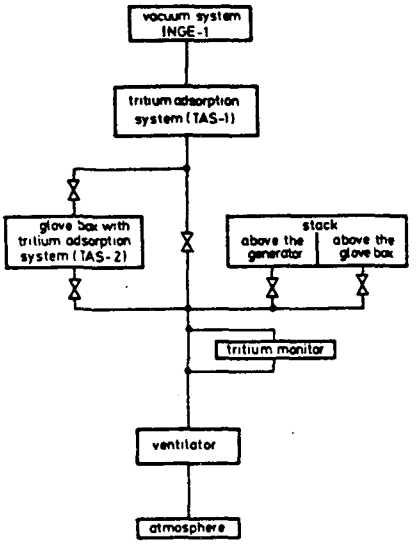

Figure 1:
Detritiation system for a high-flux neutron generator

This systems consists of three components:

(i) a tritium adsorption system (TAS-1) for cleaning of the generator exhaust gas
(ii) a glove box with a tritium adsorption system (TAS-2) for target change, waste handling and cleaning of the generator exhaust gas and
(iii) a ventilation system for air circulation above the neutron generator or the glove box.

The tritium adsorption systems TAS-1 and TAS-2 are automatically working detritiation systems based on catalytic oxidation of tritium and adsorption on a type 4A molecular-sieve dryer. The main components of these systems are a ventilator, an electrical preheater, a reaction tube filled with palladium and copper oxide, a cooler, an adsorption bed, and a flow-through ionisation chamber. The decontamination factor amounts to $\geq 10^6$ for a single-pass airflow of ≤ 10 m^3/h.

References

/1/ Lorenz, B.; ZfK-562 (1985) 68
/2/ Schmidt, D., Seeliger, D.; Experimentelle Grundlagen für neutronenphysikalische Untersuchungen für die Kernenergetik, Teil II, A 4-Abschlußbericht TU Dresden, Sektion Physik (1986)
/3/ Eckstein, P. et al.; ZfK-562 (1985) 24

OXIDATION OF HYDROGEN IN AIR AND IN INERT GAS ATMOSPHERE USING COPPER OXIDE CATALYSER

M. Rittner and U. Gohs
Technische Universität Dresden, Sektion Physik, WB Kernphysik

Tritium removal from air or inert gas atmosphere is necessary for systems involving tritium. Effluent gas streams are vented to a detritiation system based on the oxidation of tritium commonly. The choice of catalysers to be used depends on the experimental conditions. Metal oxides are usually applied for the oxidation in inert gas atmosphere. Due to their high reaction rate, precious metal catalysers are used in order to oxidize tritium gas and tritiated organic compounds in an atmosphere involving oxygen.

The oxidation of hydrogen is a first order reaction since the reaction rate is not affected by the initial concentration. Hence the reaction rate k and the decontamination factor are related as follows: $k = (\dot{V} \cdot \ln K)/V_{cat}$,

where $\dot{V}$ is the gas flow rate, and V_{cat} the reaction tube volume. The relation between the inlet and outlet gas concentration is the decontamination factor K.

The oxidation of hydrogen in inert gas atmosphere is represented in figure 1. It is shown that the decontamination factor is affected by the oxygen content of the catalyser. The reaction rate depends on the temperature according to the Arrhenius equation and is given as follows: $k = 7{,}3 \cdot 10^5 \exp(-52000/RT)$ for H_2(/1/).

The oxygen capacity for the used copper oxide catalyser (Leuna-Kontakt-4493) amounts to 56 l per liter catalyser at 190°C.
The reaction behaviour of CuO in air is represented in Figure 2. Since the reaction rate shows a linear dependence on the gas flow rate the gas phase mass transfer is the factor determining the reaction rate in the analized region.

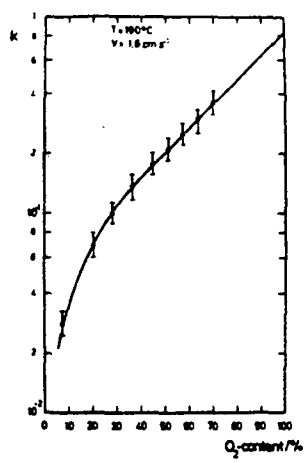

Fig. 1
Effect of oxygen content on the reaction rate

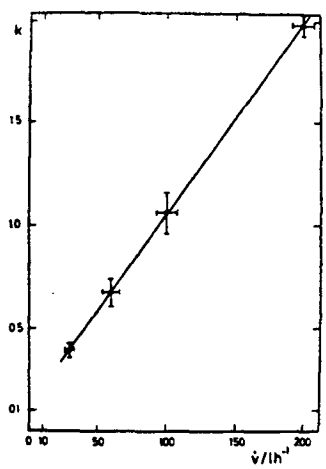

Fig. 2
Effect of gas flow rate on the reaction rate

References

/1/ Schmidt, D., Seeliger, D.; Experimentelle Grundlagen für neutronenphysikalische Untersuchungen für die Kernenergetik, Teil II, A4-Abschlußbericht TU Dresden, Sektion Physik (1986)

A DIFFUSING SYSTEM FOR PROTON BEAMS

H.U. Frey, U. Lehmann, and J. Vogt
Karl-Marx-Universität Leipzig, Sektion Physik, WB Angewandte Kernphysik

Precise PIXE measurements require a uniform particle beam. Several groups use the multiple scattering of a thin diffuser foil to produce a uniform particle distribution across the ion beam /1,2/. A diffusing system for the 2 MV Van de Graaff accelerator of the Karl Marx University was constructed and the characteristics have been determined both theoretically and experimentally.

Due to the maximum proton energy of 1.7 MeV a thin diffusing foil consisting of light elements has to be used, but better diffusing properties are provided by thicker foils of heavier elements. Following a mathematical procedure for the calculation of multiple scattering processes /3/ the properties of several diffuser materials and locations with respect to the target have been tested. As the result a carbon foil of 145 nm thickness which is 225 cm far from the target is used /4/. The intensity profiles (fig. 1) have been determined by scanning of a small piece of metal across the beam diameter /2/ and show a uniform distribution.

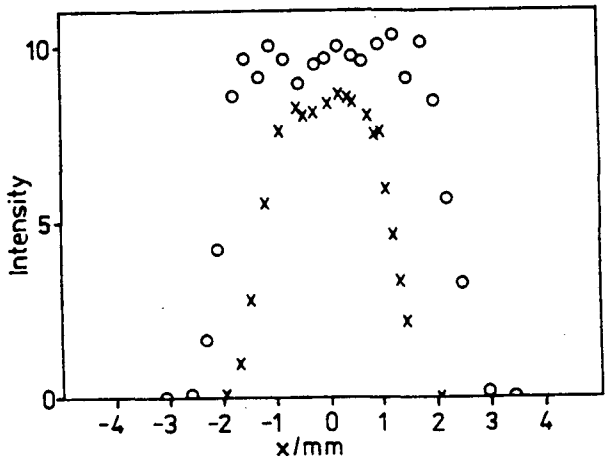

Figure 1:
Intensity profiles (arbitrarily normalized) of the diffused proton beam

The diffusing system has been used to minimize the destruction of biological samples during ion bombardment. As was shown in /5/ the normalized yield of X-rays increase with increasing accumulated ion charge. A linear function of the form

$$\sum_i \frac{Y_i}{Q_i} = a + b \sum_i Q_i = a \left(1 + \frac{b}{a} \sum_i Q_i\right) \quad (1)$$

was fitted to the X-ray yields of a certified reference material of the IAEA (rye flour, V8) /4/. The term b/a stands for the relative increase of the X-ray yield and shows the degree of the sample destruction. The values in table 1 show that the diffused ion beam causes a much lower sample destruction.

Element	with diffusing foil I = 20 nA	without diffusing foil I = 15 nA
Cl	$2.4 \cdot 10^{-3}$	$1.2 \cdot 10^{-2}$
K	$8.0 \cdot 10^{-3}$	$2.3 \cdot 10^{-2}$

Table 1:
Values of b/(a / uC) for proton bombardment of a rye flour sample (beam diameter 2.5 mm; E_p = 1.7 MeV)

R e f e r e n c e s

/1/ E.C. Montenegro et al., Nucl. Instr. and Meth. 164 (1979) 231
/2/ D.D. Jenson et al., Nucl. Instr. and Meth. B 10 (1985) 674
/3/ L. Meyer, phys. stat. sol. 44 (1971) 253
/4/ H.U. Frey, Thesis, Leipzig, 1986
/5/ J. Vogt et al., Gemeinsamer Jahresbericht 1984, ZfK-559 (1985) 85

AN INEXPENSIVE FAST-CLOSING SAFETY VALVE AGAINST VACUUM BREAKDOWN

B. Krause, and D. Lehmann
Karl-Marx-Universität Leipzig, Sektion Physik, WB Angewandte Kernphysik

To save the accelerator vacuum within the beam pipe against leakage or rupture of the exit foil of our "external ion beam" facility, mounted on the Leipzig van de Graaff accelerator, a simple and quickly acting vacuum seal has been designed, constructed and tested. The whole set-up consists of two separate units, which are fitted into two neighbouring flange ports (with 65 mm diameter) of a commercial cross piece (K 65, HV Dresden). Each unit consists of a cylindrical base plate, which carries an O-ring and the function dependent construction. On one side of the sealing component (left part of fig. 1) a cylindrical "nose" with a central bore of 6 mm diameter protrudes from the base plate. At the end of the nose a small O-ring is fixed. On the same side a bearing block with ball-bearings carries the axle of the valve plate.
In normal operation the valve plate is opened at an angle of about 45° and its position is fixed with a special latch at the end of a lifting magnet (right part of fig. 1) and with two springs, mounted on the valve base. The plate possesses an asymmetric, oval bore hole. The ion beam, having left the central bore hole, passes the asymmetric opening in the valve plate without restriction.
If the vacuum in the system begins to break down, a Penning gauge signalizes this unfavourable state and activates the lifting magnet through a relay switch. Thus the latch is reset to the upper position and the two springs accelerate the valve plate towards the small O-ring seal. Because the oval hole in the plate and the 6 mm bore in the nose do not overlap, the fast and tight closing of the opening prevents a vacuum breakdown in the beam pipe. After a foil rupture the exit foil has to be exchanged and the closed seal must be opened again, which is easily done with a special tool.
Till now the vacuum seal has worked reliably.

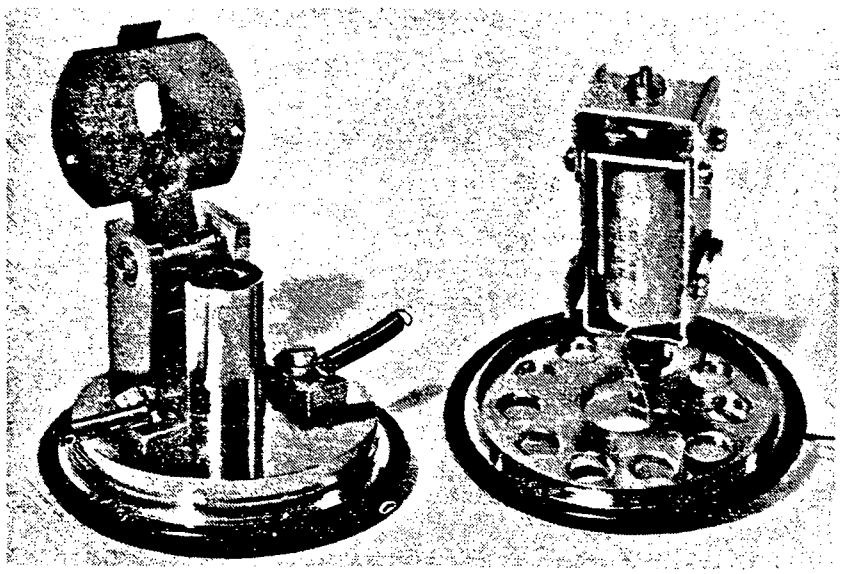

Fig. 1
View of the two components of the safety valve

A METHOD FOR COMPUTER CONTROLLED REGULATION OR STABILIZATION OF DETECTOR VOLTAGES

N.F. Bondar
Leningrad Nuclear Physics Institute, Gatchina, U.S.S.R.
J. Mösner and J. Hutsch
Zentralinstitut für Kernforschung, Rossendorf, Bereich KF

In order to stabilize or to regulate the voltage of several detectors of a computer controlled experiment a CAMAC-modul (single width) has been developed yielding 8 individually adjustable dc-levels of 0 to 10 V. These bias outputs can be selected by the CAMAC-instructions F(16)A(0 to 7) using the IC C565 for the DA-conversion. The accuracy is 12 bit ($\hat{=}$ ±0.25 %). The bias voltages are provided by detector supply units denoted HSVE /1/. They are dc-supplies with an output voltage (max. 4.8 kV) proportional to an external input dc-level of 0 to 10 V. Moreover a reference output level (also 0 to 10 V) proportional to the normal output voltage is available.
Coupling the dc-outputs of the CAMAC-modul to the external inputs of the HSVEs 8 detector voltages can be individually controlled. The measurement of the voltages (resp. the reference levels) is performed by a CAMAC-multiplexer /2/ and a 14 bit CAMAC-AD-converter /3/.
Using this configuration it is possible to realize computer controlled long term stabilization of detector responses as well as systematic investigation and test of the operational condition of gaseous multistep detectors, automatic optimization of energy and time resolution of detector telescopes and similar investigations. Of course, for such computer controlled measurements it is necessary to feed the computer with the other operational parameters of the detectors as temperature, gas pressure, gas admixture etc..
Up to now we used this configuration for an experiment measuring the differential cross section of the n-p capture reaction /4/. Because of the small cross section value of this reaction a measuring time of several weeks is necessary requiring a stable operation of the whole set-up during this time. Therefore, the used on-line computer (KRS 4201) serves for data taking as well as for recording and control of the different parameters of the experiment. With respect to the detector supplies the voltages of two MWPCs and two position-sensitive multistep avalanche chambers MSCs /5/ are checked, together with other parameters, within periodic time intervals of about 5 min and corrected if necessary. A long term stability of better than $3 \cdot 10^{-4}$ can be obtained by this method.

References.

/1/ Gerätebeschreibung HSVE 50,60,70; ZfK Rossendorf, 1984
/2/ Gerätebeschreibung MUX 5316; ZfK Rossendorf, 1981
/3/ Gerätebeschreibung ADC-DS 3526 KD; ZfK Rossendorf, 1981
/4/ this report p.126
/5/ this report p.127

COMPUTATIONAL METHODS AND CODES

EVMESS - A PROGRAM FOR EXPERIMENT DATA COLLECTION ON SM3 COMPUTERS

E. WILL

Zentralinstitut für Kernforschung Rossendorf, Bereich KF

The program has been developed for fast data collection at the double-arm time-of-flight spectrometer DEMAS /1/ in Dubna (JINR). More than 10 parameters have to be measured in a coincidence experiment depending on the experimental set-up. The data will be taken with the help of CAMAC ADC's (1024 or 4048 channels). The program is written in form of assembler subroutines for control and interrupt handling. The control routines switch on the desired measurement or display regime or execute immediately a function for example clear data memory, input or output of the displayed spectra. They will be called with short commands on the teletype in an interactive manner without a special order. Up to now 65 command words have been generated. The control of the data path takes place with the help of control words or a direct change of call and branch commands within the interrupt routines. The output to the magnetic disk, the different display and condition routines will be added in this way to the basic interrupt routine, which reads out the coincidence ADC. With this method a high working speed with only few tests in fast realtime work will be obtained. The computer waits for a command if no interrupt handling will be done. If it has obtained the first character of a command the interrupt from the coincidence unit and the monitor ADC will be blocked up. This is necessary because otherwise the fast interrupt handling blocks up the operating system (RT11SJ) at high data rates and a system crash happens in such cases. The program has a length of 61 Kbytes and is linked in 4 overlay regions. The seldom used functions have been linked in the same overlay region such as switching on of condition areas, sorting of input data from disk and the following outputs: hardcopy, protokol head to data file, program status and the help informations.

The program is able:

1. to read out up to 20 CAMAC ADC (parameters) for a coincidence event and an aditional monitor ADC. A coincidence unit has to give the LAM signal for reading out the ADC s if a coincidence event has been detected.
2. to collect the measured data event-by-event on a magnetic disk. The number of parameters, condition information (if any), start and stop time and date and a comment will be written in the first block of such a file.
3. to show up to 4 two-dimensional spectra or their projections on a color display. It is possible to choose any of the input parameters as x- or y-axis and to read/write the displayed spectra from/to disk or to make a hardcopy.
4. to write the program status with all important working parameter to the terminal.
5. to set lower und upper boundaries on each parameter or to choose condition figures with a moving mouse in the two-dimensional spectra to exclude events from display or disk output.
6. to sort the original measurement data from the disk file with new assignments of x- or y-axis and new conditions.
7. to identify x and y channel numbers and the contents in the displayed spectra with the mouse.
8. to write the contents of the displayed spectra to the lineprinter.
9. to show the input channels from an event on the terminal for checking the experiment.
10. to write an automatic measurement protocol to a special file.
11. to write a help information for all control words to the terminal.

References

/1/ Schilling, K. D., et al.; Report ZfK-586 (1986) and Nucl. Instr. Methods (submitted)

A NEW PROGRAM PACKAGE FOR THE CALCULATION OF RELATIVISTIC X-RAY EMISSION RATES

I. Reiche, G. Zschornack
Technical University Dresden, Section of Physics, Division of Applied Nuclear Physics, Mommsenstr. 13, Dresden, GDR-8027

A complete overview of relativistic X-ray emission rates for all elements was given by Scofield /1/ in 1974 for a number of different transitions in neutral atoms. In the recent time, corresponding values for the most ion ground states are not available in the literature.
Therefore, we develope a program for calculations of relativistic X-ray emission rates, running on the computer EC 1055. The program is based on the Multiconfigurational Dirac-Fock-Package of Grant, Mc Kenzie et al. /2,3/, which enables to supply corrections to the Coulomb energy levels, that result from including the transverse Breit operator (describing magnetic interaction and retardation) in first order pertubation, the second order vacuumpolarization and an approximate estimate of the self energy operator. The program allowes to include up to 32 orbitals and up to 80 configurations. X-ray emission rates are calculated in Scofields multipole approximation, either in the frozen core or in the adiabatic approximation. In the frozen core approximation the program calculates the total X-ray emission rates of all orbitals and, additionally, in the case of available fluorescence yields energetic widths of the transitions.

To check the quality of results, there were performed calculations for three elements with very different atomic numbers. Table 1 shows actual results of relative intensities in comparison with values given by Scofield and with experimental ones.
Basing on the developed program, we plan to calculate a new set of X-ray transition probabilities for all elements and the most intensive transitions up to Neptunium.

Table 1

Element	our results 1)	$K_{\alpha 2}/K_{\alpha 1}$ Scofield 2)	$\frac{1)}{2)} \cdot 100\%$	Experiment	our results 3)	$K_{\beta 3}/K_{\beta 1}$ Scofield 4)	$\frac{3)}{4)} \cdot 100\%$
$_{26}Fe$	0,5061	0,5107	99,1 %	0,506±0,01 /4/ 0,507±0,01 /5/	0,5120	0,5079	100,8 %
$_{56}Ba$	0,5407	0,5428	99,6 %	0,533±0,011 /5/ 0,562±0,022 /6/	0,5151	0,5160	99,8 %
$_{82}Pb$	0,5978	0,5950	100,5 %	0,589±0,012 /5/ 0,596±0,03 /6/	0,5201	0,5165	100,7 %

/1/ Scofield J.H., Phys. Review, A9, 1974, p. 1041
/2/ Grant I.P. et al., Comp. Phys. Commun., 1980, 21, p. 207
/3/ Mc Kenzie B.J. et al., Comp. Phys. Commun., 1980, 21, p. 233
/4/ Salem S.I. and Wimmer R.J., Phys. Rev. A2 (1970), p. 1121
/5/ Mc Crary J.H. et al., Phys. Rev. A4 (1971), p. 1745
/6/ Nelson G.C. and Saunders B.G., Phys. Rev. 188 (1969), p. 108

PROPERTIES OF A BAYES-BASED SPECTRUM UNFOLDING ALGORITHM

E. Jara, A. Reichmann, G. Zschornack

Technical University Dresden, Department of Physics, Division of Applied Nuclear Physics, Mommsenstr. 13, Dresden, GDR-8027

Every measured spectrum is a distorted representation of the original spectrum, whereby distortion is caused by the apparatus function. A mathematical formulation of this fact can be constructed by a matrix equation in the form $M_k = \sum_j R_{kj} T_j$ with T_j - searched spectrum, M_k - measured spectrum, R_{kj} - imaging matrix of the measuring apparatus.

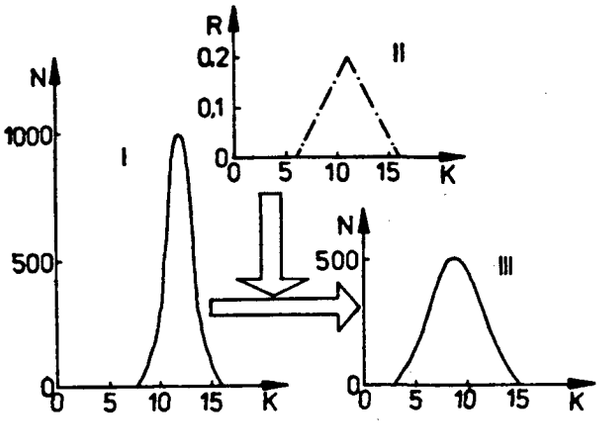

Fig. 1:

Sometime the spectrum deformation caused by the measuring apparatus is so large, that from the measured spectrum significant informations about the original spectrum can not be obtained. In such cases it is necessary to unfold the measured spectrum with respect to the imaging matrix of the measuring apparatus. For this purpose Richardson /1/ gives a Bayes-based, iterative spectrum unfolding algorithm

$$T_j^{(n+1)} = T_j^{(n)} \sum_k \left[R_{kj} M_k / \sum_i R_{ki} T_i^{(n)} \right] .$$

The analysis of properties of the unfolding algorithm was done with a corresponding computer code. As weighting criterion for the result of unfolding we calculate after each step of iteration:

- sum of absolute values of differences between the searched spectrum and the result of unfolding (Σ AB)
- difference between positions of the centre of gravity (δ_{SP})
- difference of FWHM (δ_{HWB}).

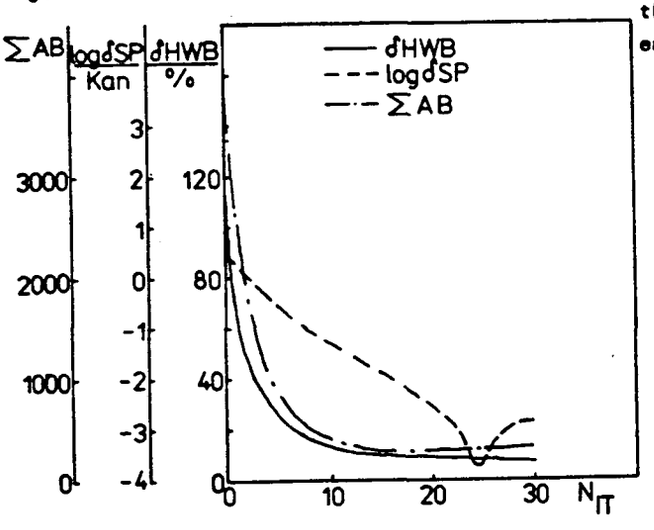

Fig. 2:

For instance, Fig. 1 shows a measured spectrum (III) with the corresponding searched spectrum (I) and the apparatus function (II). The apparatus function causes a broadening and a shift of the centre of gravity of the measured spectrum relative to the searched one. Fig. 2 shows the course of weighting values for the Bayes-unfolding as a function of the number of iterations. After a small number of steps one can get a acceptable reproduction of the searched spectrum, whereby exists a optimum number of iterations. The statistics of the measured spectrum strongly influences the result of unfolding. This influence may be reduced by smoothing with spline-based functions.

/1/ Richardson, W.H.: Journal of the Optical Society of America, 62, 1572, p. 55

LIST OF PUBLICATIONS, ACADEMIC PROMOTIONS, LECTURES AND CONFERENCE CONTRIBUTIONS, SCIENTIFIC MEETINGS, PATENTS AND AWARDS OF HONOUR

ZENTRALINSTITUT FÜR KERNFORSCHUNG, ROSSENDORF, BEREICH KF

VERÖFFENTLICHUNGEN

Aleksandrov, K.S., A.F. Bovina, V.N. Voronov, M.V. Gorev, I.M. Iskornev, S.V. Melnikova, S.V. Misjul, F. Prokert, I.N. Flerov
Ferroelastic Phase Transition in Elpasolites $A_2BB^{3+}X_6$
Jpn. J. Appl. Phys. 24 (1985) Suppl. 2, 693

Andrejtscheff, W., L.K. Kostov, L.G. Kostova, P. Petkov, H. Rotter, W.D. Fromm, H. Prade, F. Stary
Two-Quasiproton and Two-Quasineutron Excitations in the Transitional Nuclei $^{102,104,106}Pd$
Nucl. Phys. A448 (1986) 301

Andronenko, L., A.A. Kotov, L.A. Vaishnene, W. Neubert, H.W. Barz, J. Bondorf, R. Donangelo, H. Schulz
Mass yield distribution for 1 GeV proton induced nuclear reactions on Ni and Ag
Phys. Lett. 174B (1986) 18

Artemov, K.P., M.S. Golovkov, V.Z. Goldberg, V.P. Rudakov, I.N. Serikov, V.A. Timofeev, M. Andrassi, D. Wohlfarth, H.U. Gersch, G. Lang, E. Hentschel
Analysis of Angular Distributions of Deutrons Produced in the Multinucleon-group-Transfer Reaction $^{12}C(^{14}N,d)^{24}Mg$ (in russisch)
Jad. Fis. 44 (1986) 579

Beither, D., R. Kögler, D. Panknin, E. Wieser
Residual Defects in Implanted Silicon after Annealing with Incoherent Light
Phys. Status Solidi A94 (1986) 767

Balian, R., Y. Akhassid, H. Reinhardt
Dissipation in many-body systems: A geometric approach based on information theory
Phys. Rep. C131 (1986)

Barz, H.W., T.S. Biro, B. Lukacs, J. Zimanyi
Effect of correlations on entropy and hadrochemical composition in heavy ion reactions
KFKI-1986-19/A

Barz, H.W., J. Bondorf, R. Donangelo, H. Schulz
Connection between the thermodynamical and the percolation models of nuclear fragmentation
Phys. Lett. 169B (1986) 318

Barz, H.W., J. Bondorf, R. Donangelo, H. Schulz
Connection between Thermodynamical and the Percolation Models of Nuclear Fragmentation
Proc. of Workshop on Cross Properties of Nuclei and Nuclear Excitations, ed. by H. Feldmeier, p. 138 (1986)

Barz, H.W., J. Bondorf, I.N. Mushustin, H. Schulz
Statistical multifragmentation of nuclei. (III) decay of fragments. Nucl. Phys. A448 (1986) 753

Barz, H.W., H. Iwe
Cascade model studies of pion and strange particle production in C on Ta reactions at E/A ≈ 3.36 GeV. Nucl. Phys. A453 (1986) 728

Barz, H.W., B. Kämpfer, B. Lukacs
One- and two-fluid hydrodynamics applied to quark-gluon plasma formation in heavy ion collisions
Proc. of workshop on Cross Properties of Nuclei and Nuclear Excitations, ed. by H. Feldmeier, p. 186 (1986)

Betzl, M.
Internationale Schule Neutronenstreuung
Kernenergie 29 (1986) 400

Betzl, M., W. Voitus, A. Ertel, P. Bankwitz, H. Kämpf
Neutronographic Texture Investigations of Halit
ZfK-584 (1986) 68

Betzl, M., M. Voitus, A. Ertel
Methodical Investigations via Texture of Rock Salt
ZfK-584 (1986) 67

Bischoff, L., J. von Borany, M. Deutscher, U. Lorenz, G. Mende, H. Oertel, B. Schmidt, H. Schott
SiO_2-passivierte Strahlungssensoren
Tagungsbericht 17. Arbeitstagung Physik der Halbleiteroberfläche, Binz, 7.-12.4.1986

Bischoff, L., J. von Borany, H. Morgenstern, B. Schmidt, D. Schubert
Strahlenschäden in Si-Halbleiterdetektoren
ZfK-579 (1986)

Bischoff, L., D. Mademann, K. Trützschler, G. Zschornack
Der Einsatz von Mikrostreifendetektoren in der winkeldispersiven Röntgenspektrometrie
TU-Information 05-05-86, TU Dresden, 1986

Bondarenko, V.A., P.T. Prokof'ev, W. Enghardt, H. Prade, F. Stary, L. Käubler, H.-J. Keller
Protonenzustände in ^{149}Eu und Kernform im Gebiet N=84-88 (in russisch)
Izv. AN SSR, Ser. Fiz. 50 (1986) 26

Bondorf, J., R. Donangelo, I.N. Mishustin, H. Schulz
Statistical multifragmentation of nuclei. (II) Application of the model to finite nuclei disassembly. Nucl. Phys. A444 (1985) 460

Bohdorf, J., R. Donangelo, H. Schulz, K. Sneppen
Energy thresholds for fragmentation and vaporization of the atomic nucleus. Phys. Lett. 162B (1985) 30

Borany, J. von, M. Deutscher, U. Lorenz, B. Schmidt, H. Schott
Großflächige ionenimplantierte Si-Strahlungsdetektoren
Tagungsbericht zum 19. Fachkolloquium Informationstechnik, Dresden, Januar 1985, S. 134

Bordag, M., F.M. Dittes, D. Robaschik
Casimio effect with uniformly moving mirrors
J. Nucl. Phys. 43 (1986) 1606

Dittes, F.H., B. Geyer, D. Robaschik, J. Horejni
Determination of the Altarelli-Parisi-Kernel from an extended Brodsky-Lepage-Kernel
Proc. of the XX. Int. Symposium Ahrenshop, 13.-17.10.1986

Dönau, F.
Mean field theory of nuclear spin
Int. Conference "Nuclear Structure, Reactions and Symmetries", Jugoslawien, 4.-15.6.1986

Dönau, F.
Coupling of single particle and collective degrees of freedom in the light of the equation of motion method
Int. Seminar on Nuclear Physics, Sorrento, 19.-23. Mai 1986

Oshemuchadse, S., B. Kühn, W. Neubert, S. Tesch et al.
Suche nach exotischen, langlebigen Dibarionen
Kurze Mitteilungen des VIK 13 (1985) 5

Oshemuchadse, S., S. Tesch et al.
Diffraction scattering of Alphaparticles on nuclei at 17.3 GeV/c
ZfK-129 (1986)

Dubiel, M., U. Bärenwald, W. Matz
Computersimulation der Struktur von Phosphat- und Fluoroaluminatgläsern
3. Int. Otto-Schott-Kolloquium, Jena, 7.-11.7.1986

Ebert, D., H. Reinhardt
Effective chiral meson lagrangian with anomalies and Skyrme terms from quark flavour dynamics
Nucl. Phys. B271 (1986) 188

Ebert, D., H. Reinhardt
Effective chiral meson lagrangian with Weinberg and KFSR relation from microscopic four-quark interaction
Phys. Lett. B173 (1986) 453

Eichhorn, F.
Präzisionsbestimmung von Strukturfaktoren mittels dynamischen Neutroneninterferenzen
Schultagung "Dynamische Theorie der Röntgenstrahlbeugung und Röntgentopographie", Fincken, 17.-21.3.1986

Eichhorn, F., F. Häußler
Small-Angle Neutron Scattering Investigations on Cement Paste
Arbeitsberatung "Untersuchung kondensierter Medien am Reaktor IBR-2", Dubna, 16.-18.10.1986

Eichhorn, F.
Investigation of small-angle neutron scattering by double crystal diffractometry
Workshop on Neutron Physics, Budapest, 8.-10.10.1986

Eichhorn, F., F. Häußler, U. Miehe
Small-angle neutron scattering on hydrating cement paste
ZfK-584 (1986) 71

Eichhorn, F., U. Schmidt, W. Voitus
Determination of material inhomogeneities by small-angle neutron scattering
XII. Conf. on Applied Crystallography, Cieszyn, 10.-14.8.1986

Enghardt, W.
Basisrechnersystem für PET
Studie, ZfK Rossendorf, September 1986

Enghardt, W., L. Käubler, H. Prade, H.-J. Keller, F. Stary
In-Beam Study of Multiparticle Excitations in the Semi-Magic Nucleus ^{140}Ce
Nucl. Phys. A449 (1986) 417

Enghardt, W., H. Prade, H.U. Jäger, L. Käubler, H.-J. Keller, F. Stary, L.K. Kostov
Microscopic structure of semimagic nuclei with 82 neutrons or 50 protons
Ann. Phys. (Leipzig) 43 (1986) 424

Eschrig, H., R. Richter, L. Weiß, A.Y. Rumyantsev, N.L. Mitrofanov, A.S. Ivanov, N.A. Chernoplekov
Proc. of the 2nd Int. Conf. "Phonon 85", World Scientific Publishing Comp., Singapore 1985, p. 227

Feldmann, K., L. Fuentes, K. Walther
Problems in Texture Analysis of Metamorphic Rocks
Workshop on Theoretical Methods of Texture Analysis, Clausthal-Zellerfeld, 17.-21.3.1986

Fromm, W.D., D. Grambole, F. Herrmann, F. Schwarzenberg
A nuclear micro-beam probe for the investigation of surfaces
5th Int. IMEKO Symposium "Intelligent Measurement", Jena, 10.-14.6.1986, Proceedings, Vol. II, p. 271

Fromm, W.D., H.G. Ortlepp, H. Sodan, O.V. Strekalovski
Projekt der Elektronik für die Anlage PHOBOS - ein 4π Spektrometer für Vielfachereignisse aus Reaktionen mit Schweren Ionen
Projekt, VIK Dubna, Juni 1986

Fromm, W.D., F. Schwarzenberg
An intelligent multichannel analyser for the measurement of γ-spectra
5th Int. IMEKO-Symposium "Intelligent Measurement", Jena, 10.-14.6.1986, Proceedings, Vol. II, p. 268

Funke, L.
Nuclear shape transitions in the Kr isotopes
Int. Winter Meeting on Nuclear Physics, Bormio, 20.-25.1.1986, Proceedings 24, p. 599

Funke, L., J. Döring, P. Kemnitz, P. Ojeda, R. Schwengner, E. Will, G. Winter, A. Johnson, L. Hildingsson, Th. Lindblad
Yrast states in ^{81}Br and ^{82}Br
Z. Phys., A 324 (1986) 127

Funke, L., J. Döring, P. Kemnitz, E. Will, G. Winter, A. Johnson, L. Hildingsson, Th. Lindblad
Three-quasiparticle excitations in ^{81}Kr
Nucl. Phys. A455 (1986) 206

Gersch, H.U.
Second order interferometry for the study of relativistic heavy ion collisions
Proc. of the XVI. Int. Symposium on Nuclear Physics, Gaußig, November 1986

Gersch, H.U., V. Goldberg, V. Rudakov
About the possibility of a bound ^{12}C - ^{12}C quasimolecular band in ^{24}Mg
ZfK-578 (1986)

Gippner, P., K.-D. Schilling, W. Seidel, F. Stary, V.S. Salamatin, H. Sodan, S.M. Lukjanov
Berechnung der Massen-Winkel-Akzeptanz für das Doppelarm-Flugzeitspektrometer DEMAS
ZfK-572 (1985)

Gippner, P., K.-D. Schilling, W. Seidel, F. Stary, E. Will, H. Sodan, S.M. Lukyanov, G.G. Chubarian, V.S. Salamatin, Yu.E. Penionzhkevich
Fragment Mass Distributions in Heavy-Ion Reactions Leading to Composite Systems with Z=108
ZfK-592 (1986) 122

Gippner, P., K.-D. Schilling, W. Seidel, F. Stary, E. Will, H. Sodan, S.M. Lukyanov, V.S. Salamatin, Yu.E. Penionzhkevich, G.G. Chubarian, R. Schmidt
Shell effects in the evolution of the mass asymmetry in heavy-ion collisions leading to composite systems with Z=108
Z. Phys. A325 (1986) 335

Grötzschel, R., K. Brankoff, W.D. Fromm
Computerized experimental facilities for ion-beam analysis
5th Int. IMEKO-Symposium "Intelligent Measurement", Jena, 10.-14.6.1986, Proceedings, Vol. I, p. 128

Gudima,K.K., V.D. Toneev, G. Röpke, H. Schulz
Entropy evolution in heavy ion collisions
Phys. Rev. C32 (1985) 1605

Guimaraes, S., R. Kögler, E. Landi, S. Solmi, E. Wieser
Anomalous Enhanced Diffusion and Electrical Activation of Boron in Silicon after Rapid Isothermal Annealing
Phys. Status Solidi A93 (1986) 549

Heera, V., B. Rauschenbach
A simple amorphisation-recrystallisation model for boron implanted iron films
Radiat. Eff. 91 (1985) 71

Heinig, K.-H., H.-D. Geiler
Phenomenological theory of explosive solid phase crystallization of amorphous silicon
Phys. Status Solidi A93 (1986) 99

Helming, K., B. Rauschenbach
Determination of Implantation-Induced Textures by Electron Diffraction
Phys. Status Solidi B138, K1 (1986)

Hennig, K.
Texture Investigations by Neutron Diffraction
Workshop on Neutron Physics, Budapest, 8.-10.10.1986

Hennig, K., K. Feldmann
Neutron Diffractometry of Textures (in russisch)
V. Int. School on Neutron Physics, Alushta, 20.-31.10.1986

Hennig, K., Ed. Richter, Em. Richter, A. Schmidt
Oberflächenveredlung mittels Ionenstrahlen
Elektrie 40 (1986) 445

Hoffmann, W., J. Hüller, M.T. Pham
Chemische Sensoren auf der Basis von elektronischen Bauelementen
Lehrmaterial für Spezialistenweiterbildung, KdT Halle, Juni 1986

Hoffmann, W., J. Hüller, M.T. Pham
Ion-sensitive membranes applicable to ion-sensitive field effect transistors manufactured by ion implantation
4th Symposium on Ion-Selective Electrodes, Mátrafüred, 1984

Hohmuth, K., B. Rauschenbach
Bildung von Metall-Metall-Mischkristallen mittels Ionenstrahl-induzierter Mischung
Ann. Phys. (Leipzig) 43 (1986) 3

Jäger, H.U.
Model investigations of the oxidation of silicon by high dose implantation
Nucl. Instrum. Methods B15 (1986) 748

Just, G., W.D. Fromm
Quantitative Bestimmung seltener Elemente mittels INAA für 35 Zinnerzproben zur Eichung des Röntgenfluoreszenzspektrometers VRA 30 im Rahmen des Forschungsthemas "Mehrelementanalyse durch RFA"
Forschungsbericht, Leipzig/Rossendorf, November 1986

Kämpfer, B.
Phänomenologie von Phasenübergängen in Kernmaterie
ZfK-587 (1986), Promotion B

Kämpfer, B.
Entropy production during an isothermal phase transition in the early universe
Astr. Nachr. 307 (1986) 231

Kämpfer, B., H.W. Barz
Quark-gluon plasma formation in relativistic heavy ion collisions
Abstr. on contr. papers on the VIII. Seminar on High Energy Physics Problems, Dubna 1986, p. 81

Kämpfer, B., H.W. Barz, L. Münchow, B. Lukacs
Decay of the baryon-rich quark-gluon plasma produced in relativistic heavy ion collisions
Acta Phys. Pol. B17 (1986) 685

Kämpfer, B., B. Lukacs, G. Paal
Entropy production in tepid inflation
KFKI-1986-36

Kämpfer, B., B. Lukacs, G. Paal
Inflation by moderate supercooling
Abstr. of contr. papers to 11th Conf. Gen. Rel. Grav., Stockholm 1986, p. 206, poster 6.13

Kemnitz, P., J. Döring, L. Funke, G. Winter, L. Hildingsson, D. Zerrestam, A. Johnson, Th. Lindblad
Evidence for shape coexistence from few-quasiparticle excitations in ^{83}Kr
Nucl. Phys. A456 (1986) 89

Kirchbach, M.
Constraints on parity-mixing matrix elements from hard-pion exchange corrections to first-forbidden beta decay
ZfK-576 (1986)

Kirchbach, M.
Grundbegriffe der Theorie der Mesonenaustauschströme
ZfK-567 (1986)

Kirchbach, M.
Constraints on Parity-Mixing Matrix Elements from Hard-Pion Exchange Corrections to First-Forbidden 0-Decays
Contrib. to the Int. Nucl. Phys. Conf., Harrogate U.K., 25.-30.8.1986

Kirchbach, M.
The Renormalization of the Nuclear Chiral Charge Density in the Isovector $0^+ \rightarrow 0^-$ 0-Transitions in the Mass-16 Tried
Czech. J. Phys. B36 (1986) 372

Kirchbach, M., E. Truhlik
Axial exchange currents in nuclear physics
Sov. J. Part. Nucl. 17 (1986) 224

Kissener, H.R., I. Rotter, N.G. Goncharova
Microscopic studies of electric dipole resonances in 1p shell nuclei
ZfK-588 (1986)

Kleinwächter, P., I. Rotter
On the interplay between giant resonances and background
J. Phys. G 12 (1986) 821

Klimanek, P., K. Cyrener, A. Mücklich, U. Scholz
Texture development in pass-rolling of FCC metals
ZfK-584 (1986) 69

Klimanek, P., A. Kühl, A. Mücklich, U. Scholz
Texture development during cold rolling of ($\alpha + \beta$)-brass
ZfK-584 (1986) 70

Kostov, L.K., W. Andrejtscheff, L.G. Kostova, P. Petkov, W. Enghardt, H. Prade, L. Käubler, H. Rotter, F. Stary
Lifetime measurements and particle-core coupling calculations in ^{144}Sm
Z. Phys. A325 (1986) 293

Kotte, R., H.-J. Keller, H.-G. Ortlepp, F. Stary
Bragg-peak spectroscopy of low-energy heavy ions
ZfK-591 (1986)

Kovacs, Zs., H. Müller
Hadron fragment emission in cluster excitation processes at medium energies
KFKI-1985-111

Lück, H.B.
On tree initiation and propagation in electrochemical etching of particle tracks
Nucl. Tracks Radiat. Meas. 11 (1986) 17

Manfraß, P., W.D. Fromm
Zur Realisierung eines Positronen-Emissions-Tomographen
Studie, ZfK Rossendorf, März 1986

Matthies, S.
Gruppentheoretische Invarianten für Fehleruntersuchungen in der quantitativen Texturanalyse
Ann. Phys. 43 (1986) 299

Matz, W.
Neutron Diffraction on Non-crystalline Materials
Workshop on Neutron Physics, Budapest, 8.-10.10.1986

Matz, W.
The magnetic form factor of Iron in amorphous $Fe_{75}B_{25}$
ZfK-584 (1986) 66

Matz, W., E.A. Goremychkin, I. Natkaniec, D. Stachel, W. Götz
Strukturuntersuchungen an Metaphosphatgläsern (in russisch)
Arbeitsberatung "Untersuchung kondensierter Medien am Reaktor IBR-2", Dubna, 16.-18.9.1986

Matz, W., E.A. Goremychkin, I. Natkaniec, A. Wedel, D. Stachel, W. Götz
Neutron Scattering Studies of Metamorphic Glasses
3. Int. Otto-Schott-Kolloquium, Jena, 7.-11.7.1986

Mädler, P., L. Münchow, A. Pfitzner
Fluctuation induced randomization in one-body dynamics
Int. School-Seminar on Heavy Ion Physics, Dubna, 23.-30.9.1986 (Poster)

Mende, G., C. Bauer, R. Grötzschel, C. Heiser, A. Hofmann, J. Finster, W. Rudolph
Untersuchungen zum Mechanismus der anodischen Si-Oxidschichtbildung
Tagungsbericht 17. Arbeitstagung "Physik der Halbleiteroberfläche", Binz, 7.-12.4.1986, S. 169

Mende, G., J. Wende
Breakdower field strengths of anodically and thermally growes metal/oxide/semiconductor structures on polycrystalline silicon
Thus Solid Films 142 (1986) 21

Miehe, U., F. Häußler, F. Eichhorn
Neutronenkleinwinkelstreuung an Zementstein
11. Zentrale Studentenkonferenz Physik, TU Dresden, 25.-26.2.1986

Mösner, J., K. Möller, W. Pilz, G. Schmidt, T. Stiehler
A measurement of the total cross section of the capture reaction $^{2}H(n,t)\gamma$ at E_n = 25 MeV
Few Body Systems 1 (1986) 93

Mücklich, A.
Probleme der neutronographischen Texturanalyse von geologischen Proben
Vortrags- und Exkursionstagung "Gefüge im Kristallin", Mulda, 12.-14.11.1986

Mücklich, A., P. Klimanek
Texturänderungen bei der plastischen Verformung grobzweiphasiger metallischer Werkstoffe
V. Konf. "Metallkundliche Probleme der Werkstoffentwicklung" - Festigkeit und Plastizität - Freiberg, 3.-5.9.1986

Müller, H.-J.
Zustandsdichteberechnung gebundener Exzitonen in III-V-Mischkristallen
Wiss. Zeitschrift der Humboldt-Universität zu Berlin, Math.-Nat. R 35 (1986) 2

Münchow, L., R. Reif
Recent development of the nuclear many body theory
Leipzig: Teubner-Verlag 1985, Vol. I

Naumann, B., L. Naumann, W. Neubert et al.
Die Umladereaktion p(^{3}He,t) bei Impulsen von 4.4 - 18.3 GeV/c mit Produktion von Δ-Isobaren
Dubna Preprint P1-86-435

Neubert, W., H.W. Barz, H. Schulz et al.
Mass yield distributions for 1 GeV proton-induced reactions on Ni and Ag
Phys. Lett. B174 (1986) 18

Neumann, H., W. Hoyer, W. Matz, M. Wobst
Neutron Scattering Investigations on Molten Eutectic Ag-Ge Alloys
Phys. Status Solidi A92, K19 (1985)

Ortlepp, H.-G., R. Kotte, F. Stary
Low Mass Fragments from ^{252}Cf Spontaneous Fission
Proc. 15th Int. Symp. on Nuclear Physics - Nuclear Fission, Gaußig, 11.-15.11.1985; ZfK-592 (1986) 35

Petukow, V., I.B. Khaibullin, M.M. Zaripow, R. Grötzschel, M. Voelskow, R. Klabes
Investigation of Silicides obtained by Fe^{+} implantation into silicon
Phys. Status Solidi A96 (1986) 463

Pfitzner, A.
Consistent treatment of one-body dynamics and collective fluctuations
ZfK-596 (1986)

Posselt, M.
A short overview on Monte Carlo simulations of ion beam penetration into amorphous solids
Phys. Status Solidi A94 (1986) 337

Posselt, M.
Effect of subcascades on energy-loss and damage profiles
Phys. Status Solidi A94 (1986) 403

Posselt, M., J.P. Biersack
Influence of recoil transport on energy-loss and damage profiles
Nucl. Instrum. Methods B15 (1986) 20

Posselt, M., G. Diener, M. Seidel
Ideal magnetization in sintered iron materials
Phys. Status Solidi B136 (1986) 123

Prokert, F., S.V. Misjul
Anticrossing of Dispersion Branches and Exchange of Eigenvectors in the Elpasolite Type Crystal $Cs_2NaBiCl_6$
Proc. of the 2nd Int. Conf. "Phonon 85", World Scientific Publishing Comp., Singapore 1985, p. 305

Rauschenbach, B.
Formation of copper/gold solid solutions by ion beam mixing
Appl. Phys. A40 (1986) 47

Rauschenbach, B.
Synthesis of borides, carbides and nitrides in metal surfaces by high-dose ion implantation
J. Less-Common Metals 117 (1986) 115

Rauschenbach, B.
Ion beam mixing effects in Cu/Au multilayered films
Phys. Status Solidi A94 (1986) 409

Rauschenbach, B.
Formation of compounds by high-flux nitrogen ion implantation in titanium
J. Mater. Sci. 21 (1986) 395

Rauschenbach, B.
Temperature influence during high-fluence nitrogen ion implantation into iron
Nucl. Instrum. Methods B15 (1986) 756

Rauschenbach, B., C. Blochwitz
Electron microscopical investigations of ion-implanted and fatigued nickel
Phys. Status Solidi A94 (1986) 827

Rauschenbach, B., V. Heera
Formation of borides and nitrides by ion implantation in iron
J. Less-Common Metals 117 /1986) 323

Rauschenbach, B., K. Hohmuth
Synthesis of compounds by high-fluence nitrogen ion implantation in Titanium
Phys. Status Solidi A94 (1986) 833

Rauschenbach, B., K. Hohmuth, E. Richter, R. Grötzschel
Ion beam mixing of copper-gold multilayers
Nucl. Instrum. Methods B15 (1986) 692

Reichel, P., W. Matz, W. Boedess
A microprocessor controlled Mößbauer spectrometer
ZfK-584 (1986) 89

Reinhardt, H.
QCD condensates and effective quark lagrangians
NBI-HE-86-11

Reinhardt, H., B.V. Dang
Dynamical bag constant and surface tension of baryon droplets at finite temperature and density
Phys. Lett. B173 (1986) 473

Reinhardt, H., D. Ebert
Extended Skyrmion model from quark flavour dynamics
Phys. Lett. B173 (1986) 459

Reinhardt, H., D. Ebert
Extended Skyrmion model from quark flavour dynamics
Contr. to the Int. Nucl. Phys. Conf., Harrogate, U.K., 25.-30.8.1986

Reinhardt, P.G., H. Reinhardt, K. Goeke
Dissipative adiabatic mean-field theory for large amplitude collective motion
Ann. Phys. 166 (1986) 257

Reuther, H.
Conversion electron Mössbauer spectroscopy of nitrogen and phosphorus implanted iron
Phys. Status Solidi A93 (1986) 201

Rotter, I.
Spectroscopic investigation of isolated and overlapping resonance states
Atomic and Heavy Ion Reactions, Vol. II, ed. by G. Semenescu et al. (1986) p. 659

Rotter, I.
Symmetry violation caused by the boundary conditions for finite nuclei
Ann. Phys. (Leipzig) 43 (1986) 514

Rotter, I.
Many-body effects in nuclei
Czech. J. Phys. B36 (1986) 979

Rotter, I.
Self-organization in nuclei
J. Phys. G 12 (1986) 1407

Rotter, I.
Cooperative effects in nuclei and self-organization,Brasov
Int. Summer-School on Physics, Romania, 1.-13.9.1986

Rotter, I.
On charge symmetry breaking and three-body forces
Int. Conference on Atomic Physics and Few Body Systems (Few Body XI), Contributions ed. by T. Sasakawa et al., Tokyo, Sendai, August 1986, p. 376

Rotter, I.
Symmetry violation and interplay between giant resonances and background in finite nuclei
Int. Symposium on Weak and Electromagnetic Interactions in Nuclei, Heidelberg, 1.-5.7.1986. Abstracts ed. by Klapdor and Metzinger, p. 263

Rotter, I.
Symmetry violation in an open quantum mechanical system
Int. Nucl. Physics Conference, Harrogate U.K., 25.-30.8.1986, Proceedings Vol. I, p. 423

Rotter, I.
Selforganisation in nuclear systems
Int. Nucl. Physics Conference, Harrogate U.K., 25.-30.8.1986, Proceedings Vol. I, p. 31

Rotter, I.
Unified description of nuclear structure and nuclear reaction aspects
Int. Nucl. Physics Conference, Harrogate U.K., 25.-30.8.1986, Proceedings Vol. I., p. 193

Röpke, G., D. Blaschke, H. Schulz
Quark substructuce contribution to the effective mass of the nucleon
Phys. Lett. B174 (1986) 5

Rudolph, W., C. Bauer, K. Brankoff, D. Grambole, R. Grötzschel, C. Heiser, F. Herrmann
Plastic foils as primary hydrogen standards for nuclear reaction analysis
Nucl. Instrum. Methods B15 (1986) 508

Rudolph, W., K. Hennig, S. Niese
Nukleare Analytik an metallischen Werkstoffen
Elektrie 40 (1986) 451

Schilling, K.D., P. Gippner, W. Seidel, F. Stary, E. Will, K. Heidel, S.M. Lukyanov, Yu.E. Penionzhkevich, V.S. Salamatin, H. Sodan, G.G. Chubarian
The Dubna double-arm time-of-flight spectrometer for heavy-ion reaction products
ZfK-586 (1986)

Schmidt, U., F. Eichhorn
Bestimmung optimaler Anlaßbedingungen für technische Aluminiumlegierungen durch Kombination von Lichtmikroskopie und Neutronenkleinwinkelstreuung (in russisch)
6th Metallographic Symposium, Strbske Pleso, April 1986

Schulz, H., G. Röpke, K.K. Gudima, V.D. Toneev
Effective radii of light composites produced in relativistic heavy ion collisions
Phys. Rev. C33 (1986) 1095

Schwarzenberg, F., W.D. Fromm
SIF-1000-Anschluß für Digitalkassettenlaufwerke
Radio Fernsehen Elektron. 35 (1986) 4, S. 256 ff

Semmes, P.B., G.A. Leander, D. Lewellen, F. Dönau
Exchange effects in the interacting boson-fermion model
Phys. Rev. C33 (1986) 1476

Sieber, N., H. Oertel, M. Voelskow
Elektrische Eigenschaften von MOS-Strukturen, hergestellt in rekristallisiertem Silicium
Physik der Halbleiteroberfläche 17 (1986) 101

Skorupa, W., U. Kreißig, H. Oertel, H. Bartsch
Properties of Epitaxial Silicon Layers on Buried Silicon Nitride Produced by Ion Implantation
Vacuum 36 (1986) 933

Skorupa, W., H. Oertel, H. Bartsch
On the Mechanism of Carrier Lifetime Increase in Ion Beam Synthesized SOI Structures
Electron. Lett. 22 (1986) 1062

Stary, F.
Synthese von Transuranelementen
Urania 62 (1986) 4, S. 64

Stiehler, T., J. Mösner, G. Schmidt, K. Möller, W. Neubert, W. Pilz, B. Kühn, J. Hutsch
The total n-p Capture Cross Section measured at E_n = 25 MeV
Ann. Phys. (Leipzig) 43 (1986) 602

Tillack, B., P. Möck, R. Banisch, R. Reinboth, H.H. Richter, M. Voelskow, J. Matthäi, E. Wieser
Thick Monocrystalline Silicon on Oxidized Silicon Wafers Produced by a Zone Melting Process Using a Scanning Halogen Lamp
Phys. Status Solidi A94 (1986) 871

Will, E., H. Sodan, S.M. Lukjanov, V.I. Nosokin, Ju.E. Penionzhkevich, V.S. Salamatin, G.G. Chubarian, P. Gippner, W. Seidel, F. Stary, K.D. Schilling
Zweiarm-Flugzeitspektrometer der Anlage DEMAS (in russisch)
JINR 13-85-754 (1985)

Wünsch, R., L. Majling, J. Zöfka
Continuum shell-model description of baryon decays of light hypernuclei
Proc. Int. Symposium on Mesons and LIght Nuclei, Bechyne, June 1985, ed. by R. Mach, E. Truhlik and J. Zöfka; Czech. Journ. Phys. B36 (1986) 441

Wünsch, R., L. Majling, J. Zöfka
Continuum shell-model description of baryon decays of ^{14}N
Proc. Int. Symposium on Hypernuclear and Kaon Physics, Brookhaven, September 1985, ed. by R.E. Chrien; Nucl. Phys. A450 (1986) 329c

DIPLOMARBEITEN

Scholz, U.
Neutronographische Untersuchungen zur Texturentwicklung beim Kaliberwalzen von Kfz-Metallen
BA Freiberg, März 1986

Weidner, D.
Untersuchung von Aluminium-Gußlegierungen mittels Neutronenkleinwinkelstreuung am Doppelkristalldiffraktometer
Pädagogische Hochschule "N.K. Krupskaja", Halle, Juni 1986

Lopez, R.C.
Beiträge zum Aufbau eines Standardfunktions-Programmsystems unter Berücksichtigung sämtlicher Kristallklassen für die quantitative Texturanalyse
TU Dresden, Juni 1986

Mademann, D.
Untersuchung von ortsauflösenden Halbleiterdetektoren aus der DDR-Produktion hinsichtlich ihrer Eignung zum Nachweis von Röntgenstrahlung
TU Dresden, 3.7.1986

Dumschat, Chr.
Präparierung und analytische Testung von nitrat- und calciumselektiven Feldeffekttransistoren
Technische Hochschule für Chemie, Merseburg, Juni 1986

PROMOTIONEN A (Dr. rer. nat.)

Döring, J.
Einfluß von Quasiteilchen-Anregungen auf die kollektiven Eigenschaften von Atomkernen im Massengebiet um A=80
AdW der DDR, 9.5.1986

Bischoff, L.
Optimierung der Materialparameter von hochohmigem neutronendotiertem Silicium und dessen Einsatz für Zähldetektoren
ZfK Rossendorf, 24.10.1986

PROMOTIONEN B (Dr. sc. nat.)

Kämpfer, B.
Phänomenologie von Phasenübergängen in Kernmaterie
TU Dresden, 9.10.1986

Klabes, R.
Nichtkonventionelle Kurzzeit-Temperverfahren zur Modifizierung der strukturellen und elektrischen Eigenschaften von Silicium
AdW der DDR, 5.12.1986

VORTRÄGE

Andrä, G., H.-D. Geiler, E. Glaser, G. Götz, M. Wagner, K.-H. Heinig
Explosive crystallization of ion-implanted silicon layers
Int. Conference IBMM 86, Catania, 9.-13.6.1986

Andrä, G., E. Glaser, M. Wagner, H.-D. Geiler, G. Götz, H. Bartsch, K.-H. Heinig, K. Hennig
Explosive crystallization in amorphous silicon layers
E-MRS Conference 1986 Meeting, Strassbourg, 17.-20.6.1986

Armigliato, A., S. Guimaraes, S. Solmi, R. Kögler, E. Wieser
Comparison of Boron Diffusivity During Rapid Thermal Annealing in Predamaged, Preamorphized and Crystalline Silicon
Int. Conference "Ion Beam Modification of Materials", Catania, 9.-13.6.1986

Bankwitz, P., H. Kämpf, M. Betzl, C. Legler
Zur Textur von Magnetiten und Granaten a)

Barz, H.W.
One and two fluid hydrodynamics applied to quark-gluon-plasma formation in heavy ion collision
Workshop on Gross Properties of Nuclei and Nuclear Excitations, Hirschegg, Januar 1986

Barz, H.W.
Multifragmentation b)

Barz, H.W.
Energy spectra of fragments calculated within the statistical multifragmentation model d)

Bauer, C., W. Rudolph, C. Heiser, D. Grambole, F. Herrmann
Low-Z element analysis by nuclear reactions
XXI. Winter School on Physics, Zakopane,

Betzl, M., K. Feldmann, W. Voitus, K. Walther
Texture Investigations by Neutron Diffraction - Progress in Neutron Time-of-flight Texture Studies at Pulsed Reactors
Workshop on Neutron Physics, Budapest, 8.-10.10.1986

Bischoff, L.
Application of NTD-Si Detectors in Research and Industry
Konf. Naukowa i Spotkanie Przyjazni zwiazkow mlodzierzy z panstw RWPG, Swierk, 4.-7.11.1986

Bischoff, L., J. von Borany, M. Deutscher, U. Lorenz, G. Mende, H. Oertel, B. Schmidt, H. Schott
SiO_2-passivierte Strahlungssensoren k)

Borany, J. von, M. Deutscher, U. Lorenz, B. Schmidt, H. Schott
Großflächige ionenimplantierte Strahlungsdetektoren
19. Fachkolloquium Informationstechnik, TU Dresden, Januar 1986

Dönau, F.
Mean field theory of nuclear spin
Institutsseminar, Niels-Bohr-Institut, Februar 1986

Dönau, F.
Mean field theory of nuclear spin
Institutsseminar, Lund University, März 1986

Dönau, F.
Mean Field theory of Nuclear spin
Int. Winter School of Nuclear Physics, Zakopane, April 1986

Dönau, F.
Coupling of single particle and collective degrees of freedom in the light of the equation of motion method
Int. Seminar on Nucl. Physics, Sorrento, Mai 1986

Dönau, F.
Mean Field Theory of Nuclear spin
Int. Conference "Nuclear Structure, Reactions and Symmetries", Dubrovnik, Juni 1986

Dönau, F.
Spin orientation in deformed nuclei
Seminarvortrag, UT Knoxville, September 1986

Dönau, F.
Cranking about non-symmetry axes
Workshop on Nuclear Theory, Oak Ridge, Oktober 1986

Dönau, F.
Cranking about non-symmetry axes
Institutsseminar, Vanderbuilt University, Nashville, Oktober 1986

Döring, J.
Neuere Methoden der γ-Meßtechnik
Methodisches Seminar des ZfK, Rossendorf, 22.5.1986

Dubiel, M., U. Bärenwald, W. Matz
Computermodell zur Glasstruktur von $Ba(PO_2)_2$ zur Interpretation von Neutronenstreuexperimenten [a)]

Ebert, D., H. Reinhardt
Effective chiral lagrangian and Skyrme quark flavour dynamics
High Energy Physics Seminar, Dubna, June 1986

Eichhorn, F.
Neutronenkleinwinkelstreuung am Beton [a)]

Ertel, A., H. Kämpf, M. Betzl
Texturuntersuchungen an Salinargesteinen mittels Neutronendiffraktion [a)]

Feldmann, K.
Texturuntersuchungen an sächsischen Granuliten [a)]

Fromm, W.D.
Das elektronische Projekt für die Anlage PHOBOS (in russisch)

Fromm, W.D.
Datensammel- und Speichersysteme in Vieldetektor-Experimenten (in russisch)
Arbeitsberatung zur Anlage PHOBOS, Dubna, 22.1.1986

Fromm, W.D.
Das modulare System MMS-16 und der Arbeitsplatzcomputer AC 7100 [b)]

Fromm, W.D.
A nuclear micro-beam probe for the investigation of surface [f)]

Fromm, W.D.
Überblick über die Arbeiten zur Automatisierung kernphysikalischer Experimente am ZfK (in russisch) [e)]

Funke, L.
Nuclear shape transitions in the Kr isotopes
24. Int. Winter Meeting on Nuclear Physics, Bormio, 20.-25.1.1986

Funke, L.
Shell effects observed in nuclei of the mass 80 region
Institutsseminar, Gustaf-Werners-Institut, Uppsala, 13.11.1986

Funke, L.
Shell effects observed in nuclei of the mass 80 region
Experimental group meeting im NBI, Kopenhagen, 24.11.1986

Gersch, H.U.
Coulomb final-state interaction in identical boson interferometry
Arbeitstagung GIBS, VIK Dubna, April 1986
Int. Summer School on Nuclear Dynamics, Poiana Brasov, September 1986

Gippner, P.
Shell effects in the evolution of the mass asymmetry in HIC [d)]

Gippner, P., K.D. Schilling, W. Seidel, F. Stary, E. Will, H. Sodan, S.M. Lukyanov, V.S. Salamatin, Yu.E. Penionzhkevich, G.G. Chubarian, R. Schmidt
Shell effects in the evolution of the mass asymmetry in heavy-ion collisions leading to composite systems with Z=108
18th Masurian Summer School on Nuclear Physics, Mikolajki, 1.-13.9.1986

Grambole, D., F. Herrmann, W.D. Fromm, F. Schwarzenberg
A nuclear micro-beam probe for the investigation of surfaces [f)]

Grambole, D., F. Herrmann
Mikrosonde am Tandem-Beschleuniger [c)]

Grötzschel, R., K. Brankoff, W.D. Fromm
Computerized experimental facilities for ion beam analysis at the Rossendorf accelerators [f)]

Häßner, A., R. Portius, E. Wieser
Silicierung mit Lichtofen
IV. Symposium Physikalische Grundlagen zu Beauelementetechnologien der Mikroelektronik, Frankfurt/O., 10.-12.9.1986

Heera, V.
Amorphisierung durch Ionenimplantation - Modellvorstellungen [c)]

Heera, V., B. Rauschenberg
Quasikristalline Strukturen
Seminar, ZfW Dresden, 9.9.1986

Heera, V., B. Rauschenbach
Quasikristalle
Seminar des WB Theoretische Physik der TU Dresden, 7.5.1986
Institutskolloquium, ZfW Dresden, 9.9.1986

Heider, M., H. Schott, M. Stäck, B. Schmidt
Möglichkeiten der Nutzung der Optoelektronik für die Bestimmung geometrischer Parameter von Bauteilen großer Abmessungen
Int. Tagung INFERT '86, Dresden, September 1986

Heinig, K.-H.
Optimierung des Kleinwinkelkongrenzenfangs bei lateralem Zonenschmelzen durch Computersimulation [c)]

Heinig, K.-H.
Ionenstrahlgestützte Umordnungsprozesse in Halbleitern [c)]

Heinig, K.-H., H.-J. Müller
Ionenbeschleunigte Festphasenepitaxie - Literaturübersicht [c)]

Heinig, K.-H., H.-J. Müller
Computersimulation zum Korngrenzenfangen beim lateralen Zonenschmelzen von Siliciumschichten [c)]

Heinig, K.-H., H.-J. Müller
Computersimulation von Korngrenzenevolution und Korngrenzenfang beim lateralen Zonenschmelzen
Seminar KÜL 4, Rossendorf, 13.12.1985

Heinig, K.-H., H.-J. Müller
Zelluläre Automaten, Selbstorganisation und Schmelzinstabilität bei Lichtheizung
Seminar an der Sektion Physik der Friedrich-Schiller-Universität, Jena, 18.12.1986

Heinig, K.-H., H.-J. Müller, G. Otto, K. Hennig
Conditions of grain boundary confinement during lateral zone-melting studied by computer simulation
E-MRS Conference 1986 Meeting, Strassbourg, 17.-20.6.1986

Helming, K.
Unvollständige Polfiguren und erweitertes MPDS-Konzept [a)]

Hensel, E.
Möglichkeiten der Nutzung des Ion Beam Mixing zur Veränderung der Eigenschaften von Metalloberflächen [c)]

Herberg, H., H. Schott, Ch. Hesse, B. Schmidt
Mikrorechnergesteuertes Positioniersystem
Int. Tagung INFERT '86, Dresden, September 1986

Hermann, H., W. Matz, N. Mattern
Partielle Strukturfaktoren für amorphes $Fe_{75}B_{25}$ und Beschreibung der Struktur mit einem mikroheterogenen Modell
Workshop AdW-Zusammenarbeit zum Thema 1.10.3.3., Tiblissi, 12.-14.5.1986

Hoffmann, W., J. Hüller, M.T. PHam, G. Lauschke, R. Schuster, H.J. Köhler, M. Thümmler
Continuous measurement of pH and alkali ion activity in biomedical experiments
Bioelectroanalytical Symposium 1986, Mátrafüred, Oktober 1986

Hoffmann, W., J. Hüller, M.T. Pham
Chemisch sensitive Feldeffekttransistoren, Eigenschaften und Anwendung
Kolloquium "Elektrochemische Methoden in der Labordiagnostik", Greifswald, 6.-8.5.1986

Hoffmann, W., J. Hüller, M.T. Pham
Integration - Lösungsweg für ionenselektive Sensoren
Institutsseminar, TU Karl-Marx-Stadt, Mai 1986

Hoffmann, W., J. Hüller, M.T. Pham
pH-sensitive Feldeffekttransistoren für Biosensoren
Institutsseminar, Zentralinstitut für Molekularbiologie, Berlin-Buch, Mai 1986

Hoffmann, W., J. Hüller, M.T. Pham
Technologie und Applikation von chemisch sensitiven Feldeffekttransistoren
Institutsseminar, TH Leuna-Merseburg, Juni 1986

Iwe, H.
Kernphysikalische Forschungstechnologie der Zukunft [g)]

Iwe, H.
Teilchenerzeugung in relativistischen Kern-Kern-Stößen
Institutsseminar, KMU Leipzig, Sektion Physik, Juni 1986

Iwe, H.
Strangeness production in the cascade model
High Energy Physics Seminar, Dubna, June 1986

Iwe, H.
A production in head-on collisions of CüC
Workshop, Budapest, July 1986

Iwe, H.
Strangeness production in relativistic heavy-ion reactions
Institutsseminar, LTF Dubna, Sektor Lukyanov, July 1986

Jäger, H.-U.
Traceruntersuchungen zur SOI-Herstellung durch Sauerstoff-Hochdosisimplantation [c)]

Kahn, A.
Flüssigmetallionenquellen für Mikrostrahlanlagen: Messung von Eigenschaften [c)]

Kaun, K.H., L. Funke
Nuclear physics and applications in Rossendorf and the accelerator problem
Vortrag und Diskussionsrunde im AFI, Stockholm, 18.11.1986

Kämpfer, B.
Relativistische Schwerionenstöße [g)]

Kämpfer, B.
Two-fluid model applied to relativistic heavy-ion collisions
Workshop, Budapest, Mai 1986

Kämpfer, B.
Deconfinement transitions in relativistic heavy ion collisions
Institutsseminar, LTF Dubna, Sektor Lukyanov, Mai 1986

Kämpfer, B.
Urformen der Materie: Kernmaterie - Quarkmaterie - Inomaterie
ZfK-Institutskolloquium, Rossendorf, September 1986

Käubler, L.
Yrast spectroscopy in ^{138}Ba and ^{140}Ce; g-factor for a 10^+ isomer in ^{140}Ce
36. Allunionskonferenz über Kernphysik, Charkow, 15.-18.4.1986

Käubler, L.
Hyperfeinwechselwirkung
Methodisches Seminar des ZfK, Rossendorf, 22.5.1986

Käubler, L.
In-beam investigations and structure studies of the N=82 nuclei ^{138}Ba and ^{140}Ce; the magnetic moment of the 10^+ isomer in ^{140}Ce
18. Sommerschule über Kernphysik, Mikolajki, 1.-13.9.1986

Kirschbaum, D.
On a possible supersymmetric structure in non-Hamiltonian mechanics
Institutsseminar, LTF Dubna, Sektor 6, Juli 1986

Kirschbaum, D.
On the structure of the canonical transformation group
Herbstmeeting zu Problemen der mathematischen Physik, Wroclaw, 12.12.1985

Klimanek, P., K.-E. Hensger, A. Mücklich
Umwandlungstexturen in metallischen Werkstoffen [a)]

Kotte, R., W. Seidel, H.J. Keller, H.-G. Ortlepp, F. Stary
Detector module for the 4 -spectrometer PHOBOS
Int. School-Seminar on Heavy Ion Physics, Dubna, 23.-30.9.1986 (Poster)

Kögler, R., R. Grötzschel, G. Otto, E. Wieser
Anormal erhöhte Diffusion an Arsen in Silicium bei Kurzzeittemperung c)

Kögler, R., E. Wieser, G. Otto
Diffusionsbeschleunigung und elektrische Aktivierung von As in Si bei Kurzzeittemperung (RTA) h)

Kögler, R., E. Wieser, M. Voelskow, G. Otto
Transient Enhanced Diffusion and Electrical Activation of As in Si During Rapid Thermal Annealing i)

Lehmann, D., C. Ascheron, C. Bauer
Nondestructive determination of the hydrogen depth distribution in semiconductor material using ion beam methods
IX. CANAS, Neubrandenburg, 15.-19.9.1986

Lück, H.B.
Kernspurmikrofilter-Eigenschaften und Einsatzmöglichkeiten
Informationstagung der KdT "Aufarbeitung in der Biotechnologie", Leipzig, 4.12.1986

Manfraß, P.
Das Rossendorfer PET-Projekt
Nuklearmedizinisches Kolloquium der MAD/ZfK, Medizinische Akademie Dresden, 4.12.1986

Matthäi, J.
Methoden zur Herstellung korngrenzenfreier SOI-Schichtbereiche beim lateralen Zonenschmelzen
Fachtagung mit internationaler Beteiligung: "Schichtsysteme für zukünftige Bauelemente der Mikro-, Opto- und Molekularelektronik", Karl-Marx-Stadt (TH), 11.-13.11.1986

Matthäi, J., M. Voelskow, H.H. Stegemann
Elektrische Aktivierung und Dotantenumverteilung in SOI-Schichten beim lateralen Zonenschmelzen c)

Matthies, S.
Zur Struktur der universellen Standardprogramme PSGL 33 und FFSGL 33
Seminarvortrag, Universität Metz, 15.6. - 19.7.1986

Matthies, S.
Eine einheitliche Konzeption zur Wahl der Kristallkoordinatensysteme und Grundbereiche im G-Raum für alle existierenden Kristallsymmetrien
Seminarvortrag, Universität Metz, 15.6.-19.7.1986

Matthies, S.
Kriterien und numerische Beispiele für Vergleiche verschiedener Reproduktionsmethoden
Seminarvortrag, Universität Metz, 15.6.-19.7.1986

Matthies, S.
Methodische Weiterentwicklungen bezüglich der zentralen Aufgabe der quantitativen Texturanalyse a)

Matz, W.
Strukturuntersuchungen an Gläsern mit Neutronendiffraktion a)

Matz, W.
Untersuchung der Genauigkeit des neuen Mößbauerspektrometers auf Mikroprozessorbasis
Mößbauerkolloquium, Freiberg, 18.-19.3.1986

Matz, W.
Einsatz der Neutronenflugzeitdiffraktionsmethode zur Strukturanalyse nichtkristalliner Systeme i)

Matz, W.
Flugzeitneutronendiffraktion zur Untersuchung der Struktur amorpher Stoffe a)

Matz, W., H. Hermann
Mössbauer Studies of the Average Magnetic Moment's Dependence on Boron Concentration in Amorphous Fe-B Alloys j)

Matz, W., A. Wedel
Neutronendiffraktionsuntersuchungen an Metaphosphatgläsern i)

Märten, H., W. Neubert, D. Richter, D. Seeliger
Energy and angular distribution of ^{252}Cf(s.f.) neutrons
Int. Conference on Nuclear Physics, Harrogate, 24.-30.8.1986
IAEA Nuclear Data Meeting, Leningrad, Juni 1986

Melzer, U., M. Lukasiak, J. Suwalski, W. Matz
^{119}Sn Hyperfine Field Distributions in Tin-containing Ferrites [j)]

Mende, G., C. Bauer, R. Grötzschel, C. Heiser, A. Hofmann, J. Finster, W. Rudolph
Investigations on the mechanism of the anodic oxidation of Si
37. Tagung der Int. Society of Electrochemistry, Vilnius, 24.-31.8.1986

Mende, G., C. Bauer, J. Finster, R. Grötzschel, C. Heiser, A. Hofmann, W. Rudolph
Untersuchungen zum Mechanismus der anodischen Si-Oxidschichtbildung
11. Arbeitstagung der AG Elektrochemie der Chemischen Gesellschaft der DDR, Garzau, 14.-16.1.1986 und [k)]

Mende, G., C. Bauer, C. Heiser, A. Hofmann, J. Finster, R. Grötzschel, W. Rudolph
Untersuchungen zum Mechanismus der anodischen Oxydation von Silicium [k)]

Mende, G., C. Bauer, C. Heiser, A. Hofmann, J. Finster, R. Grötzschel, W. Rudolph
Investigations on the mechanism of the anodic oxidation of silicon
37. Tagung der Int. Society of Electrochemistry, Vilnius, 24.-31.8.1986

Mende, G., M. Deutscher, H. Flietner, B. Schmidt
Die anodische Si-Oxydation als Methode zur Herstellung von MOS-Strukturen und Detektoren für ionisierende Strahlung
Institutsseminar, Institut für Physik der lettischen AdW, Riga, 22.8.1986

Michel, P.
Eine Meßanordnung zur Bestimmung des differentiellen n-p-Einfang-Querschnitts (in russisch)[e)]

Morgenstern, H.
DLTS-Untersuchungen an Mo-Schottky-Barrieren [c)]

Morgenstern, H.
Bildung von Schottky-Barrieren und tiefen Störstellen
19. Fachkolloquium Informationstechnik und 1. Tagung Schaltkreisentwurf, TU Dresden, 21.-23.1.1986

Möller, K.
Offshell information on the singlett neutron-proton interaction from the capture reaction $n + p = d + \gamma$
XI. Int. IUPAP Conf. on Few Body Systems ..., Tokio/Sendai, 24.-30.8.86 (Contributions p. 314)

Mösner, J.
Experimental Investigation on Few-Nucleon Systems at the Rossendorf Tandem Accelerator
Seminarvortrag, Institut für Kernphysik, Novosibirsk, 27.11.1986

Mösner, J., K. Möller, W. Pilz, G. Schmidt, T. Stiehler
A measurement of the total cross section of the caoture reaction $^2H(n,t)\gamma$ at E_n = 25 MeV
XI. Int. IUPAP Conf. on Few Body Systems ..., Tokio/Sendai, 24.-30.8.86 (Contributions p. 410)

Müller, H., H.W. Barz
A phase space model for the description of hadron-hadron interactions
VIII. Int. Symposium über Probleme der Hochenergiephysik, Dubna, 19.-24.6.1986

Müller, H.-J.
Computersimulation der Bildung von kristallinen Siliciumschichten [c)]

Müller, H.-J., K.-H. Heinig
Theoretische Beschreibung der Phasentransformation in Si
Seminar, Zentralinstitut für Werkstofforschung der AdW der DDR, Dresden, 15.1.1986

Müller, H.-J., K.-H. Heinig
The theoretical description of the solid-phase transformation a-Si into poly-Si
Seminar, Phys.-Techn. Institut der AdW der UdSSR, Kazan, 27.2.1986

Müller, H.-J., K.-H. Heinig
Computersimulation contra analytische Transformationsformeln der primären Kristallisation [c)]

Müller, H.-J., K.-H. Heinig
Computersimulation der Festphasentransformation a-Si zu poly-Si
Sektionskolloquium Physik, Friedrich-Schiller-Universtität, Jena, 20.3.1986

Müller, H.-J., K.-H. Heinig
Amorphous-to-polycrystalline transformation of Si at rapid thermal annealing studied by computer simulation [1)]

Müller, H.-J., K.-H. Heinig
Computer experiments on macroscopic phenomena of structural phase transformations
Institutsseminar, LTF Dubna, 24.6.1986

Müller, H.-J., K.-H. Heinig, K. Hennig
Computer simulation of primary crystallisation
E-MRS Conference 1986 Meeting, Strassbourg, 17.-20.6.1986

Müller, H.-J., K.-H. Heinig, M. Voelskow, J. Matthäi
SOI-Schichten durch sekundäre Rekristallisation - Stand der theoretischen und experimentellen Untersuchungen
Seminar KÜL 4, Rossendorf, 13.12.1985

Naehring, F., A. Hofmann
Ionenmikrostrahlanlage: Eigenschaften, erste Ergebnisse und Weiterentwicklung [c]

Neuber, W.
Mass loss and linear momentum transfer in 1 GeV proton-induced reactions on U, Bi, Sm [d]

Neubert, W.
Entwicklung von ortsauflösenden Teilchendetektoren in Rossendorf (in russisch)
Institutsseminar, Institut für Kernphysik, Novosibirsk, 27.11.1986

Neumann, H., W. Hoyer, W. Matz
Nahordnung in geschmolzenen Ge-Eutektika [a]

Neumann, H., W. Hoyer, W. Matz, M. Wobst
Strukturuntersuchungen an geschmolzenen und amorphen Germaniumlegierungen [i]

Ortlepp, H.-G.
Detektor-Elektronik (in russisch) [n]

Ortlepp, H.-G.
Neuentwicklungen bei Teilchendetektoren
Methodisches Seminar der HFR 2.12 zur Entwicklung der experimentellen Kernphysik - Anwendung moderner kernphysikalischer Meßmethoden, ZfK Rossendorf, 22.5.1986

Ortlepp, H.-G., K. Heidel, E. Will
Untersuchung der Zeitnahme an sehr kurzen Detektorstromsignalen (in russisch)
Seminar der Abteilung für Elektronikentwicklung des LJaR, VIK Dubna, 10.12.1986

Panknin, D., E. Wieser, R. Grötzschel, C.-E. Richter, M. Gericke, Ya.V. Fattachov, I.B. Khaibullin
Elektrische Aktivierung und Dotandenverteilung von Si-implantiertem GaAs nach Kurzzeitausheilung im Festphasenregime [h]

Panknin, D., E. Wieser, R. Grötzschel, C.-E. Richter, M. Gericke, Ya.V. Fattachov, I.B. Khaibullin
Dopant Distribution and Electrical Activation of Silicon Implanted GaAs by Short Time Annealing
II. Conference on Physics and Technology of GaAs and other III-V Semiconductors, Budapest, 8.-11.9.1986

Panknin, D., E. Wieser, R. Grötzschel, C.-E. Richter, M. Gericke, Ya.V. Fattachov, I.B. Khaibullin
Dopant Distribution and Electrical Activation of Silicon Implanted GaAs by Short Time Annealing [l]

Panknin, D., E. Wieser, C.-E. Richter
Ausheilung und elektrische Aktivierung von implantiertem GaAs durch Kurzzeittemperung im Festphasenregime [c]

Pfitzner, A.
Consistent description of s.p. motion and collective fluctuations [b]

Pfitzner, A.
Randomization of s.p. motion by collective fluctuations [d]

Posselt, M.
Theoretische Beschreibung der Ionenimplantation in Schichtstrukturen [c]

Posselt, M.
Kaskadentheoretische Beschreibung der Ionenimplantation in Schichtstrukturen [c]

Posselt, M., W. Skorupa, A. Beyer, W. Markgraf
The electronic stopping and range profile calculations for high energy implantation of phosphorous into silicon
16. Allunionskonferenz über die Physik der Wechselwirkung geladener Teilchen mit Kristallen, Moskau, 26.-28.5.1986

Prade, H.
Yrast spectroscopy on N=82 and Z=50 nuclei
Europhysicss Study Conference on the Structure of Cold Nuclei, Albena, 14.-18.9.1986

Prade, H., Yrast spectroscopy in semi-magic nuclei with N=82
Seminarvortrag, Gustaf-Werners-Institut, Uppsala, 13.11.1986

Prade, H.
Yrast spectroscopy in semi-magic nuclei with N=82
Experimental group meeting im NBI, Kopenhagen, 24.11.1986

Prokert, F.
Untersuchungen von Phasenübergängen an Perovskiten und verwandten Strukturen mittels Neutronenstreuung a)

Prokert, F.
The TOF diffractometer DN-2 at the pulsed reactor IBR-2 of JINR Dubna
14. Frühjahrsschule Ferroelektrizität '86, Fincken, 7.-11.4.1986

Rauschenbach, B.
Hochdosis-Ionenimplantation und Ionenstrahl-induzierte Mischung von Metallen
Seminar, ZfW Dresden, Mai 1986

Rauschenbach, B., K. Helming
Determination of implantation -induced textures by electron diffraction
10. European Crystallographic Meeting, Wroclaw, 5.-9.8.1986

Reinhardt, H.
Extended Skyrmion model from low-energy QCD
Seminarvortrag, Niels-Bohr-Institut, Dezember 1985

Reichel, P.
Aufbau eines mikroprozessorgesteuerten Mößbauerspektrometers im ZfK
Mößbauerkolloquium, Freiberg, 18.-19.3.1986

Reuther, H.
Mößbaueruntersuchungen an implantierten Metallen c)

Reuther, H.
Conversion electron Mößbauer spectroscopic studies of ion implanted iron j)

Richter, E.
Ion implantation into metals
Seminar der Berg- und Hüttenuniversität, Krakow, Mai 1986

Richter, E.
Veränderung von Metalloberflächen durch Ionenimplantation
Seminar des Politechnikum, Lublin, Mai 1986

Richter, E., A. Kolitsch
Veränderung der mechanischen Eigenschaften von Stahl
KdT-Vortrag, Frühjahrsmesse, Leipzig,

Rotter, I.
Selbstorganisation in Kernen
Institut für Hochenergiephysik (Theorieseminar), Zeuthen, 16.1.1986

Rotter, I.
Nicht-selbstadjungierte Hamiltonoperatoren in der Kerntheorie
Seminarvortrag, Institut für Mathematik der AdW, Berlin, 16.4.1986

Rotter, I.
Strukturen in Kernsystemen
Vereinigtes Theorieseminar der Friedrich-Schiller-Universität, Jena, 21.4.1986

Rotter, I.
Selbstorganisation in Kernen
Seminar, Institut für Kernphysik der Lomonossow-Universität, Moskau, 4.6.1986

Rotter, I.
Strukturen in einem offenen Kernsystem
Seminar, Laboratorium für Theoretische Physik des VIK Dubna, 6.6.1986

Rotter, I.
Irreversibilität und Strukturen in Kernsystemen
Seminar, Humboldt-Universität, Sektion Physik, Bereich Statistische Thermodynamik und Theoretische Biophysik, Berlin, 24.6.1986

Rotter, I.
Cooperative effects in nuclei and selforganization
Int. Summer School on Physics, Brasov, 1.-13.9.1986

Rotter, I.
Der Atomkern als offenes quantenmechanisches System
Seminar, Institut für Kernphysik der AdW der UdSSR (Sibirische Abteilung), Novosibirsk, 14.10.1986

Rudolph, W.
Application of nuclear methods for solid state analysis
Seminarvortrag, Institute for Nuclear Chemistry and Technology, Warschau, Februar 1986

Rudolph, W.
Anwendung von Ionenstrahlmethoden für die Festkörperanalyse
Arbeitstagung des KME, Eisleben, März 1986

Rudolph, W.
Nukleare Analysenmethoden für Festkörperuntersuchungen
Seminarvortrag, Bergakademie Freiberg, Sektion Physik, Dezember 1986

Rudolph, W., C. Bauer, K. Brankow, D. Grambole, R. Grötzschel, C. Heiser, F. Herrmann, K. Hennig
H- und O-Ausdiffusion beim Ionenbeschuß von Plastfolien
7. Arbeitstagung "Energiereiche atomare Stöße", Oberstdorf, Januar 1986

Rudolph, W., C. Bauer, C. Döring, D. Grambole, R. Grötzschel, C. Heiser, F. Herrmann, P. Urwank, K. Hennig
Analysis of boron doped silicon oxide layers by means of the backscattering and prompt nuclear reactions
MRS-Tagung, Strasbourg, Juni 1986

Schmidt, B.
Sensoren für Strahlung und chemische Signale
Vortrag zur Frühjahrsmesse, Leipzig,

Schmidt, B.
Herstellung und Anwendung von Siliciumsensoren
Weiterbildungslehrgang für Fachschullehrer, Ing.-Schule für Lebensmittelindustrie, Dippoldiswalde, 6.2.1986

Schmidt, B., J. von Borany
Entwicklung und Herstellung von Halbleiterdetektoren im ZfK Rossendorf
Seminarvortrag, PTI Leningrad , Oktober 1986

Schmidt, B., H. Schott, H.-J. Just
Hybridintegrated Sensor for Position Measurement
IMEKO Symposium TC2 Photon Detectors, Varna, 22.-24.5.1986

Schmidt, B., D. Schubert
Herstellung mikromechanischer Bauelemente mit Hilfe mikroelektronischer Technologie
Jahrestagung der Physikalischen Gesellschaft der DDR, Leipzig, 9.-12.2.1986

Schott, H., H. Herberg
Microcomputer controlled position sensitive measurement system [f)]

Schott, H., H. Herberg, B. Schmidt
Mikrorechnergesteuertes Positioniersystem mit hybridintegriertem Positionierschaltkreis
4. Fachtagung "Anwendung von Mikrorechnern in der Meß- und Automatisierungstechnik", Magdeburg, September 1986

Schubert, D., U. Lorenz, W. Jenschke, T. Uhlig
Sensoren in SOI-Technologie
19. Fachkolloquium Informationstechnik, Dresden, Januar 1986

Schulz, H.
Impact Parameter Dependence of the Specific Entropy
High Energy Physics Seminar, Dubna, June 1966

Schulz, H.
Onset of Multifragmentation
Seminarvortrag, Niels-Bohr-Institut, November 1985

Schulz, H.
Connection between Thermodynamical and the Percolation Models of Nuclear Fragmentation
Workshop on Cross Properties of nuclei and Nuclear Excitations, Hirschegg, January 1986

Schulz, H.
Limiting temperature of finite nuclei [d)]

Seidel, W.
Parameter positionsempfindlicher Lawinenzähler (in russisch) n)

Sieber, N., H. Oertel
Elektrische Eigenschaften von MOS-Strukturen in SOI-Schichten c)

Sieber, N., H. Oertel, M. Voelskow
Elektrische Eigenschaften von MOS-Strukturen, hergestellt im rekristallisierten Si
17. Arbeitstagung Physik der Halbleiteroberfläche, Binz, 7.-12.4.1986

Skorupa, W.
Hochenergieimplantation in Si - Übersicht und erste Ergebnisse c)

Skorupa, W.
Hochenergieimplantation in Silicium
Problemseminar ZfK/ZFTM, Rossendorf, 6.2.1986

Skorupa, W.
Erzeugung von SOI-Strukturen durch Hochdosis-Ionenimplantation m)

Skorupa, W.
Erzeugung von Siliciumnitrid durch Stickstoff-Hochdosisimplantation in Silicium
Bereichsseminar KB des ZfK, Rossendorf, 20.6.1986

Skorupa, W.
Erzeugung von SOI-Strukturen mit Ionenstrahlverfahren
Fachtagung mit internationaler Beteiligung "Schichtsysteme für zukünftige Bauelemente der Mikro-, Opto- und Molekularelektronik", Karl-Marx-Stadt (TH), 11.-13.11.1986

Skorupa, W., U. Kreißig, H. Oertel, H. Bartsch
Properties of epitaxial silicon layers on buried silicon nitride produced by ion implantation
4. Int. Conference Low Energy Ion Beams, Brighton, 7.-11.4.1986

Skorupa, W., E. Wieser, R. Grötzschel, M. Posselt, A. Armigliato, A. Garulli, A. Beyer, W. Markgraf
Hochenergieimplantation und Ausheilung von Phosphor in Silicium h)

Skorupa, W., E. Wieser, R. Grötzschel, M. Posselt, H. Bueeke, A. Armigliato, A. Garulli, A. Beyer, W. Markgraf
High Energy Implantation and Annealing of Phosphorus in Silicon l)

Skorupa, W., K. Wollschläger, R. Grötzschel, H. Bartsch
Erzeugung vergrabener Si_3N_4 Schichten mit rechteckförmigen Stickstoffprofilen durch Ionenimplantation c)

Skorupa, W., K. Wollschläger, U. Kreißig, R. Grötzschel, H. Bartsch
Properties of Ion Beam Synthesized Buried Silicon Nitride Layers with Rectangular Nitrogen Profiles l)

Skorupa, W., K. Wollschläger, U. Kreißig, R. Grötzschel, H. Bartsch
Erzeugung von SOI-Strukturen mit vergrabenen Si_3N_4-Schichten mit rechteckförmigen Stickstoffprofilen durch Ionenimplantation h)

Sobeslavsky, E.
Modelluntersuchungen zur Stickstoffimplantation in Silicium
Herbstschule Isolatorphysik, Ahrenshoop, 27.-29.11.1985 und c)

Stary, F.
Erprobung der Bragg-Ionisationskammer am Tandem des ZfK Rossendorf (in russisch) n)

Stary, F.
Physik mit schweren Ionen
Festkolloquium zum 30. Jahrestag der Gründung des VIK Dubna, ZfK Rossendorf, 3.4.1986

Stary, F.
Gasgefüllte Detektoren für schwere Ionen
Kolloquium der physikalischen Institute der Technischen Universität Braunschweig, 16.12.1986

Stegemann, K.H., M. Voelskow
SOI-Substrate für die Mikroelektronik - Stand der Herstellungstechnologie c)

Teichfuß, M.
Detektionssysteme für geladene Teilchen geringer Energie und Reichweite c)

Teichfuß, M.
Evidence of low energy charged particles
Konf. Naukowa i Spotkanie Przyjazni zwiazkow mlodzierzy z panstw, Swierk, 4.-7.11.1986

Tesch, S.
Scattering and fragmentation of relativistic deuterons and helium nuclei
Int. Symposium on Hadron Structure, Smolenice, 2.-8.11.1986

Voelskow, M., J. Matthäi
Stand der Arbeiten zur Herstellung von SOI-Substraten und apparative Weiterentwicklung im ZfK m)

Voelskow, M., J. Matthäi
Stand und Perspektiven einer SOI-Technologie m)

Voelskow, M., J. Matthäi, K.H. Stegemann, Ch. Höppner
Methoden zur Herstellung korngrenzenfreier SOI-Gebiete beim lateralen Zonenschmelzen c)

Voelskow, M., K.H. Stegemann
Stand und Perspektiven einer SOI-Technologie
Kolloquium (KME), Erfurt, 4.4.1986

Walther, K.
Ein Steuerprogramm für den automatischen Betrieb des Spektrometers NSWR a)

Walzog, D.
Vakuum- und Gasversorgungssystem (in russisch) n)

Weiß, L., H. Eschrig
Messung und theoretische Interpretation von Kohn-ähnlichen Anomalien in der Elektron-Phonon-Wechselwirkung a)

Weiß, L.
INS-Untersuchungen an Halbleitern ($Pb_{1-x}SN_xTe$, $CoSi_2$) a)

Wieser, E., A. Häßner, R. Portius
Bildung von Molybdänsilicid-Polysiliciumstrukturen durch Kurzzeittemperung c)

Winter, G.
Yrast properties in the Kr nuclei
Europhysics Study Conference on the Structure of Cold Nuclei, Albena, 14.-18.9.1986

Wollschläger, K., W. Skorupa
Phasenbildungskinetik an vergrabenen Si_3N_4-Schichten aus IR-spektroskopischen Untersuchungen c)

Wünsch, R.
Production, Structure and Decay of Hypernuclei
Seminarvortrag, Institute for Nuclear Research, Moscow State University, December 1985

Wünsch, R.
Atomkerne und Quarks
6. Tagung über Probleme der theoretischen Physik, Leipzig, Februar 1986;
Radio DDR II, Wissenschaftsredaktion, April 1986

Wünsch, R.
The Rossendorf Continuum shell-model, formalism and application
Seminarvortrag, Institute for Nuclear Research, Novosibirsk, August 1986

Wünsch, R.
URANIA-Vortrag "Neutrinos", Dresden, September 1986

a) Int. Winterschule Neutronenstreuung, Stadt Wehlen, 27.-31.1.1986

b) Int. Frühjahrsschule Kernphysik und Analytik, Holzhau, 6.-11.4.1986

c) Arbeitstagung "Ionenstrahltechnologie 86", Papstdorf, 14.-18.4.1986

d) XVI. Int. Symposium on Nucl. Physics, Gaussig, 10.-14.11.1986

e) Expertenberatung zur Automatisierung wissenschaftlicher Forschungen AWF, Kiev, 18.-22.11.1986

f) 5th Int. IMECO Symposium, Jena, 10.-14.6.1986

g) Festseminar zum 30. Jahrestag des ZfK, Rossendorf, Februar 1986

h) IV. Symposium "Physikalische Grundlagen zu Bauelementetechnologien der Mikroelektronik, Frankfurt/O., 10.-12.9.1986

i) IX. Arbeitstagung "Struktur nichtkristalliner und partiellkristalliner Systeme", Biesenthal, 24.-27.3.1986

j) Int. Meeting on Application of Mössbauer Spectroscopy in Physics of Metals and Physical Metallurgy, Valtice, 12.-16.5.1986

k) 17. Arbeitstagung Physik der Halbleiteroberfläche, Binz, 7.-12.4.1986

l) Int. Conference "Ion Beam Modification of Materials", Catania, 9.-13.6.1986

m) DDR-SOI Workshop, Dresden (ZfK), 13.12.1986

n) Arbeitsberatung zum 4 π-Detektor (Anlage PHOBOS), Dubna, 21.-23.1.1986

VERANSTALTUNGEN

Int. Winterschule "Neutronenstreuung", Stadt Wehlen, 27.-31.1.1986

Int. Frühjahrsschule "Kernphysik und Analytik", Holzhau, 6.-11.4.1986

Arbeitstagung "Ionenstrahltechnologie 86", Papstdorf, 14.-18.4.1986

PATENTE

Altmann, J., C. Blochwitz, B. Rauschenbach, G. Schmidt
Verfahren zur Erhöhung der chemischen Resistenz von Nickelwerkstoffen
DD 227 457

Böhme, H., R. Kirchbach, H.B. Lück, G. Schmidt
Verfahren zur Erzeugung von Kernspuren in Hohlfäden
DD 238 466

Jörren, C., E. Richter
Verfahren zur Erhöhung des Verschleißwiderstandes von Hartmetallerzeugnissen
DD 227 455 (11.7.1985/18.9.1986)

Lück, H.B.
Herstellung von Kernspurmikrofiltern sehr geringer Porenverengung
DD 239 068

Lück, H.B.
Asymmetrischer Kernspurmikrofilter und Verfahren zu seiner Herstellung
DD 238 467

Lück, H.B., R. Korf, P. Hörl, W. Fischer, V. Preißler
Separator mit gefalteter Membran
DD 233 489

Poitz, T., E. Richter, S. Schneider, G. Beister
Verfahren zur Farbumwandlung bei Titannitriddekoren
DD 224 839 (21.6.1984/17.7.1985)

WISSENSCHAFTLICHE PREISE

Institutspreis Kategorie I, 2. Preis 1985/1986

Enghardt, W., H.-U. Jäger, L. Käubler, H.-J. Keller, H. Prade, F. Stary
Experimentelle und theoretische Untersuchungen von Mehrteilchenanregungen in halbmagischen Kernen mit 82 Neutronen oder 50 Protonen

Institutspreis Kategorie II, 2. Preis 1985/1986

Schott, H., B. Schmidt
Entwicklung und Herstellung eines hybridintegrierten optoelektronischen Positionierschaltkreises

Institutspreis Kategorie III, 1. Preis 1985/1986

Fromm, W.D., P. Manfraß, M. Sobiella, D. Wohlfahrt
Positronenkamera mit Gasdetektoren

Bereichspreis Kategorie I, 1. Preis 1985/1986

Müller, H.J., K.H. Heinig
Computersimulation der primären Kristallisation von amorphen zu polykristallinen Silicium

Bereichspreis Kategorie I, 2. Preis 1985/1986

Matz, W., H. Herrmann, N. Mattern
On the Structure of Amorphous Fe75B25

Bereichspreis Kategorie II, 1. Preis 1985/1986

Jäger, H.-U.
Modellierung der Sauerstoffumverteilung im Target bei Sauerstoff-Hochdosisimplantation in Silicium

Bereichspreis Kategorie II, 2. Preis 1985/1986

Skorupa, W., K. Wollschläger, U. Kreißig, R. Grötzschel, H. Bartsch
Vergrabene Si_3N_4-Schichten mit steilen Halbleiter/Isolator-Übergängen in Silicium

Bereichspreis Kategorie III, 1. Preis 1985/1986

Kotte, R., H.J. Keller, H.-G. Ortlepp, F. Stary
Weiterentwicklung der Bragg-Peak-Spektroskopie

Bereichspreis Kategorie III, 2. Preis 1985/1986

Fromm, W.D.
Das Farbdisplay 4791 als autonomer 2D-Analysator

Bereichspreis Kategorie IV, 1. Preis 1985/1986

Bischoff, L., J. von Borany
Strahlenschäden in Si-Halbleiterdetektoren

Bereichspreis Kategorie V, 1. Preis 1985/1986

Tesch, S.
Öffentlichkeitsarbeit

ZENTRALINSTITUT FÜR KERNFORSCHUNG, ROSSENDORF, BEREICH G

VERÖFFENTLICHUNGEN

Baldauf, D., M. Borkenhagen, R. Fülle, B. Hartmann, S. Hiekmann, G. Hofmann, W.-J. Linnemann
Prozeßführung an Beschleunigern
ZfK-594 (1986) 30

Bergmann, W.
Erhöhte Rechenleistungen durch Vektorprozessing
ZfK-594 (1986) 36

Böttger, H.
RATARI - A. Programm System of Rational Arithmetic
Proc. Int. Conference Computing Algebra and its Application in Theoretical Physics 1985
Dubna 1986, 160

Brückner, R., H. Guratzsch
Irradiation System for Target Materials with Low Heat Transmission
ZfK-594 (1986) 16

Büttig, H.
Beam Profile Monitor System Based on Infrared Thermography
ZfK-594 (1986) 19

Dietrich, J., M. Friedrich
Experimentelle und theoretische Untersuchungen am Fokussiersystem einer HF-Ionenquelle
Exp. Tech. Phys. 34 (1986) 263

Dietrich, J. H. Guratzsch, G. Kerber, W. Naumann, H. Odrich
Die Beschleunigung von $^{20}Ne^{3+}$- und $^{20}Ne^{4+}$-Ionen mit dem Rossendorfer Zyklotron U-120
Kernenergie 29 (1986) 392

Dietrich, J., G. Kerber, W. Naumann, H. Odrich
Erzeugung und Beschleunigung von Li^{3+}-Ionen am Rossendorfer Zyklotron U-120
Exp. Tech. Phys. 34 (1986) 191

Eichhorn, K., St. Preusche
Ionenstrahlablenkung mit Hilfe eines Statormagnetes
ZfK-594 (1986) 12

Eichhorn, K., E. Richter, H. Taubert
Anwendung der Dünnschichtaktivierung auf Kavitationsuntersuchungen
ZfK-594 (1986) 22

Friedrich, M.
Erhöhung der Transmission des Tandembeschleunigers EGP-10-1
Pribory i Tekhnika Ehksperimenta 4 (1986) 33 (in russ.)

Friedrich, M.
BROHR und SYSFIT - ein Programmsystem zur Berechnung der Strahlführung an elektrostatischen Beschleunigern
ZfK-577 (1986)

Friedrich, M.
Ionenoptische Untersuchungen am Rossendorfer Tandembeschleuniger EGP-10-1
ZfK-593 (1986)

Fromm, U., R. Hammer, H. Kirsch, M. Kunicke
JOBMIT - Ein Programmpaket zur gezielten Bearbeitung von TSO-Stapeljobs
ZfK-594 (1986) 41

Hartmann, P.
Rekonstruierte Impulsspannungsquelle für die Zyklotron-Ionenquelle
ZfK-594 (1986) 11

Hieronymus, W., B. Schneider, J. Günther, A. Findeisen, K. Franke
Der Rossendorfer Forschungsreaktor RFR - ein kerntechnisches Großgerät im Bereich Großgeräte des ZfK
ZfK-594 (1986) 48

Matthes, H., W. Pfestorf
The Negative Ion Sputter Source MISS-585
NIM A244 (1986) 155

Regel, K.
Certain Pattern of DNA Double Strand Breaks in Membrane Attached Superstructure Units Cause Cell Killing: A Radiation Action Model
ZfK-594 (1986) 25

VORTRÄGE, DIE AUSSERHALB DES EIGENEN KOLLEKTIVS GEHALTEN WURDEN

Friedrich, M.
Die elektrostatischen Beschleuniger des ZfK Rossendorf
Bereichsseminar IJF Novosibirsk, 11.11.1986

Hammer, P., Ch. Eifrig, K. Eichhorn
A Study of Wear in Refrigeration Compressors Using Deuteron Activation
Fachtagung INSYCONT 86, Krakow, Sept. 1986

PROMOTIONEN B (Dr. sc. nat.)

Dietrich, J.
Beiträge zur Strahlextraktion und -formierung bei Plasmaionenquellen und zum Transport intensiver Ionenstrahlen
TU Dresden, 14.11.1986

Regel, K.
Zur Bedeutung der DNS-Superstrukturen für das Verständnis des Strahlenwirkungsmechanismus
Akademie der Wissenschaften der DDR, 4.4.1986

VERANSTALTUNGEN

XIII. Frühjahrsschule für Beschleunigungstechnik, Hörnitz 10.-14.3.1986

TECHNISCHE UNIVERSITÄT DRESDEN, SEKTION PHYSIK, WB THEORETISCHE PHYSIK

VERÖFFENTLICHUNGEN

Münchow, L., R. Reif: Recent Developments in the Nuclear Many-Body Problem
Vol. 1 Strong Interactions and Nuclear Structure. Teubner-Texte zur Physik, Band 7,
BSB B.G. Teubner Verlagsgesellschaft, Leipzig 1985

Biedermann, M., P. Mädler: A two-stage model for fast particle emission in heavy-ion collisions. Z. Phys. A323 (1986) 315

Milek, B., R. Reif: Gamow states in a realistic two-center potential and nucleon emission in heavy-ion collisions. Nucl. Phys. A458 (1986) 354

Schmidt, R.: Critical distance for fusion and fusion barriers of very-heavy-ion collisions. Z. Phys. A325 (1986) 239

Gippner, P., K.D. Schilling, W. Seidel, F. Stary, E. Will, H. Sodan, S.M. Lukyanov, V.S. Salamatin, Yu.E. Penionzhkevich, G.G. Chubarian, R. Schmidt: Shell effects in the evolution of the mass asymmetry in heavy-ion collisions leading to composite systems with Z = 108. Z. Phys. A325 (1986) 335

Knospe, O., R. Schmidt, H. Schulz: Site-percolation approach for mass and isotopic distributions in fragmentation reactions. Phys. Lett. B182 (1986) 293

Mädler, P., B. Milek, R. Reif: On the possibility of post-equilibrium polar particle emission in heavy-ion induced fusion-fission reactions.
VIK Dubna Report E7-86-558, Dubna 1986

DIPLOMARBEITEN

Fandrich, J.: Differentielle Emissionsspektren leichter Teilchen im Zwei-Zentren-Schalenmodell für Schwerionenreaktionen

PROMOTIONEN A (Dr. rer. nat.)

Milek, B.: Adiabatische Basis im Zwei-Zentren-Potential endlicher Tiefe und Nukleonenemission in schwerioneninduzierten Kernreaktionen.

VORTRÄGE, DIE AUSSERHALB DES EIGENEN KOLLEKTIVS GEHALTEN WURDEN

Mädler, P.: Fragen des Mechanismus von Schwerionenreaktionen bei mittleren Energien. (in russ.) Internationale Arbeitstagung zum 4 π-Detektor "Phobos", Dubna, Januar 1986

Reif, R.: Schwerionenphysik - Grundlagenforschung und Anwendung.
Kolloquium der Sektion Physik der Bergakademie Freiberg, Februar 1986

Mädler, P.: Two-stage model for HIC a)

Milek, B.: Emission of polar particles in fission a)

Schmidt, R.: Dynamics of the mass asymmetry in HIC a)

Reif, R.: Semiclassical one-body dynamics of heavy-ion collisions
International School-Seminar on Heavy-Ion Physics, Dubna, September 1986

Mädler, P.: Description of fast nucleon emission within a phenomenological two-stage model
International School-Seminar on Heavy-Ion Physics, Dubna, September 1986

Schmidt, R.: Semiklassische Theorie dissipativer Schwerionenreaktionen
Seminar des Instituts für Physikalische Chemie, AdW, Berlin-Adlershof, Oktober 1986

Biedermann, M.: Fast nucleon emission in HIC within the two-stage model b)

Knospe,O.:Site-percolation approach for isotopic distributions in fragmentation reactions b)

Milek, B.: One-body dynamics in a semiclassical model of HIC and fission b)

Schmidt, R.: Semiclassical treatment of dissipative HIC-Nucleonenexcitation and -transfer b)

a) Internationale Frühjahrsschule des ZfK Rossendorf, Holzhau, April 1986
b) XVI. International Symposium on Nuclear Physics, Gaussig, November 1986

VERANSTALTUNGEN

XVI. International Symposium on Nuclear Physics - Dynamics of Heavy-Ion Collisions - Gaussig, 10. - 14. November 1986

TECHNISCHE UNIVERSITÄT DRESDEN, SEKTION PHYSIK, WB KERNPHYSIK

VERÖFFENTLICHUNGEN

Böttger, R., W.D. Fromm, H. Klein, H. Märten, D. Richter, D. Seeliger: The Cf-252(sf) Neutron Spectrum in the High-Energy Range, Radiation Effects 96 (1986) 129

Eckstein, P., F. Gleisberg, U. Jahn, R. Krause, E. Paffrath, D. Schmidt, R. Schwierz, D. Seeliger, A.I. Glotov, V.A. Romanov: Intense Neutron Generator Project at the TUD, Proc. IV. Int. Symp. on Neutron Induced Reaction, Smolenice, June 1985, p. 417

Elfruth, T., D. Hermsdorf, H. Kalka, D. Seeliger, K. Seidel, S. Unholzer: The Neutron Emission from Lead Bombarded with 14 MeV Neutrons, Proc. IV. Int. Symp. on Neutron Induced Reaction, Smolenice, June 1985, p. 68

Elfruth, T., D. Hermsdorf, H. Kalka, J. Pöthig, D. Seeliger, K. Seidel, S. Unholzer: Neutron emission from lead bombarded with 14 MeV neutrons, Proc. of the Int. Conf. on Fast Neutron Physics, Dubrovnik, 26.5.-31.5.1986, p. 282, INDC(Yug)-010/G (1986)

Florek, M., I. Szarka, J. Oravec, K. Holy, E. Misianikova, H. Helfer, U. Jahn, YU.P. Popov: The (n,α) reactions on the ^{95}Mo and ^{143}Nd isotopes with 3 MeV neutrons, Proc. IV. Int. Symp. on Neutron Induced Reaction, Smolenice, June 1985, p. 74

Hermsdorf, D.: Description of File 8201 for Lead for the Library BROND, INDC(GDR)-39/L (1986)

Hermsdorf, D.: Description of File 1402 for Silicon for the Library BROND - Revision of MAT 2015 and Integral Data Tests -, INDC(GDR)-38/L (1986)

Hermsdorf, D., H. Kalka, D. Seeliger, U. Steininger: Phenomenology of angular distributions of neutron-induced particle emission at 14 MeV, Proc. of the Int. Conf. on Fast Neutron Physics, Dubrovnik, 26.5.-31.5.1986, p. 87, INDC(Yug)-010/G (1986)

Ignatovich, V.K., A. Meister, S. Mittag, W. Pilz, D. Seeliger, K. Seidel: Temperature Shift of Neutron Resonances, ZfK-592 (1986) 74

Ignatovich, V.K., A. Meister, S. Mittag, W. Pilz, D. Seeliger, K. Seidel: Temperature Shift of Neutron Resonances, Proc. IV. Int. Symp. on Neutron Induced Reaction, Smolenice, June 1985, p. 304

Kalka, H., D. Hermsdorf, D. Seeliger: Excitonmodel and Multistep-Compound Reactions, Proc. IV. Int. Symp. on Neutron Induced Reaction, Smolenice, June 1985, p. 78

Märten, H., D. Richter, D. Seeliger, W. Neubert, A. Lajtai: Energy and Angular Distribution of ^{252}Cf Fission Neutrons in the low Energy Range, Proc. Int. Nucl. Phys. Conf., Harrogate, Aug. 1986, Vol. 1, B123, p. 149

Märten, H., D. Seeliger: Description of the ^{252}Cf(sf) neutron spectrum in the framework of a generalized Madland-Nix model, Nucl. Sci. Eng. 93 (1986) 370

Märten, H., D. Richter, D. Seeliger, W. Neubert: On the Mechanism of Fission Neutron Emission, ZfK-592 (1986) 1

Märten, H., D. Richter, D. Seeliger, W.D., Fromm, W. Neubert: Experimental Arrangement for the Measurement of Correlations Between Fission Products and Neutrons, ZfK-592 (1986) 39

Märten, H., D. Seeliger: Investigation of the 252 Cf spontaneous fission neutron spectrum, Proc. IV. Int. Symp. on Neutron Induced Reactions, Smolenice, June 1985, p. 322

Märten, H., D. Richter, D. Seeliger, W.D. Fromm, D. Neubert: Differential Study of ^{252}Cf (sf) Neutron Emission, Proc. IV. Int. Symp. on Neutron Induced Reactions, Smolenice, June 1985, 368

Märten, H., D. Seeliger, W. Neubert, D. Richter: Detailed Investigations of Fission Neutron Emission, Radiation Effects 93 (1986) 41

Märten, H., D. Seeliger: Theoretical Study of the Cf-252(sf) Neutron Spectrum, Radiation Effects 93 (1986) 99

Meister, A., S. Mittag, L.W. Pikelner, W. Pilz, D. Seeliger, K. Seidel: Chemically Shifts of Uranium Neutron Resonances, Proc. IV. Int. Symp. on Neutron Induced Reactions, Smolenice, June 1985, p. 315

Meister, A., S. Mittag, L.B. Pikelner, W. Pilz, D. Seeliger, K. Seidel: Measurement of the Mean-Square Charge Radii of Neutron Resonance States in Uranium Nuclei, ZfK-592 (1986) 65

Meister, A., S. Mittag, W. Pilz, D. Seeliger, K. Seidel, L.B. Pikelner: Mean-square radii of the ^{236}U nucleus in excited states with different fission widths, ZfK-592 (1986) 70

Pretzsch, G., B. Dörschel, H. Seifert, T. Streil, D. Seeliger: Measurement of Tritium Activity Concentration in Air by Means of the Electret Ionisation Chambers, Radiation Protection Dosimetry 12, Nr. 4 (1986) 345

Schmidt, D., D. Seeliger: Experimentelle Grundlagen für neutronenphysikalische Untersuchungen für die Kernenergetik (Teil I: Einsatzvorbereitung des intensiven Neutronengenerators INGE-1, Teil II: Beiträge zur Tritiumtechnologie), A4-Abschlußbericht TU Dresden, Sektion Physik (1986)

Seeliger, D., K. Seidel, H. Märten: Proceedings of the XV-th International Symposium on Nuclear Physics - Nuclear Fission - November 11 - 15 1985, Gaußig, p. 1 - 194 (Editor), ZfK-592

Szarka, S., M. Florek, J. Oravec, K. Holy, H. Helfer, U. Jahn: Gas Proportional Telescope used to Investigate Rare Reactions Induced by 3 MeV Neutrons, Nucl. Instr. and Meth. B17 (1986) 472

DIPLOMARBEITEN

Almeroth, L.: Beiträge zur Entwicklung einer elektronisch steuerbaren Hochspannungsversorgungseinheit 40 kV/25 mA

Blanco, L.E.: MOCCA - ein Programm zur Simulation von Mehrfachstreueffekten bei der Streuung schneller Neutronen in endlichen Streugeometrien

Hildebrandt, B.: Entwicklung, Aufbau und Erprobung eines Monitor-Systems für den Intensiven Neutronengenerator INGE-1

Krimmling, P.: Analyse mehrfachdifferentieller Wahrscheinlichkeiten der Neutronenemission aus der Spontanspaltung von ^{252}Cf im Rahmen des erweiterten Kaskadenverdampfungsmodells

Steininger, U.: Beiträge zur Entwicklung und Aufbau einer Impulsionenquelle

Töpfer, M.: Herstellung von Gruppendaten und Berechnung von Neutronenausflußspektren für ein Bleikugelbenchmarkexperiment

PROMOTIONEN A (Dr.rer.nat.)

Gleisberg, F.: Beiträge zu Entwurf und Anwendung steuerbarer Stromversorgungseinheiten auf Schaltreglerbasis in rechnergeführten physikalischen Experimentanordnungen, TU Dresden, 30.5.1986

Jahn, U.: Dimensionierung, Aufbau und Erprobung des ionenoptischen Systems für den intensiven Neutronengenerator INGE-1, TU Dresden, 12.12.1986

Köhler, M.: Beitrag zur Applikation des 1-Chip-Mikrorechners U 882 im wissenschaftlichen Gerätebau am Beispiel eines einfachen Vielkanalysator, TU Dresden, 1.8.1986

VORTRÄGE, DIE AUSSERHALB DES EIGENEN KOLLEKTIVS GEHALTEN WURDEN

Eckstein, P., U. Jahn, E. Paffrath, D. Schmidt, D. Seeliger: Intense Neutron Generator Development at the TU Dresden, IAEA Advisory Group Meeting on Neutron Source Properties, Leningrad, 9. - 13.6.1986

Elfruth, T., D. Hermsdorf, H. Kalka, J. Pöthig, D. Seeliger, K. Seidel, S. Unholzer: Differential Neutron Emission Cross Section from Lead and Carbon Bombarded with 14 MeV Neutrons, IAEA Vienna, 1986

Märten, H.: Theoretical Description of the Cf-252 Fission Neutron Spectrum, IAEA Advisory Group Meeting on Neutron Source Properties, Leningrad, 9. - 13.6.1986

Märten, H., D. Richter, D. Seeliger, W. Neubert, A. Lajtai: Energy and Angular Distribution of ^{252}Cf Fission Neutrons in the Low Energy Range, IAEA Advisory Group Meeting on Neutron Source Properties, Leningrad, 9. - 13.6.1986

Märten, H., D. Richter, D. Seeliger, W.D. Fromm, W. Neubert: New Experimental and Theoretical Results of Cf Neutron Emission, IAEA Advisory Group Meeting on Neutron Source Properties, Leningrad, 9.-13.6.1986

Märten, H., A. Ruben, D. Seeliger: Calculation of Prompt Fission Neutron Spectra for Applied Purposes, IAEA Advisory Group Meeting on Neutron Source Properties, Leningrad, 9.-13.6.1986

Seeliger, D.: Status of experimental and theoretical double-differential neutron data, IAEA Advisory Group Meeting on Nuclear Data for Fusion Reactor Technology (in Cooperation with the Technical University Dresden), Gaußig, 1.12.-5.12.1986

Seidel, K.: Benchmark testing of nuclear data on Pb-spheres, IAEA Advisory Group Meeting on Nuclear Data for Fusion Reactor Technology (in Cooperation with the Technical University Dresden), Gaußig, 1.12.-5.12.1986

Seidel, K., L.B. Pikelner: Messung der mittleren quadratischen Radien der Kerne von Uraniumisotopen beim Einfang von Resonanzneutronen (in russ.), V. Int. Schule über Neutronenphysik, Aluschta (UdSSR), Okt. 1986.

VERANSTALTUNGEN

IAEA Advisory Group Meeting on Nuclear Data for Fusion Reactor Technology (in Cooperation with the Technical University Dresden), Gaußig, 1.12.-5.12.1986

BERUFUNGEN

Doz. Dr. sc. nat. K. Seidel wurde am 1.9.1986 zum außerordentlichen Professor an die TU Dresden, Sektion Physik, berufen.

TECHNISCHE UNIVERSITÄT DRESDEN, SEKTION PHYSIK, WB ANGEWANDTE KERNPHYSIK

VERÖFFENTLICHUNGEN

Bischoff, L.; Mademann, D.; Trützschler, K.; Zschornack, G.: Der Einsatz von Mikrostreifendetektoren in der winkeldispersiven Röntgenspektrometrie, TU-Preprint 05-05-86

Heinrich, B.; Irmer, K.; Pötschke, R.: Fast analysis of carbon content by inelastic scattering of neutrons, Third Working Meeting Radioisotope Application and Radiation Processing in Industry Leipzig, 23-27. Sept. 1985, Vol. III, S. 841-847

Herbach, C.M.; Merla, K.; Musiol, G.; Ortlepp, H.-G.; Pausch, G.; Alkhazov, I.D.; Drapchinsky, L.V.; Ganza, E.A.; Kovalenko, S.S.; Kostochkin, O.L.; Solovjev, S.M.; Shpakov, V.I.: Absolute fission cross-section measurement of Pu-239 at 4.8, 8.65 and 18.8 MeV and of U-235 at 4.45 and 18.8 MeV neutron, XV. Intern. Symp. on Nucl. Phys. "Nuclear Fission" Gaussig, GDR, Nov. 1985, ZfK-592 (1986) 152-155

Irmer, K.; Pötschke, R.: Die Untersuchung der Messung der Kohlenstoffkonzentration mit Hilfe der unelastischen Neutronenstreuung, Isotopenpraxis 22 (1986) 9, S. 316-320

Irmer, K.; Siebert, H.-U.; Theilig, B.: Bestimmung des ^{235}U-Gehaltes in großen Proben - Messung und Monte-Carlo-Experiment, Isotopenpraxis 22 (1986) 7, S. 225-232

Kreisler, D.; Zschornack, G.: Temperaturregelung am Analysatorkristall eines Kristalldiffraktionsspektrometers mit einem diskreten parameteroptimierten Regler, TU-Preprint 05-03-86

Ortlepp, H.-G.; Herbach, C.M.; Merla, K.; Musiol, G.; Pausch, G. Identification of associated particles in the TCAPM fission cross-section measurements at the tandem accelerator of the CINR Rossendorf, XV. Intern. Symp. on Nucl. Phys. "Nuclear Fission" Gaussig, GDR, Nov. 1985, ZfK-592 (1986) 156-159

Pausch, G.; Fromm, W.D.; Herbach, C.M.; Merla, K.; Musiol, G.; Ortlepp, H.-G.: CAMAC data acquisition system and data analysis in TCAPM fission cross-section measurements at the tandem accelerator of the CINR Rossendorf, XV. Intern. Symp. on Nucl. Phys. "Nuclear Fission" Gaussig, GDR, Nov. 1985, ZfK-592 (1986) 160-163

Musiol, G.; Gromow, K.J.; Chalkin, A.: Internationale Zusammenarbeit im Programm JASNAPP, Energoatomizdat Moskau 1986, S. 185-192

Schiekel, M.; Jugelt, P.: State and Trends in energy dispersive X-Ray analysis, Third Working Meeting Radioisotope Application and Radiation Processing in Industry Leipzig, 23-27. Sept. 1985, Vol. II, S. 511-537

Zschornack, G.; Musiol, G.; Reichmann, A.; Karrasch, G.; Kreiseler, D.; Schulze, W.; Tänzer, W.; Wagner, W.: A Computer-Aided Bragg Crystal Diffraction Spectrometer for X-Ray Analysis, Third Working Meeting Radioisotope Application and Radiation Processing in Industry Leipzig, 23.-27. Sept. 1985, Vol. II, S. 589-593

Zschornack, G.: A Systemization of X-Ray Energies and Electron Binding Energies in Free Highly Charged Ions, TU-Preprint 05-06-86

Zschornack, G.: Eine Systematisierung von atomaren Eigenschaften hochgeladener Ionen, 7. Tagung "Energiereiche atomare Stöße" in Oberstdorf/BRD vom 26.1.-1.2.1986, EAS-7, S. 18-20

Zschornack, G.; Musiol, G.; Wagner, W.: Dirac-Fock-Slater X-Ray Energy Shifts and Electron Binding Energy Changes for all Ion Ground States in Elements up to Uranium, Rossendorf, ZfK-574

Zeuner, A.; Henning, K.; Kießling, M.: Investigation of the Material transport Behaviour of Tube- and Though-Vibration mills by radioactive indicators, Third Working Meeting Radioisotope Application and Radiation Processing in Industry Leipzig, 23-27. Sept. 1985, Vol. III, S. 1021-1027

Zeuner,A.; Hartmann, F.: Residence time investigation and material balance for fresh and waste water in a rayon by radioisotope application, Third Working Meeting Radioisotope Application and Radiation Processing in Industry Leipzig, 23-27. Sept. 1985, Vol. IV., S. 1271-1278

VORTRÄGE, DIE AUSSERHALB DES EIGENEN KOLLEKTIVS GEHALTEN WURDEN

Jugelt, P.: Anwendung energiedispersiver Röntgenspektrometer in der Festkörperanalytik, ZfK Rossendorf, Anwenderkolloquium 20.5.1986

Musiol, G.: Pausch, G.: Absolut- und Präzisionsbestimmung von Spaltquerschnitten mit der Methode der zeitlich korrelierten assoziierten Teilchen, TU Dresden, 24.4.1986

Musiol, G.: Irmer, K.: Zur Entwicklung der Forschung auf dem Gebiet der Angewandten Kernphysik, TU Dresden, 13.9.1986

Musiol, G.: Kernenergetik und Umwelt, Gaußig, 27.11.86, Dresden, 3.12.86

Pausch, G., Herbach, C.M.: Absolutbestimmung von Spaltquerschnitten mit der Methode der zeitlich korrelierten assoziierten Teilchen, III. Interdisziplinäre Zentrale Wissenschaftl. Konferenz der Studenten und jungen Wissenschaftler, Zittau, 20./21. Febr. 1986

Reiche, I.: Geometriefaktoren für ß-Rückstreuanordnungen, XI. Zentrale Studentenkonferenz, Dresden,

Schiekel, M.; Heckel, J.; Heinrich, B.: Elementanalyse an historischem Glas, Wiss. Zeitschrift d. TU Dresden 35/4, S. 41-42

Schmidt-Böcking, H.; Zschornack, G.; Dangendorf, V.; Euler, J.; Hagmann, S.; Ulrich, J.; Schmidt, S.: "Search for Metastable Highly Charged Recoil Ions", Intern. Konferenz "Physics of Multiply Charged Ions" in Groningen/Niederlande, 17.-19.9.86

Zeuner, A.: Einsatz von Radiotracern zur Prozeßanalyse, Tagung "25 Jahre Radionuklidanwendung in der landtechnischen Forschung", Potsdam-B., 11.9.1986

Zschornack, G.: A Systemization of X-Ray Energies and Electron Binding Energies in Free Highly Charged Ions, Intern. Konferenz "Physics of Multiply Charged Ions" in Groningen/ Niederlande, 17.-19.9.86

Zschornack, G.: Einsatz eines rechnergesteuerten Kristall-Diffraktionsspektrometers zur Untersuchung der Röntgenspektren hochionisierter Atome, Seminar am ZWG der AdW, Bereich Schöneweide, 6.6.86

Zschornack, G.: Röntgenspektroskopie hochionisierter Schwerionen an den Ionenquellen des VIK Dubna, Inst. f. Kernphysik d. Joh.Wolfg.Goethe-Universität, Frankfurt/Main, 18.3.86

Zschornack, G.: Wellenlängendispersive Röntgenspektroskopie hochgeladener Schwerionen, Institut f. Kernphysik der KFA Jülich, 25.3.86

DIPLOMARBEITEN

Döring, Uwe: Aufbau und Erprobung einer speziellen α-Impulskammer

Klein, Jens-Peter: Methodische Untersuchungen zu einer hybriden Auswertemethode in der quantitativen Röntgenfluoreszenzanalyse an geologischen Proben

Kießling, Andreas: Entwicklung und Untersuchung von Sensoren für die Flächenmassemeßtechnik

Mademann, Dirk: Untersuchung von ortsauflösenden Halbleiterdetektoren aus der DDR-Produktion hinsichtlich ihrer Eignung zum Nachweis von charakteristischer Röntgenstrahlung

Steininger, Angela: Berechnung der räumlichen Verteilung und der Energie der Neutronen bei Spaltquerschnittsmessungen nach der Methode der zeitlich korrelierten assoziierten Teilchen

Todt, Ulrich: Weiterentwicklung des Experimentiersystems zur Absolut- und Präzisionsbestimmung von Spaltquerschnitten auf der Grundlage eines neuen ADC-Typs

PROMOTIONEN A (DR. RER. NAT.)

Pausch, G.: Absolutmessung des Spaltquerschnitts von ^{235}U bei 4.45 MeV Neutronenenergie unter Nutzung einer rechnergekoppelten Meßapparatur im CAMAC-Standard

Theilig, B.: Untersuchungen zur Bestimmung des ^{235}U-Gehaltes in großvolumigen Proben

Pötschke, R.: Die Untersuchung der radiometrischen Kohlenstoffgehaltsbestimmung in Rohbraunkohle mit Hilfe eines Strahlungstransportmodells für unelastische Neutronenstreuung

Thiek, P.-A.: Die Berechnung der mittleren ß-Teilchen-Registrierwahrscheinlichkeit für zylinderförmige Elektronen-Emissionsdetektoren mit einem statistischen Modell

KARL-MARX-UNIVERSITÄT LEIPZIG, SEKTION PHYSIK, WB ANGEWANDTE KERNPHYSIK

VERÖFFENTLICHUNGEN

Ascheron, C., G. Otto, R. Flagmeyer, H.-E. Zschau, V.N. Bugrov, S.A. Karamyan: Damage Profile on High Energy Ion Implanted GaP. phys. stat. sol. (a) 97, K 15 (1986)

Ascheron, C., A. Schindler, R. Flagmeyer, G. Otto: Swelling, Strain, and Radiation Damage of He^+ Implanted GaP. phys. stat. sol. (a) 96, 555 (1986)

Ascheron, C., H. Neumann, G. Dlubek, R. Krause: Microhardness of Proton Bombarded GaP Single Crystals. J. Mat. Sci. Lett. 5, 891 (1986)

Ascheron, C., G. Otto, R. Flagmeyer, H.-E. Zschau, V.N. Bugrov, S.A. Karamyan: Damage Profiling on High ... . Preprint VIK, E 14-86-448, Dubna (1986)

Flagmeyer, R., B. Schumann: Rutherford Backscattering/Channeling Analysis of Lattice-Matched $Ca_{0.43}Sr_{0.57}F_2$ Films on GaAs. phys. stat. sol. (a) 93, K 117 (1986)

Frey, H., J. Vogt, G. Otto: Evaluation of Thick Target PIXE Analysis with a Minicomputer. J. Radioanal. Nucl. Chem. 99, 193 (1986)

Stephan, D., V. Geist: Theoretische Intensitätsprofile von Kossel-Linien und Vergleich mit experimentellen Linienprofilen. Exp. Techn. Phys. 34, 153 (1986)

DIPLOMARBEIT

Koch, Andreas: Ein Programmpaket für den EMG-666- zur Aufnahme und Auswertung von Rutherfordrückstreu-/Kanalisierungs-Spektren und seine Anwendung auf die Analyse mehrkomponentiger dünner Schichten. KMU Leipzig, Juli 1986

PROMOTION A (Dr. rer. nat.)

Frey, Herald: Spurenelementanalytik an vorwiegend biologischen Proben durch Spektroskopie protoneninduzierter Röntgenstrahlung (PIXE). KMU Leipzig, 29. 7. 1986

PROMOTION B (Dr. sc. nat.)

Ascheron, Claus: Veränderungen physikalischer Eigenschaften von GaP-Einkristallen und einkristalliner Vergleichsmaterialien durch Protonenbeschuß. KMU Leipzig, 16. 12. 1986

BERUFUNG

Herr Dr. sc. nat. Volker Geist wurde mit Wirkung vom 1. 2. 1986 zum Dozenten an die Sektion Chemie der Karl-Marx-Universität Leipzig, WB Kristallografie, berufen.

VORTRÄGE

Ascheron, C., G. Otto, R. Flagmeyer, H.-E. Zschau, V.N. Bugrov, S.A. Karamjan: Damage Profiling on High Energy Ion Implanted GaP. XVI. Allunionstagung "Physik der Wechselwirkung geladener Teilchen mit Einkristallen", Moskau, 27. 5. 1986

Fechner, R., A. Schindler, R. Flagmeyer, F. Bigl: Untersuchung von Strahlenschäden nach Ionenstrahlätzprozessen im GaAs mittels Cn-64-Adsorption und Autoradiografie sowie RBS-Channeling. 4. Symposium "Physikalische Grundlagen der Bauelementetechnologien der Mikroelektronik", Frankfurt/O., September 1986

Flagmeyer, R.: Analyse von MBE-Schichtstrukturen mittels RBS/Channeling-Technik. Bereichsseminar, ZIE Berlin der AdW, Berlin, 6. 3. 1986

Flagmeyer, R.: Möglichkeiten der Rückstreuspektrometrie zur Stoffanalyse an organischem Material. 3. Frühjahrsschule +), April 1986

Flagmeyer, R.: Rutherford-Rückstreuspektrometrie. Bereichsseminar, Sektion Physik der MLU, Halle, 2. 4. 1986

Flagmeyer, R.: RBS/Channeling an Supergitterstrukturen. 1. Frühjahrsschule "Nukleare Analytik an Beschleunigern" des ZfK Rossendorf der AdW, Holzhau, 7. - 12. 4. 1986

Flagmeyer, R.: Charakterisierung von Heteroepitaxieschichten auf GaAs-Substraten mittels RBS/Channeling. 1. Fachtagung "Schichtsysteme für zukünftige Bauelemente der Mikro-, Opto- und Molekularelektronik", TU Karl-Marx-Stadt, 11. - 13. 11. 1986

Flagmeyer, R.: Rutherford-Rückstreuung (RBS). "Tage der Wissenschaft" der KMU, Leipzig, 4. - 6. 11. 1986

Flagmeyer, R.: Gitterplatzlokalisierung in III-V-Halbleitereinkristallen mittels Channeling. Bereichsseminar, Sektion Chemie der KMU, Leipzig, 11. 12. 1986

Frey, H.U., H.-E. Zschau, J. Vogt, G. Otto: PIGE and PIXE analyses of elemental distributions in biological samples. Int. Conf. IX. CANAS, Neubrandenburg, 15. - 19. 9. 1986

Frey, H.U.: Erfahrungen mit dem EDR 184 bei PIXE-Messungen. Anwenderseminar VKA/EDR des ZWG Berlin der AdW, Wernsdorf, 8. 10. 1986

Lehmann, D.: Einsatzvorbereitung für externen Strahl am 2-MeV-Beschleuniger der Sektion Physik. 3. Frühjahrsschule +), April 1986

Lehmann, D., C. Ascheron, C. Bauer-Neelmeijer: Nondestructive Determination of the Hydrogen Depth Distribution in Semiconductor Material Using Ion Beam Methods. Int. Conf. IX. CANAS, Neubrandenburg, 15. - 19. 9. 1986

Lehmann, D.: Zu Ursachen und Auswirkungen der Havarie von Tschernobyl. Kolloquium, DHfK Leipzig, 15. 10. 1986

Otto, G.: Stoffanalytik mit kernphysikalischen Methoden an biologischen Substanzen. Sektion Stomatologie der KMU, Leipzig, 3. 2. 1986

Otto, G.: Specifics of IBA of biological samples. 1. Frühjahrsschule "Nukleare Analytik an Beschleunigern" des ZfK Rossendorf der AdW, Holzhau, 7. - 12. 4. 1986

Otto, G.: Ionenstrahlverfahren (PIXE, PIGE, RBS) zur Stoffanalytik. Bereichsseminar, Sektion Chemie der KMU, Leipzig, 12. 5. 1986

Otto, G.: Stoffanalyse an biologischen Proben mittels kernphysikalischer Verfahren (in russisch). XVI. Allunionstagung Physik der "Wechselwirkung geladener Teilchen mit Einkristallen", Moskau, 28. 5. 1986

Rentsch, H., H.-E. Zschau, J. Vogt, H. Zeuner, S. Herrmann, H. Dettmar: Quantitative Bestimmung demineralisationsbedingter Mineralgehaltsveränderungen der äußeren Schmelzoberfläche. Symposium, Gesellschaft für konservierende Stomatologie der DDR, Reinhardsbrunn, 3. - 7. 11. 1986

Vogt, J.: Charakterisierung von Kohle, -produkten und -rückständen mittels Spektrometrie ioneninduzierter Röntgen- und Gammastrahlung. Seminar, VEB Kombinat Chemieanlagenbau Leipzig-Grimma, Leipzig, 9. 6. 1986

Vogt, J., H.U. Frey: Analyse biologischer Proben mittels PIXE. 3. Frühjahrsschule +), April 1986

Zschau, H.-E.: Eigenschaften und Dosimetrie ionisierender Strahlung. Lehrgang, KMU Leipzig, 24. 2. 1986

Zschau, H.-E.: PIGE- und RBS-Untersuchungen zur Konzentrationsverteilung der Elemente F, Na und P in Zähnen. 3. Frühjahrsschule +), April 1986

Zschau, H.-E.: Die Reaktorsicherheit bei der friedlichen Nutzung der Kernenergie. Wurzen, 12. 6. 1986

Zschau, H.-E.: PIGE-, PIXE- und RBS-Untersuchungen an Zähnen zur Bestimmung der Tiefenprofile von F, Na, P und Ca. Seminar, Technische Universität Prag, 2. 7. 1986.

VERANSTALTUNG +)

3. Frühjahrsschule "Stoffanalyse mit dem Ionenstrahl an biologischem Material", Klingenthal (Vogtland), 10. - 14. 3. 1986

HUMBOLDT-UNIVERSITÄT ZU BERLIN, SEKTION PHYSIK, BEREICH 06 - ATOMSTOSSPROZESSE DER FESTKÖRPERPHYSIK

VERÖFFENTLICHUNGEN

M. Fried, T. Lohner, E. Jároli, G. Vizkeletky, E. Kotai, J. Gyulai, A. Biro, J. Adam, M. Somogyi, and H. Kerkow: Optical Properties of Thermally Stabilized Ion Implantation Amorphized Silicon, Proc. Int. Conf. on Ion Beam Modification, Catania 1986

N. M. Kabachnik, H. Kerkow, V. P. Petuchov, E. A. Romanowski, and R. Wedell: Ion-Induced Characteristic X-Ray Emission in solids (b), phys. stat. sol. (b) 139, 1, (1987), Review Article

K. Holldack, H. Kerkow, and W. Prentrup: Anomalous Diffusion of Boron in Silicon due to Heavy Ion Bombardment, phys. stat. sol. (a) 94, 357 (1986)

J. Bollmann, H. Klose, and A. Mertens: Formation of Schottky-junctions in silicon by ion implantation, phys. stat. sol. (a) 97, K95 (1986)

R. Wedell: Multiple Scattering Effects of Light Relativistic Particles Under Channeling Conditions, Konferenzmaterialien der Arbeitstagung "Relativistic Channeling", Acquafredda di Maratea/Italien, 31.3.86-4.4.86

R. Wedell: Some aspects of relativistic particle collision processes in solids, Proc. of the XVI International Symposium on Nuclear Physics, Gaussig 1986

J. Bollmann, H. Klose, and A. Mertens: Big channeling effects at low-energy ion implantation in silicon, phys. stat. sol. (a) 97, K135 (1986)

A. Schenk, K. Irmscher, D. Suisky, R. Enderlein, F. Bechstedt, and H. Klose: Field dependence of the emission rate at deep centres in Si and GaAs, Acta Phys. Pol. 67, 73 (1985)

K. Irmscher, A. Schenk, R. Enderlein, H. Klose, and D. Suisky: Electric Field enhanced thermal Emission from charged deep Levels in Si, Proc. 18th Int. Conf. Sem. Phys., Stockholm 1986

F. G. Rüdenauer, M. Riedel, H. E. Beske, H. Düsterhöft et al.: Cross Calibration for SIMS Quantification, Springer Series in "Chemical Physics", Bd. 44, SIMS V

J. Bollmann, H. Klose, and A. Mertens: Kanalleitungseffekte bei niederenergetischer Ag-Implantation in Si, Proc. "Physik der HL-Oberfläche" 17, 55 (1986)

S. Mechahougui, G. Lehmann, and U. Müller-Jahreis: The Use of secondary Ion Mass Spectrometry for Steel Analysis, ZFK-Bericht 584, 77 (1986)

B. Lukasch: Depth Resolution in Differential Hall-Effekt Measurements for Shallow Implantation Profils, ZFK-Bericht 584, 76 (1986)

J. Bollmann, H. Klose, and A. Mertens: Deep Levels in n-Si caused by Low Energy Ion Implantation, ZfK-Bericht 584, 79 (1986)

H. Düsterhöft and A. Lüders: A Method of Quantification of Mass Spectra in Secondary Ion Mass Spectrometry (SIMS), ZfK-Bericht 584, 78 (1986)

DIPLOMARBEITEN

U. Krause: Statische Modellrechnungen zum Vakanzkomplexbildungsprozeß.

A. Lüders: Untersuchungen von Energieverteilungen und quantitative Analysen bei der positiven Sekundärionenemission aus sauerstoffbedeckten Metallen und isolierenden Proben beim Beschuß mit 10 keV Ar^+-Ionen.

M. Schade: Verfahren zur berührungslosen Drahtdickenmessung.

DISSERTATIONEN A

P. Gehrmann: Untersuchungen zur Richtungsabhängigkeit des Energieverlustes und anderer Effekte bei der Bewegung leichter Ionen in Einkristallen. Juni 1986

VORTRÄGE

H. Kerkow: Nutzung von Kleinbeschleunigern für Festkörperuntersuchungen mit kernphysikalischen Methoden, Int. Arbeitstagung ZfK Rossendorf, Holzau, 1986

P. Gehrmann, K. Lenkeit, R. Stolle und R. Wedell: Theoretische und experimentelle Untersuchungen der Energieverluste von Protonen in Silizium unter Kanalleitungsbedingungen, XVI. Allunionskonfernez über Physik der Wechselwirkung geladener Teilchen mit Kristallen, Moskau, Mai 1986

P. Gehrmann, K. Lenkeit, R. Stolle und R. Wedell: Bestimmung des Durchbruchswinkels unter den Bedingungen des Axial-Flächenüberganges, XVI. Allunionskonferenz über Physik der Wechselwirkung geladener Teilchen mit Kristallen, Moskau, Mai 1986

G. Ferenczi, C. A. Londos, T. Pavelka, M. Somogyi, and A. Mertens: Identification of the carbon associated radiation damage levels in silicon, ICDS - 14, Paris, August 1986

R. Wedell: Multiple Scattering Effects of Light Relativistic Particles Under Channeling Conditions, Hauptvortrag auf der Arbeitstagung "Relativistic Channeling", Acqafredda di Maratea/Italien, April 1986

B. Gruska, W. Frentrup und J. Gerlach: Kurzzeittemperung an Be-implantierten GaAs-Epitaxieschichten, Arbeitstagung ZfK Rossendorf "Ionenstrahltechnologie '86", Papstdorf, April 1986

B. Gruska, W. Frentrup und J. Gerlach: Kurzzeittemperung implantierter A_3B_5-Epitaxieschichten, Fachtagung "Schichtsysteme für zukünftige Bauelemente der Mikro-, Opto- und Molekularelektronik", TH Karl-Marx-Stadt, Oktober 1986

U. Schade, Ch. Rosinska und W. Frentrup: Untersuchungen zur Langzeitausheilung durch Ionenimplantation amorphisierter Siliziumschichten, 9. Zentrale Leistungsschau der Studenten und jungen Wissenschaftler, Leipzig, 1985

H. Klose, J. Bollmann und A. Mertens: Elektronische Eigenschaften oberflächennaher Implantationsdefekte in Si, Problemseminar "Tiefe Störstellen", TH Karl-Marx-Stadt, Dezember 1985

H. Klose und K. Irmscher: Zur Feldabhängigkeit der Einführungs- und Emissionsprozesse tiefer Zentren - experimentelle Ergebnisse, Problemseminar "Tiefe Störstellen", TH Karl-Marx-Stadt, Dezember 1985

M. Griepentrog: Ionenstrahlgestützte Untersuchungen an Katodenmaterialien, Herbstschule des ZIE, Bad Stuer, Dezember 1986

H. Düsterhöft und M. Griepentrog: Einsatz der SIMS für Analytik von Metalloberflächen, NARVA-Herbstschule, Berlin, September 1986

U. Müller-Jahreis: Méthodes analytiques á l'aide des faisceaux d'ions, Universität Sétif (Algerien), Juni 1986

M. Abbas, H. Kerkow, M. Klein und R. Wedell: Experimentelle und theoretische Untersuchungen der Energie- und Temperaturabhängigkeit der Amorphisierungsdosis in Silizium, Belorussische Staatliche Leninuniversität Minsk, Juni 1986

H. Klose, A. Mertens, and J. Bollmann: Channeling of heavy ions at low energies in Si, TU Prag, März 1986

H. Klose: Electronical properties of implantation defects in Si, TU Prag, März 1986

U. Krause: Statistische Modellrechnungen zum Vakanzkomplexbildungsprozeß, Belorussische Staatliche Leninuniversität, Minsk, September 1986

H. Klose: O raspredelenije radiazionnych defektov v poluprovdnikach, IFP der SOAN, Novosibirsk, November 1986

H. Klose: Vorlesungen an der MGU zum Thema "Elektritscheskije i ionometritscheskije metody v issledo vanijach svoistv implantivo vannych poluprovodnikov, November 1986

K. Holldack: Diffusionsanomalien in Silizium infolge Ionenbeschusses, 11. Nationale Studentenkonferenz, Dresden, 1986

K. Holldack: Diffusionsanomalien von B in Si infolge Ionenbeschusses, Studententage WPU Rostock, Februar 1986

M. Griepentrog: Internationale Trends der Geräteentwicklung für die Festkörperanalytik, SIMS-Kolloquium, Dresden, November 1986

H. Düsterhöft und W. Schneider: Oberflächenanalytik in der Festkörperphysik, Vortrag auf dem E-Kolloquium im Kombinat NARVA (BGW), November 1986

H. Kerkow: Nukleare Analytik an Kleinbeschleunigern, 1. Frühjahrsschule des ZfK, April 86

P. Gehrmann: Untersuchungen zur Richtungsabhängigkeit des Energieverlustes und anderer Effekte, Kolloquium ZfK Rossendorf, Juni 1986

BERUFUNGEN

Doz. Dr. sc. U. Müller-Jahreis zum a.o. Professor für Experimentalphysik an der Humboldt-Universität zu Berlin, Februar 1986

Dr. sc. R. Wedell zum a.o. Dozenten für Theoretische Physik an der Humboldt-Universität zu Berlin, Februar 1986

FRIEDRICH-SCHILLER-UNIVERSITÄT JENA, SEKTION PHYSIK, WISSENSCHAFTSBEREICH IONOMETRIE

VERÖFFENTLICHUNGEN

Bartsch, H., G. Andrä, E. Glaser;
TEM cross-sectional imaging of laser-induced crystallization after ion implantation; phys. stat. sol. (a) 94 (1986) 773-779

Fuschini, E., A. Uguzzoni, K. Gärtner, K. Hehl;
Axial blocking in a master equation approach; Nucl. Instr. & Meth. in Physics Research B 12 (1985) 334-342

Gärtner, K., E. Glaser, G. Götz, K. Hehl;
Defect analysis by dechanneling; Nucl. Instr. & Meth. in Physics Research B 15 (1986) 317-321

Geiler, H.-D., E. Glaser, G. Götz, M. Wagner;
Explosive crystallization in silicon; Journal of Appl. Physics 59 (1986) 3091-3099

Glaser, E., G. Andrä, H. Bartsch, K. Drenda, G. Götz;
Formation of monocrystalline layers by explosive crystallization of ion implanted amorpheus Silicon; phys. stat. sol. (a) 94 (1986) 781-786

Götz, G.;
Explosive crystallization processes in Silicon; Appl. Phys. A 40 (1986) 29-36

Götz, G.;
Radiation effects in optoelectronic materials; Radiation effects 98 (1986) 189-210

Götz, G., K. Gärtner, E. Glaser, B. Weber, W. Wesch, A. Witzmann, A. Dittmar;
High energy ion beam analysis of solids; Lehrmaterial zur CIBAS-Sommerschule, S. 1-405

Heinig, K.-H., H.-D. Geiler;
Phenomenological theory of explosive crystallization of amorpheus Silicon; Part I: Stationary Solutions; phys. stat. sol. (a) 92 (1985) 421-430

Heinig, K.-H., H.-D. Geiler;
Phenomenological theory of explosive crystallization of amorphous Silicon; Part II: Dynamical Solutions; phys. stat. sol. (a) 93 (1986) 99-104

Kaschner, C., A. Witzmann, K. Gärtner, G. Götz;
Laser annealing of ion implanted NiSi layers; phys. stat. sol. (a) 94 (1986) 787-791

Uguzzoni, A., E. Fuschini, K. Gärtner, K. Hehl;
Axial blocking dips from the master equation for the transverse energy distribution; Nucl. Instr. & Meth. in Physics Research B 13 (1986) 32-37

Wagner, M., H.-D. Geiler, G. Götz;
Time-resolved investigation of large - area explosive crystallization of amorphous silicon layers; phys. stat. sol. (a) 92 (1985) 413-420

Wendler, E., W. Wesch, G. Götz;
Near edge optical absorption behaviour in weakly damaged ion implanted GaAs; phys. stat. sol. (a) 93 (1986) 207-212

Wesch, W., G. Götz;
Rapid annealing of ion implanted GaAs;phys. stat. sol. (a) 94 (1986) 745-766

Wesch, W., K. Gärtner, E. Wendler, G. Götz;
RBS and optical investigations of defects in weakly damaged GaAs; Nucl. Instr. & Meth. Phys. Research B 15 (1986) 431-434

Wesch, W., K. Gärtner, E. Wendler, G. Götz;
Investigation of defects in weakly damaged GaAs layers; Rad. eff. 97 (1986) 313-320

Witzmann, A., A. Dittmar, K. Gärtner, G. Götz;
Formation of Ni silicides on As-doped silicon; phys. stat. sol. (a) 91 (1985) 439-445

DIPLOMARBEITEN

Heiber, U.: Ionenimplantation magnetischer Werkstoffe.

Machalett, F.: Einsatz eutektischer Systeme als Quellenmaterial in Flüssigmetallionenquellen.

Müller, B.: Untersuchung der nichtionischen Komponente des von Flüssigmetallionenquellen emittierten Strahles in Abhängigkeit von den Betriebsparametern der Quelle.

Stiebritz, I.: Untersuchungen an Flüssigmetallionenquellen für Gallium und Goldsilizium.

PROMOTIONEN A (DR. RER. NAT.)

Dittmar, A.; Nickelsilizidbildung bei Kurzzeittemperprozessen; 18. 3. 1986.

Stock, D.: Phänomenologische Beschreibung laserinduzierter Phasenübergänge 1. Art aus metastabilen Zuständen ; 18. 3. 1986.

VORTRÄGE

Andrä, G.: Einfluß dotandeninduzieter Keimbildung auf den Prozeß und das Ergebnis der Flüssigphasenexplosivkristallisation in amorphem Silizium auf SiO_2. Arbeitstagung "Ionenstrahltechnologie", Papstdorf, April 1986.

Andrä, G., H.-D. Geiler, E. Glaser, G. Götz: Explosive crystallization of ion implanted silicon layers. IBMM '86, Catania, June 1986.

Andrä, W., G. Götz, U. Pusa, W. Einbrodt: Eigenschaften ionenimplantierter pn-Übergänge mit kleinen Eindringtiefen. IV. Symposium Physik. Grundlagen zu Bauelemente-Technologien der Mikroelektronik, Frankfurt/Oder, Sept. 1986.

Bachmann, T., P. Ressel, W. Wesch; Einfluß von Restdefekten auf die elektrischen Eigenschaften von ionenimplantierten GaAs-Schichten nach ns-Impulslaserausheilung. Arbeitstagung "IOnenstrahltechnologie", Papstdorf, April 1986.

Dittmar, A., K. Gärtner, G. Götz.: Bildung von Ni-Silizid durch ms-Laserbestrahlung. BGU Minsk, Juni 1986.

Gärtner, K.: Information about crystall defects from the energy dependence and temperature dependence of dechanneling. KFKI Budapest, November 1986.

Gärtner, K.: Lokalisierung von Defekten mit Hilfe der Dekanalisierung. BGU Minsk, Juni 1986.

Gärtner, K.: Dekanalisierung an Kristalldefekten. Frühjahrsschule "Nukleare Analytik an Beschleunigern", Holzhau , April 1986.

Geiler, H.-D.: Explosivkristallisation amorpher Si-Schichten auf kristallinen und amorphen Trägern. TU Berlin (West), Opt. Inst., Febr. 1986.

Geiler, H.-D.: Rapid solidification phenomena in undercooled molten silicon. Univ. Sofia, November 1986.

Geiler, H.-D.: Laserprozesse zur Herstelung von SOI-Strukturen. 3. Nationale Tagung "Lasertechnologie", Karl-Marx-Stadt, November 1986.

Geiler, H.-D., G. Andrä, E. Glaser, G. Götz: Study of the ignition behaviour of explosive crystallization in ion implanted silicon. IBMM '86, Catania, June 1986.

Geiler, H.-D., Stock, D., G. Götz: Modelling of ultrafast melting and solidification of implanted amorphous silicon. IBMM '86, Catania, June, 1986.

Geiler, H.-D., D. Stock, G. Götz, K. Hennig: Modelling of ultrafast solidification in highly undercooled molten silicon. Int. Conf. E-MRS Meeting, Strasbourg, June 1986.

Glaser, E.: Explosivkristallisation in ionenimplantierten amorphen Siliziumschichten. Arbeitstagung "Ionenstrahltechnologie", Papstdorf, April 1986.

Glaser, E., Andrä, G., H.-D. Geiler, G. Götz, M. Wagner: Explosive crystallization in ion implanted silicon layers on crystalline substrates. IBMM '86, Catania, June 1986.

Götz, G.: Generation of crystalline layers by laser induced processes. KFKI Budapest, Mai 1986.

Götz, G.: Defects in ion implanted and laser annealed GaAs. Univ. Aarhus, Sept. 1986.

Götz, G.: Laser assisted formation of epitaxial silicides. Univ. Aarhus, Sept. 1986.

Götz, G.: Explosive crystallization in silicon. Univ. Aarhus, Sept. 1986.

Götz, G.: Ionenimplantation und Ausheilung von Strahlenschäden. Bergakademie Freiberg, Okt. 1986.

Herold, J.: Untersuchung der Festphasenkristallisation von ionenimplantierten GaAs im Temperaturbereich bis 400° C. Arbeitstagung "Ionenstrahltechnologie", Papstdorf, April 1986.

Kaschner, C.: Markerexperimente zur Aufklärung der $NiSi_2$-Bildung durch ns-Laserbestrahlung. Arbeitstagung "Ionenstrahltechnologie", Papstdorf, April 1986.

Kaschner, C.: Bildung von epitaktischen $NiSi_2$ durch Laserbestrahlung. Kolloquium junger Physiker, , Mai 1986.

Kaschner, C., A. Witzmann, K. Gärtner, G. Götz: Epitaktisches Wachstum von $NiSi_2$ durch Laserbestrahlung. BGU Minsk, Juni 1986.

Kaschner, C., A. Witzmann, K. Gärtner, G. Götz: Liquid phase silicide formation. KFKI Budapest, Nov. 1986.

Mühle, R., J. Mittenbacher: Untersuchungen an Flüssigmetall-Ionenquellen. Arbeitstagung "Ionenstrahltechnologie", Papstdorf, April 1986.

Wesch, W.: Short time annealing of ion implanted GaAs. Univ. Tbilissi, Okt. 1986.

Wesch, W., P. Ressel, D. Stock, E. Wendler, G. Götz: Short time annealing of ion implanted GaAs. 2nd Conf. Physics and Technology of GaAs and other III-V Semiconductors, Budapest , Sept. 1986.

Wesch, W., E. Wendler, G. Götz: Investigation of defects in ion implanted GaAs by means of RBS and optical transmission spectroscopy. 2nd Conf. Physics and Technology of GaAs and other III-V Semiconductors, Budapest , Sept. 1986.

Winkler, N.: Eletrische Messungen an explosivkristallisierten Silizium. Arbeitstagung "Ionenstrahltechnologie", Papstdorf, April 1986.

Stock, D., H.-D. Geiler, G. Götz: Modelling of ultrafast solidification in highly undercooled molten silicon. JPJ Swierk, Okt. 1986.

BERGAKADEMIE FREIBERG, SEKTION PHYSIK, WB ANGEWANDTE PHYSIK

VERÖFFENTLICHUNGEN

Degering, D. and S. Unterricker: Determination of small yttrium concentrations in geological samples by charged particle activation analysis. Proceedings 3rd Working Meeting "Radioisotope Application and Radiation Processing in Industry", Leipzig, 23. - 27. Sept. 1985, p. 921.

Hebert, D., K. Fröhlich, T. Franke, R. Gellermann, S. Unterricker, J. H. Kim: Underground laboratory in Freiberg, GDR. Nucl. Instr. Methods in Phys. Res. B 17 (1986) 427.

Blankenburg, H. J., S. Unterricker, B. Eichler, R. Starke, W. Stolz, H. J. Rösler: Natürliche Radioaktivität, chemische und Phasenzusammensetzung der Eisenoxide aus Vulkanitachaten. Chem. Erde 45 (1986) 159.

Bergelt, H., H. Militzer, W. Stolz: Die Radonexhalation von Festgesteinsproben unter Druckeinwirkung. Gerl. Beitr. Geophys. 95 (1986) 7.

Reichel, W. und W. Stolz: Apparatur zur Auswertung fadenförmiger Thermolumineszenzdosimeter. Isotopenpraxis 22 (1986) 313.

Pietzsch, C.: Nomenklatur und Vereinbarungen für die Veröffentlichung mößbauerspektroskopischer Daten. IUPAC Nomenklaturregeln für die Analytik Nr. 15, übersetzt und bearbeitet. Chemische Gesellschaft der DDR, Berlin 1986.

DIPLOMARBEITEN

Müller, S.: Seltene Erden in hydrothermalen Calciten. Freiberg, Juli 1986.

Docekal, A.: Fission-track-Untersuchungen an natürlichen Gläsern. Freiberg, Juli 1986.

PROMOTIONEN A (DR.-ING.)

Feddersen, Ch.: Erfassung der durch kurzlebige Radonfolgeprodukte bedingten Strahlenbelastung von Bergarbeitern durch ein integrierendes am Arbeitsplatz auswertbares Dosimetersystem. Freiberg, April 1986.

PROMOTIONEN B (DR. SC. NAT.)

Unterricker, S.: Die Anwendung der Methode 'Gestörte Winkelkorrelationen' TDPAC zur Untersuchung der Strahlenschädigung und der Struktur von tetraedrisch koordinierten Verbindungshalbleitern unter besonderer Berücksichtigung der Verhältnisse nach einer Ionenimplantation. Bergakademie Freiberg, 21. 5. 1986.

VORTRÄGE

Unterricker, S.: Korrelation von Bindungstyp und Ausheilverhalten von Strahlenschäden bei halbleitenden Verbindungen.

Pietzsch, C., U. Thieme: Mößbaueruntersucnungen zur Karbidbildung in HTMB-Stählen.

Pietzsch, C.: Mößbaueruntersuchungen zur Fe^{2+}, Fe^{3+}-Verteilung in Chromspinellen. Mößbauerkolloquium, Freiberg 18./19. 3. 1986.

Unterricker, S.: TDPAC-Untersuchungen zur Strahlenschädigung und zur Struktur von implantierten halbleitenden Substanzen. Vortrag vor der Fakultät Math.-Nat. der Bergakademie Freiberg, 18. 11. 1986.

Stolz, W., S. Unterricker, J. H. Kim: Germanium als Detektor für ionisierende Strahlung. Berg- und Hüttenmännischer Tag, Freiberg 25. 6. 1986.

Stolz, W.: Die Entwicklung der Radiumforschung im sächsischen Raum. Vereinigung für Strahlenforschung und Strahlenschutz der DDR, Berlin 24. 6. 1986.

Stolz, W.: Radon - Geowissenschaftliche Anwendungen und Quelle der natürlichen Strahlenbelastung. Kolloquiumsvortrag ZfI-Leipzig, 14. 5. 1986.

VERANSTALTUNGEN

Mößbauerkolloquium, 18. - 19. 3. 1986 in Freiberg, Bergakademie Freiberg, Sektion Physik.

NOTIZEN